

ANNUAL REVIEW

***INSTITUTE
FOR
MOLECULAR
SCIENCE***



1980

Errata

p.79—80,

III—H Single Vibronic Level Fluorescence Spectroscopy

Yasuo UDAGAWA, Yoko MOCHIZUKI, Koji KAYA (*Tohoku Univ.*),
Isamu SUZUKA (*Nippon Univ.*), and
Mitsuo ITO (*Tohoku Univ. and IMS*)

The fluorescence spectroscopy of aromatic molecular vapors has been stimulated by the "single vibronic level" (SVL) excitation technique. Much information about primary photophysical processes can be obtained from measuring SVL fluorescence spectra, quantum yields and lifetimes. The experiments are carried out in the gas phase at low pressure where the time interval between subsequent collisions is large compared with the lifetime of the excited vibronic levels. Therefore, the SVL fluorescence spectra reflect properties of the isolated molecule.

The present research project aims at elucidating

the adiabatic vibrational potentials of the excited state molecules by use of the SVL fluorescence spectroscopy. The adiabatic vibrational potentials are essential in understanding photochemical and photophysical behaviors of the excited state molecules. The SVL fluorescence spectra of several N-heterocyclic molecules (pyridine, pyrazine and s-tetrazine) obtained by excitations to their various vibronic levels have been observed by use of a high power dye laser. From the analysis of the observed spectra, detailed information about the geometrical structure and adiabatic potentials of the excited state molecules have been obtained.

p.6, line 11,

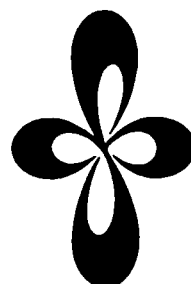
Keiya KANDA should be Yoshiya KANDA.

p.152, line 17 from bottom,

J. Chem. Phys. should be *J. Phys. Chem.*

ANNUAL REVIEW

***INSTITUTE
FOR
MOLECULAR
SCIENCE***



1980

Published by

The Institute for molecular Science
Myodaiji, Okazaki 444, Japan
Phone 0564—52—9770
December 1, 1980

Editorial Committee: Tasuku Ito (Chairman),
Yasuki Endo, Kazuo Kitaura,
Akira Miyashita, Tadayoshi Sakata,
Kosuke Shobatake, Makoto Watanabe

IMS 1980

The Institute for Molecular Science is an inter-university national research institute which was established in 1975. This, the third issue of IMS Annual Review, is the report on the state and activities of IMS during the year since August 1979.

On the 8th of November, IMS held a ceremony celebrating its establishment and the completion of the buildings and facilities. On the next day, the institute was opened to the public. In the first five years the cumulative sum of equipment funds for IMS amounted to 2,549 million yen and the construction costs amounted to 3,900 million yen.

The Laboratory of Molecular Dynamics started in January when Prof. T. Fujiyama moved from Tokyo Metropolitan University to the chair of the Laboratory. Dr. Y. Udagawa came to the same Laboratory as Assoc. Professor. Thirteen Research Laboratories are presently engaged in research, and IMS will have two more Research Laboratories, upon completion.

The accidental death of Dr. G. Soda in February was a matter of deep regret for all of us. He had just arrived at IMS as Assoc. Professor of the Instrument Center in October, 1979. Mr. S. Takahashi, Technical Chief, retired in March. He has established the basis for the Development Workshop and contributed a great deal to the research activities of IMS.

In, 1980, two special research projects contained in the second five-year plan have been initiated in place of those of the first five-year plan. They are supported by a total of 84 million yen for the first year of the five-year plan. The first of these research projects is 'Energy Transfer and Energy Conversion through Molecular Processes', which is concerned with the experimental and theoretical studies of the intra- or inter-molecular energy transfer and photochemical conversion of energy. The second research project is 'The Development and Control of Molecular Functions', which is concerned with the molecular design of materials and the control of chemical reactions at the molecular level. These subjects are not only fundamentally interesting in molecular science but also currently important from the viewpoint of social needs.

The interaction between photons and molecules is one of the principal subjects in molecular science. The lasers have accelerated the rapid progress of molecular spectroscopy and photochemistry. Funded by the program for the Installation of Large Scale Research Equipment, IMS have developed four laser-based systems for both time-resolved spectroscopy and high resolution spectroscopy. The pico-second continuously tunable laser from UV to IR is working successfully. In recent years, synchrotron orbital radiation (SOR) has received considerable attention because of its unique characteristics as a light source. Since the foundation of IMS, the need for a SOR facility with 0.6 GeV storage ring, which is called UVSOR, has been strongly felt for research in molecular science and related fields. The UVSOR project is now ready to be realized by 203 million yen grant awarded this year.

The inter-university national research institutes have been established with the purpose of promoting science in collaboration with universities. These two systems are complementary to each other. Because of this the research facilities of IMS are open to the scientists in the universities for common use. Furthermore, the most important role that IMS is playing is to encourage the scientists who are doing research in molecular science and its related fields. IMS entertains proposals for Cooperative Research from scientists throughout the country. IMS also solicits applications for the programs of Joint Studies and Research Symposia, both carried out by a group of scientists. All of these activities are highly appreciated among the scientists. The total number of visitors who have used the facilities or attended symposia amounts to 7,000 man-days a year.

IMS is now widely known among the molecular scientists in the world. The number of foreign scholars who visit IMS has increased yearly and amounted to about 140 during the past year. The international collaborative activities at IMS is supported by the Invited Foreign Scholars Program and the Okazaki Conference which is held twice a year with participation of invited speakers from abroad. IMS is a unique institute in Japan in that it has distinguished foreign scientists as members of its Council. Dr. G. Herzberg and Prof. H. Gerischer served as foreign members of the Council for two years and four years, respectively. Prof. Melvin Calvin and Prof. Sir George Porter are the current members of the Council. The presence of these distinguished scientists in the Council encourages international collaborative activities among the molecular scientists not only at IMS but throughout the country. The Eighties are hoped to be an era for international collaboration. It will be a great pleasure to watch IMS develop its potential as it contributes to greater international collaboration through the scientific activities. (September, 1980)



Hideo Akamatsu
Director

CONTENTS

IMS 1980	i
ORGANIZATION	1
SCIENTIFIC STAFF	1
COUNCIL	6
BUILDINGS AND CAMPUS	7
RESEARCH ACTIVITIES I THEORETICAL STUDIES	9
A. Potential Energy Surfaces for Chemical Reactions	9
1. Ab Initio Calculations of the $a^3\Pi-b^3\Sigma^-$ Transition of CH^+	9
2. Potential Energy Surfaces of the Reaction $C^+ + H_2 \rightarrow CH^+ + H$	9
3. Reaction Coordinate Properties of $HFCO \rightarrow HF + CO$ Reaction	10
4. The Reaction Mechanism of Hydroboration. An Ab Initio MO Study on the $C_2H_4 + BH_3$ Reaction	11
5. Photoisomerization Processes of Polyenes in Singlet Mechanism: Potential Surfaces	12
6. Photoisomerization Processes of Polyenes in Singlet Mechanism: Radiationless Transition from Zwitterionic State	13
B. Problems in Molecular Structure and Molecular Interaction	14
1. An Ab Initio MO Study on the Stability and Nature of the Si-C Double Bond	14
2. An Ab Initio MO Study on the Stability and Nature of the Si-C and Si-Si Triple Bonds	15
3. Theoretical Evidences for Intramolecular Hydrogen Bonding in Syn-7-Norbornenol	16
4. MO Study on the Mechanism of Heat-Resistance of Thermophilic Bacteria	17
5. Ab Initio SCF MO Calculation of Force Constants and Dipole Derivatives on Trans- and Cis-N-Methylformamide	17
6. Ab Initio MO Study on Amine Molecules	18
C. Structure, Bonding and Reactivity of Transition Metal Complexes	18
1. Energy Gradient in the Ab Initio MO Method with the Effective Core Potential Approximation	18
2. An Ab Initio MO Study on the Reaction Mechanism of $Co^+ + C_2H_6$	19
3. Ab Initio MO Study on Hydrolysis of $PtCl_2(NH_3)_2$ and Trans-Effect	20
4. An Ab Initio MO Study of the Structure and Coordinate Bonding Nature of $Ni(PH_3)_2L$ ($L = H_2CO$ or $(CO)_2$)	20
5. The Mutual Influence of Ligands in Pentaammine Co(III) Complexes. Ab Initio MO Study	21
6. MO Study of Catalytic Specificity of Manganic Ion in Photosynthetic Water Decomposition	22
D. Surface Electronic Structure of Metal Oxides and Chemisorption Mechanisms	22
1. Theory of the Electronic Structure of ReO_3 (001) Surface and the Surface Oxygen Vacancy	23
2. Self-consistent Madelung Potential for the Cluster Calculation of Partially Ionic Solids — Application to ReO_3 —	23
3. Theoretical Study of Ethylene Metathesis Reaction on the ReO_3 Surface by DV- $X\alpha$ Cluster Calculation	24
4. Electronic Structure of ZrO_2 by the DV- $X\alpha$ Cluster Method	25
E. Theory of Transition-Metal Surfaces and Interaction with Adparticles	25
1. Chemisorption of Oxygen Atom on bcc Metal Surfaces	26
2. Electronic Structure of the Chemisorption System of Oxygen on the Mo (100) Surface	26
3. Chemisorption of Oxygen Atoms on Zinc (0001) Surface by DV- $X\alpha$ Cluster Calculations	27
4. Theoretical Study of Chemisorption of Underlayer Type	28

F. Electronic Structure of Low Dimensional Materials	29
1. Self-consistent Electronic Band Structure of Polyacetylen and Polyethylene	29
2. The Electronic Structure Calculations of the Graphite Intercalation Compounds Based on the SCF-DV-X α Cluster Model	30
G. Electron Theory of Semiconductor Surfaces	31
1. Self-consistent DV-X α Cluster Calculation of Electronic Structure on the Si (111) 7 \times 7 Model Surface	31
2. Electronic Structure of Chemisorption Systems: H and Cl Chemisorbed on Si (111) 7 \times 7 Reconstructed Surface	32
3. Chemical Pseudopotential Theory of Surface Reconstruction and Chemisorption	32
H. Development of Density Functional Approaches for the Potential Energy Surface	34
1. Density Functional Approach to the Total Energies of Molecules, Surface and Bulk Systems	34
I. The Analysis of the Electron Distribution in Molecules	35
1. The Electron Density Analysis and the Oxydation Number. I. Some Sulpher and Chlorine Compounds	35
J. Theoretical Study of Molecular Photoionization and Molecular Inner Shell Excitation	36
1. The Boron K Absorption Spectra of BF ₃ , BCl ₃ , and BBr ₃	36
RESEARCH ACTIVITIES II MOLECULAR STRUCTURE	38
A. High Resolution Spectroscopy of Transient of Molecular Species	38
1. Microwave Spectroscopy of HSO and DSO	38
2. Vibronic Interactions between \tilde{A} and \tilde{X} via the ν_3 Mode in BO ₂	39
3. Pertubations in the \tilde{A} State of HCCl	40
4. Dye Laser Excitation Spectroscopy of Deuterated Fluorocarbene DCF	40
5. Microwave Optical Double Resonance of HNO: Rotational Spectrum in \tilde{A}^1A'' (100)	41
6. Microwave Spectrum of CF in $^2\Pi_{1/2}$	42
7. The ν_3 Band of the Trifluoromethyl Radical by Diode Laser Spectroscopy	42
8. Hyperfine Structures of PH ₂ in \tilde{X}^2B_1 and \tilde{A}^2A_1 from Intermodulated Fluorescence	43
9. Vibration-Rotation Bands of the FCO Radical by Diode Laser Spectroscopy	44
10. Infrared-Optical Double Resonance Spectroscopy. Application to the Vibration-Rotation Spectrum of the NH ₂ Radical in Excited Electronic States	45
11. Microwave Spectrum of the SF Radical	46
12. Microwave Spectrum of the ClSO Radical	47
13. Diode Laser Spectroscopy of the HO ₂ ν_2 Band	47
14. Dye Laser Excitation Spectroscopy of SiH ₂	48
15. The HO ₂ ν_1 Band Observed by a Difference-Frequency Laser	48
16. Laser Excitation Spectroscopy of the Singlet Methylene Produced by UV Photodissociation of Ketene	49
17. Diode Laser Spectroscopy of the FSO ν_1 Band	49
B. Microwave Spectroscopy of Non-polar Molecules	50
1. Microwave Spectra of Deuterated Ethylenes: Molecular Structure and Intramolecular Potential Function	50
2. Microwave Spectra of Deuterated Ethanes: Internal Rotation Potential and r_z Structure	51
C. Development of New Instruments for High Resolution Spectroscopy	52
1. Computer-Aided Diode Laser Spectroscopy	52
2. A Near-Infrared Diode Laser Spectrometer	53
D. Development of New Instruments for Condensed Phase Spectroscopy	53
1. Light Scattering Spectrometer for Intensity Measurement	53
2. Light Scattering Spectrometer for Line-Shape Measurement	54
3. Dual-beam Thermal Lensing Spectrometer	55
E. Local Structure Formations in Solutions	55

1. Light Scattering Study of Local Structures in Solutions. Mean Association Numbers and Concentration Fluctuation for Alcohol-Carbon Tetrachloride Systems	55
2. Light Scattering Study of Local Structures in Solutions. Cooperative Translational Motion of Alcohol Molecules in Carbon Tetrachloride Solutions	56
F. Intensity Distributions of Vibration Spectra	57
1. Shapes of the ν_1 Band of Liquid Chloroform and Intermolecular Interaction	57
2. Fluctuation of Local Field and Depolarization Degree of the ν_1 Line of Carbon Tetrachloride	58
G. Double Resonance Spectroscopy Using a Tunable Diode Laser	59
1. Pure Rotational Spectrum of CF_4 in the $\nu_3 = 1$ State	59
2. Dipole Moment and Pure Rotational Transitions of SiH_4 and GeH_4 in the $\nu_3 = 1$ Vibrational State	59
H. Large Amplitude Intra-Molecular Motions	60
1. Diode Laser Spectroscopy of Hydrazine $-\text{NH}_2\text{NH}_2$	60
I. Production of Highly Excited Atoms from Molecules	60
RESEARCH ACTIVITIES III ELECTRONIC STRUCTURE	63
A. Primary Photochemical Reactions of Organic Compounds	63
1. Direct Measurement of the Reaction Rate for cis \rightarrow trans Photoisomerization of Stilbene	63
B. Electronic Structures of Excited States	63
1. Laser Flash Photolysis of Benzene. II. Laser-Induced Cluster Formation in Gas Phase	63
2. Laser Flash Photolysis of Benzene. III. $S_n \rightarrow S_1$ Absorption of Gaseous Benzene	64
3. Time-resolved Measurements of Electron and Energy Transfer of Rhodamine B Monolayer on Surface of Organic Crystals	64
4. Biphotonic Ionization of 8-Anilino-1-Naphthalemesulfonate in Polar Solvents	64
5. Picosecond Time-Resolved Fluorescence Studies of Interamolecular Heteroexcimers	64
6. Picosecond Laser Spectroscopy of Intramolecular Heteroexcimer Systems. 1. Time-Resolved Fluorescence Studies of $p\text{-(CH}_3)_2\text{NC}_6\text{H}_4 - (\text{CH}_2)_n$ $= (9\text{-Anthryl})$, $p = (\text{CH}_3)_2\text{NC}_6\text{H} = (\text{CH}_2)_n = (1\text{-Pyrenyl})$ Systems and 9,9'-Bianthryl	64
C. Studies on Transient Phenomena in Biology	65
1. Picosecond Fluorescence Lifetime of the Coenzyme of D-Amino Acido Oxidase ..	65
2. Picosecond Transient Behavior of the Reaction-Center Particles of Photosystem I Isolated from Spinach Chloroplast. I. Decay Characteristics of Excited Chlorophylls	65
3. Picosecond Transient Behavior of the Reaction-Center Particles of Photosystem I Isolated from Spinach Chloroplast. II. Energy Transfer and Electron Transfer at Weak Light Excitation	65
D. Solar Energy Conversion by Using Photocatalytic Effects of Semiconductors — Decomposition of Water and Hydrogen Evolution	66
1. Photocatalytic Decomposition of Gaseous Water over TiO_2 and $\text{TiO}_2\text{-RuO}_2$ Surfaces	66
2. Photocatalytic Decomposition of Water by Solar Energy — Hydrogen Evolution, CO_2 Fixation on Powdered Semiconductors and their Mechanisms with Pulsed Laser-Dynamic Mass Technique —	66
3. Photocatalytic Hydrogen Production from Liquid Methanol and Water	67
4. Conversion of Carbohydrate into Hydrogen Fuel by a Photocatalytic Process	67
5. Hydrogen Production from Biomass and Water by Photocatalytic Reactions	69
6. Heterogeneous Photocatalytic Production of Hydrogen and Methane from Ethanol and Water	69
7. Photocatalytic Reaction of Benzene, Naphthalene and Coal with Water	70
8. Luminescence of $\text{Ru (bipy)}_3 \text{Cl}_2$ Adsorbed on Semiconductor or Insulator	71

E. Study of Elementary Processes in Chemical Reaction	71
1. Construction of Crossed Molecular Beam Apparatus	71
2. Formation of Chlorine Atoms by the Infrared Multiphoton Dissociation of Trichloroethylene under the Molecular Beam Condition	72
F. Chemical Reactions Through Highly Excited Vibrational States	73
1. Infrared Multiphoton Dissociation of Ammonia: Laser Energy and Pressure Dependence of the Emission from NH and NH ₂	73
2. Infrared Multiphoton Dissociation of Ammonia (II): Optoacoustic Measurement of Vibrational Distribution	74
3. State-Selective Chemistry in the Electronic Ground State	74
G. Study on Photochemical Processes Related to Planetary Space Chemistry	75
1. A Ultra-High-Vacuum, Pulsed Molecular Beam Apparatus for the Study of Electronically Excited Cometary Molecules	75
2. Photochemical Conversion from Methylamine to Hydrogencyanide with an ArF Laser at 193 nm	77
3. Excited State Dynamics and Quenching Rates for NH (A ³ Π _i) Radical	78
4. ArF Laser Photolysis of Cometary Molecules — Product Analysis by a High Resolution Mass Spectrometer —	78
5. Vacuum Ultraviolet Laser Photolysis of Carbon Suboxide — Emissions from Electronically Excited Atomic and Diatomic Carbons —	78
H. Single Vibronic Level Fluorescence Spectroscopy	80
I. Picosecond-Backward Echo in Molecular Sodium	80
RESEARCH ACTIVITIES IV MOLECULAR ASSEMBLIES	81
A. Photoelectric and Optical Properties of Organic Solids in Vacuum Ultraviolet Region	81
1. Polarization Energies of Organic Solids Determined by Ultraviolet Photoelectron Spectroscopy	81
2. Ultraviolet Photoelectron Spectroscopy of Aliphatic Hydrocarbon Solid Films	82
3. Photoelectron Spectroscopy of 2,2-Diphenyl-1-picrylhydrazyl (DPPH) and 2,2-Diphenyl-1-picrylhydrazine (DPPH ₂)	83
4. Anisotropic Vacuum UV Absorption Spectra of Oriented Polyacrylonitrile Films	84
5. Ultraviolet Photoelectron Spectra of Tetrahalogeno- <i>p</i> -benzoquinones and Hexahalogenobenzenes in the Solid State	84
6. Polarization Energies of Tetrathiafulvalene Derivatives	85
B. Photoconduction in Organic Solids	86
1. Purification of Tetrabenz[<i>a,c,d,j,l,m</i>]perylene	86
2. Detrapping of Charge Carriers by Singlet Excitons in Naphthalene Single Crystal	86
C. Reduction Kinetics and Electron Transport Behavior of Cytochrome c₃	87
1. Kinetics of Cytochrome c ₃ Reduction with Hydrogenase: A Mössbauer Effect Study	87
2. Electrical Conductivity of an Anhydrous Cytochrome c ₃ Film as a Function of Temperature and Ambient Pressure	87
D. Chemistry and Physics of Graphite Intercalates	88
1. Graphite Filaments and Their Alkali-metal Intercalation Compounds	88
2. Raman Scattering from Graphite Intercalated with FeCl _{3-y}	89
E. Organic Metals	90
1. Requirements for an 'Organic Metal'	90
F. Studies of Ion-Molecule Reactions by a Threshold Electron-Secondary Ion Coincidence Technique	91
1. Determination of Separate Reaction Cross Sections for the Two Spin-Orbit States Ar ⁺ (2P _{3/2} , 2P _{1/2})	91
2. Theoretical Studies of the State Selected Reaction Ar ⁺ (2P _{3/2} , 2P _{1/2}) + H ₂ (D ₂) → ArH ⁺ (ArD ⁺) + H (D)	92
3. Direct Observation of Enhanced Charge-Transfer Cross Section at Near-Resonance: H ₂ ⁺ (ν) + Ar → Ar ⁺ + H ₂	93

4. Calculation of Ion Trajectory and Potential Mapping for TEPSICO Ion Optics	93
G. Photoionization Processes in Small Molecules	95
H. Studies of Formation and Destruction Mechanisms of Interstellar Molecules	95
I. Spectroscopy and Chemical Dynamics Using Supersonic Nozzle Beams	95
1. Construction of a Molecular Beams Apparatus for Spectroscopic and Dynamical Studies	96
J. Several Topics in HeI Photoelectron Spectroscopy	96
1. Systematic Assignments of HeI Photoelectron Spectra of 100 Fundamental Organic Compounds	96
2. Cyclic Peroxides: Dihedral Angle around the Peroxide Bond by Microwave and Photoelectron Spectroscopic Studies	97
3. Automatic Data-Processing System for Photoelectron Intensity Measurements	98
K. Studies of Molecular Complexes and Clusters by HeI Photoelectron Spectroscopy	98
1. Photoelectron Spectroscopic Study of EDA Complex of (CH ₃) ₂ O with BF ₃ in the Gas Phase	99
2. Construction of a New Photoelectron Spectrometer for Studying Molecular Complexes and Clusters in the Gas Phase	99
L. Photoelectron-Mass Spectroscopy of Multiphoton Ionization	100
1. Construction of an Apparatus for Studying Multiphoton Ionization Electron and Mass Spectroscopy	100
M. Production, Characterization and Spectroscopic Studies of Molecular Complexes and Clusters	101
1. Construction of an Apparatus for Molecular Beam Chemistry	102
RESEARCH ACTIVITIES V APPLIED MOLECULAR SCIENCE	103
A. Nature and Its Chemical Consequences of Interaction Between Benzene Rings in Bridged Aromatic Compounds	103
1. Formation of <i>o</i> -(9-Fluorenyl)phenylnitrene in the Photoisomerization of 1-Azatriptycene	103
2. Contrasting Photochemical Bridging Regioselectivity in Bridgehead-Substituted 9,10-Etheno- vs. 9,10-(<i>o</i> -Benzeno)-9,10-dihydroanthracenes	104
3. Synthesis of 2,7-Bis(dimethylamino)pyrene and the Electrical Conductivity of Its CT Complex with TCNQ	105
4. Radical Anions of 9,10-Dihydro-9,10[1',2']-benzenoanthracene-1,4,5,8-tetraone	106
5. Syntheses, Structures, and Redox Reactions of 5,18;7,16;9,14-Tris(<i>o</i> -benzeno)heptacene-1,4,6,8,10,13,15,17-octaones	106
B. Stereochemical Consequences of the Non-Bonded Interaction in Overcrowded Molecules	107
1. Unconventional Synthesis and Conformational Flexibility of Bis(1-triptycyl) Ether	107
2. Rotational Barriers in Bisadducts of 1-Cyano-1-methylethyl Radicals with Nitrones and Nitroso Compounds	108
3. Out-of-Plane Deformation of a Benzene Ring Incorporated in Cyclophanes	109
C. Structural Studies by Means of NMR of Other Nuclei	110
1. ¹⁷ O NMR Chemical Shifts of Tungsten Carbonyl Carbene Complexes. An Independent Experimental Measure for the Moss Reactivity Parameter m_{CXY} of Carbene :CXY	110
2. The Anomeric Effect in 2-Alkoxytetrahydropyrans as Revealed by the ¹⁷ O NMR Chemical Shifts	111
D. Spin-state Variations among Nickel(II) Complexes Containing Macrocyclic Ligands	112
1. The Role played by Water in Spin-state Variations among Nickel(II) Halide Complexes Containing 7 <i>R</i> (<i>S</i>),14 <i>S</i> (<i>R</i>)-5,5,7,12,12,14-Hexamethyl-1,4,8,11-tetra-tetraazacyclotetradecane	112

2. Dehydration Associated with High-spin to Low-spin Conversion of 5,5,7,12,12,14-Hexamethyl-1,4,8,11-tetraazacyclotetradecanenickel(II) Halide Dihydrate	113
3. Spin-state Equilibria of the Nickel (II) Complexes of 2,12-Dimethyl-3,7,11,17-tetraazabicyclo[11.3.1]-heptadeca-1(17),2,11,13,15-pentaene Analogs in Water	113
E. Structure Determination of New or Chemically Interesting Coordination Compounds by X-ray Diffractometry	113
1. Crystal and Molecular Structure of a Silver (II)Complex with a Macrocyclic Ligand	113
2. Optical Resolution of 7 <i>R</i> (<i>S</i>),14 <i>R</i> (<i>S</i>)-5,5,7,12,12,14-Hexamethyl-1,4,8,11-tetraazacyclotetradecanenickel(II) Ion and the Absolute Configuration of the (+) ₅₈₉ -Isomer	114
3. The Crystal and Molecular Structure of meso-1,4,7,10,13,16-Hexaazacyclooctadecanecobalt(III) Chloride	114
4. The Crystal and Molecular Structure of <i>Trans</i> -Dichloro-bis-(+)- <i>S,S</i> -trans-1,2-diaminocyclopentane)cobalt(III) Chloride Hydrogen Chloride Dihydrate, <i>trans</i> -[CoCl ₂ (+cptn) ₂]Cl·HCl·2H ₂ O	115
F. Preparation and Stereochemistry of Metal Complexes Containing Amino-phosphine Chelate Ligands	115
1. Preparation and Circular Dichroism of Dichloro-(<i>S</i>)-2-(butylphenylphosphinomethyl)pyrrolidine-palladium(II) ([PdCl ₂ L]) and Its Related Complexes, and the Absolute Configuration of [PdCl ₂ L] Determined by X-Ray Analysis	115
2. Preparation and Resolution of the <i>fac</i> -Tris(2-aminoethyldimethylphosphine)-cobalt(III) Complex and the Absolute Configuration of Its (+) ₅₈₉ -Isomer Determined by X-Ray Analysis	116
3. Optical Resolution of 2-Aminoethylbutylphenylphosphine and the Absolute Configuration Assigned on the Basis of Circular Dichroism Spectra of Its Palladium (II) Complexes	116
G. Chiral Recognition in Catalytic Hydrogenation of α-Acylaminoacrylic Acids by Cationic Rhodium(I) Complexes of Chiral Aminophosphines Derived from (<i>R,R</i>)-1,2-Cyclohexanediamine or (<i>R</i>)-1,2-Propanediamine	116
RESEARCH ACTIVITIES VI	118
COMPUTER CENTER	118
A. Theoretical Investigations of Metalloporphyrins and Charge-Transfer Complexes by the Ab Initio SCF MO Method	118
1. Potential Energy Surfaces for Out-of-Plane Movement of Fe Ion in Fe-Porphine	118
2. Theoretical Analysis of Mössbauer Spectra of Fe-Porphines	118
3. Ab Initio MO Study of Charge Transfer Complexes, Benzene + TCNE and Naphthalene + TCNE	119
4. Ab Initio SCF Calculation of Chlorophyll	120
B. Implementation of On-Line QCLDB System	121
LOW TEMPERATURE CENTER	121
C. A Cryostat for AC Magnetic Susceptibility Measurements	121
D. The Solid State Properties of Triphenylene-Potassium Complexes in Hydrogen Atmosphere	122
E. X-Ray Study of Partially Oxidized Derivative of Magunus Green Salt	123
CHEMICAL MATERIALS CENTER	124
F. Synthesis of a New Atropisomeric Diphosphine Ligand and its Use in Rh(I)-Catalyzed Asymmetric Hydrogenation of α-Acylaminoacrylic Acids	124
G. Selective 1,4-Addition of diethylaluminum Benzenethiolate to Vinyloxiranes. Stereoselective Synthesis of Allylic Alcolols	125
H. Organometallic Synthesis by Use of Transition Metal Vapors	126

DEVELOPMENT WORKSHOP	126
I. Design Study of UVSOR (Ultraviolet Synchrotron Orbital Radiation) Light Source	126
J. Designing of a High-Speed Image Processor and its Use for Picosecond Time-Resolved Spectroscopy	127
RESEARCH FACILITIES	129
Computer Center	129
Low Temperature Center	130
Chemical Materials Center	131
Instrument Center	131
Development Workshop	133
LARGE SCALE RESEARCH EQUIPMENTS	135
1. Picosecond Continuously Tunable Laser from UV to IR	135
2. High Resolution spectroscopy	135
3. High Resolution Spectroscopic System in the Far-Infrared Region	136
4. Ultraviolet Synchrotron Orbital Radiation (UVSOR) Facility— Experiment Systems	136
SPECIAL RESEARCH PROJECTS	138
OKAZAKI CONFERENCES	142
JOINT STUDIES PROGRAMS	144
1. Joint Studies	144
2. Research Symposia	145
3. Cooperative Researches	146
4. Use of Facilities	146
SATELLITE MEETINGS FOR THE INTERNATIONAL CONFERENCES	147
FOREIGN SCHOLARS	148
LIST OF PUBLICATIONS	151

ORGANIZATION AND STAFF

Organization

The Institute for Molecular Science, upon completion, will comprise 15 research laboratories —each staffed by a professor, an associate professor, two research associates and a few technical associates— and five research facilities. The laboratories are grouped into five divisions as follows:

Division of Theoretical Studies	Theoretical Studies I Theoretical Studies II ²⁾ Theoretical Studies III ¹⁾
Division of Molecular Structure	Molecular Structure I Molecular Structure II ²⁾ Molecular Dynamics
Division of Electronic Structure	Excited State Chemistry Excited State Dynamics Electronic Structure ²⁾
Division of Molecular Assemblies	Solid State Chemistry Photochemistry Molecular Assemblies Dynamics ¹⁾ Molecular Assemblies ²⁾
Division of Applied Molecular Science	Applied Molecular Science I Applied Molecular Science II ²⁾
Five Research Facilities are:	Computer Center Instrument Center Low-Temperature Center Chemical Materials Center Development Workshop

1) To be established.

2) Professors and associate professors are adjunct professors from universities.

Scientific Staff

Hideo AKAMATU	Professor, Director-General
<i>Division of Theoretical Studies</i>	
<i>Theoretical Studies I</i>	
Keiji MOROKUMA	Professor
Masaru TSUKADA	Associate Professor
Shigeki KATO	Research Associate
Chikatoshi SATOKO	Research Associate
Shigeru OBARA	Technical Associate
Iwao OHMINE	Research Fellow (—March 80)
Toshiharu HOSHINO	Research Fellow (April 80—)
Masami KUSUNOKI	Visiting Scholar from Meiji Univ. (—March 80)
Keiichi YANO	Graduate Student from Waseda Univ.* (—September 79)
Mitsuyasu HANAMURA	Graduate Student from Tohoku Univ.* (April 79—)

Theoretical Studies II

Teijiro YONEZAWA
Suehiro IWATA

Kazuo KITAURA

Adjunct Professor from Kyoto Univ. (April 79—)
Adjunct Associate Professor from the Inst. for Phys.
Chem. Res. (April 79—)
Research Associate

Division of Molecular Structure

Molecular Structure I

Eizi HIROTA
Shuji SAITO
Chikashi YAMADA
Yasuki ENDO
Kentarou KAWAGUCHI
Tetsuo SUZUKI
Masao KAKIMOTO
Keiichi NAGAI
Susumu SOFUE

Professor
Associate Professor
Research Associate
Research Associate
Technical Associate
Technical Associate
Research Fellow (—September 79)
Research Fellow
Graduate Student from Tokyo Metropolitan Univ.*
(October 79—)

Molecular Structure II

Masamichi TSUBOI

Michio TAKAMI

Tamotsu KONDOW

Adjunct Professor from the Univ. of Tokyo
(April 79—)
Adjunct Associate Professor from the Inst. for Phys.
Chem. Res. (—March 80)
Adjunct Associate Professor from the Univ. of Tokyo
(April 80—)

Molecular Dynamics

Tsunetake FUJIYAMA
Yasuo UDAGAWA
Tadashi KATO
Nobuyuki ITO

Shiaki HYODO

Fumisato IIDA

Professor
Associate Professor
Research Associate
Graduate Student from Tokyo Metropolitan Univ.*
(October 79—)
Graduate Student from Tokyo Metropolitan Univ.*
(October 79—)
Graduate Student from Tokyo Metropolitan Univ.*
(April 80—)

Division of Electronic Structure

Excited State Chemistry

Keitaro YOSHIHARA
Tadayoshi SAKATA
Nobuaki NAKASHIMA
Tomoji KAWAI
Minoru SUMITANI
Kazuhito HASHIMOTO
Keiji KAMOGAWA
Katsumi TANIMURA

Professor
Associate Professor
Research Associate
Research Associate
Technical Associate (Unit Chief)
Technical Associate
Research Fellow
Visiting Scientist

Excited State Dynamics

Ichiro HANAZAKI
Nobuyuki NISHI
Iwao NISHIYAMA
Hisanori SHINOHARA
Ryoichi NAKAGAKI
Susumu KUWABARA
Masayuki UMEMOTO

Professor
Associate Professor
Research Associate
Research Associate
IMS Fellow (May 80—)
Graduate Student from Osaka Univ.* (April 79—)
Graduate Student from Kyushu Univ.* (April 80—)

Electronic Structure

Mitsuo ITO
Hiroshi TSUBOMURA
Masahiro MATSUOKA

Adjunct Professor from Tohoku Univ. (—March 80)
Adjunct Professor from Osaka Univ. (April 80—)
Adjunct Associate Professor from Kyoto Univ.
(June 78—)

Division of Molecular Assemblies

Solid State Chemistry

Hiroo Inokuchi
Inosuke KOYANO
Kenichiro TANAKA
Kazuhiko SEKI
Naoki SATO
Tatsuhisa KATO
Kenji ICHIMURA
Kazumichi NAKAGAWA
Masako YUDASAKA

Professor
Associate Professor
Research Associate
Research Associate
Technical Associate
Technical Associate
IMS Fellow (May 80—)
Research Fellow (—March 80)
Graduate Student from Tokyo Metropolitan Univ.*
(April 80—)

Photochemistry

Katsumi KIMURA
Kosuke SHOBATAKE
Yohji ACHIBA
Kiyohiko TABAYASHI
Kenji SATO
Shinji TOMODA
Noriyoshi KAKUTA

Professor
Associate Professor
Research Associate
Research Associate
Technical Associate
Research Fellow (April 80—)
Graduate Student from Hokkaido Univ.*
(—March 80)

Molecular Assemblies

Yuji MORI

Mizuka SANO

Katsuhide YOSHIDA

Gunzi SAITO

Adjunct Professor from Tokyo Inst. of Tech.
(April 79—)
Adjunct Associate Professor from Univ. of Electro-Communications (—March 80)
Adjunct Associate Professor from Univ. of Tokyo
(April 80—)
Research Associate

Division of Applied Molecular Science

Applied Molecular Science I

Hiizu IWAMURA
Tasuku ITO
Tadashi SUGAWARA
Koshiro TORIUMI
Yuzo KAWADA
Yoshinori NISHIZAWA
Morimatsu KATOH

Takahiko OOSUMI
Kazumasa KOBAYASHI

Fumio UENO

Professor
Associate Professor
Research Associate
Research Associate
Technical Associate
Research Fellow
Graduate Student from Nagoya Inst. of Tech.*
(—March 80)
Graduate Student from Ehime Univ.* (—March 80)
Graduate Student from Yamaguchi Univ.*
(April 80—)
Graduate Student from Tohoku Univ.* (April 80—)

Applied Molecular Science II

Junnosuke FUJITA
Teruyoshi SAKATA

Adjunct Professor from Nagoya Univ. (April 79—)
Adjunct Associate Professor from Osaka Univ.
(—March 80)

Nobuyuki HARADA

Adjunct Associate Professor from Tohoku Univ.
(April 80—)

Research Facilities

Computer Center

Hiroshi KASHIWAGI
Shigeyoshi YAMAMOTO
Unpei NAGASHIMA

Associate Professor
Technical Associate
Graduate Student from Hokkaido Univ.* (April 80—)

Instrument Center

Keisaku KIMURA
Toshiro MURAO

Research Associate
Technical Associate

Low-Temperature Center

Toshiaki ENOKI

Research Associate

Chemical Materials Center

Hidemasa TAKAYA
Akira MIYASHITA
Arata YASUDA

Associate Professor
Research Associate
Technical Associate

Development Workshop

Makoto WATANABE
Yoshihiro TAKAGI

Associate Professor
Research Associate

Technical Staff

Akira UCHIDA	Technical Head
Kusuo SAKAI	Technical Section Chief
Satoshi INA	Computer Center
Fumio NISHIMOTO	Computer Center
Kenichi IMAEDA	Low-Temperature Center
Kazuo HAYAKAWA	Electronic Shop
Hisashi YOSHIDA	Electronic Shop
Masaaki NAGATA	Glassblowing Shop
Toshio HORIGOME	Machine Shop
Nobuo MIZUTANI	Machine Shop
Norio OKADA	Machine Shop
Mitsukazu SUZUI	Machine Shop

Foreign Visiting Staff

C. Bradley Moore	Univ. of California, Berkeley, USA	May 14, 1979—Aug. 13, 1979
Jean Durup	Univ. de Paris-Sud, Orsay, France	Aug. 25, 1979—Dec. 24, 1979
Anton Rieker	Univ. Tübingen, Germany	Sept. 1, 1979—Nov. 30, 1979
Robert G. Parr	Univ. of North Carolina, USA	Oct. 1, 1979—Nov. 25, 1979
Naba K. Ray	Delhi Univ. India	Oct. 1, 1979—Nov. 22, 1979

David Fox	State Univ. of New York, Stony Brook, USA	Dec. 28, 1979—Mar. 31, 1980
Jon T. Hougen	NBS, Washington, D.C., USA	Feb. 4, 1980—April 26, 1980
Richard L. Jaffe	NASA, Ames Research Center USA	Feb. 18, 1980—April 26, 1980
Imre G. Csizmadia	Univ. of Toronto, Toronto, CANADA	April 7, 1980—April 26, 1980
Ronald D. McKelvey	Univ. of Wisconsin, La-Crosse, USA	May 19, 1980—Aug. 18, 1980

*The cooperative education programs of IMS with graduate schools.

COUNCIL

Hideo AKAMATU, Director-General

Councillors

<i>Chairman</i>	Masao KOTANI	President, The Science University of Tokyo
<i>Vice-Chairman</i>	Saburo NAGAKURA	Professor, The University of Tokyo
	Melvin CALVIN	Professor, University of California, U.S.A.
	Kenichi FUKUI	Professor, Kyoto University
	Sir George PORTER	Director, The Royal Institution, U.K.
	Kodi HUSIMI	President, Japan Science Council
	Naotaka ISHIZUKA	President, Nagoya University
	Keiya KANDA	President, Kyushu University
	Yonezo MORINO	Professor Emeritus, The University of Tokyo
	Sogo OKAMURA	Director, Japan Society for the Promotion of Science
	Kazuo SAITO	Professor, Tohoku University
	Shoji SHIBATA	Professor Emeritus, The University of Tokyo
	Yataro TAJIMA	Director-General, National Institute of Genetics
	Yasutada UEMURA	Professor, The University of Tokyo
	Tadao UMESAO	Director-General, National Museum of Ethnology
	Itaru WATANABE	Professor, Keio University
	Yasuhide YUKAWA	President, Osaka Women's University

The Council is the advisory board for the Director-General. Two of the counsellors are selected among distinguished foreign scientists.

Administration Bureau

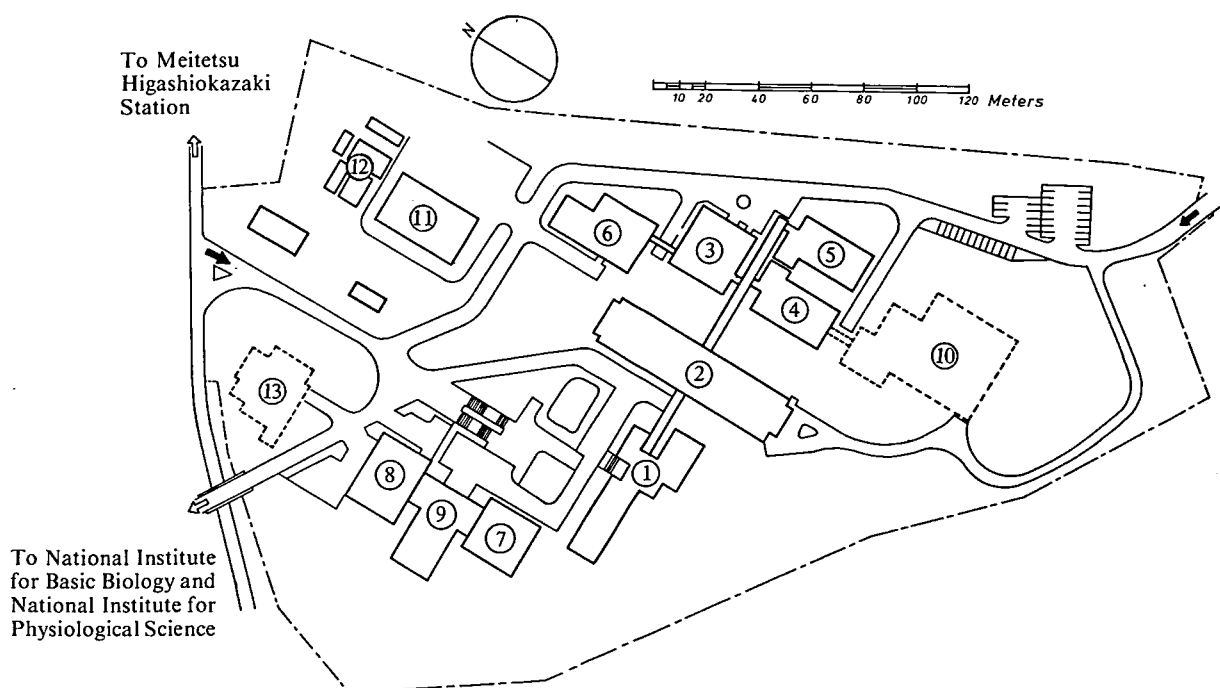
Hiroaki MIZUMURA	Director-General Administration Bureau
Minoru SHIMIZU	Director, General Affairs Department
Hiroshi HIGURASHI	Director, Budgeting and Accounting Department

BUILDINGS AND CAMPUS

The IMS campus covering 62,561 m² is located on a low hill in the middle of Okazaki City. The inequality in the surface of the hill and growing trees are preserved as much as possible, and low-storied buildings are adopted for conservation of the environment. The buildings of IMS are separated according to their functions as shown in the map. The Research Office Building and all Research Facilities except for the Computer Center are linked organically to the Main Laboratory Building by corridors. Computer Center, Library, and Administration Buildings are situated between IMS and the neighboring National Institute for Basic Biology and National Institute for Physiological Sciences, because the latter two facilities are common to these three institutes.

The lodging facility of IMS called Yamate Lodge, located within 10 min. walk, has sleeping accommodations for 20 guests. Scientists who visit IMS can make use of this facility. Foreign visiting scientists can also live at this lodge with their families during their stay.

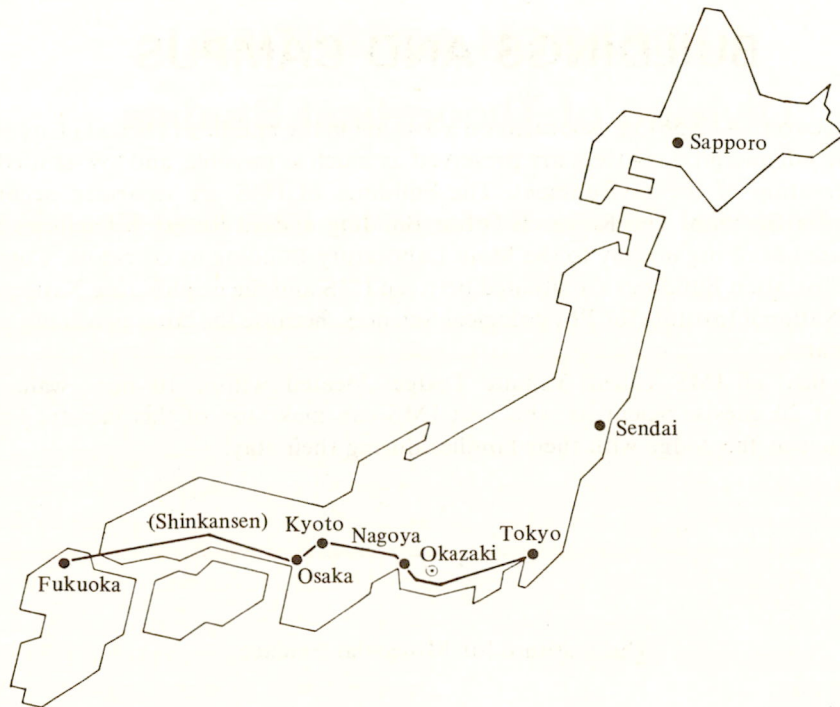
The Institute for Molecular Science



- | | |
|------------------------------|--|
| 1. Research Office Building | 8. Library |
| 2. Main Laboratory Building | 9. Central Administration |
| 3. Development Workshop | 10. Special Experiment Building† |
| 4. Instrument Center | 11. Power Station |
| 5. Chemical Materials Center | 12. Waste-Water Disposition Facilities |
| 6. Low-Temperature Center | 13. Faculty Club†† |
| 7. Computer Center | |

† In the planning stage

†† Under construction



Okazaki (population 250,000) is 260 km southwest of Tokyo, and can be reached by train in about 3 hours from Tokyo via New Tokaido Line (Shinkansen) and Meitetsu Line.
The nearest large city is Nagoya, about 40 km west of Okazaki.



IMS, 1980

RESEARCH ACTIVITIES I

Division of Theoretical Studies

I—A Potential Energy Surfaces for Chemical Reactions

In the molecular quantum chemistry group, the determination and characterization of potential energy surfaces for chemical reactions remained to be one of the most important areas of studies. The first two projects (A-1 and A-2) are concerned with potential energy surfaces for $C^+ + H_2 \rightarrow CH^+ + H$ reactions, which have recently been experimentally studied by Prof. Kusunoki, one of the collaborators in our calculation.

The other projects, intended to determine potential energy surfaces for specific reactions of timely interest, use heavily the method of energy gradient. The power of the method is being recognized by many groups in the world, and the extension of the method to cover MCSCF and CI wave functions has been established. Our group not only uses it to determine the equilibrium geometry, the transition state geometry and vibrational frequencies, but also tries to characterize the potential energy characteristics by the aid of the energy gradient. It is our feeling that in the near future energy gradient method will be an essential tool in quantum chemistry.

I-A-1 Ab Initio Calculations of the $a^3\Pi - b^3\Sigma^-$ Transition of CH^+

Isao KUSUNOKI (*Tohoku Univ.*), Shogo SAKAI (*Kansai Univ.*), Shigeki KATO and Keiji MOROKUMA

[*J. Chem. Phys.*, **72**, 6813 (1980)]

Emission band spectra of the CH^+ ($b^3\Sigma^- \rightarrow a^3\Pi$) transition have recently been observed in studies of chemiluminescent ion-molecule reactions of $C^+ + H_2$. A set of vibrational constants of these states have been determined from the spectra.¹⁾ In order to confirm the spectroscopic assignments we have carried out an ab initio calculation of the potential energy curves, spectroscopic constants and transition moment for $a^3\Pi$ and $b^3\Sigma^-$, using the configuration interaction (CI) method. The spectroscopic constants calculated from the ab initio potential curves are compared with experimental values in Table I. The agreement between theoretical and experimental values is

Table. I Theoretical and Experimental (in parentheses) Spectroscopic Constants for the $a^3\Pi$ and $b^3\Sigma^-$ States on CH^+ .^a

	T_e (cm ⁻¹)	ω_e (cm ⁻¹)	$\omega_e x_e$ (cm ⁻¹)	r_e (Å)
$b^3\Sigma^-$	29750 (28872)	2103 (2040)	55 (50)	1.237 (1.245)
$a^3\Pi$	0	2764 (2631)	85 (64)	1.130 (1.136)

^a In parentheses are experimental values, taken from Ref. 1, except for r_e which are obtained by RKR calculations.

good. The calculated electronic transition moment decreases with an increasing internuclear distance R . The Franck-Condon factors, r centroid, and oscillator strengths for each band have also been calculated.

Reference

- 1) I. Kusunoki and Ch. Ottinger, *J. Chem. Phys.* (in press).

I-A-2 Potential Energy Surfaces of the Reaction $C^+ + H_2 \rightarrow CH^+ + H$

Shogo SAKAI (*Kansai Univ.*), Shigeki KATO, Isao KUSUNOKI (*Tohoku Univ.*) and Keiji MOROKUMA

The $C^+ + H_2$ reaction is a prototype ion-molecular reaction which has received much attention from experimental and theoretical points of view. Kusunoki and Ottinger¹⁾ have recently observed the chemiluminescence from CH^+ ($A^1\Pi$) produced by the reaction $C^+(^2P) + H_2 \rightarrow CH^+(A^1\Pi) + H$ and determined the product rotational-vibrational population distributions. Interpretation of this reaction requires a knowledge of potential energy surfaces beyond the previous calculations.²⁾ We have performed ab initio MO calculations of potential surfaces for several low-lying electronic states of CH_2^+ . The polarization CI method was used, where the primary orbital set was determined by a 7-configuration MCSCF calculation with the 6-31G** basis set. We have first considered the $C_{\infty v}$ and C_{2v} symmetries of the nuclear configuration and found that there is no

feasible reaction path leading to the desired high energy reaction product CH^+ ($A^1\Pi$) within these symmetries. In the $C_{\infty v}$ symmetry, the energy difference between the second and the third potential surface is too large to cause the non-adiabatic transition between them. The region of avoided crossing was next determined in the C_s nuclear framework. A profile of $^2A'$ (in C_s symmetry) surfaces is shown in Figure 1. The avoided crossing between the second and the third surface is seen at the CCH angle of about 95° . The results are consistent with the experimental observation of high product rotational energy.

Reference

- 1) I. Kusunoki and Ch. Ottinger, *J. Chem. Phys.*, **71**, 4227 (1979).
- 2) D. H. Liskow, C. F. Bender and H. F. Schaefer, *J. Chem. Phys.*, **61**, 2507 (1974); P. K. Pearson and E. Roueff, *J. Chem. Phys.*, **64**, 1240 (1976).

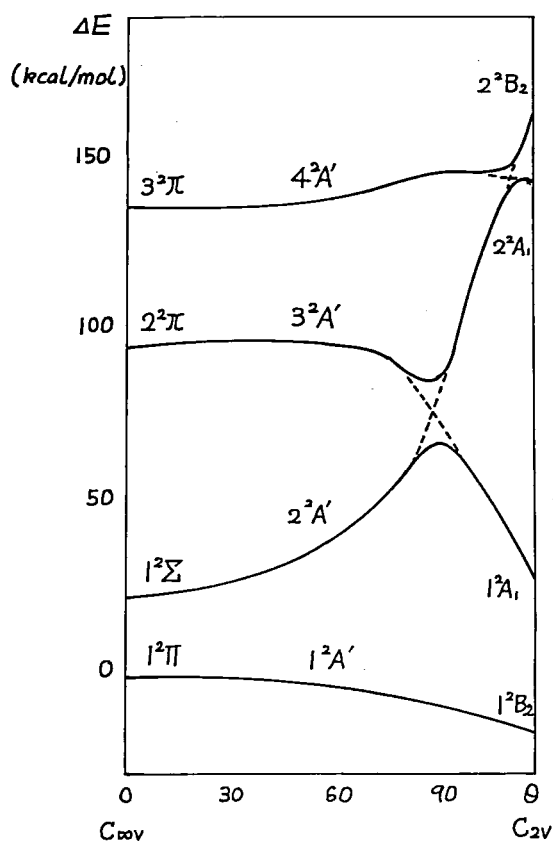


Figure 1.

I-A-3 Reaction Coordinate Properties of $\text{HFCO} \rightarrow \text{HF} + \text{CO}$ Reaction

Shigeki KATO and Keiji MOROKUMA

Theoretical characterization of the potential

energy surface for chemical reactions provides information essential to better understanding of the reaction mechanism. In our previous studies we have attempted to interpret the energy partitioning in reaction products in terms of the transition state structure and the reaction coordinate.^{1,2)} It has been shown that the curvature property of the reaction coordinate and the change of vibrational force constants along the reaction coordinate are critical factors determining the dynamic properties of chemical reactions.²⁾ In the present work, we have performed ab initio MO calculations for the intrinsic reaction coordinate (IRC) of $\text{HFCO} \rightarrow \text{HF} + \text{CO}$ reaction. The Hartree-Fock energy gradient method with the 4-31G basis set was employed. The force constant along the IRC was calculated by the numerical differentiation of analytically evaluated gradient.

In Figure 1 changes in geometric parameters along the IRC are shown. The 'normal coordinate' vibrational frequencies as functions of the reaction coordinate and the projection of the curvature of IRC to these normal coordinates are given in Figure 2 and 3, respectively. We can make the following observations. (1) At the initial stage of reaction, the reaction coordinate is mainly composed of the OCF bending and CF stretching modes and the H atom moves rapidly as the reaction proceeds. (2) The change in frequency of the highest frequency mode is large, reflecting the change in the main component of this mode from the CH stretching to the HF stretching. (3) The curvature of IRC is large before and after, not at the transition state. The reaction coordinate at the transition state is well separated from the other modes.

References

- 1) S. Kato and K. Morokuma, *J. Chem. Phys.*, **72**, 206 (1980).
- 2) S. Kato and K. Morokuma, *J. Chem. Phys.*, **73**, 3900 (1980).

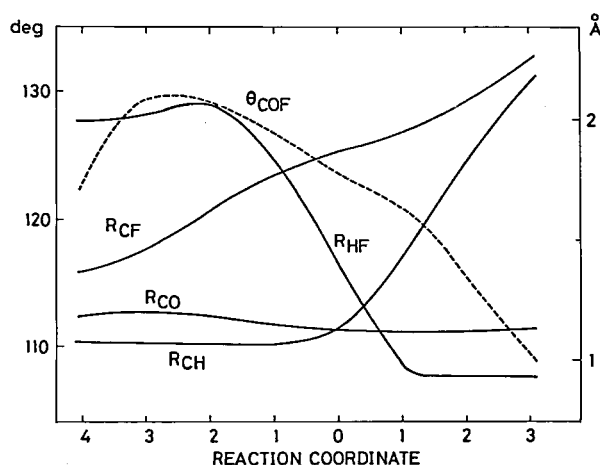


Figure 1.

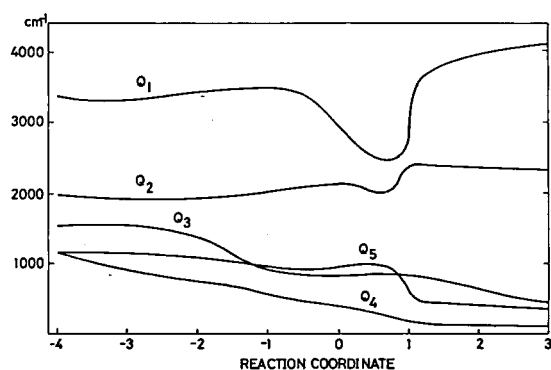


Figure 2.

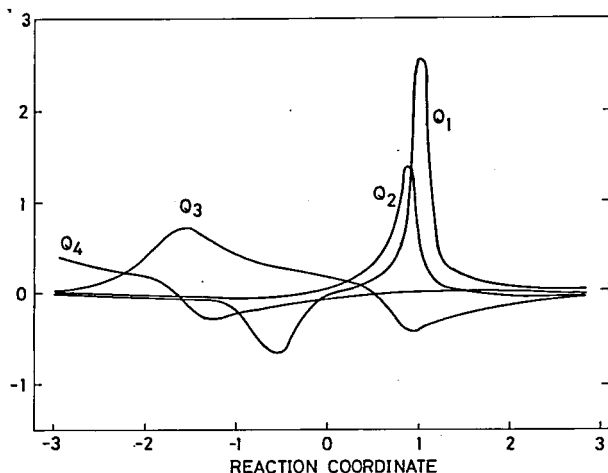


Figure 3.

I-A-4 The Reaction Mechanism of Hydroboration. An Ab Initio MO Study on the $C_2H_4 + BH_3$ Reaction

Shigeru NAGASE, N. K. RAY (*IMS and Univ. of Delhi*) and Keiji MOROKUMA

[*J. Am. Chem. Soc.* **102**, 4536 (1980)]

Despite its great synthetic usefulness and applicability, the detailed mechanism of the hydroboration reaction has been a matter of a considerable dispute. In order to resolve the reaction mechanism, we have searched carefully for the stationary points on the potential energy surface of the title reaction with the ab initio SCF energy gradient method.

Upon going from the reactant, $C_2H_4 + BH_3$, to the final product, ethylborane, with a C_s symmetry constraint, we found two stationary points, an intermediate π complex and a transition state (saddle point), as shown in Figure 1. The energy profile at the SCF level is given in Figure 2. The calculated SCF overall barriers were further refined with CI calculations. The results are summarized in Table I.

Table I. Overall Barrier Height (ΔE) for the $C_2H_4 + BH_3$ Reaction.

Method ^a	ΔE (kcal/mol)
4-31G	11.7
4-31G + CI (S + D)	9.7
6-31G**	6.7
4-31G + CI (S + D + Q)	5.6
Exp.	2 ± 3

^a S = single excitation, D = double excitation, and Q = quadruple excitation correction.

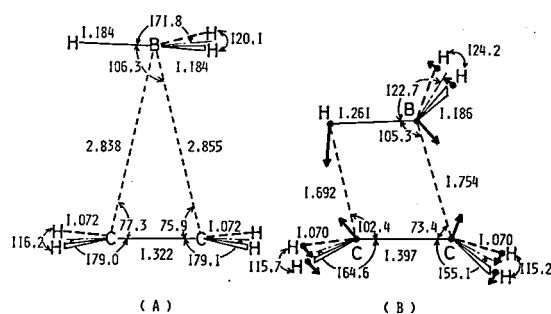


Figure 1. Optimized geometries (in ångströms and degrees) for the intermediate π -complex (A) and the transition state (B) at the 4-31G SCF level. The arrows in (B) indicate the displacement vector of the reaction coordinate at the transition state.

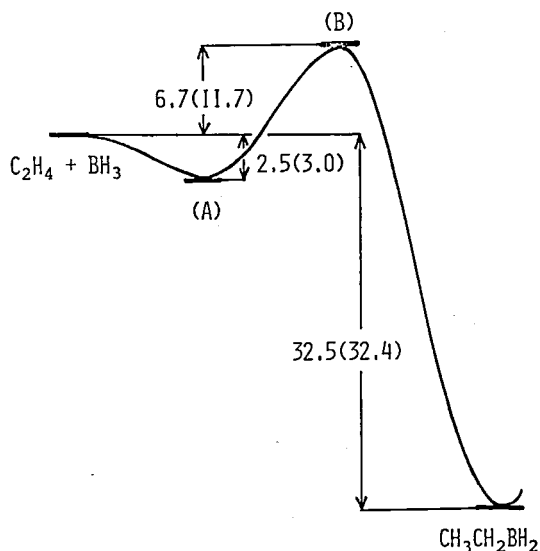


Figure 2. The energy profile (kcal/mol) for the reaction of C_2H_4 with BH_3 at the 4-31G (in parentheses) and 6-31G** SCF levels. Geometries used are optimized at the 4-31G SCF level. (A) and (B) are the π -complex and the transition state, respectively.

It is concluded that the hydroboration reaction proceeds through a two-step process. First, a loose three-center π complex is formed in the early stage without an energy barrier, and then it is transformed to the product via a four-center transition state, this process being the rate-determining step. The overall mechanism proposed here is significantly different from any previous study, though it in part supports some of previous findings.

I-A-5 Photoisomerization Processes of Polyenes in Singlet Mechanism: Potential Surfaces

Iwao OHMINE and Keiji MOROKUMA

The singlet state potential energy surfaces for the C-C torsional isomerization are determined by employing the GVB-CI method. The two configurations, the ground state and $\pi^2 \rightarrow \pi^{*2}$, are included in the GVB procedure. The full π -CI calculation is performed on the GVB orbitals. The results of butadiene potential surfaces are shown in Figure 1 for the single torsion around the C₁-C₂ bond and in Figure 2 for the double torsion around the C₁-C₂ and C₃-C₄ bonds. We partially include the geometrical relaxation effects by allowing the C-C bond length changes along the isomerization.¹⁾ At the equilibrium of the planar geometry the 1A_g state has a long bonded nature^{2, 3)} and the C-C bond alternation of this state is completely different from the ground state case. The noncovalent 1B_u state, optically allowed from the ground state, has the less bond alternation. Thus even if the 1A_g state exists above the 1B_u state for the vertical transition from the ground state, their energy ordering might be reversed when the geometrical relaxation (the relaxation energy) is taken into account. In the 4-31G basis set calculation, we found that the relaxation energy is about 1 eV for the 1A_g and is about 0.5 eV for the 1B_u state.

We can see in Figure 1 that the energies of the noncovalent 1B_u and 1A_g states decrease along the C₁-C₂ torsion, while the energy of the covalent 1A_g state stays rather constant. Two non-covalent states 1B_u and 1A_g become near degenerate at the 90° C₁-C₂ twisted region, resulting in so-called sudden polarized states Z₁ and Z₂.⁴⁾ In butadiene, the Z₂ state with the anionic methylene and cationic allyl group is lower in energy than the Z₁ with the cationic methylene and anionic allyl group.

We can see in Figure 2 that a simultaneous double torsion around two C-C bonds might be feasible on the potential surface of the covalent 1A_g

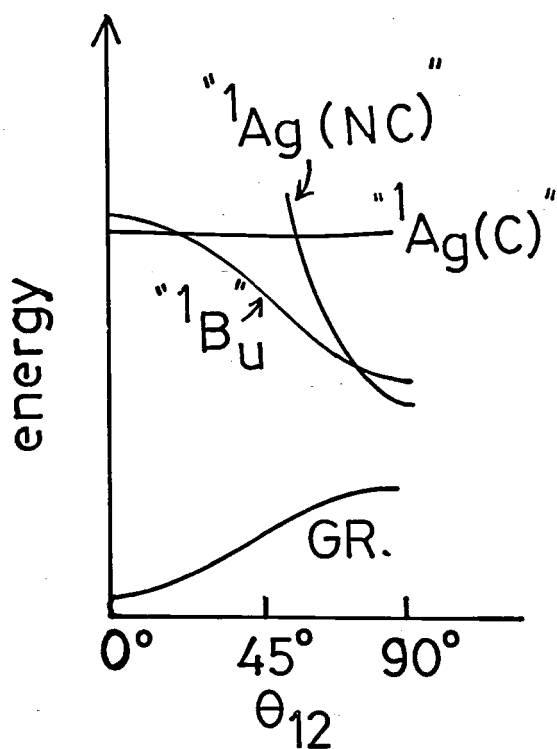


Figure 1. Energy profile for the C₁-C₂ torsion.

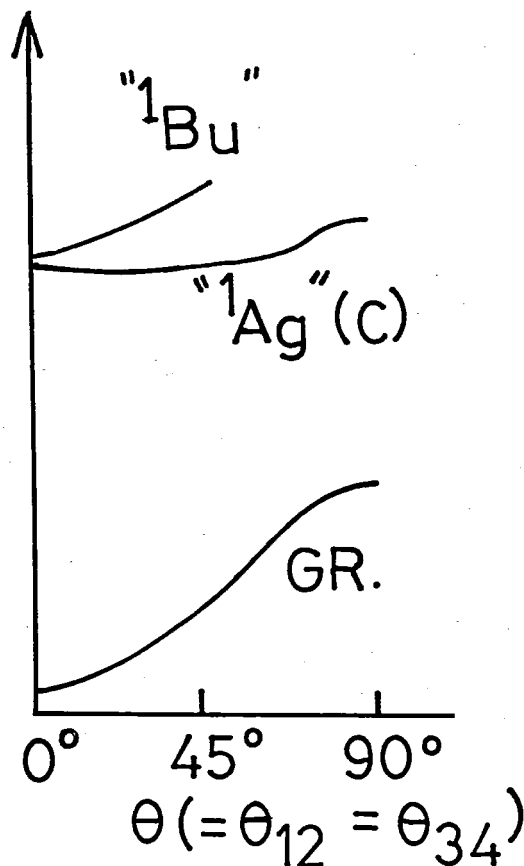


Figure 2. Energy profile for C-C double torsion.

state but not on the 1B_u state surface. In the localized orbital description, the 1A_g state consists mainly of two triplet excitations at the two ethylenic units, which couple to form a singlet state.^{2,3)} The double torsion around two C-C bonds of these ethylenic units can be favorable, as the ethylenic triplet state has the equilibrium at the C-C twisted geometry.

References

- 1) I. Ohmine and K. Morokuma, *J. Chem. Phys.* **73**, 1907 (1980).
- 2) K. Schulten, I. Ohmine and M. Karplus, *J. Chem. Phys.* **64**, 4422 (1976).
- 3) R. P. Hosteny, T. H. Dunning Jr., R. R. Gilman, A. Pipano and I. Shavitt, *J. Chem. Phys.* **62**, 4764 (1975).
- 4) L. Salem, *Acc. Chem Res.* **12**, 87 (1979).

I-A-6 Photoisomerization Processes of Polyenes in Single Mechanism: Radiationless Transition from Zwitterionic States

Iwao OHMINE and Keiji MOROKUMA

A considerable interest has recently been paid in sudden polarized states (zwitter ionic states) of polyenes.¹²⁾ Roles of these states in photoisomerization processes were discussed by Salem et al.¹⁾ and Warshel et al.²⁾ We here examine the mechanism of vibrational excitation associated with the radiationless transition from these states to the ground state. The geometries of the sudden polarized states for butadiene and PSB-butadiene are determined by using the restricted Hartree-Fock (RHF) procedure. The C_1 - C_2 90°-twisted conformation with C_s -symmetry is assumed in the optimization of geometrical variables. Figure 1 (A) and (B) present the butadiene equilibrium geometry for the zwitter ionic state (Z_1) corresponding to the cationic methylene and the anionic allyl group and that for the anionic methylene and cationic allyl (Z_2), respectively.¹⁾ We can see in the figure that there exists a significant pyramidalization of the twisted methylene group in Z_2 ($\phi \approx 64^\circ$) as expected from an analogy to the CH_3^- structure and almost none in Z_1 ($\phi \approx 5^\circ$) as expected from CH_3^+ . These two minima on the singlet excited state potential surface act as two distinct funnels in the radiationless transition process. Comparing the Z_1 and Z_2 geometries with the ground state geometry shown also in Figure 1, we expect that the deactivation process from Z_2 to the ground state induces a strong flapping motion of the twisted methylene group and that from Z_1 promotes mainly C-C stretching motion. For butadiene, the Z_2 is more stable than Z_1 (see Table I) and the deactivation pathway from Z_2 is expected to be

Table I Energies and Bond Lengths of the C_1 - C_2 90°-twisted Butadiene and PSB-Butadiene Singlet States.^a

State	Energy (Bond Lengths) ^b
Butadiene	
Ground state ^c	-154.6597 (1.471, 1.395, 1.378)
Z_1 - State ^d	-154.4952 (1.395, 1.422, 1.340)
Z_2 - State ^d	-154.5239 (1.432, 1.436, 1.332)
PSB-Butadiene	
Ground State ^c	-170.9959 (1.463, 1.408, 1.300)
Z_1 - State ^d	-170.9427 (1.429, 1.388, 1.339)
Z_2 - state ^d	-170.8114 (1.369, 1.515, 1.270)

^a Adiabatic mapping with the 4-31G basis set. C_s symmetry.

^b Energies are in hartree and bond lengths are in Å.

^c Singlet UHF solution.

^d RHF solutions. The Z_1 -state with a cationic methylene group ($H_1C_1H_1$)⁺ and the Z_2 -state with an anionic methylene group ($H_1C_1H_1$)⁻.

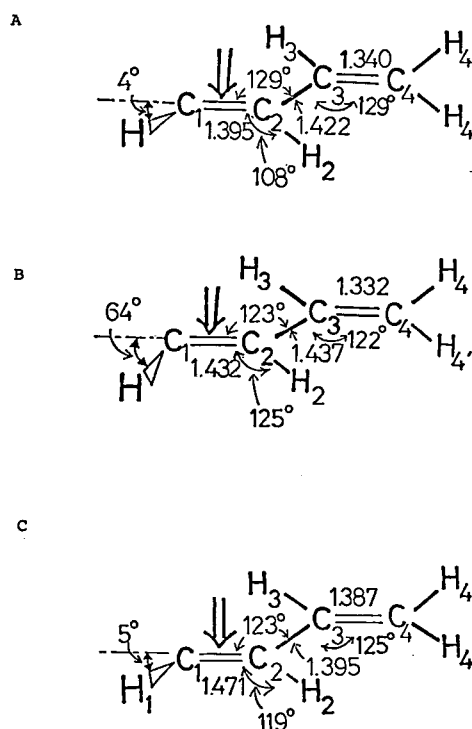


Figure 1. The optimized geometries of twisted butadiene. (A) the Z_1 -zwitter ionic state, (B) the Z_2 -zwitter ionic state (see Text) and (C) the transition state of the ground state.

An arrow indicates the twisted C-C bond. Bond lengths are in Å and bond angles are in degrees. See the footnote of Table I.

predominant and thus the methylene flapping motion will be enhanced. The energy difference between the Z_1 states with and without pyramidalization ($\phi \approx 64^\circ$ and 0°) is about 7 kcal/mole in the RHF approximation with the 4-31G basis. Inclusion of d orbitals (4-31G + d with the exponent 0.8 on C) increases this difference to 12 kcal/mole, while configuration interaction (CI) decreases it; for example, the full CI of valence π orbitals predicts the energy difference to be 4 kcal/mole in the 4-31G basis. Though an extensive CI with a large basis set is required for a more quantitative treatment of this pyramidalization,³⁾ the difference in geometry and hence in vibrational excitation between Z_1 and Z_2 should be given a serious consideration.

In PSB-butadiene, the Z_1 state is greatly stabilized by the coulomb attraction between the protonated nitrogen N^+ and the excess π -electron located at the C-C- N^+ segment. We can see in Table I that Z_1 is 82 kcal/mole more stable than Z_2 . The energy difference between the lowest singlet state (Z_2 for butadiene and Z_1 for PSB-Butadiene) and

the ground state at the respectively optimized twisted geometry decreases from 85 kcal/mole for butadiene (78 kcal/mole in the 4-31G + diffused orbitals with the exponent 0.05) to 33 kcal/mole for PSB-butadiene (32 kcal/mole). The Z_1 state has a small pyramidalization angle and a deactivation from the lowest singlet to the ground state in PSB-butadiene is expected to introduce significant stretching motions of the C-C bonds but not much flapping motion of the twisted methylene group, in clear contrast to the butadiene case.

References

- 1) (a) L. Salem, *Acc. Chem. Res.* **12**, 87 (1979); (b) L. Salem and P. Bruckmann, *Nature* (London), **258**, 526 (1975); (c) L. Salem, *Science*, **191**, 822 (1976); (d) P. Bruckmann and L. Salem, *J. Am. Chem. Soc.* **98**, 5037 (1976).
- 2) (a) A. Warshel, *Proc. Natl. Acad. Sci. U.S.A.* **75**, 2558 (1978); (b) R. Weiss and A. Warshel, *J. Am. Chem. Soc.* **101**, 6131 (1979).
- 3) (a) B. R. Brooks and H. F. Schaefer III, *J. Am. Chem. Soc.* **101**, 307 (1979); (b) W. V. Volland, E. R. Davidson and W. T. Borden, *J. Am. Chem. Soc.* **101**, 533 (1979); (c) V. Bonacic-Koutecký, R. J. Buenker and S. D. Peyerimhoff, *J. Am. Chem. Soc.* **101**, 5917 (1979).

I—B Problems in Molecular Structure and Molecular Intraction

In the 9th Okazaki Conference last February we learned a lot on reactive intermediates in organic chemistry. The discussion inspired our work on reactive intermediates involving silicon (B-1 and B-2). More work is in progress where we are determining transition states connecting various reactants and intermediates or reactions involving silicon compounds. The energy gradient method is fully utilized.

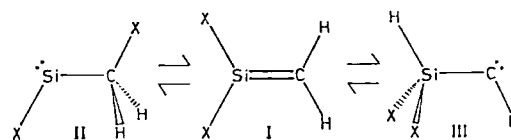
We continued to collaborate with the group of Prof. Tsuboi, who became Adjunct Professor in the Division of Molecular Structure. We feel that the MO method is providing a great service in understanding molecular vibrations. (B-5 and B-6)

I-B-1 An Ab Initio MO Study on the Stability and Nature of the Si-C Double Bond

Mitsuyasu HANAMURA,¹⁾ Shigeru NAGASE (Yokohama National Univ.) and Keiji MOROKUMA

In an attempt to clarify the stability and nature of the Si-C double bond, we have carried out ab initio MO calculations for $X_2Si = CH_2$ ($X = H, CH_3, F$). All calculations were carried out with split-valence 4-31G basis set by means of the closed-shell Hartree-Fock (RHF) and the generalized valence bond (GVB) method. Geometries were fully optimized by the use of the energy gradient. Energies were also calculated with the configuration interaction (CI) method including all the single and double excitations from the valence orbitals relative to the RHF reference configuration.

We first examine the thermodynamic stability of the following three isomers of $X_2Si = CH_2$ in the singlet state. The results for $X = Me$ are shown in Table I. Silylcarbene (III) is the most unstable. For



$X = Me$, silaethylene (I) is more stable than silylene (II) by 22 kcal/mol in our best calculations; we believe that 1,1-dimethylsilaethylene is a thermodynamically stable molecule. It is interesting to point out that the preference of I is further enhanced by $X = F$.

In Figure 1 are shown the equilibrium geometries predicted by GVB and RHF for I. This planar singlet ground state is found to lie 36 kcal/mol below the lowest triplet.

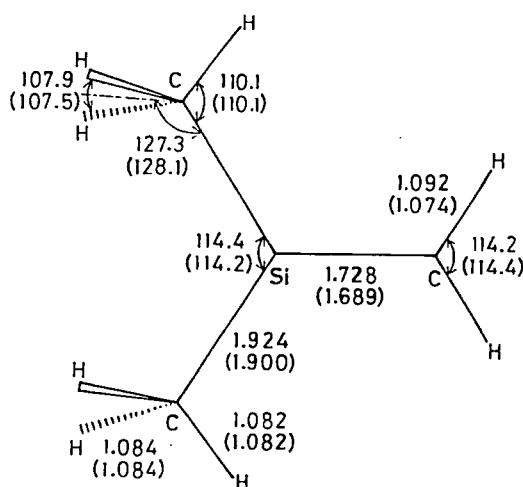


Figure 1. Optimized geometries (in Å and degrees) for $\text{Me}_2\text{Si} = \text{CH}_2$ in the GVB and the RHF (parenthesis) method.

Table I Energies (kcal/mol) of Isomers of $\text{Me}_2\text{Si} = \text{CH}_2$ relative to I.^a

Method	II	III
RHF	16.0	58.7
GVB	18.0	62.4
RHF + CI (S + D) ^b	20.5	70.8
RHF + CI (S + D + QC) ^b	21.8	73.1

^a at the RHF optimized geometries.

^b S + D = all single and double excitations, QC = correction for quadruple excitation.

Reference

1) IMS Graduate Student 1980— from Tohoku Univ.

I-B-2 An Ab Initio MO Study on the Stability and Nature of the Si-C and Si-Si Triple Bonds

Mitsuyasu HANAMURA,¹⁾ Keiji MOROKUMA and Shigeru NAGASE (Yokohama National Univ.)

In order to elucidate the thermodynamic and kinetic stabilities of the Si-C and Si-Si triple bonds, we have carried out ab initio MO calculations of i) $\text{XSi} \equiv \text{CH}$ (X = H, F, CH_3) and ii) $\text{HSi} \equiv \text{SiH}$. The method of calculation is described in the preceding section.

i) $\text{XSi} \equiv \text{CH}$: The relative energies of the three isomers and with X = H and F are shown in Table I. Carbene is the most unstable. Silyne is less stable than silylene by 27 kcal/mol for X = H and 3 kcal/mol for X = F. It might be possible with appropriate substituents to make silyne the most stable.

In Figure 1 is shown the potential profile from $\text{H}_2\text{Si} = \text{C}$: through $\text{HSi} \equiv \text{CH}$ to $:\text{Si} = \text{CH}_2$. The barrier heights for the rearrangements are very small (1.6 kcal/mol and 4.0 kcal/mol).

ii) $\text{HSi} \equiv \text{SiH}$: Table II reveals that the most stable isomer is the bridged form (IV). Normal coordinate analysis identifies the isomers II-V correspond to energy minima, whereas disilyne (I) does not.

Reference

1) IMS Graduate Student 1980— from Tohoku Univ.

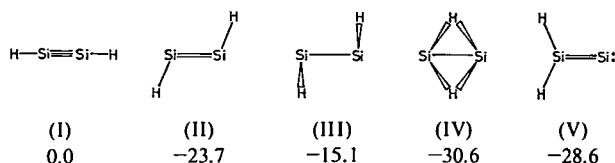
Table I. Energies (kcal/mol) of Isomers of $\text{XSi} \equiv \text{CH}$ (X = H, F) relative $\text{XSi} \equiv \text{CH}$.^a

Method	X = H		X = F	
	$:\text{Si} = \text{CH}_2$	$\text{H}_2\text{Si} = \text{C}$:	$:\text{Si} = \text{CHF}$	$\text{FHSi} = \text{C}$:
RHF	-43.5	33.2	-14.3	16.1
RHF + CI (S + D) ^b	-30.0	45.0	-5.4	27.5
RHF + CI (S + D + QC) ^b	-26.9	46.0	-3.4	28.8

^a at the RHF optimized geometries.

^b S + D = all single and double excitation, QC = correction for quadruple excitation.

Table II. Relative Energies (kcal/mol) of Five Isomers of $\text{HSi} \equiv \text{SiH}$ in RHF + CI (S + D + QC) Method with 4-31G** Basis Set at the 4-31G RHF Optimized Geometries.



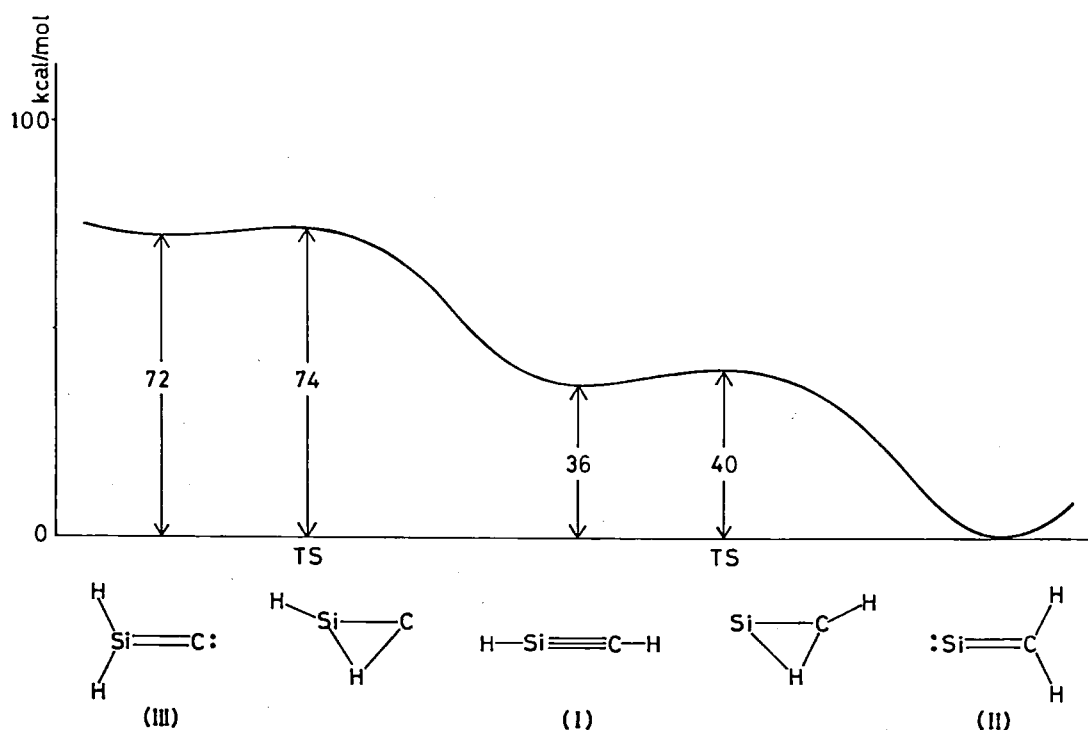


Figure 1. Relative energies (kcal/mol) of $\text{HSi}\equiv\text{CH}$ system in RHF + CI (S + D + QC) method with 4-31G** RHF optimized geometries.

I-B-3 Theoretical Evidences for Intramolecular Hydrogen Bonding in Syn-7-Norbornenol

Keiji MOROKUMA and Georges WIPFF (*Univ. of Strasbourg*)

[*Chem. Phys. Lett.* 74, 400 (1980)]

Syn-7-norbornenol exhibits the best known 'experimental evidences' for intramolecular hydrogen bonding to a π -electron system: a shift in the OH stretching frequency from 3630 cm^{-1} to 3574 cm^{-1} and a decrease in the splitting between the $\text{C}=\text{C}$ π and the oxygen lone pair ionization potential from 0.85 eV to 0.30 eV . Despite advances in MO studies on hydrogen bonding, no direct 'theoretical evidences' have yet been available, because a comparison of small changes in the stability and spectral properties requires a careful geometry optimization.

We have used the ab initio SCF energy gradient method with a minimal basis set, and fully optimized the geometries of four forms of norbornenol: syn-cis (SC), syn-trans (ST), anti-cis (AC) and anti-trans (AT). The results are summarized in Table I. Our findings are as follows. (1) SC, the only form that can have intramolecular

hydrogen bonding, has the lowest energy. (2) The OH distance is the largest and the COH angle is the smallest in SC. (3) The frequency ω_{OH} , estimated from the calculated diagonal force constant and scaled to fit the experiment for AC, shows a red shift of 30 cm^{-1} going from AC to SC. (4) The $\text{C}=\text{C}$ π orbital is destabilized in SC, whereas the oxygen lone pair energy changes little, relative to AC.

All the 'theoretical evidences' above clearly indicate that there exists an intramolecular hydrogen bond. 'Experimental evidences', such as the ir shift and pe splitting, can really be attributed to hydrogen bonding.

Table I. Optimized Geometries, Relative Energies, Vibrational Frequencies and Ionization Potentials of 7-Norbornenol.

Conformation	SC	ST	AC	AT
ΔE (kcal/mol)	-1.68	1.56	(0)	0.38
R_{OH} (Å)	0.990 ₆	0.987 ₆	0.988 ₄	0.987 ₅
COH (°)	103.9	104.5	105.3	104.3
ω_{OH} (cm^{-1})	3601	3639	(3630)	3639
Ionization potential (eV)				
I_{OH}	8.87	8.84	8.92	8.85
$\text{C}=\text{C } \pi$	8.24	7.81	8.09	7.99

I-B-4 MO Study on the Mechanism of Heat-Resistance of Thermophilic Bacteria

Chikayoshi NAGATA*, Misako AIDA* (*National Cancer Center Research Institute), Iwao OHMINE and Keiji MOROKUMA

Many experimental studies on the structure of tRNA from an extremely thermophilic bacteria, which can grow even at 85°C, showed that ribothymidine (T) in the T ψ C loop is replaced by 2-thioribothymidine (s²T). The replacement of an atom O with S in tRNA has been considered to increase the stability of the tertiary structure.¹⁾ Although the reason has not been clear, the following suggestion has been proposed: the stacking energy for ⁵³G : ⁵⁴T : ⁵⁵ ψ becomes stronger by substitution of s²T for T, thus leading to a stronger association of T ψ C loop with D loop.

It is aimed, by the MO calculation, to clarify whether the S-substituted pyrimidine contributes to increase the stacking energy. The interaction energies between T and s²T have been calculated with the 4-31G basis set by ab initio SCF MO method augmented with the perturbation treatment for the dispersion energy. The conformation of the bases was taken from X-ray crystallography of tRNA^{Phe} (YEAST).²⁾ (Figure 1) For s²T-containing tRNA, the same conformation as that for the yeast tRNA was assumed. For the distance between the T: ψ base pair, the observed value of 3.54 Å was used, and calculation was carried out also at 3.4 Å for comparison. For G : T base pair, the observed value 3.45 Å was used.

The results are summarized in Table I. Only a small increase in the stacking energy for ⁵⁴T : ⁵⁵ ψ was obtained by replacement of O with S. However, this displacement increases the stacking energy for ⁵³G : ⁵⁴T by 1 kcal/mol and this seems to contribute partly to the heat stability of the thermophile tRNA. But, this is not enough to explain all of it, and other effects such as strengthening of hydrogen bond and stabilization effect of magnesium ion, might also contribute.

Table I. Calculated Interaction Energies. (kcal/mol)

	T(O) - ψ		T(S) - ψ		T(O) - G		T(S) - G
	3.54Å	3.4Å	3.54Å	3.4Å	3.45Å	3.45Å	
ΔE_{SCF}	+1.17	+2.71	+1.82	+2.77	+3.87	+3.37	
ΔE_{disp}	-3.80	-4.68	-4.06	-4.98	-6.55	-7.00	
ΔE_{total}	-2.03	-1.97	-2.24	-2.21	-2.68	-3.63	

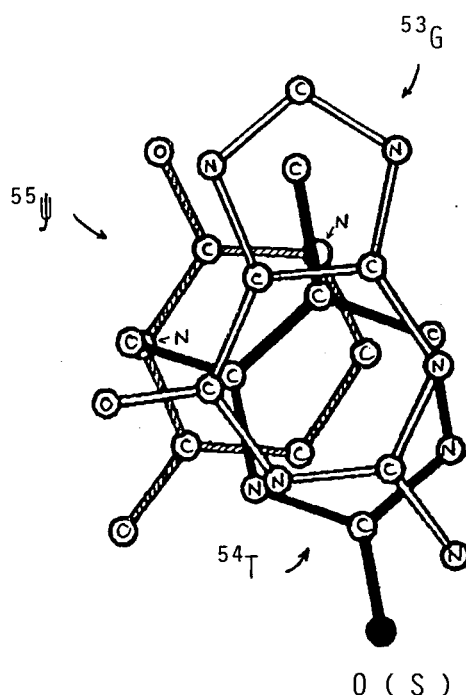


Figure 1. Conformation of bases, ⁵³G, ⁵⁴T and ⁵⁵ ψ . Hydrogen atoms are neglected here.

References

- 1) K. Watanabe, T. Oshima and S. Nishimura, *Nucleic Acids Res.*, **3**, 1703 (1976).
- 2) B. E. Hingerty, R. S. Brown and A. Jack, *J. Mol. Biol.*, **124**, 523 (1978).

I-B-5 Ab Initio SCF MO Calculation of Force Constants and Dipole Derivatives on Trans- and Cis-N-Methylformamide

Yoko SUGAWARA,* Akiko Y. HIRAKAWA,* Masamichi TSUBOI* (Univ. of Tokyo), Shigeki KATO and Keiji MOROKUMA

Recently we have carried out ab initio SCF MO calculation of force constants and dipole derivatives on formamide¹⁾ and the results have shown that such a calculation is quite useful in determining and improving the molecular force field of amide compounds.

This time we have extended calculations trans and cis isomers of N-methylformamide, using the 4-31G basis set for in-plane modes, and the 4-31G* basis set (containing polarization function for C, N, and O atoms) for out-of-plane modes. The main conformer of N-methylformamide in gas phase is trans, the other, 10% being as cis form; the calculated energy difference between the two isomers was 1.4 kcal/mol. For the trans form, calculated normal frequencies were generally, as

expected,¹⁾ 10 – 15% greater than the observed fundamental frequencies; however, the normal modes coincided with those estimated in the previous experimental studies. There were no significant differences in the force field of the two isomers. The isomer shifts in frequencies and infrared intensities were reasonably reproduced.

Reference

Y. Sugawara, Y. Hamada, A. Y. Hirakawa, M. Tsuboi, S. Kato and K. Morokuma, *Chem. Phys.* **50**, 105 (1980).

I-B-6 Ab Initio MO Study on Amine Molecules

Yoshiaki HAMADA,* Naoki TANAKA,* Yoko SUGAWARA,* Akiko Y. HIRAKAWA,* Masamichi TSUBOI* (*Univ. of Tokyo*), Shigeki KATO and Keiji MOROKUMA

Ab initio MO calculations were performed to investigate their practical abilities of the understanding and prediction of the vibrational spectra of amines. Three basis sets, STO-3G, 4-31G and 4-31G* (including the polarization function), were used and compared with one another in the Hartree-Fock approximation. As spectroscopical observables, we calculated the fully optimized

geometry, the force constants (frequencies and modes), the dipole moment, and the dipole moment derivatives (infrared intensity, direction of the transition moment). These calculations were compared with the experimental values. New experiments were also made. Methylamine, hydrazine and hydroxylamine, which have a C-N, N-N and N-O single bond, respectively, were investigated as the simplest representative amines. The relationship between the calculated variables and the bonding character was examined.

Some of the results are summarized as follow. 1) Inclusion of the d-function of the N atom is essential to reproduce the geometry and frequencies for an amino group. 2) The calculated frequencies ω_i , nearly equally higher by the factor of 1.15 – 1.25 than the observed frequencies ν_i , can be used to identify the vibrational mode and to predict the unassigned spectrum. The calculated intensity pattern and polarization are very helpful for the prediction. 3) The experimentally unsolved position of the amino twisting frequency is predicted; it should be in the region of 1200 – 1300 cm^{-1} .

For the completeness and extension of this work, we are investigating a) the vibrational anharmonicity in the Hartree-Fock approximation, b) the effect of CI and c) the transferability or correlation of force constants between amines described above and other simple molecules.

I—C Structure, Bonding and Reactivity of Transition Metal Complexes

We have put in a substantial effort in this area of theoretical studies. Our goal is to understand not only the structure and bonding of transition metal complexes but also their reactivity and reaction mechanisms.

As is becoming clear with simpler theoretical reactions, the full geometry optimization is more or less mandatory for the determination of transition state and activation barrier. For systems involving transition metals such an optimization is very expensive. In order to open an avenue for efficient geometry determination, we have recently developed an energy gradient program for the effective core potential approximation (C-1). The program has been used so far for geometry optimization of reactants and products of a few reaction systems (C-2 and C-3). We also continued to work on the energy decomposition analysis in transition metal complexes for the interaction between a ligand and the remaining fragment of a complex (C-4 and C-5). In the Annual Review next year we hope to report the determination of transition states for some reaction systems.

I-C-1 Energy Gradient in the Ab Initio MO Method with the Effective Core Potential Approximation

Kazuo KITAURA, Shigeru OBARA and Keiji MOROKUMA

The efficiency of the energy gradient method in

the ab initio MO scheme has been established by now for calculating equilibrium and transition state geometries and vibrational frequencies of polyatomic molecules. The direct application of the gradient method, however, to systems containing heavy atoms has been very limited, because the method still requires too much computer time. The use of the effective core potential approximation¹⁾

may enable one to circumvent this practical difficulty and open a way of applying the energy gradient method to systems such as transition metal complexes. In addition to integrals required for the usual gradient calculation, one needs the matrix elements of the derivative of the effective core potential with respect to the nuclear coordinates. They can be easily obtained by using the translational invariance of the matrix elements, namely,

$$\begin{aligned} & \langle \chi_A | \frac{\partial V_c^{\text{ECP}}}{\partial R_C} | \chi_B \rangle \\ &= - \langle \frac{\partial \chi_A}{\partial R_A} | V_c^{\text{ECP}} | \chi_B \rangle \\ & - \langle \chi_A | V_c^{\text{ECP}} | \frac{\partial \chi_B}{\partial R_B} \rangle . \end{aligned}$$

Once the derivatives are obtained, the energy gradient in the SCF, MCSCF²⁾ and CI³⁾ methods can be calculated with the effective core potential approximation. We now have a computer program for SCF and MCSCF.

The method has been applied for optimizing equilibrium geometries of some transition metal complexes. The results are shown in Figure 1.

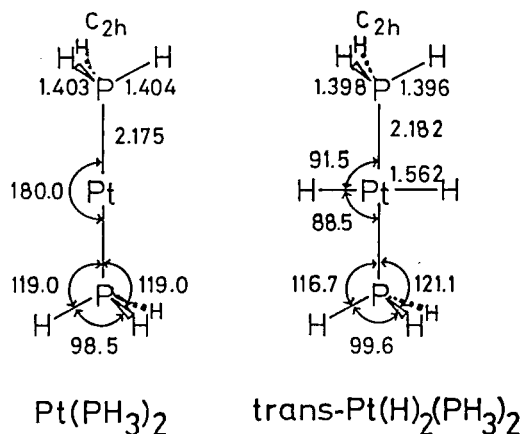


Figure 1. Optimized equilibrium geometries (distances in Å, bond angles in degrees) with a basis set of double- ζ quality. The relativistic effective core potential of Basch and Topiol (*J. Chem. Phys.* **71**, 802 (1979)) was used for Pt.

References

- 1) L. R. Kahn, P. Baybutt and D. G. Truhlar, *J. Chem. Phys.* **65**, 3826 (1979).
- 2) S. Kato and K. Morokuma, *Chem. Phys. Lett.* **65**, 19 (1979).
- 3) B. R. Brooks, W. D. Laidig, P. Soxe, J. D. Goddard, Y. Yamaguchi and H. F. Schaefer III, *J. Chem. Phys.* **72**, 4652 (1980); R. Krishnan, H. B. Schlegel and J. A. Pople, *J. Chem. Phys.* **72**, 4654 (1980).

I-C-2 An Ab Initio MO Study on the Reaction Mechanism of $\text{Co}^+ + \text{C}_2\text{H}_6$

Shigeru OBARA, Kazuo KITAURA and Keiji MOROKUMA

A recent ion beam study of the reaction of Co^+ with isobutane¹⁾ has shown that a reaction product is the cobalt-olefin adduct. A proposed reaction mechanism is the insertion of Co^+ into a C-H or C-C bond, followed by the migration of a β -H or β -CH₃ group to Co, and the elimination of H₂ or CH₄.

We are studying the reaction mechanism of $\text{Co}^+ + \text{C}_2\text{H}_6$ as a model system for this reaction by using the ab initio SCF and MCSCF gradient method with the effective core potential.²⁾

We have searched the equilibrium geometry of reaction intermediates: the olefin adduct $[\text{H}_2\text{CoC}_2\text{H}_4]^+$. The ground state of Co^+ ion is ^3F and the second lowest is ^5F , and the spin state of reaction intermediates can be a triplet, a quintet or a singlet. The optimized geometry of a triplet state of the olefin adduct is shown in Figure 1. Further studies searching for geometries of the transition state for each spin state and possible reaction schemes are in progress.

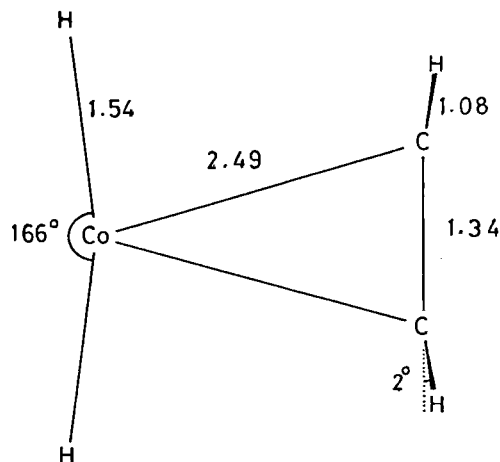


Figure 1. Optimized geometry (in Å and degrees) of $[\text{H}_2\text{CoC}_2\text{H}_4]^+$ ($^3\text{B}_1$). Basis sets with double-zeta quality and Co effective core potential are used. Constrained to C_{2v} .

References

- 1) P. B. Armentrout and J. L. Beauchamp, *J. Am. Chem. Soc.* **102**, 1736 (1980).
- 2) K. Kitaura, S. Obara and K. Morokuma, *IMS Ann. Rev.* **18** (1980).

I-C-3 Ab Initio MO Study on Hydrolysis of $\text{PtCl}_2(\text{NH}_3)_2$ and Trans-Effect

Kazuo KITAURA, Shigeyoshi SAKAKI (*Kumamoto Univ.*) and Keiji MOROKUMA

The ligand substitution reactions have been well studied for square-planar Pt(II) complexes.¹⁾ The hydrolysis of $\text{PtCl}_x(\text{NH}_3)_{4-x}$ is one of the most systematically studied systems. We intend to investigate the trans-effect on hydrolysis of $\text{PtCl}_2(\text{NH}_3)_2$: $\text{PtCl}_2(\text{NH}_3)_2 + \text{H}_2\text{O} \rightarrow [\text{PtCl}(\text{NH}_3)_2(\text{H}_2\text{O})]^+ + \text{Cl}^-$.

Ab initio MO calculations were carried out with the double- ζ set for Pt and the minimum basis set for the ligand atoms. The relativistic effective core potential approximation was used for Pt.²⁾ Geometries of the reactants and the products were

fully optimized using the energy gradient.³⁾ The results (Figure 1) show the order of ligand trans-influence on the geometry to be: $\text{Cl} > \text{NH}_3 > \text{H}_2\text{O}$. Energetically trans- $\text{PtCl}_2(\text{NH}_3)_2$ is obtained to be more stable by 17 kcal/mol than the cis isomer, while cis- $[\text{PtCl}(\text{NH}_3)_2(\text{H}_2\text{O})]^+$ is more stable by 8 kcal/mol than the trans isomer.

The determination of geometries of five coordinated intermediates and transition states of the reaction is in progress.

Reference

- 1) F. Basolo and R. G. Pearson, "Mechanisms of Inorganic Reactions", John Wiley, 1967, Chap. 5.
- 2) H. Basch and S. Topiol, *J. Chem. Phys.* **71**, 802 (1979).
- 3) K. Kitaura, S. Obara and K. Morokuma, *IMS Am. Rev.* **18** (1980).

I-C-4 An Ab Initio MO Study of the Structure and Coordinate Bonding Nature of $\text{Ni}(\text{PH}_3)_2\text{L}$ ($\text{L} = \text{H}_2\text{CO}$ or $(\text{CO})_2$)

Shigeyoshi SAKAKI (*Kumamoto Univ.*), Kazuo KITAURA and Keiji MOROKUMA

An ab initio MO study was performed on $\text{Ni}(\text{PH}_3)_2\text{L}$ ($\text{L} = \text{H}_2\text{CO}$ or $(\text{CO})_2$), and the results are compared with those for the previously studied $\text{Ni}(\text{PH}_3)_2\text{L}$ ($\text{L} = \text{C}_2\text{H}_2$, C_2H_4 , CO_2).¹⁾ The $[4s3p2d]$ basis set was used for the Ni atom, the 4-31G for the other atoms. Possible structures we examined are shown in Figure 1. The geometries of these complexes were constructed referring to experimental structures of related complexes, and we optimized some bond distances and angles. (See Figure 1.) As shown in Table 1, the side-on $\text{Ni}(\text{PH}_3)_2(\text{H}_2\text{CO})$ is more stable than the end-on. In the latter, the optimized Ni-O distance 1.97 Å is longer than the corresponding experimental distance 1.76 Å for the side-on complex. In the side-on $\text{Ni}(\text{PH}_3)_2(\text{H}_2\text{CO})$, the H_2CO ligand is distorted out of its planarity; The distortion reduces the

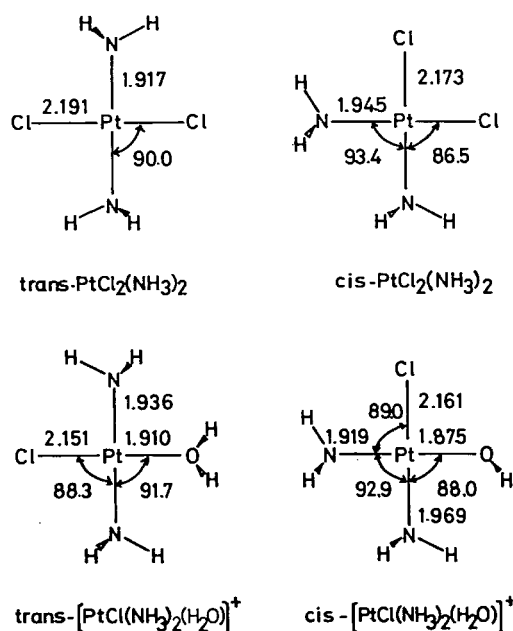


Figure 1. Optimized geometries. (distances in Å and angles in degrees)

Table 1. Energy Components of Interaction between $\text{Ni}(\text{PH}_3)_2$ and L (kcal/mol).

L	H_2CO			CO		CO_2	C_2H_2	C_2H_4
	end-on	$\theta = 0^\circ$	32°	Td	Pl	42°	40°	26°
BE	-7	-32	-42	-25	8	-27	-37	-30
DEF	0	11	20	0	0	34	40	15
INT	-7	-43	-62	-25	8	-61	-77	-45
ES	-27	-101	-102	-101	-115	-76	-148	-132
EX	42	161	157	138	181	131	189	168
BCTPLX	-13	-67	-74	-43	-42	-70	-75	-54
FCTPLX	-7	-15	-17	-19	-16	-16	-24	-16
R	-2	-21	-26			-30	-19	-11

exchange repulsion EX and increases the backdonative stabilization BCTPLX. In $\text{Ni}(\text{PH}_3)_2(\text{CO})_2$, the tetrahedral-like structure is more stable than the planar, because of the smaller EX destabilization. The back bonding energy of the CO ligand is only about a half of the other ligands, and therefore BE per ligand is the smallest. However, CO is an unidentate ligand and two CO molecules can coordinate to $\text{Ni}(\text{PH}_3)_2$, which results in the largest overall BE and BCTPLX.

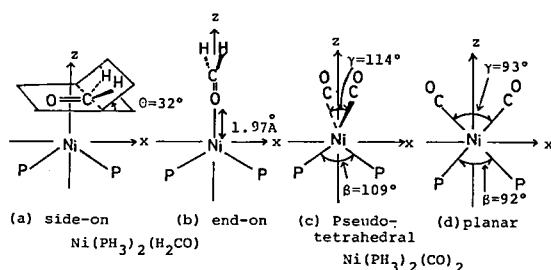


Figure 1. Geometries and optimized geometrical parameters of $\text{Ni}(\text{PH}_3)_2\text{L}$ ($\text{L} = \text{H}_2\text{CO}$ or $(\text{CO})_2$).

Reference

- 1) K. Kitaura, S. Sakaki and K. Morokuma, *IMS Ann. Rev.* 19, 20 (1979).

I-C-5 The Mutual Influence of Ligands in Pentaammine Co(III) Complexes. Ab Initio MO Study

Toshiharu HARA (*Wakayama Tech. College*),
Kazuo KITAURA and Keiji MOROKUMA

The mutual influence of ligands in $[\text{Co}(\text{NH}_3)_5\text{X}]^{3+}$ ($\text{X} = \text{NH}_3$, H_2O and CN^-) was studied through an analysis of bonding between NH_3 (both cis and trans to X) and the $[\text{Co}(\text{NH}_3)_4\text{X}]$ fragment.

The ab initio SCF MO calculations were carried out with the basis set of double- ζ quality. The effective core potential approximation¹⁾ was used for Co. The interaction energy between NH_3 and $[\text{Co}(\text{NH}_3)_4\text{X}]$ was decomposed into components of the steric (electrostatic + exchange-repulsion), the donative (from NH_3 to $[\text{Co}(\text{NH}_3)_4\text{X}]^{3+}$), the back-donative and the remaining (coupling) interactions.²⁾ The calculated binding energy of $\text{Co} \cdots \text{trans NH}_3$ is larger in $[\text{Co}(\text{NH}_3)_5(\text{H}_2\text{O})]^{3+}$ and smaller in $[\text{Co}(\text{NH}_3)_4\text{CN}]^{2+}$ than in $[\text{Co}(\text{NH}_3)_6]^{3+}$ (Table I), the order being in accord with that of the experimentally observed trans influence of ligands: $\text{CN}^- > \text{NH}_3 > \text{H}_2\text{O}$. Energy components show that the substitution of NH_3 by the weaker ligand increases the donative interaction and reduces the

exchange-repulsion between NH_3 and Co, while the opposite is true in case of the stronger ligand. The change in electron distributions also reflect the trend mentioned above (Figure 1).

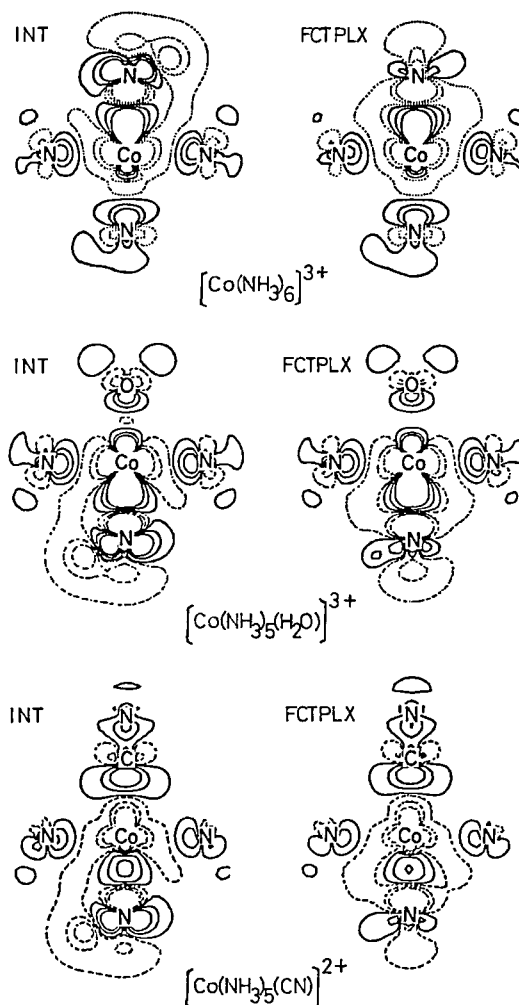


Figure 1. The difference density maps for the interaction of $\text{trans NH}_3 \cdots [\text{Co}(\text{NH}_3)_4\text{X}]^{n+}$. The solid and the dotted lines show the increase and the decrease in densities. The contours are ± 0.01 , ± 0.005 and $\pm 0.001 \text{ e} \cdot \text{bohr}^{-3}$, respectively.

References

- 1) S. Topiol, J. W. Moskowitz and F. Melius, *J. Chem. Phys.* 68, 2364 (1978).
- 2) K. Kitaura, S. Sakaki and K. Morokuma, *Inorg. Chem.* in press.

Table I. The Interaction Energy (kcal/mol) between NH_3 and $[\text{Co}(\text{NH}_3)_5\text{X}]^{3+}$ and its Components in $[\text{Co}(\text{NH}_3)_5\text{X}]^{3+}$ (X = NH_3 , H_2O and CN).^a

Complex	$[\text{Co}(\text{NH}_3)_6]^{3+}$	$[\text{Co}(\text{NH}_3)_5(\text{H}_2\text{O})]^{3+}$		$[\text{Co}(\text{NH}_3)_5\text{CN}]^{2+}$	
		cis	trans	cis	trans
INT	-70	-74	-75	-60	-51
ES + EX	-21	-23	-24	-14	-7
FCTPLX	-36	-38	-38	-34	-30
BCTPLX	-10	-8	-8	-11	-12
R	-4	-5	-4	-2	-2

^a The minus sign shows stabilization. INT, ES + EX, FCTPLX, BCTPLX and R are total, steric, donative, back-donative and remaining interaction energies, respectively.

I-C-6 MO Study of Catalytic Specificity of Manganic Ion in Photosynthetic Water Decomposition

Masami KUSUNOKI (*Meiji Univ.*), Kazuo KITAURA, Keiji MOROKUMA and Chikayoshi NAGATA (*National Cancer Center Research Institute*)

Though the necessity of Mn for photosynthetic decomposition of H_2O is well established, its molecular mechanism remains to be elucidated. Our previous MO study¹⁾ has suggested that a cooperative action between a neutral H_2O and Mn(III) can give an attractive double minimum potential for proton transfer. Here we compare Mn(III) with Mn(II), Fe(III) and Cu(II) for their proton transfer capability. The adopted model system is shown in Figure 1. The relative energies as functions of R_{OH} in Figure 1 indicate that Mn(III) has a deeper second minimum than any other metals (Table I). Table I also shows that Mn(III) has the largest charge transfer from the water molecule to the metal complex. These results suggest that Mn(III) might be a best metal ion for water-splitting.

Reference

- 1) M. Kusunoki, K. Kitaura, K. Morokuma and C. Nagata, *FEBS Letters*, **117**, 179 (1980).

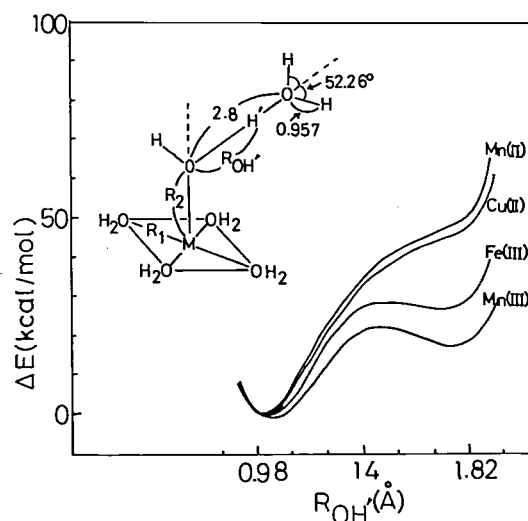


Figure 1. The adopted model system and the potential energy curves for the proton transfer. The R_1 and R_2 distances were optimized for each system: $R_1 = 2.00\text{Å}$, 1.93Å , 1.83Å and 1.86Å , and $R_2 = 2.00\text{Å}$, 2.00Å , 2.06Å and 1.95Å for the Mn(II), Cu(II), Fe(III) and Mn(III), respectively.

Table I. The proton transfer energy (ΔE_{pt}) as a function of the charge transfer (δ) from the water molecules to the catalytic metal-complex.

Systems	spin	ΔE_{pt} (kcal/mol) ^a	δ
Mn(II)	5/2	49	0.068
Cu(II)	1/2	48	0.075
Fe(III)	1/2	26	0.11
Mn(III)	2	19	0.12

^a $\Delta E_{\text{pt}} \equiv E(R_{\text{OH}} = 1.82) - E(R_{\text{OH}} = 0.98)$

I—D Surface Electronic Structure of Metal Oxides and Chemisorption Mechanisms

Metal oxides provide us inexpensive and practical catalysts with a great variety of properties. They are also important as electrode materials on which many interesting electrode and photo-electrode processes take place. Though any of real reactions on surfaces include many intricate processes, fundamental physical and chemical investigations are now becoming increasingly important.

In this project theoretical studies have been worked out for the electronic structure of bulk and ideal surface of metal oxides, surface defects and interaction with adsorbates. Through the investigations of many prototype oxides, cardinal characteristics of the surface electronic structure have been elucidated. We concentrated in this year mainly on ReO_3 surface, which exhibits a high catalytic activity for olefin metathesis reactions.

I-D-1 Theory of the Electronic Structure of ReO_3 (001) Surface and the Surface Oxygen Vacancy

Masaru TSUKADA, Nobuo TSUDA,* Fujio MINAMI* (*National Inst. Res. Inorg. Mat.)

[*J. Phys. Soc. Jpn.*, 49, 1115 (1980)]

The DV- $X\alpha$ method is applied to various clusters representing the ReO_3 (001) surface and an oxygen vacancy on it. Two models of the neutral (001) surface are proposed: a) rough surface model (RSM) and b) smooth surface model (SSM). In the former model one half of the top Re ions are covered by oxygen ions, while in the latter the formal charge of the top Re ion is reduced from that of the bulk Re ions. For the SSM, the accumulation of the electrons on the top layer is caused by the drastic lowering and thus resulted occupation of the intrinsic surface state level, which is mainly localized on the top Re ion. On the other hand the surface of the RSM is structurally neutral.

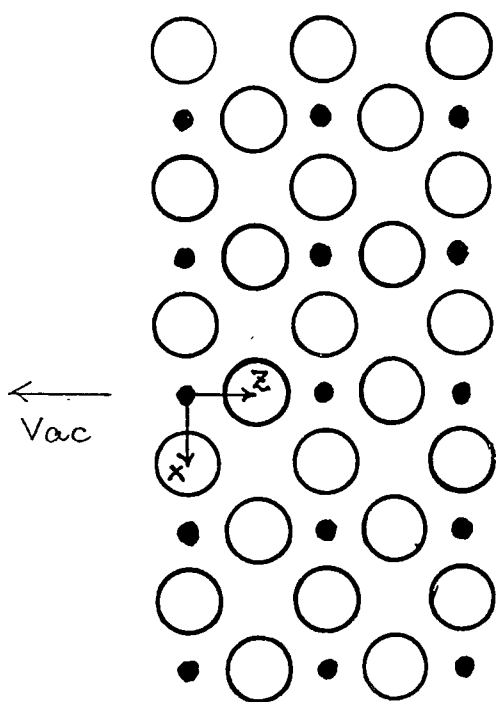


Figure 1. The (001) ReO_3 surface of SSM. Open and filled circles represent respectively O and Re ions.

Therefore, though the ionicity on the surface is somewhat reduced due to the Madelung potential reduction effect,¹⁾ the electron accumulation on the top Re ion is not conspicuous. This corresponds to the fact that the intrinsic surface state is not so lowered to accommodate electrons, because the field at the top Re sites is moderated by the presence of the oxygen half monolayer.

Since the electronic state of O and Re ions on the top layer differs remarkably between the two models, several experiments are suggested which can be used to determine which of the two models is realized. The orbital of the defect state associated with the surface oxygen vacancy is composed mainly of Re 6p, 6s, 5d orbitals and is stuck out of the surface.²⁾

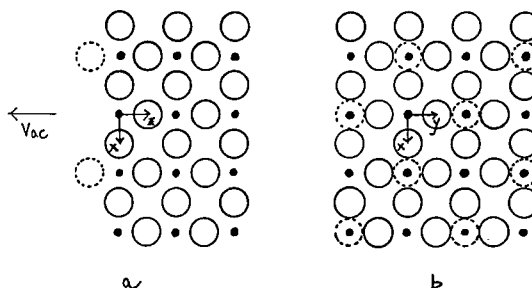


Figure 2. a) Side view and b) front view of the (001) ReO_3 surface of RSM.

References

- 1) C. Satoko, M. Tsukada and H. Adachi, *J. Phys. Soc. Jpn.*, 45, 1333 (1978).
- 2) M. Tsukada, C. Satoko and H. Adachi, *J. Phys. Soc. Jpn.*, 48, 200 (1980).

I-D-2 Self-consistent Madelung Potential for the Cluster Calculation of Partially Ionic Solids —Application to ReO_3 —

Masaru TSUKADA

[*J. Phys. Soc. Jpn.*, 49, 1183 (1980)]

A self-consistent Madelung potential (SCMP) is proposed which can be combined with the DV- $X\alpha$ cluster method for partially ionic solids. The SCMP is based on the following rules established by many cluster calculations worked out in our

group.¹⁾ 1) An almost equal amount of charge back flow measured from the perfectly ionized state takes place through the bond joining the nearest neighbor cation-anion pair. 2) The charge of a central or inner cluster ion is obtained by Mulliken population analysis with much better accuracy than the boundary cluster ion. 3) An excessive charge is accumulated on the boundary cluster ions due to the lack of the charge back flow through the artificially cut boundary bonds.

In SCMP the charge of the exterior ions not joined to the cluster ions are so chosen that they are consistent with the Mulliken charge of the central cluster ion. The net charge of the cluster is assumed as the sum of the formal charge of component ions. The charge α of the boundary exterior ions approximately compensates the excessive charge described in rule 3).

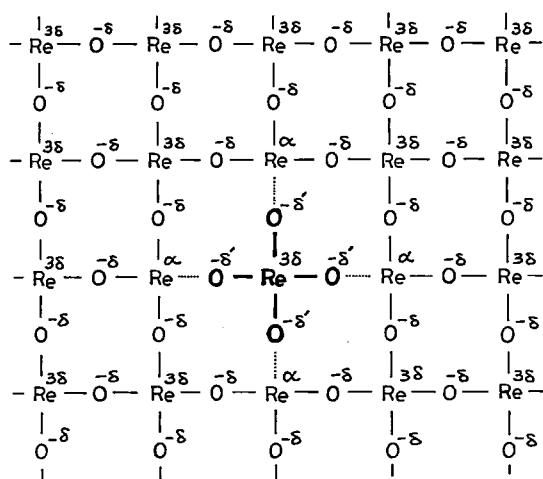


Figure 1. The self-consistent Madelung potential (SCMP) for the cluster calculation of $(\text{ReO}_6)^{6-}$ in ReO_3 . The dotted line means the truncated bond between the boundary oxygen ion in the cluster and the exterior Re ion. The figure shows the (001) plane including the central cluster Re ion.

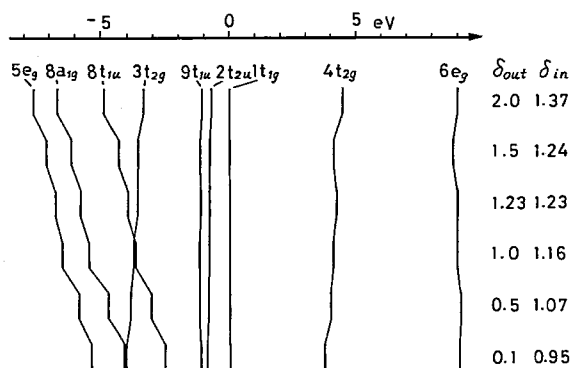


Figure 2. The change of the level structure of $(\text{ReO}_6)^{6-}$ with the value of δ_{out} , the parameter for the outer ionic charge. The selfconsistent value of δ is given by $\delta_{\text{out}} = \delta_{\text{in}} = 1.23$ in this case.

The method is applied to the $(\text{ReO}_6)^{6-}$ cluster in ReO_3 crystal.²⁾ The agreement of the valence electronic structure with XPS³⁾ and APW band calculation⁴⁾ is considerably improved by the use of SCMP instead of the MP with formal ionic charge.

References

- 1) M. Tsukada, C. Satoko and H. Adachi, *J. Phys. Soc. Jpn.*, **48**, 200 (1980).
- 2) M. Tsukada, N. Tsuda and F. Minami, *J. Phys. Soc. Jpn.*, **49**, 1115 (1980).
- 3) G. K. Wertheim, L. F. Mattheiss, M. Campagna and T. P. Persall, *Phys. Rev. Lett.*, **32**, 997 (1974).
- 4) L. F. Mattheiss, *Phys. Rev.*, **181**, 987 (1969), **B2**, 3918 (1970), **B6**, 4718 (1972).

I-D-3 Theoretical Study of Ethylene Metathesis Reaction on the ReO_3 Surface by DV-X α Cluster Calculation

Masaru TSUKADA, Nobuo TSUDA,* Atsushi FUJIMORI* (*National Inst. for Inorg. Mater.)

The olefin metathesis reactions catalyzed by the trioxide of Re, Mo, and W attracted much attention because of their technological importance. Experimental study of the metathesis reaction of propylene on a single crystal ReO_3 surface is recently worked out by Tsuda et al.¹⁾ They found that the catalytic activity of the surface increases sharply with a slight reduction of the

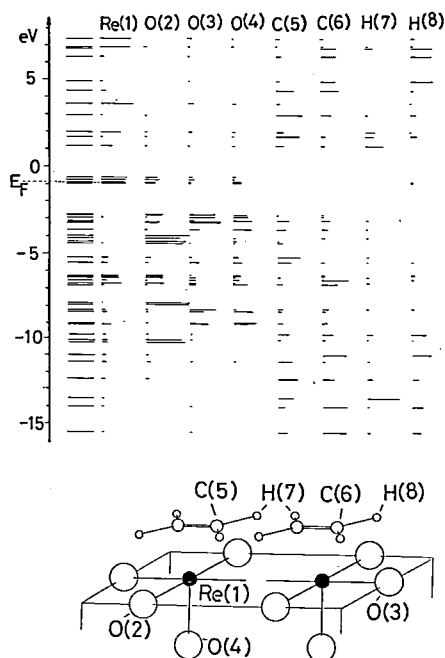


Figure 1. a) Energy levels and b) structure of the cluster $\text{Re}_2\text{O}_8-(\text{C}_2\text{H}_4)_2$ for the case of the molecular plane parallel to the crystal surface.

surface. To elucidate the reaction mechanism, the effect of the ReO_3 surface on the interaction between two ethylene molecules is theoretically investigated.

We made DV- $X\alpha$ calculations for clusters $\text{Re}_2\text{O}_8-(\text{C}_2\text{H}_2)_2$ modelled on the two ethylene molecules chemisorbed on ReO_3 (001) surface. In these clusters, the double bond, and the molecular plane of the two molecules are assumed, respectively to lie on the same line or on the same plane. Two cases are investigated on which the ethylene molecular plane is either parallel or perpendicular to the ReO_3 (001) surface of SSM.

In all the cases investigated, the overlap population of the ethylene double bond is found to be negative, indicating a cut off of the double bond. On the other hand, a new formation of C-C bond between the nearest carbon atoms of the two molecules is found. A flow of electrons from the catalyst to the reactants is revealed. The sharp raise of the reactivity with slight reduction seems to correspond the increase of the number of the pairs of nearest neighbor top Re ions uncovered by oxygen ions.²⁾

References

- 1) N. Tsuda, A. Fujimori and M. Tsukada, to be submitted in *J. Catal.*
- 2) M. Tsukada, N. Tsuda and F. Minami, *J. Phys. Soc. Jpn.*, **49**, 1115 (1980).

I-D-4 Electronic Structure of ZrO_2 by the DV- $X\alpha$ Cluster Method

Masahiko MORINAGA (*Toyohashi Univ. of Tech.*), Hirohiko ADACHI (*Osaka Univ.*) and Masaru TSUKADA

[*J. Solid State Ionics*, in press]

In this work the electronic structure of cubic and tetragonal ZrO_2 is calculated and the stability of

cubic phase¹⁾ is examined. The DV- $X\alpha$ calculations are made for the cluster $(\text{ZrO}_8)^{12-}$, which is shown in Figure 1(a), 1(b) for the cubic and the tetragonal phase, respectively. The following results were obtained; 1) The net charge at Zr is +3.1 for the cubic phase, whereas it is +2.9 for the tetragonal phase. 2) The bond order is higher in the tetragonal phase than in the cubic phase, indicating the stronger covalency in the former phase. 3) The energy gap between the O-2p and the Zr-4d band is larger in tetragonal ($\sim 8\text{eV}$) than in cubic ($\sim 7\text{eV}$) ZrO_2 .

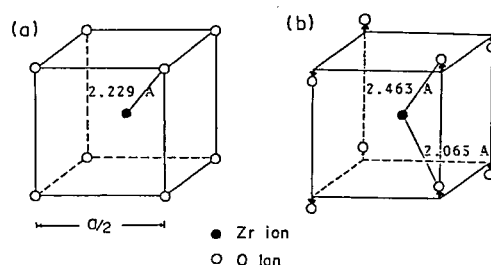


Figure 1. Cluster of $(\text{ZrO}_8)^{12-}$ used in the calculation of (a) cubic ZrO_2 and (b) tetragonal ZrO_2 . The magnitude of displacements of anions is from Teufer (*Acta Cryst.*, **19**, 486 (1962)).

The result 2) implies that the tetragonal ZrO_2 is more stable than the cubic one. The oxygen ions at a shorter Zr-O distance stabilize the tetragonal phase by making the covalent bonds with the Zr ions. The change in the magnitude of the energy gap may be another indicator for the higher stability of tetragonal phase than the cubic one. Relations between the change in the electronic structure and the stability of the cubic phase are discussed in full detail.

Reference

- 1) B. C. Weber, *J. Amer. Ceram. Soc.*, **45**, 614 (1962)

I—E Theory of Transition-Metal Surfaces and Interaction with Adparticles

Transition-metal surfaces are important for various fields of applications including catalyses, magnetic and electronic devices and ultra-high vacuum technology. It is needless to say that they are among the recent most attractive subjects for solid state physicists and quantum chemists. The presence of partially filled d band results in a wide variety of physical properties and chemical activities of these surfaces.

In this project clarification of the interplay between the electronic structure and the local atomic arrangement is aimed at. Investigations are also made into the way of the interaction of the transition-metal surfaces with adparticles. The subjects we studied in this year include the chemisorption of oxygen onto bcc transition-metal surfaces, under-layer type chemisorption of titanium and chemisorption on zinc surface.

I-E-1 Chemisorption of Oxygen Atom on bcc Metal Surfaces

Hirohiko ADACHI (*Osaka Univ.*) and Masaru TSUKADA

Recently many studies for chemisorption on transition metal surfaces, especially on fcc metal surfaces¹⁻³⁾ such as Ni, Pd and Pt have been performed. For chemisorption on bcc Fe and Cr surfaces, there have been few investigations reported both from experimental and theoretical view points. For bcc Mo and W surfaces, though various experimental works have been performed, surface electronic structure and chemisorption mechanisms have still been in question. In the present work, we investigate oxygen chemisorptions on bcc V, Cr, Fe and Mo surfaces. Figure 1 shows model cluster OMe_9 ($\text{Me} = \text{V}, \text{Cr}, \text{Fe}, \text{and Mo}$) used in the present calculation. We calculate chemisorptions for hollow site and on-top site of bcc(001) surfaces varying the oxygen position. The level structures for chemisorption on Vanadium surfaces are shown in Figure 2. For on-top-site chemisorption bonding levels due to interactions between O-2p and V-3d orbitals appear lower part of the d band, and are shifted downward when oxygen approaches the surface. The bonding levels are split off below d band for the hollow-site chemisorption. Similar level structures have been obtained for Cr and Fe surfaces. The adsorbed oxygen has negative ionicity both on the hollow and on-top sites.

In the on-top chemisorptions, strong interactions between O-2p_{x,y} and Me(2) orbitals take place. On the other hand, mixings of O-2p_{x,y,z} and Me(3) orbitals are predominant for the hollow site chemisorptions.

Reference

- 1) D. E. Ellis, H. Adachi and F. W. Averill, *Surface Sci.*, **58** 497 (1976).
- 2) H. Adachi, *J. Phys. Soc. Jpn.*, **47** 1903 (1979).
- 3) D. E. Ellis, E. J. Baerends, H. Adachi and F. W. Averill, *Surface Sci.*, **64** 649 (1977).

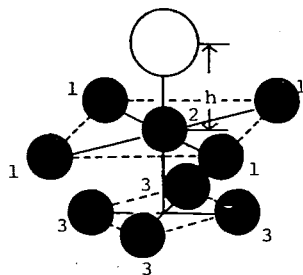


Figure 1. Structure of OMe_9 cluster for on-top chemisorption.

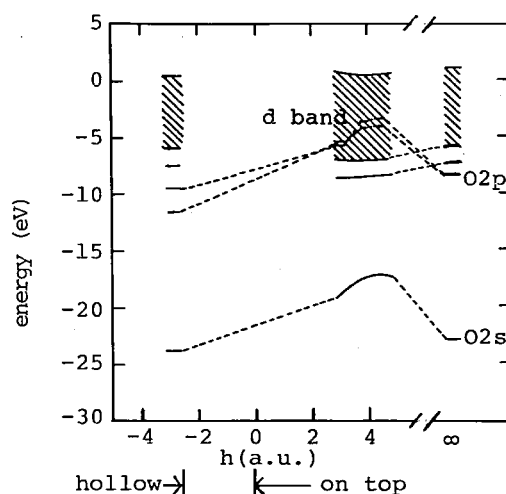


Figure 2. Level structure of OV_9 cluster.

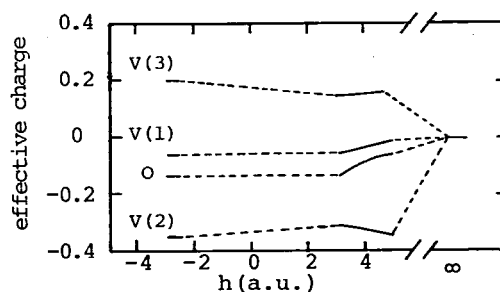


Figure 3. Effective charge of atoms in OV_9 cluster.

I-E-2 Electronic Structure of the Chemisorption System of Oxygen on the Mo (100) Surface

Masaru TSUKADA and Hirohiko ADACHI (*Osaka Univ.*)

The (100) surface of Mo, W shows a peculiar reconstructed structure due to the dangling bond like surface states locating close to the Fermi level.¹⁾ The purpose of this work is to investigate the special role of such surface states on the chemisorption of atoms and molecules onto the molybdenum surface. We have chosen the Mo/O system because of the abundance of experimental informations.

The DV- $X\alpha$ calculations are made for the clusters Mo_9 , $\text{O-Mo}_5\text{Mo}_4$, $\text{O-Mo}_4\text{Mo}_5$ modelled on the clean Mo (100) surface, on-top and hollow chemisorption, respectively. The calculated total density of states of Mo_9 resembles well with that by the band calculation of thin layer.²⁾ The change of the chemisorbed oxygen 2p levels with the distance h from the surface is shown in Figure 1 for both the

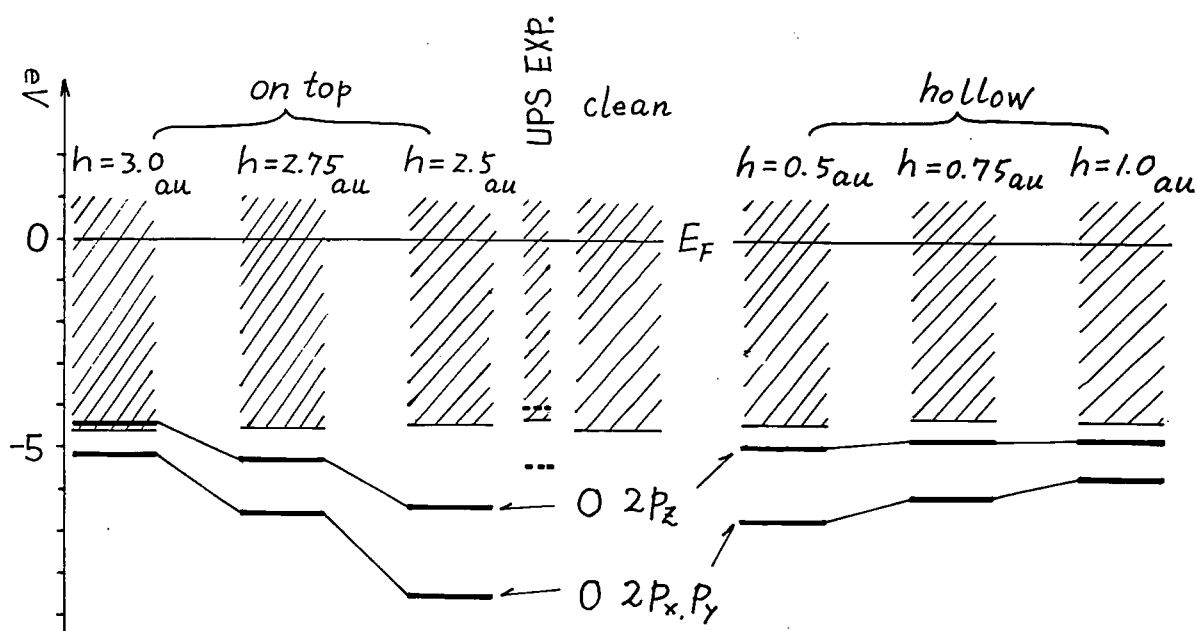


Figure 1. Level structures of Mo₉/O system.

on-top and the hollow type chemisorption. The shaded region in the figure represents the band region of the substrate. It is seen that the oxygen 2p level is considerably lowered when the distance from the surface decreases. For the on-top chemisorption with $h \approx 3.0$ a.u., one finds the oxygen level position nearly correspond to those obtained by UPS experiments.³⁾ For the hollow chemisorption with $h \approx 0.5 \sim 1.0$ a.u., the oxygen levels are located at too low positions to be compared with the experiment. Mulliken population analysis revealed that the oxygen net charge is about $-0.6|e|$, $-0.7 \sim -0.9|e|$ for the on top and the hollow site, respectively. The role of the dangling bonds on the chemisorption is now being studied.

References

- 1) I. Terakura, K. Terakura and N. Hamada, *J. Phys. Soc. Jpn.*, in press.
- 2) G. P. Kerker, K. M. Ho and M. L. Cohen, *Phys. Rev.*, **B18**, 5473 (1978).
- 3) S. L. Wang and E. W. Plummer, *Solid State Commun.*, **23**, 515 (1977)

I-E-3 Chemisorption of Oxygen Atoms on Zinc (0001) Surface by DV-X α Cluster Calculations

Eizo MIYAZAKI (Tokyo Inst. Techn.), Masaru TSUKADA and Hirohiko ADACHI (Osaka Univ.)

Zinc has an interesting character from the chemisorptive or catalytic view point; metallic zinc does not indicate any catalytic activity under

moderate reaction conditions, however, when it is oxidized, the activity is greatly enhanced. The DV-X α calculations have been performed varying the oxygen-surface distance h for Zn (0001). Figure 2 shows the valence levels of cluster Zn₄/O (Figure 1) for various h along with UPS spectrum. The calculated d-band width and the level of adsorbate oxygen 2p state are in good agreement with the experiment.¹⁾ We found that a large amount of electrons flow into the oxygen atom mainly from the nearest Zn atoms in the 1st layer. This electron transfer causes 1) remarkable upward shift (~ 2 eV) of the oxygen 2p level compared with the free atom state, and 2) creation of unoccupied level, which is mainly composed of the Zn-4s orbital of the top layer. There exists a maximum value in the bond order at $h = 2.8$ a.u. and the value of the total bond order shows similar trend in this region, suggesting the equilibrium distance between the adsorbed oxygen atom and the surface to be ~ 2.8 a.u. (See Figure 3).

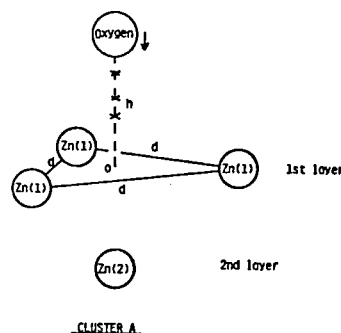


Figure 1. Structure of the model cluster Zn₄/O.

center. Namely it interacts with the N-2s state, forming widely separated bonding and antibonding level, i.e. the $9a_{1g}$, $15a_{1g}$ of Ti_6N (P_5) cluster. The charge deficiency from the unoccupied $15a_{1g}$ level may cause the elongation of Ti-Ti bond on the chemisorption process.

Reference

- 1) H. D. Shih, F. Jona, D. W. Jepsen and P. M. Marcus, *Phys. Rev. Lett.*, **36**, 789 (1976), *Surf. Sci.*, **60**, 445 (1976).
- 2) D. E. Eastman, *Solid State Commun.*, **10**, 933 (1972).
- 3) H. Adachi, M. Tsukada and C. Satoko, *J. Phys. Soc. Jpn.*, **45**, 875 (1978).

I—F Electronic Structure of Low Dimensional Materials

Recently a great deal of attention is concentrated on the development of new low-dimensional compounds with the practical importance. Typical example may be the search of one-dimensional metals or superconductors. Intercalated compounds of graphite or other layer crystals have attracted much interest from the view point of superconductivity, catalyses, batteries and photovoltaic cells.

Reliable first principle calculations of the electronic structure is essential for the study of the properties of these materials. In this year we performed the energy band calculation of polyacetylene, polyethylene and polydiacetylene. The DV- $X\alpha$ cluster calculation is also made for various intercalation compounds of graphite.

I-F-1 Self-consistent Electronic Band Structure of Polyacetylene and Polyethylene

Chikatoshi SATOKO and Masaru TSUKADA

One-dimensional organic conductor shows characteristic properties such as charge density wave, impurity-doped high conductivity, and Peierls transition. It has been uncertain whether these experimental properties can be understood on a one-electron band scheme. Band calculations for

the one-dimensional crystal have been made by several methods.³⁾ The results, however, were different among each other.

Our self-consistent results are presented in Figure 1 (a) and (b) for $cis-(CH)_x$ and $trans-(CH)_x$, respectively. The calculated band gaps of them agree well with the experimental values (1.17 eV and 0.8 eV), respectively. The lowest transitions for the $trans-(CH)_x$ are theoretically allowed by the optical polarization parallel to the axis. This polarization dependence has been observed in the reflection spectra.¹⁾

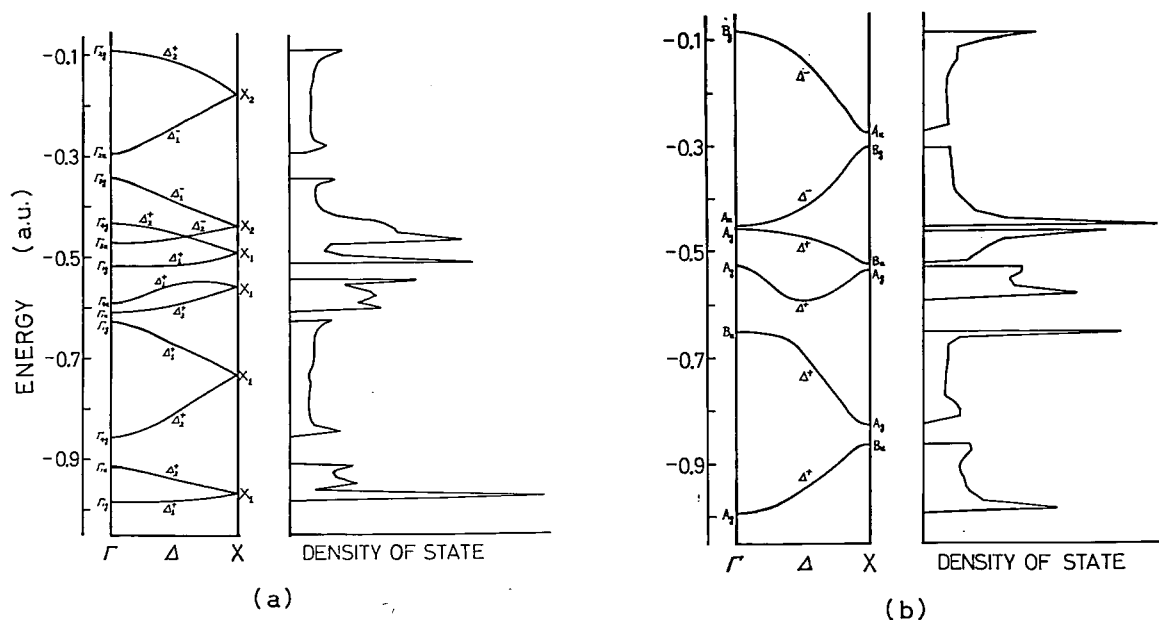


Figure 1. (a) Energy band of $cis-(CH)_x$. (b) Energy band of $trans-(CH)_x$.

X-ray photoemission spectra show a structure which is different from that of the density of states. This discrepancy occurs due to the small transition probability of C-2p electrons in the X-ray region. The XPS shows a good agreement with C-2s partial density of state.²⁾

In polyethylene the band gap between Γ_{3g} and Γ_{1u} states is ~ 10 eV which is larger than the observed value (8 eV). This may show the exciton formation in the excitation due to the small screening effect. The lowest transition allowed by the polarization perpendicular to the chain axis is consistent with the observed selection rule.

References

- 1) C. R. Fincher, Jr., D. L. Peebles, A. J. Heeger, M. A. Drug, Y. Matsumura, A. G. MacDiarmid, H. Shirakawa and S. Ikeda, *Solid State Commun.*, **27**, 489 (1978).
- 2) C. B. Duke, A. Paton, W. R. Salaneck, H. R. Thomas, E. W. Plummer and A. G. MacDiarmid, *Chem. Phys. Letters*, **59**, 146 (1978).
M. Tokumoto, to be published.
- 3) J. M. Andre, L. A. Burke, J. Delhalle, G. Nicolas, Ph. Durand, *Int. J. Quantum Chem. Symp.*, **13**, 283 (1979).
P. M. Grant and I. P. Batra, *Solid State Commun.*, **29**, 225 (1979).
J. E. Falk and R. J. Fleming, *J. Phys. C: Solid State Phys.*, **8**, 627 (1975).
M. Kertesz, J. Koller and A. Azman, *J. Chem. Phys.*, **67**, 1180 (1977).

I-F-2 The Electronic Structure Calculations of the Graphite Intercalation Compounds Based on the SCF-DV X α Cluster Model

Shuhei OHNISHI,* Masaru TSUKADA, Satoru SUGANO* (*Tokyo Univ.)

[Physica B, in press]

Self-consistent DV-X α calculations are performed for seven types of clusters, $C_{48}H_{24}A$, $C_{48}H_{24}A$ ($A = K, Li, Fe, Cl, Br, Br_2$) simulating graphite and its intercalation compounds. The cluster includes upto the third neighbor carbon atoms of a intercalant with attached H atoms to the outermost carbon atoms. The following results are obtained. 1) For $C_{48}H_{24}Li$ and $C_{48}H_{24}K$, the energy levels of Li-2s, 2p and K-4s, 4p orbitals lie far above E_F , so that alkali metals are fully ionized in graphite.¹⁾ 2) The peak of the Fe-3d states lies just below E_F and clings to it due to the large inter-layer separation of the transition-metal-graphite intercalation compounds.²⁾ 3) The calculated state density of the halide clusters are shown in Figure 1. In the figure, σ and π -bond peaks just below E_F are Cl-3p and Br-4p valence states, which are pinned at the Fermi level. The gross orbital populations indicated that the halide-intercalants are between neutral and monovalent in graphite. 4) In the Br_2 -intercalation cluster, the atomic 4s and 4p states of Br split into the σ and π bond orbitals with different energies. The Br_2 molecule in graphite is found to be neutral, consistent with the experimental results.³⁾ The position of 4p(σ) peak corresponds to that observed in XPS⁴⁾ within 5 eV below E_F .

References

- 1) D. Guerard, G. M. T. Foley, M. Zanini and J. E. Fischer,

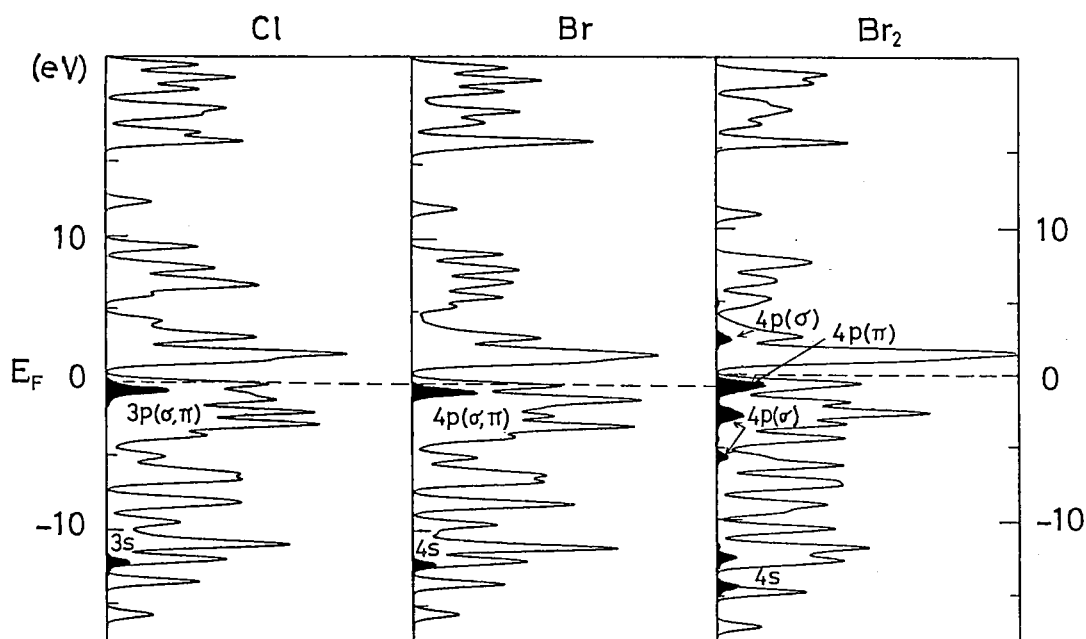


Figure 1. Calculated state densities for the clusters, $C_{48}H_{24}Cl$, $C_{48}H_{24}Br$, $C_{48}H_{24}Br_2$.

Nuovo Cimento, **38 B**, 410 (1977).

- 2) J. E. Fischer, *Comments on Solid State Phys.*, **9**, 93 (1979).
M. E. Vol'pin et al *J. Am. Chem. Soc.*, **97**, 3366 (1975).
- 3) D. A. Platts, D. D. L. Chung and M. S. Dresselhaus, *Phys.*

Rev., **B15**, 1087 (1977).

- 4) B. Bach, E. L. Evans, J. M. Thomas and M. Barer, *Chem. Phys. Lett.*, **10**, 547 (1971).

I—G Electron Theory of Semiconductor Surfaces

Physical and chemical properties of covalent semiconductor surfaces are quite different from those of metals or ionic crystals. Especially surface reconstruction is generally observed, which is closely related with the presence of the dangling bonds. Study of the surface atomic structure based on the electron theory is indispensable for the elucidation of the various properties of the covalent semiconductor surfaces. Moreover the chemisorption mechanisms are closely related with the electronic and the atomic structure of the surfaces.

Our attention is now mainly focussed on Si (111) 7×7 reconstructed surface. The DV- $X\alpha$ cluster theory has been proved successful to clarify the direct correlation between the characteristics in the electronic structure and the local atomic arrangement.

I-G-1 Self-consistent DV- $X\alpha$ Cluster Calculation of Electronic Structure on the Si(111) 7×7 Model Surface

Toshiharu HOSHINO, Masaru TSUKADA, Katsuhiko NAKAMURA (*Fukuoka Inst. of Tech.*), Shuhei OHNISHI* and Satoru SUGANO* (**Tokyo Univ.*)

[*J. Phys. Soc. Jpn.* in press]

The long-period reconstruction found in the Si (111) 7×7 surface has received much theoretical as well as experimental interest.¹⁾ Recently two promising models have been proposed. The first one is a low density vacancy model proposed by Ino.²⁾ This model explains quite well RHEED patterns and LEED-IV spectra.³⁾ The other model assumes the buckling of the surface plane. Chadi *et al*³⁾ proposed in their recent letter a buckled ring-like structure for the 7×7 surface, emphasizing the 2×1 -like electronic structure of this surface.

To obtain theoretical informations on the electronic structures for various reconstruction models of the Si (111) 7×7 surface, we adopted the first principle DV- $X\alpha$ cluster method. In the present work, we have used the surface cluster without a vacancy (A) $\text{Si}_{13}\text{H}_{15}$ and that with it (B) $\text{Si}_{12}\text{H}_{15}$ (Figure 1). Studies are made for unrelaxed, relaxed and reconstructed cases of these systems, respectively. Calculated spectra of both total and local densities (Figure 2) for various systems have been investigated in detail. We have concluded, from a comparison between our calculations and recent ultraviolet photoemission spectroscopy results,⁴⁾ that the presence of vacancies on the surface is essential to the reconstruction of the Si (111) 7×7 surface. The same calculations have been done in the cases of the clusters $\text{Si}_{16}\text{H}_{21}$ ($\text{Si}_{15}\text{H}_{21}$)

and $\text{Si}_{19}\text{H}_{21}$ ($\text{Si}_{18}\text{H}_{21}$). The qualitative results are not different from the one of $\text{Si}_{13}\text{H}_{15}$ ($\text{Si}_{12}\text{H}_{15}$).

Reference

- 1) J. J. Lander and J. Morrison, *J. Appl. Phys.*, **34**, 1403 (1963);
J. J. Lander, in *Progress in Solid State Chemistry*, ed. H. Reiss (Pergamon, Oxford 1965) Vol. 2, p. 26.
- 2) S. Ino, Japan. *J. Appl. Phys.*, **19**, L61 (1980).
- 3) D. J. Chadi et al, *Phys. Rev. Lett.*, **44**, 799 (1980).
- 4) F. Houzay (to be published).

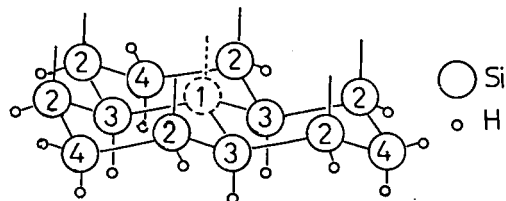


Figure 1. Surface cluster $\text{Si}_{13}\text{H}_{15}$ including Si (1) and $\text{Si}_{12}\text{H}_{15}$ without it.

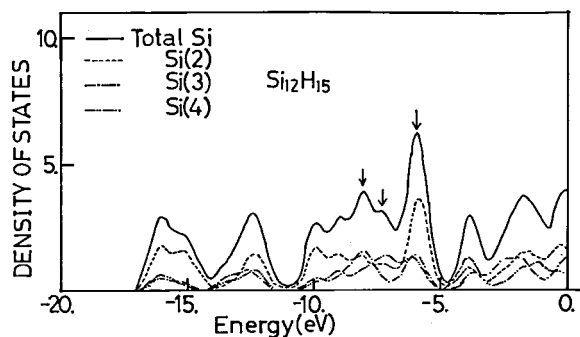


Figure 2. The total and local density of states for $\text{Si}_{12}\text{H}_{15}$ cluster simulating Si (111) 7×7 reconstructed surface. The Si (2) atoms in Figure 1 are lowered by 0.5 a.u. and the Si (3) atoms are displaced in the second layer toward the vacancy, keeping the bond length between Si (2) and Si (3) constant. The three peaks shown by arrows agree with those of recent UPS results [F. Houzay et al].

I-G-2 Electronic Structure of Chemisorption Systems: H and Cl Chemisorbed on Si (111) 7×7 Reconstructed Surface

Toshiharu HOSHINO and Masaru TSUKADA

Recently many ultraviolet photoemission spectroscopy (UPS) experiments have been made to investigate electronic structure of reconstructed semiconductor surfaces with chemisorbed overlayers of H, Cl, Ag and Au.¹⁾ On the other hand, there have not existed any theoretical investigations on these systems. It does hardly seem possible, at present, to calculate electronic structure of the chemisorption systems, incorporating both surface reconstruction and bulk effect.

We have successfully applied the DV- $X\alpha$ cluster method²⁾ to Si (111) 7×7 reconstructed surface. This has encouraged us to apply the method to chemisorption systems with surface reconstruction. In the present work, we made DV- $X\alpha$ cluster calculations to study electronic structure of Si (111) 7×7 surface with chemisorbed atoms of H and Cl. The used surface clusters are shown in Figure 1. The substrate is modelled by either $\text{Si}_{13}\text{H}_{15}$ or $\text{Si}_{12}\text{H}_{15}$ (vacancy cluster). The four kind of chemisorption sites (Figure 1) on these surfaces are investigated.

Calculated spectra (Figure 2) of H and Cl chemisorbed to site (A') and site (C) on Si (111) 7×7 vacancy cluster reproduces fairly well the results of recent UPS experiments. The further detailed analysis of our calculations is now in progress. We are planning to investigate the chemisorption systems of Ag and Au on Si (111).

References

- 1) T. Sakurai and H. D. Hagstrum, *Phys. Rev.*, **B 15**, 5349 (1975); J. E. Rowe, G. Margaritondo and S. B. Christman, *Phys. Rev.*, **B 15**, 1581 (1977); F. Wehking, H. Beckermann and R. Niedermayer, *Surf. Sci.*, **71**, 364 (1978); L. Braicovich, C. M. Garner, P. R. Skeath, C. Y. Su, P. W. Chye, I. Lindau and W. E. Spicer, *Phys. Rev.*, **B 20**, 5131 (1979).
- 2) K. Nakamura, T. Hoshino, M. Tsukada, S. Ohnishi and S. Sugano, to be published in *J. Phys. Soc. Jpn.* and to be submitted in *J. Phys. C*.

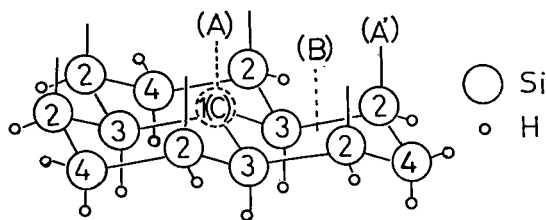


Figure 1. Substrate surface clusters, $\text{Si}_{13}\text{H}_{15}$ including Si (1) and $\text{Si}_{12}\text{H}_{15}$ without it, and the four chemisorption sites (A), (A'), (B) and (C) are shown.

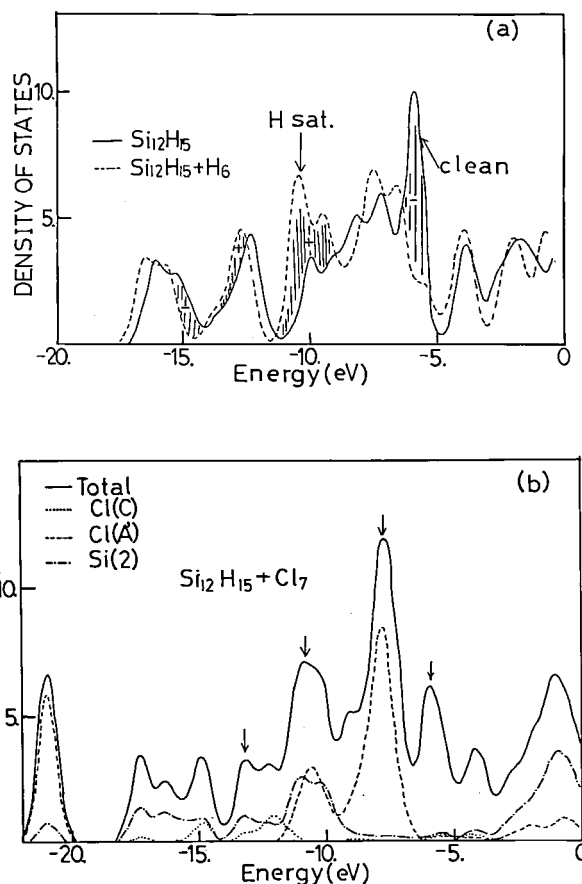


Figure 2. (a) The total density of states for Si (111) 7×7 reconstructed clean surface cluster $\text{Si}_{12}\text{H}_{15}$ and it with the atoms H chemisorbed to site (A'). (b) The total and local density of states for Si (111) 7×7 reconstructed surface cluster $\text{Si}_{12}\text{H}_{15}$ with the Cl atoms chemisorbed to site (A') and (C). Our calculations reproduce main features of ultraviolet photoemission spectroscopy made recently by Sakurai and Hagstrum, and by Rowe, Margaritondo and Christman.

I-G-3 Chemical Pseudopotential Theory of Surface Reconstruction and Chemisorption

Toshiharu HOSHINO, Katuhisa SUZUKI (Osaka Univ.) and Masaru TSUKADA

Since Harrison's bond theory¹⁾ determining surface reconstructions at semiconductor surfaces from energy minimum principles, several theories²⁾ have been presented which aim at accounting for every detail of LEED and photoemission spectra. These theories involve either a couple of four constant parameters or a few scaling functions for interaction. Therefore, the obtained results depend always on the parameters used in the work.

On the other hand, Bullett et al.³⁾ and the authors⁴⁾ have successfully applied the chemical pseudopotential (CCP)⁵⁾ method to the bulk band

structure, the bulk moduli and the imperfections of covalent semiconductors. The electronic structure of ideal and relaxed (but not reconstructed) silicon surfaces was discussed by Casula, Ossicini and Selloni⁶⁾ in this method. The CPP method is based on first principles and requires no external parameters. It is a local theory that fits to the chemical bond concept. In addition self-consistency is in principles built in.

We have applied the CPP method to the problem of determining surface reconstruction in the simplest version. Numerical calculations on two surfaces of silicon, Si (111) 2×1 and Si (001) 2×1 , were carried out.⁷⁾ Simple models (Figure 1) for these surfaces of silicon lead to a reconstruction in agreement with current pictures (Table I). Application of the present method is now studied to various problems including the formation energy of surface vacancy and determining chemisorption geometry on semiconductor surfaces.

References

- 1) W. A. Harrison, *Surf. Sci.*, **55**, 1 (1976).
- 2) J. A. Appelbaum and D. R. Hamann, *Surf. Sci.*, **55**, 1 (1976); D. J. Chadi, *Phys. Rev. Lett.*, **41**, 1062 (1978); **43**, 43 (1979); *Phys. Rev.*, **B 19**, 2074 (1979).
- 3) D. W. Bullet, *J. Phys. C (GB)*, **8**, 2695 (1975); **8**, 2707 (1975).
- 4) T. Hoshino and K. Suzuki, *J. Phys. Soc. Jpn.*, **47**, 1141 (1979); **48**, 2031 (1980).
- 5) P. W. Anderson, *Phys. Rev.*, **181**, 25 (1969).
- 6) F. Casula, S. Ossicini and A. Selloni, *Solid State Commun.*, **30**, 309 (1979).
- 7) K. Suzuki and T. Hoshino, to be published in *J. Phys. Soc. Jpn.*
- 8) A. Taloni and d. Haneman, *Surf. Sci.*, **10**, 215 (1968).
- 9) K. C. Pandey and J. C. Phillips, *Phys. Rev. Lett.*, **34**, 1450 (1975).
- 10) M. Schlüter, J. R. Chelikowsky, S. G. Louie and M. L. Cohen, *Phys. Rev.*, **B 12**, 4200 (1975).

- 11) J. A. Appelbaum and D. R. Hamann, *Phys. Rev.*, **B 12**, 1410 (1975).

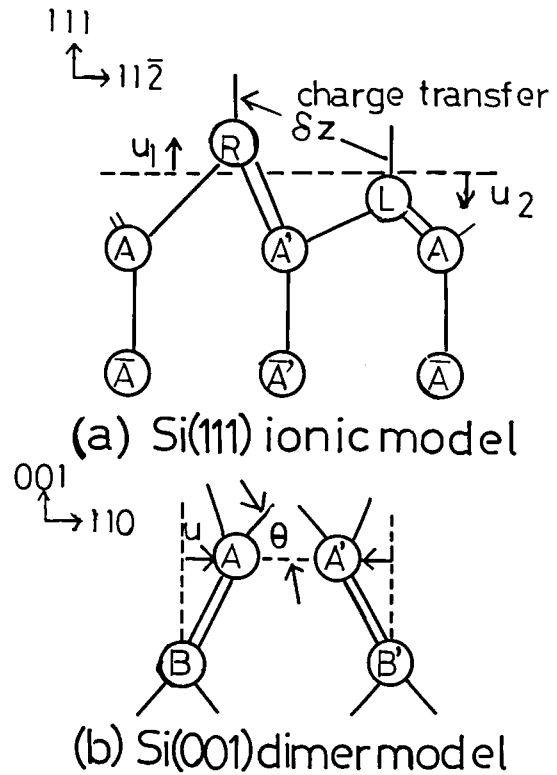


Figure 1. Reconstruction models for Si surfaces: (a) alternate rows of surface atoms are subjected to vertical displacements u_1 and u_2 , with accompanying charge transfer δz from the lowered atom L to the raised atom R. (b) the surface atom has two back bonds and two dangling bonds. The direction θ of one of its dangling bonds and the atom's parallel displacement u can be taken as independent variables.

Table I. Displacements in A of the first layer atoms in the (2×1) reconstruction at the (111) and (001) surfaces of silicon, either assumed or determined. The primed and unprimed displacements correspond to the two inequivalent atoms in the surface unit cell, and z and z' are perpendicular to the surface.

(111)	Authors			z	z'
	Suzuki and Hoshino [7]			0.47	-0.42
	Taloni and Haneman [8]			0.13	-0.11
	Pandey and Phillips [9]			0.35	-0.29
	Schlüter, Chelikowsky, Louie and Cohen [10]			0.18	-0.11
	Appelbaum and Hamann [11]			0.16	-0.35
	Harrison [1]			0.78	-0.78
	Chadi [2]			0.31	-0.44
(001)	Authors	x	x'	z	z'
	Suzuki and Hoshino [7]	0.42	-0.42	0	0
	Appelbaum and Hamann [2]	0.69	-0.69	0.09	0.09
	Chadi [2]	0.46	-0.18	0.04	-0.44

I—H Development of Density Functional Approaches for the Potential Energy Surface

Reliable first principle calculations of the Born-Oppenheimer adiabatic potential surface are most important for the studies of various problems such as the determination of structure of solid surface, chemisorption geometry, defect formation in the bulk and the surface and numerous elementary chemical processes on solid surfaces. Development of a trustworthy numerical method feasible to large clusters and infinite systems is the main target of our effort in these years. Considerable progress in the calculational technics has been made in this year.

I-H-1 Density Functional Approach to the Total Energies of Molecules, Surface and Bulk Systems

Chikatoshi SATOKO and Masaru TSUKADA

In the electron gas model proposed by Gordon and Kim,¹⁾ interaction potentials were calculated using the sum of the electron densities of individual atoms. However, they didn't perform the variation of electron densities. So we calculate the binding energy of molecules to give the minimum of the density functional. The kinetic and correlation energies are calculated using the Gaussian quadrature integration over each Wigner-Seitz cell²⁾ and the other terms are analytically integrated.

The results of the total energy are shown in Figure 1 for alkali chlorides, KCl and NaCl. In the figure zero points of the energy are taken as the sum of the total energy of the dissociated neutral atoms. We also calculated the potential curve for KCl using the Gordon-Kim approximation, shown with the dotted line in Figure 1. The equilibrium bond distance is near the experimental value, but the binding energy is negative. This is due to the overestimate of the kinetic energy change from neutral K to cation K^+ or from anion Cl^- to neutral Cl. We scale the Thomas-Fermi energy terms to get the correct ionization energy and electron affinity. The scaled values are 1.200 for K, 1.131 for Na, and 0.797 for Cl. The Weizsacker terms are taken as zero. The scaled potential curves are shown by the solid lines in Figure 1. The equivalent bond distance and bond energy show the good agreements with the experiments.

The scaled values of the Thomas-Fermi term for MgO are 1.143 for Mg and 0.895 for O. These values give a longer equivalent bond distance than the experimental value. We choose the Weizsacker term as $Cw = 0.006$ for Mg, $Cw = 0.01$ for O. The orbital populations near the equivalent bond distance are $Mg^{+0.6}(3s)^{1.4}O^{-0.6}(3p)^{4.6}$.

There is another method in which we solve the

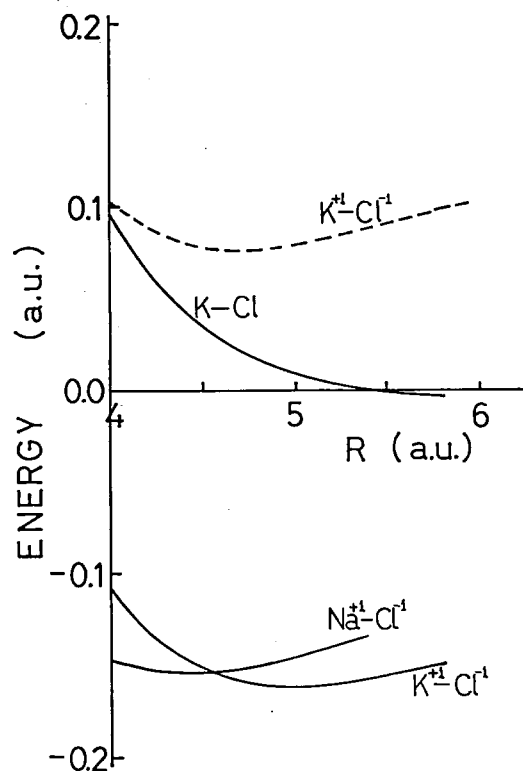


Figure 1. Potentials for KCl and NaCl. Dotted line is from Gordon-Kim model. Full lines are from the modified model.

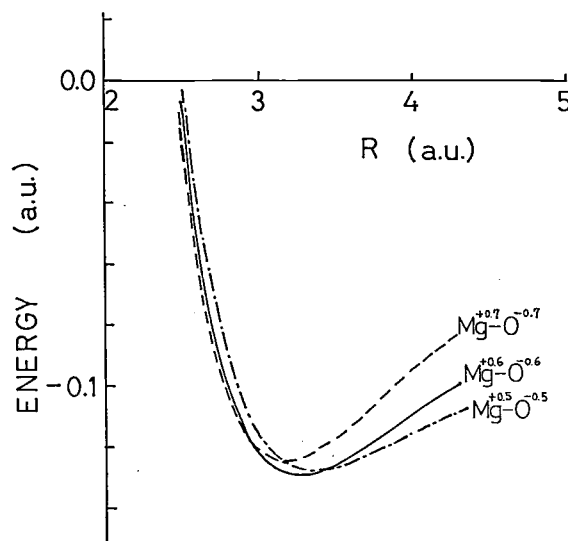


Figure 2. Potentials for MgO.

eigen-function of the HFS one-electron equation self-consistently and calculate the total energies using the electron densities of this solution.³⁾ We are now in progress.

References

- 1) Marvin Waldman and Roy G. Gordon, *J. Chem. Phys.*, **71**, 1 (1979).
- 2) H. Gollish and L. Fritsche, *Z. Physik*, **B 33**, 11 (1979).
- 3) Tom Ziegler and Arvi Rauk, *Theoret. Chim. Acta (Berl.)* **46**, 1 (1977).

I—I The Analysis of the Electron Distribution in Molecules

The ab initio method is a quantitative technique in nature. Besides, it can provide the qualitative picture of the chemical bonds and of the electron distribution in molecules. In addition to the traditional ways such as the Mulliken population analysis and the electron density map, a new method to see the electron distribution in molecules is developed. The change of the electron distribution around an atom in molecules with the oxidation numbers and with the excited states is examined.

I-I-1 The Electron Density Analysis and the Oxidation Number. I. Some Sulphur and Chlorine Compounds.

Suehiro IWATA¹⁾ (*Inst. Phys. Chem. Res. and IMS*), and Keiko YAMADA and Haruo HOSOYA (*Ochanomizu Univ.*)

The number of electrons in a sphere with radius R at a center (C) and the averaged electron density in the sphere are proved to be easily computed without any numerical integration.²⁾ In order to extend the coding to including the d type function, a simpler method to derive the analytical expression was found. The number of electrons in a sphere is defined as

$$N(l, m, n, \mathbf{P}; R, C)$$

$$= \int_0^{2\pi} d\phi \int_0^\pi \sin \theta d\theta \int_0^R r^2 dr \rho(l, m, n, \mathbf{P}; r)$$

where the electron density ρ is assumed to be given in terms of gaussian type function (GTF):

$$\rho(l, m, n, \mathbf{P}; r)$$

$$= (x - P_x)^l (y - P_y)^m (z - P_z)^n$$

$$\exp \left\{ -\alpha (r - \mathbf{P})^2 \right\}.$$

After some manipulation, the recurrence formula,

$$N(l, m, n, \mathbf{P})$$

$$= 1/(2\alpha) [(l-1) N(l-2, m, n, \mathbf{P})$$

$$+ (\partial/\partial P_x) N(l-1, m, n, \mathbf{P})],$$

can be derived.

The electron distribution of two series of molecules were studied:

- (1) H_2S , H_2S_2 , S_2F_2 , FS_2F , S_2O_2 , SF_2 , SO_2 , SF_4 , and SO_3 .
- (2) HCl , HOCl , Cl_2O , ClFO_2 , ClF_3 , ClFO_3 , HClO_4 .

They are listed as increasing the oxidation number of sulphur and chlorine. Two basis sets, STO-6G and 4-31G, were examined. In Figure 1, the density difference from free atoms are shown for STO-6G calculations.

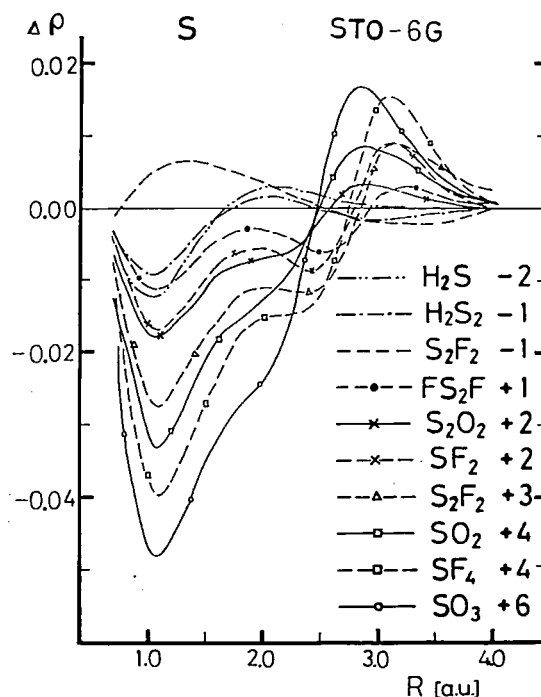


Figure 1. The difference of the spherically averaged electron density between molecules and free atoms.

References

- 1) IMS Adjunct Associate Professor for 1979 — 1980.
- 2) S. Iwata, *Chem. Phys. Letters*, **69**, 305 (1980).

I—J Theoretical Study of Molecular Photoionization and Molecular Inner Shell Excitation

The photoabsorption spectra of molecules in the soft X-ray and X-ray energy region are theoretically studied. The so-called discrete shape resonance and Rydberg series lying below the inner shell ionization threshold (I_p) and the strong resonance embedded in the continuum above I_p are discussed. The ab initio method based on the square integrable basis set is used both for the discrete and continuum spectra.

I-J-1 The Boron K Absorption Spectra of BF_3 , BCl_3 , and BBr_3 .

Suehiro IWATA¹⁾ (*Inst. Phys. Chem. Res. and IMS*), Eiji ISHIGURO (*Osaka City Univ.*), Yoshio SUZUKI, Akira MIKUNI, and Taizo SASAKI (*Univ. of Tokyo*)

In the molecular electronic spectra of the inner shell region the strong and sharp bands below I_p and the broad and intense structures in the continuum above I_p are often observed simultaneously. The B K spectra of BF_3 are one of such examples. Using the synchrotron radiation from SOR-RING at ISSP, Univ. of Tokyo, the B K spectra of BF_3 , BCl_3 , and BBr_3 were observed with the almost same accuracy in terms of energy and cross section. The spectra are given in Figure 1 along with the theoretical spectra for BF_3 . In the figure the B K ionization threshold (I_p) are shown, which are independently determined by XPS. Below I_p both spectra of BCl_3 and BBr_3 are almost identical. The bands of BCl_3 above I_p (B K) are Rydberg series converging to the $L_{2,3}$ of Cl. The ab initio calculations with extensive basis sets were performed for BF_3 and BCl_3 . The Hole SCF — Hole Potential (IVO) method was applied to evaluating the term values and the transition probabilities. The results are summarized in Table I. To construct the continuum spectra the Stieltjes procedure was used. The assignment is given in the table. In three B K spectra, the band a is the $1s$ to the non-bonding π excitation. In BCl_3 and BBr_3 the $1s$ to the valence anti-bonding σ^* excitation is lying below I_p and is assigned to d and d', while the same excitation in BF_3 is embedded in the continuum and is broadened as the band e.

References

- 1) IMS Adjunct Associate Professor for 1979 — 1980.

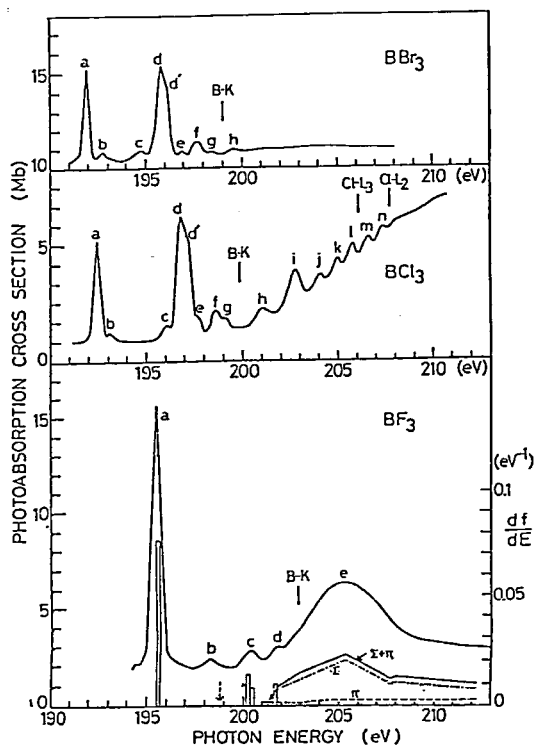


Figure 1. Experimental Photoabsorption Spectra of BF_3 , BCl_3 , and BBr_3 , and theoretical spectra of BF_3 .

Table I. Theoretical and Experimental Term Values of BF_3 and BCl_3 .

	Experimental		Calculated		
	Energy	Term Value	Term Value	Trans. Dipole	Assign.
BF_3					
a	195.50ev	7.30ev	7.22ev	0.078A	$2p\pi(a_2')$
b	198.24	4.56	4.01	forbidden	3s (a_1')
c	200.30	2.50	{ 2.50 2.27	0.014 0.004	3p (a_2') 3p (e')
d	201.7	1.08	{ 1.19 1.12	0.005 0.005	4p (a_2') 4p (e')
e	205.1	-2.3	-4.45	0.058	$2p\sigma^*(e')$
BCl_3					
a	192.43	7.37	7.04	0.076	$2p\pi(a_2')$
b	193.1	6.7			?
c	196.1	3.7	3.04	forbidden	3s (a_1')
d	196.87	2.93	0.63	0.040	$2p\sigma^*(e')$
e	197.6	2.2	{ 2.09 2.02	0.003 0.009	3p (a_2') 3p (e')
f	198.69	1.11	{ 1.11	0.000	4p (a_2')
g	199.0	0.8	{ 1.07	0.018	4p (e')

RESEARCH ACTIVITIES II

Division of Molecular Structure

II—A High Resolution Spectroscopy of Transient Molecular Species

The open-shell electronic structure characterizes most unstable species as free radicals, and causes additional complexities in their high-resolution spectra which are ascribed to fine structure and hyperfine structure interactions of unpaired electrons. Analyses of these structures provide us with information on the electronic properties of the molecules which is not obtainable for molecules without unpaired electrons. High resolution spectroscopy not only provides molecular constants at very high precision, but also allows us to unambiguously identify transient species in chemical reaction systems and to unravel the details of reaction mechanisms. Besides these fundamental implications in the fields of molecular science and chemical reaction, the present project will be of significance in related fields such as astrophysics and environmental researches.

II-A-1 Microwave Spectroscopy of HSO and DSO

Yasuki ENDO, Shuji SAITO, and Eizi HIROTA

We have recently carried out dye laser excitation spectroscopy on HSO¹⁾ and DSO²⁾; the radical has been assumed as an intermediate in chemical reactions involving both sulfur and oxygen, but its structure, or even its existence has not been elucidated unambiguously. Our molecular constants obtained from dye laser spectroscopy have allowed us to observe microwave spectra of these

species in the ground electronic state. Although one of the centrifugal distortion constants Δ_K could not be determined, other molecular constants were very much improved in precision, as shown in Table I. The hyperfine structures were well resolved for HSO, and the Fermi and dipole-dipole constants were well determined, as listed in Table II. In contrast, the resolution was insufficient for DSO. The $3_{12} \leftarrow 2_{11}$, $J = 3.5 \leftarrow 2.5$ transition, shown in Figure 1, is an exception, which was found widely split, by the interactions of 3_{12} and 2_{11} , respectively, with 4_{04} and 3_{03} through the off-diagonal term ($\epsilon_{ab} + \epsilon_{ba}$) of the spin-rotation coupling. The off-diagonal

Table I. Rotational, Centrifugal Distortion, and Spin-Rotation Coupling Constants of HSO and DSO (MHz)^a

Constant	HSO		DSO	
	Present	Ref. 1)	Present	Ref. 2)
A	299 484.63 (49)	299 478 (20)	158 726.938 (71)	158 750 (18)
B	20 504.56 (59)	20 504.4 (17)	19 836.533 (89)	19 836.2 (28)
C	19 133.93 (58)	19 135.6 (17)	17 570.206 (87)	17 573.6 (26)
Δ_N	0.030 70 (52)	0.031 8 (25)	0.026 46 (31)	0.028 1 (41)
Δ_{NK}	0.896 0 (26)	0.857 (58)	0.669 8 (13)	0.847 (55)
Δ_K	27.2 ^b	27.2 (20)	8.9 ^b	8.9 (10)
δ_N	0.001 93 (22)	0.002 02 (56)	0.003 23 (23)	0.001 92 (84)
δ_K	0.89 (29)	0.45 (38)	0.558 (42)	-0.15 (20)
ϵ_{aa}	-10 365.99 (55)	-10 292 (64)	-5 646.83 (42)	-5 668 (101)
ϵ_{bb}	-426.7 (11)	-433 (32)	-393.997 (37)	-347 (38)
ϵ_{cc}	0.23 (16)	-5 (32)	0.053 (56)	51 (36)
$ \epsilon_{ab} + \epsilon_{ba} /2$	378.0 (27)		322.667 (78)	
Δ_{NK}^s	0.038 (43)			
Δ_K^s	2.95 (12)		0.67 (10)	

^a Values in parentheses denote 2.5 times standard errors and apply to the last digits of constants.

^b Fixed.

element of the dipole-dipole tensor term, T_{ab} , was determined to be $-1.2(3)$ MHz from an analysis of the transition, where the diagonal terms were calculated from the HSO constants. The minus sign of T_{ab} means that it is opposite in sign to the $(\epsilon_{ab} + \epsilon_{ba})/2$ constant. The hyperfine constants of Table II clearly indicate that the HSO radical has the A'' ground state.

References

- 1) M. Kakimoto, S. Saito, and E. Hirota, *J. Mol. Spectrosc.* **80**, 334 (1980).
- 2) N. Ohashi, M. Kakimoto, S. Saito, and E. Hirota, *J. Mol. Spectrosc.*, in press.

Table II. Hyperfine Coupling Constants of HSO and DSO (MHz)^a

Constant	HSO	DSO
σ	$-36.37(142)$	-5.58^b
T_{aa}	$-11.96(24)$	-1.84^b
T_{bb}	$10.44(38)$	1.60^b
$ T_{ab} $	$(-)\ 7.8^{c,d}$	$(-)\ 1.2(3)^c$

^a Values in parentheses denote 2.5 times standard errors and apply to the last digits of constants.

^b Calculated from the HSO constants without corrections for axis rotation on isotopic substitution.

^c The minus sign means that T_{ab} is opposite in sign to $(\epsilon_{ab} + \epsilon_{ba})$.

^d Calculated from the DSO constant and fixed in the least-squares analysis for HSO.

DSO

$3_{12}-2_{11}$ 35-2.5

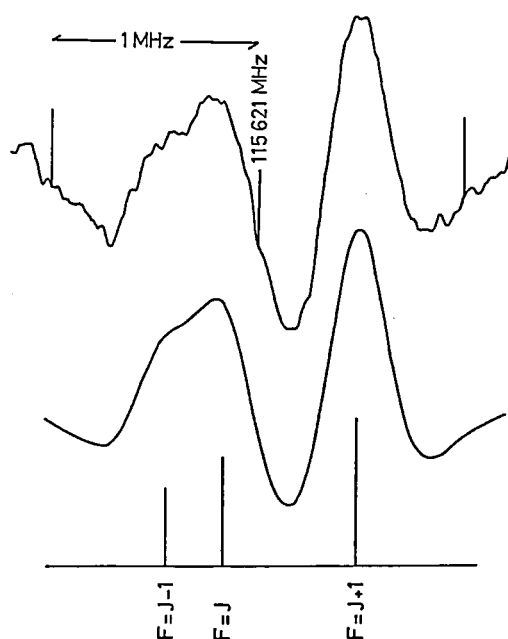


Figure 1. The $3_{12} - 2_{11}$, $J = 3.5 - 2.5$ transition of DSO.

II-A-2 Vibronic Interactions between \tilde{A} and \tilde{X} via the ν_3 Mode in BO_2

Kentarou KAWAGUCHI, Eizi HIROTA, and Chikashi YAMADA

We have recently carried out high-resolution diode laser spectroscopy of BO_2 , which has revealed an interesting problem.¹⁾ The ν_3 fundamental band we observed is located at 1278.2590 cm^{-1} , which is much smaller than half of $2\nu_3$ (2640.6 cm^{-1}) obtained by Johns²⁾ from electronic spectra. We explain this observation by a vibronic interaction between $\tilde{A}^2\Pi_u$ and $\tilde{X}^2\Pi_g$. The two states may interact with each other through excitation of the ν_3 or the antisymmetric stretching mode. As a simplest form we may assume the interaction Hamiltonian as follows:

$$H' = h'x_3 \quad (1)$$

where h' has a matrix element between \tilde{A} and \tilde{X} , given by

$$a = \langle \tilde{A} | h' | \tilde{X} \rangle, \quad (2)$$

and x_3 denotes an internal coordinate corresponding to the ν_3 mode. The effective potential functions for the ν_3 modes in \tilde{A} and \tilde{X} are given by

$$V(\tilde{A}/\tilde{X}) = \frac{1}{2} kx_3^2 + \frac{1}{2} \Delta E \pm \frac{1}{2} (\Delta E^2 + 4a^2x_3^2)^{1/2}, \quad (3)$$

where k is the harmonic force constant and ΔE the unperturbed energy difference between \tilde{A} and \tilde{X} . By using our value of $\tilde{\nu}(\nu = 1 \leftarrow 0)$ and Russell et al.'s value³⁾ of $\tilde{\nu}(\nu = 2 \leftarrow 0)$, we obtained $k = 9.01\text{ md/\AA}$ and $2a^2/\Delta E = 5.62\text{ md/\AA}$, where corrections were made for vibrational anharmonicities. These results account for the vibrational frequency in the \tilde{A} and \tilde{X} states are drawn in Figure 1.

References

- 1) K. Kawaguchi, E. Hirota, and C. Yamada, to be published.
- 2) J. W. C. Johns, *Canad. J. Phys.* **39**, 1738 (1961).
- 3) D. K. Russell, M. Kroll, and R. A. Beaudet, *J. Chem. Phys.* **66**, 1999 (1977).

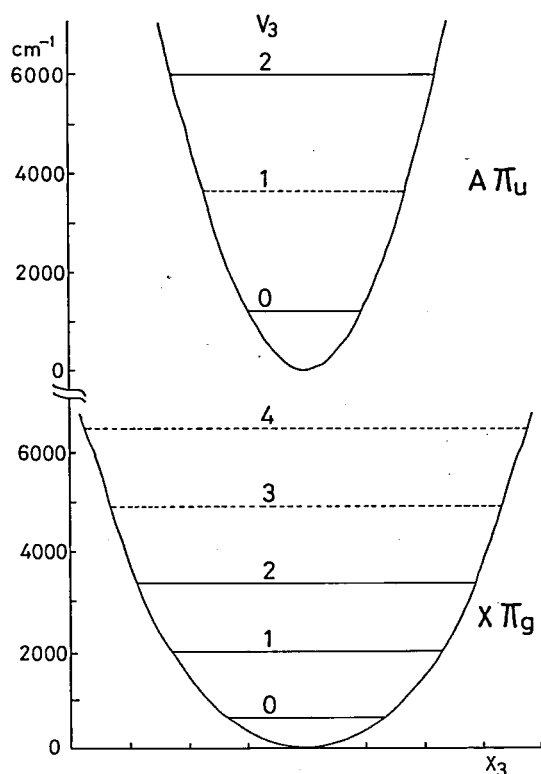


Figure 1. Potential functions for the ν_3 mode of BO_2 in the $\tilde{A}^2\Pi_u$ (upper trace) and $\tilde{X}^2\Pi_g$ (lower trace) states.

II-A-3 Perturbations in the \tilde{A} State of HCCl

Eizi HIROTA, Masao KAKIMOTO, and Shuji SAITO

The $\tilde{A}^1A''(050) - \tilde{X}^1A'(000)$ band of HCCl was recorded with Doppler-limited resolution by observing fluorescence excited by a dye laser. The observed branches are pP_1 , pQ_1 , and pR_1 which satisfy c-type selection rules. In addition to these, axis-switching induces two more branches, qQ_0 and oR_2 . The assignment was made by taking ground-state combination differences. Only $J_{0,J}$ levels were thus detected for the upper vibronic levels. As noted by Meter and Travis¹⁾, the series of levels are perturbed drastically at $J = 8$ to 10 . The effect is largest for $J = 9$; lines terminating at this level were all found split into two with nearly equal intensities. Weak satellites were observed also for transitions with $J' = 8$ or 10 . Figure 1 shows the observed term values of the upper vibronic state, plotted versus $J(J+1)$. It is apparent that a perturbing series approaches $J_{0,J}$ from the higher frequency side, crosses the latter near $J = 9$, and goes to lower frequencies with increasing J .

There are three explanations for the

perturbation. The first is vibration-rotation interactions within the manifold of the \tilde{A} state. However, this mechanism fails to explain the Zeeman effects (~ 0.15 MHz/G) observed for transitions with $J' = 9$. The second one may be called an electronic Coriolis interaction with a high vibrational state associated with the ground electronic state. A matrix element of the orbital angular momentum which was calculated from the zero-field spectra did not reproduce the observed Zeeman effects, which required a much larger value for the matrix element. Furthermore, at higher magnetic fields (larger than 10 kG or so) the Zeeman effects of $J' = 9$ lines deviate considerably from the first order. These observations cannot be explained by pair-wise interactions of two levels. On the other hand, the last mechanism, the singlet-triplet interaction, seems to be more reasonable.

Reference

- 1) A. J. Merer and D. N. Travis, *Canad. J. Phys.* **44**, 525 (1966).

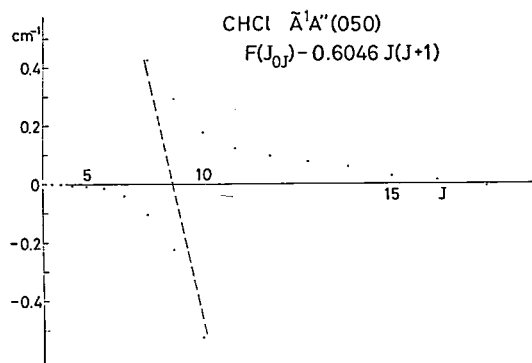


Figure 1. Term values of HCCl $\tilde{A}^1A''(050)$ $J_{0,J}$ levels versus $J(J+1)$. A term $0.6046 J(J+1)$ cm^{-1} has been subtracted for ease of drawing. A broken line shows the perturbing series of levels qualitatively.

II-A-4 Dye Laser Excitation Spectroscopy of Deuterated Fluorocarbene DCF

Tetsuo SUZUKI and Shuji SAITO

It is well recognized that carbenes in singlet states behave quite differently from those in triplet states in chemical reactions they participate. The fluorocarbene molecule is one of the simplest carbenes which have singlet ground states, in contrast to the parent carbene CH_2 , but its triplet states have not been detected. We have recently investigated the HCF molecule by dye laser excitation spectroscopy and evaluated the

rotational and centrifugal distortion constants precisely.¹⁾ From our experience on HCCI, we had expected to find a clue to triplet states through the observations of a singlet-singlet transition. However, the $\tilde{A}^1A''(000) - \tilde{X}^1A'(000)$ band of HCF we observed did not show any large perturbations, although a few perturbed lines did show very weak Zeeman effects. To obtain more information we investigated the same band of DCF by dye laser excitation spectroscopy. The previous study of Meter and Travis²⁾ using conventional high-resolution spectroscopy is limited to the parent species HCF, and no other high-resolution works have been reported. We have scanned in a region from 17200 to 17400 cm^{-1} . The analysis is being carried out, and is expected to provide information not only on the lowest triplet state but also on molecular structure.

References

- 1) M. Kakimoto, S. Saito, and E. Hirota, to be published.
- 2) A. J. Meter and D. N. Travis, *Canad. J. Phys.* **44**, 1541 (1966).

II-A-5 Microwave Optical Double Resonance of HNO: Rotational Spectrum in \tilde{A}^1A'' (100)

Kojiro TAKAGI (*Toyama Univ.*), Shuji SAITO, Masao KAKIMOTO, and Eizi HIROTA

Although the ground state is a single state, the HNO molecule has attracted much attention, because of its important role as an intermediate in chemical reactions involving nitrogen and oxygen. Many spectroscopic works have already been published on this molecule, which cover wide wavelength regions from microwave (or rf) to ultraviolet. However, still our knowledge on excited electronic states of HNO is rather limited, and in the present work we attempted to determine rotational energy levels in a few low-lying vibrational states associated with the \tilde{A} state, by using the microwave-optical double resonance (MODR) technique.

We generated the HNO molecule by the reaction of discharged oxygen with a mixture of propylene and NO at a total pressure of 10 to 20 mTorr. The $\tilde{A}-\tilde{X}$ electronic transition was excited by a dye laser (CR 599-21), whereas rotational transitions within the $\tilde{A}^1A''(100)$ state were pumped by either rf (0-1000 MHz) or microwave (7.8 - 157 GHz) radiation. The double-resonance signal was observed as a change in the fluorescence intensity upon irradiation of rf or microwave. We thus

observed 14 a-type and 4 b-type transitions, as listed in Table I. Figure 1 shows the observed $K_{-1} = 1$ K-type doubling frequencies divided by $J(J+1)$. This clearly indicates the presence of perturbations, particularly for $J = 3$ and 4, which could not be detected by conventional electronic spectroscopy. In spite of these perturbations we could improve molecular constants of HNO in the \tilde{A} state. We are extending a similar measurement to the (020) level to trace the origin of the perturbations.

Table I. Observed Rotational Transitions of HNO in $\tilde{A}^1A''(100)$

Rotational transition	Observed frequency (MHz)	Pumped optical transition
a-type $1_{01} - 0_{00}$	75 919.03 (7)	$^3P_1(1), ^3Q_1(1)$
$2_{02} - 1_{01}$	153 827.90 (30)	$^3Q_1(2)$
$2_{11} - 1_{10}$	156 305.49 (30)	$^3R_0(1)$
$2_{12} - 1_{11}$	151 050.96 (30)	$^3Q_0(1)$
$2_{11} - 2_{12}$	7 883.37 (10)	$^3Q_0(2)$
$3_{12} - 3_{13}$	15 707.41 (15)	$^3Q_0(3)$
$4_{13} - 4_{14}$	26 306.19 (10)	$^3Q_0(4)$
$5_{14} - 5_{15}$	39 256.52 (10)	$^3Q_0(5)$
$6_{15} - 6_{16}$	54 931.10 (15)	$^3Q_0(6)$
$7_{16} - 7_{17}$	73 022.9 (1)	$^3Q_0(7)$
$3_{21} - 3_{22}$	13.82 (2)	$^3Q_1(3)$ lower
$5_{23} - 5_{24}$	11.12 (8)	$^3Q_1(5)$ upper
$6_{24} - 6_{25}$	192.09 (8)	$^3Q_1(6)$ upper
$7_{25} - 7_{26}$	856.81 (5)	$^3Q_1(7)$ upper
b-type $5_{15} - 6_{06}$	101 043.48 (20)	$^3P_1(7), ^3Q_0(5)$
$6_{16} - 7_{07}$	16 250.13 (8)	$^3Q_0(6)$
$8_{08} - 7_{17}$	69 666.38 (3)	$^3Q_0(7)$
$9_{09} - 8_{18}$	156 352.88 (20)	$^3Q_0(8)$

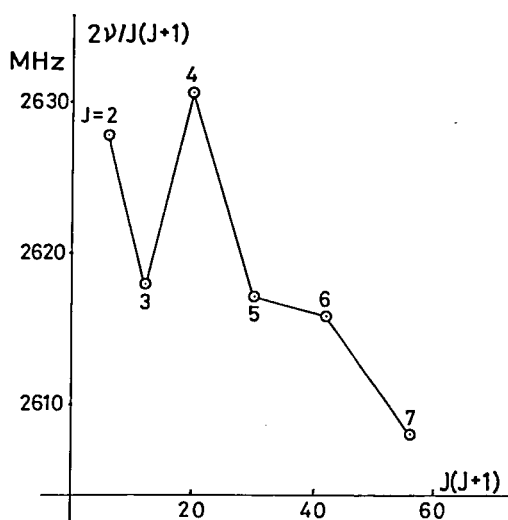


Figure 1. The $K_{-1} = 1$ K-type doubling frequencies of HNO in $\tilde{A}^1A''(100)$, divided by $J(J+1)/2$ and plotted against $J(J+1)$.

II-A-6 Microwave Spectrum of CF in $^2\Pi_{1/2}$

Shuji SAITO, Yasuki ENDO, and Eizi HIROTA

The CF molecule is a typical Hund's case (a) diatomic free radical, however the rotational constant is so large that it has escaped microwave observation. The molecular constants available were thus obtained from either electronic spectra or electron-paramagnetic-resonance spectra in the gas phase. We have recently observed and analyzed the fundamental band of CF using infrared diode laser spectroscopy.¹⁾ In this experiment we found that even $^2\Pi_{1/2}$ lines could be easily modulated because of a small ratio of the spin-orbit coupling constant A to the rotational constant B. This observation encouraged us to observe the lowest rotational transition of CF in $^2\Pi_{1/2}$, which is only the transition accessible with our present microwave spectrometer.

The CF radical can be produced by a DC discharge in either CF₄ or C₂F₄. We found that, in the case of CF₄, addition of a small amount of CH₃F (CF₄: 17 mTorr, CH₃F 0.7 mTorr) increased the number of CF molecules by a factor of 9 or so. A glow discharge cell was used, and a Zeeman coil wound on it, which produced the magnetic field up to 24 G, was actually found useful in picking paramagnetic CF lines from among other lines. The observed transitions are listed in Table I, and Table II summarizes the molecular constants derived therefrom. The dipole moment obtained from Stark effect measurements was also included in Table II. To determine all the hyperfine coupling constants we have to wait for data on higher-J transitions in both $^2\Pi_{1/2}$ and $^2\Pi_{3/2}$; the J = 5/2 ← 3/2, the next lowest one, which will appear at 207 GHz, may be readily observed. The present data have been incorporated with infrared data in determining the rotational and centrifugal distortion constants precisely.¹⁾

Reference

- 1) K. Kawaguchi, C. Yamada, Y. Hamada, and E. Hirota, *J. Mol. Spectrosc.*, in press.

Table I. Observed Frequencies of J = 3/2 ← 1/2 of CF in $^2\Pi_{1/2}$ (MHz)

	F' - F''	ν_{obs}
f	2 ← 1	124 309.999 (6)
	1 ← 0	124 708.812 (12)
	1 ← 1	123 682.520 (9)
e	2 ← 1	124 001.566 (18)
	1 ← 0	124 185.447 (10)
	1 ← 1	124 217 490 (10)

Table II. Molecular Constants of CF (MHz)

ν_0 ($^2\Pi_{1/2}$, J = 3/2 \leftarrow 1/2)	124 201.973 (24)	
p_{eff}	256.679 (12)	
$a - (b + c)/2$	747.61 (3)	
b	270 (1)	
d	792.16 (3)	
μ	0.645 (5) D	
<hr/>		
Derived parameters		
B_0	42 199.5 (7)	(a)
a	705.3 (15)	(b)
c	-354.7 (40)	(b)

(a) A = 77.11 cm⁻¹, D₀ = 0.2015 MHz assumed.

(b) a + (b + c)/2 = 662.9 MHz assumed.

II-A-7 The ν_3 Band of the Trifluoromethyl Radical by Diode Laser Spectroscopy

Chikashi YAMADA and Eizi HIROTA

In contrast to the CH₃ radical, the trifluoromethyl radical was shown by Fessenden and Schuler¹⁾ using the observed ¹³C hyperfine structure to have a non-planar structure. Carlson and Pimentel²⁾ observed three fundamental bands, ν_1 , ν_2 , and ν_3 , of CF₃ in the gas phase, using a rapid-scan infrared spectrometer. Milligan and Jacox³⁾ have reported all the four fundamental bands of CF₃, generated by flash photolysis of a CF₂N₂ and trans-N₂F₂ mixture frozen at low temperature.

We generated the CF₃ radical by a 60 Hz discharge in a mixture of CF₃I (50 ~ 100 mTorr) and Ar or N₂ (0.5 ~ 1 Torr) directly in a multiple-reflection cell. It was necessary to maintain the discharge as mild as possible. Because C₂F₆ generated by the recombination of CF₃ has a strong absorption of ν_{10} at 1251 cm⁻¹, we had to use Zeeman modulation. When we increased the DC magnetic field, paramagnetic lines disappeared.

Table I. Molecular Constants Associated with the ν_3 Band of CF₃ (cm⁻¹)^a

Constant	Value
α_3^B	0.679 33 (78) × 10 ⁻³
α_3^C	0.422 (14) × 10 ⁻³
C ζ_3	0.140 625 (26)
q ₃	-0.625 7 (24) × 10 ⁻³
r ₃	0.321 1 (53) × 10 ⁻³
$\tilde{\nu}_0$	1260.164 74 (14)

^a Values in parentheses denote standard deviation.

This observation suggests that the spin-rotation coupling constant is small. We have observed about 1300 lines in the region 1233 to 1269 cm^{-1} , of which 230 lines were assigned to Q branches. Figure 1 shows a part of the observed spectrum. The least-squares analysis was carried out by taking into account the so-called "2,2" as well as "2, -1" interactions. The former, which results in l-type doubling, is characterized by the constant q,

whereas the latter by r. The molecular constants obtained are summarized in Table I.

References

- 1) R. W. Fessenden and R. H. Schuler, *J. Chem. Phys.* **43**, 2704 (1965).
- 2) G. A. Carlson and G. C. Pimentel, *J. Chem. Phys.* **44**, 4053 (1966).
- 3) D. E. Milligan and M. E. Jacox, *J. Chem. Phys.* **48**, 2265 (1968).

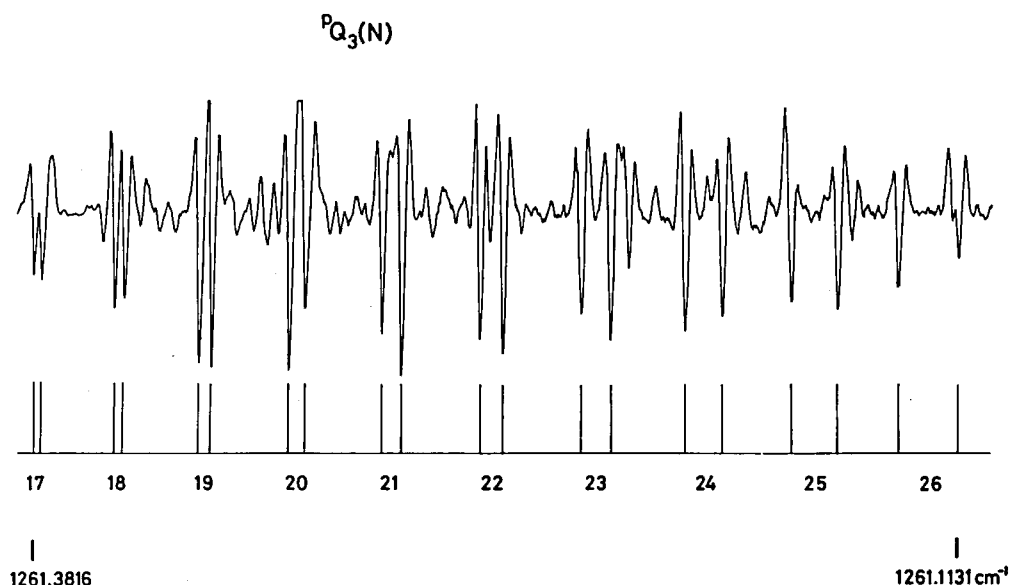


Figure 1. A part of the observed spectrum of the $\text{CF}_3 \nu_3$ band.

II-A-8 Hyperfine Structures of PH_2 in $\tilde{\text{X}}^2\text{B}_1$ and $\tilde{\text{A}}^2\text{A}_1$ from Intermodulated Fluorescence.

Masao KAKIMOTO and Eizi HIROTA

We have perviously reported that the $0_{00} - 1_{10}$ transition in the $\tilde{\text{A}}^2\text{A}_1(000) - \tilde{\text{X}}^2\text{B}_1(000)$ band of PH_2 showed splittings even with Doppler-limited resolution, and have ascribed the splitting mainly to the Fermi term of the P nucleus in the $\tilde{\text{A}}$ state.¹⁾ In the present work we improved the resolution by introducing the intermodulated fluorescence technique to completely resolve the hyperfine structure.

We generated the PH_2 radical by the reaction of H_2 discharge products with powdered red phosphorus placed in a fluorescence cell. It was imperative to thoroughly pump water from all materials in the cell. The dye laser beam was split into two, which, after chopped at 390 Hz and 540 Hz, were introduced into the cell from opposite

ends. The fluorescence was lock-in-detected at 930 Hz, the sum frequency. The resolution we achieved was about 10 MHz, which was determined by the two following reasons: (1) the dye laser beams were focused to the center of the cell by lenses with $F \cong 20$ cm, (2) to eliminate feedback to the source laser, we were forced to cross the two beams at a small angle (~ 10 mrad). To measure splittings we employed a temperature-stabilized confocal etalon of 50 cm length, and calibrated its FSR by observing a rotational transition of the NO_2 5933 Å band. We thus resolved hyperfine structures of 15 $I_H = 0$ and 16 $I_H = 1$ transitions of the PH_2 $\tilde{\text{A}}^2\text{A}_1(000) - \tilde{\text{X}}^2\text{B}_1(000)$ band. As an example, Figure 1 shows the $3_{30}, J' = 7/2 - 4_{40}, J'' = 9/2$ transition. The least-squares analysis gave hyperfine constants, as listed in Table I, which clearly indicate that PH_2 is a π and a σ radical in $\tilde{\text{X}}$ and $\tilde{\text{A}}$, respectively.

Reference

- 1) R. F. Curl, Y. Endo, M. Kakimoto, S. Saito, and E. Hirota, *Chem. Phys. Lett.* **53**, 536 (1978).

Table I. Hyperfine Coupling Constants of PH₂ (MHz)^a

Nucleus	Constant	\tilde{A}^2A_1 (000)	\tilde{X}^2B_1 (000)
P	Fermi	1748.0 (2.1)	208.2 (1.7)
	T _{aa}	-264.7 (6.0)	-311.5 (4.8)
	T _{bb}	485.1 (5.3)	-315.0 (3.7)
H	Fermi	189.8 (1.8)	-48.9 (1.5)
	T _{aa}	9.2 (3.3)	-6.0 (3.5)
	T _{bb}	-6.4 (4.2)	-3.2 (2.8)

^a Values in parentheses denote standard error.

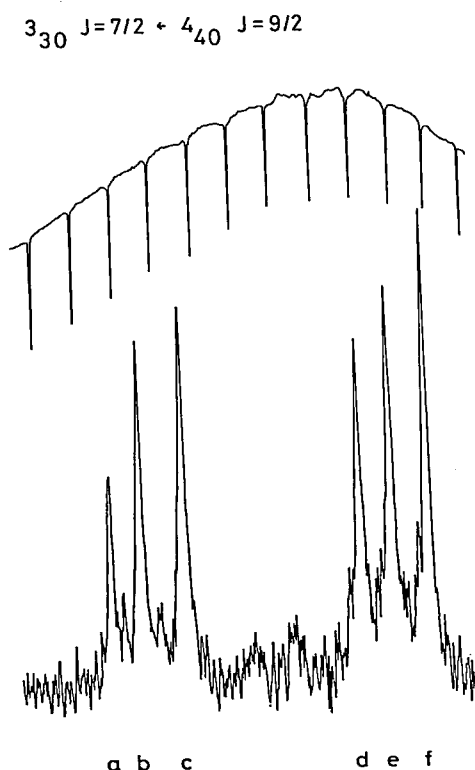


Figure 1. Intermodulated fluorescence spectrum of the $3_{30}, J' = 7/2 - 4_{40}, J'' = 9/2$ transition of the $\text{PH}_2\tilde{A}^2A_1(000) - \tilde{X}^2B_1(000)$ band. The upper trace is the Doppler-limited spectrum with 150 MHz markers from the etalon.

II-A-9 Vibration-Rotation Bands of the FCO Radical by Diode Laser Spectroscopy.

Keiichi NAGAI, Chikashi YAMADA, Yasuki ENDO, and Eizi HIROTA

Little is known about the molecular structure of the FCO radical. Only UV as well as IR spectra in low-temperature matrices have been reported.¹⁾ In the present work we succeeded in observing infrared spectra of FCO, which we assigned to the ν_1 (C = O stretch) and ν_2 (C-F stretch) bands.

We observed identical spectra with nearly equal intensities for the following three reaction systems: C₂F₄ (100 mTorr) + O₂ (100 mTorr), SF₆ (80 mTorr) + CO (150 mTorr), and C₂F₄ (80 mTorr) + CO (150 mTorr), all diluted with He to about 1 Torr and excited by 60 Hz discharges in a cell. Both Zeeman and source modulation were employed. The latter was found more suitable for observing closely spaced lines. The wavenumber of an absorption line was determined using either N₂O (5 μm) and CO₂ (10 μm) as references or our high-precision λ -meter.²⁾ Figure 1 shows Q-branch series of the 10 μm band. Both bands obeyed a-type selection rules. When they were analyzed separately, the lower-state parameters agreed with each other within experimental errors. Therefore, later the two bands were subjected to a joint analysis, leading to molecular constants listed in Table I. Some high-K lines showed spin-rotation splittings, from which the coupling constants were calculated (Table I). Although we could assign our spectra to FCO with almost 100% confidence, we got an additional evidence from the observation of the ν_1 band of F¹³CO. This band appeared at the frequency that was just expected from the isotope shift observed in an Ar matrix. The molecular constants of F¹³CO are listed in Table II. It is unfortunate that our data are almost useless in determining the molecular structure. This is because the C atom is located closely to the b-axis and because the A constants are poorly determined. We needed higher-order centrifugal distortion terms in fitting the ν_1 band of F¹²CO, whereas such terms were unnecessary for F¹³CO. This observation may be explained by the fact that the $3\nu_3$ state is close to the ν_1 state in F¹²CO. The matrix frequencies reported¹⁾ support this explanation. The calculated inertia defect (0.09780 amu \AA^2), combined with the B and C constants, allows us to estimate the A constant to be 191 271 MHz, which agrees with the observed value 191 062 (514) MHz within the experimental error.

References

- 1) D. E. Milligan, M. E. Jacox, A. M. Bass, J. J. Comeford, and D. E. Mann, *J. Chem. Phys.* **42**, 3187 (1965); M. E. Jacox, *J. Mol. Spectrosc.* **80**, 257 (1980).
- 2) K. Nagai, K. Kawaguchi, C. Yamada, K. Hayakawa, Y. Takagi, and E. Hirota, *J. Mol. Spectrosc.*, in press.

Table I. Molecular Constants of $F^{12}CO$ (MHz)^a

State	ν_2	ν_1	Ground
A	—	—	191 062 (514)
ΔA	1 454.15 (71)	−596.1 (33)	
B	11 367.21 (66)	11 413.8 (12)	11 466.39 (69)
C	10 695.59 (66)	10 741.8 (12)	10 795.30 (69)
Δ_N	0.012 38 (29)	0.013 00 (41)	0.012 46 (33)
Δ_{NK}	−0.559 5 (37)	−0.584 2 (48)	−0.529 7 (40)
Δ_K	42.685 (36)	75.72 (51)	39.5 ^b
δ_N	0.002 03 (73)	0.001 9 (13)	0.002 11 (30)
δ_K	0.115 (24)	0.56 (40)	0.080 ^b
H_K	0.004 96 (50)	1.165 (30)	
L_K		−0.020 17 (74)	
P_K		0.000 139 3 (63)	
ϵ_{aa}	1 834 (28)	1 829 (27)	1 838 (28)
$\epsilon_{hh} + \epsilon_{cc}$	11 (10)	13 (10)	14 (10)
$\tilde{\nu}_0$ (cm ^{−1})	1 026.1282 (2)	1 861.6386 (2)	

^a Values in parentheses denote standard errors and apply to the last digits of constants.

^b Calculated using force constants and fixed.

Table II. Molecular Constants of $F^{13}CO$ (MHz)^a

State	ν_1	Ground
A	180 939.46 (67)	182 148 ^b
B	11 413.2 (64)	11 463.5 (64)
C	10 710.3 (65)	10 760.5 (65)
Δ_N	0.016 2 (16)	0.018 0 (19)
Δ_{NK}	−0.508 (14)	−0.478 (16)
Δ_K	35.779 (21)	35.2 ^b
δ_N	0.017 (45)	0.013 (52)
δ_K	−1.03 (30)	0.080 ^b
H_K	0.003 42 (16)	
ϵ_{aa}	2 150 (204)	2 167 (203)
$\epsilon_{hh} + \epsilon_{cc}$	350 (138)	396 (150)
$\tilde{\nu}_0$ (cm ^{−1})	1 821.1775 (2)	

^a See the footnote a of Table I.

^b See the footnote b of Table I.

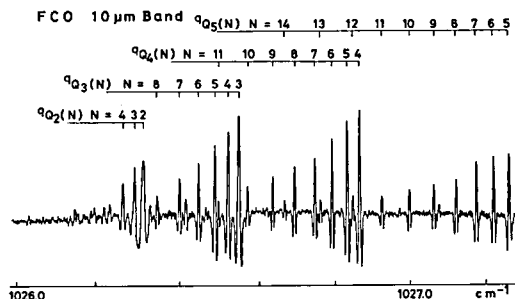


Figure 1. Q-branch series of the $F^{12}CO$ ν_2 band.

II-A-10 Infrared-Optical Double Resonance Spectroscopy. Application to the Vibration-Rotation Spectrum of the NH_2 Radical in Excited Electronic States.

Takayoshi AMANO (*Univ. of Tokyo*), Kentarou KAWAGUCHI, Masao KAKIMOTO, Shuji SAITO, and Eizi HITORA

Few examples have been reported on double resonance experiments using a dye laser and an infrared laser as sources. We have carried out such double resonance spectroscopy on NH_2 , which permitted us to determine upper-state molecular constants at high precision. Our infrared source was a CO_2/N_2O laser, and thus we had to apply the magnetic field to “scan” infrared spectra in the laser magnetic resonance fashion. This disadvantage was compensated by the fact that we were allowed to place the cell inside the infrared-laser cavity; the intracavity arrangements did not require any careful alignment for the two laser beams. The dye laser beam was introduced into the cell through an end mirror made of ZnSe, which has the reflectivity of 90% for the infrared beam and passes about a quarter of the dye laser power. We normally observed the change in fluorescence intensity upon infrared laser pumping. When the infrared source (actually the magnetic field) is swept, the observed hyperfine splitting $\Delta\nu_{obs}^{IR}$ is slightly different from the true splitting $\Delta\nu^{IR}$, as given by

$$\Delta\nu_{obs}^{IR} = \Delta\nu^{IR} \pm (\nu^{IR}/\nu^{OP}) \Delta\nu^{OP}, \quad (1)$$

Where ν^{IR} and ν^{OP} denote the infrared and optical transition frequencies, $\Delta\nu^{OP}$ the splitting in the optical transition, and the + and − signs apply to the cases where the two beams proceed in the opposite and same directions, respectively. Figure 1 shows an example of the observed spectrum. Because the total spin of the protons is zero, the

transition is split into three components due to the ^{14}N nucleus, and two triplets appear as expected from Eq(1). We also observed infrared transitions to a vibronic level (referred to as "u" level) as decreases in fluorescence intensities. It is most probable that this level is a highly excited vibrational level in the ground electronic state. Molecular constants obtained from the observed spectrum are summarized in Table I. It is interesting that g_1^{aa} changes its value on the vibrational transition $(0, 10, 0) - (0, 9, 0)$.

Table I. Molecular Constants of NH_2 in \tilde{A}^2A_1 $(0, 9, 0)$ and $(0, 10, 0)^a$

	$(0, 10, 0)$	$(0, 9, 0)$	Unit
$(0)_1$	148.52 (95)	85 (47)	MHz
$(bb)_1$	71.1 (16)	[33.2] ^b	MHz
g_1^{aa}	-0.0552 (55)	-0.2144 (39)	
g_1^{bb}	-0.259 (73)	[0.] ^b	
Spin-rotation	-4128.99 (8) MHz for $(0, 10, 0)$ 2_{11} level		
Splitting	-7818 (180) MHz for "u" level		
V (interaction constant between 2_{11} and "u")	1895 (250) MHz		
ν [$(0, 10, 0) 2_{11} - (0, 9, 0) 2_{20}$]		958.6773 (5) cm^{-1}	
ν ["u" $- (0, 9, 0) 2_{20}$]		959.752 (8) cm^{-1}	

^a Values in parentheses denote standard errors and apply to the last digits.

^b Assumed.

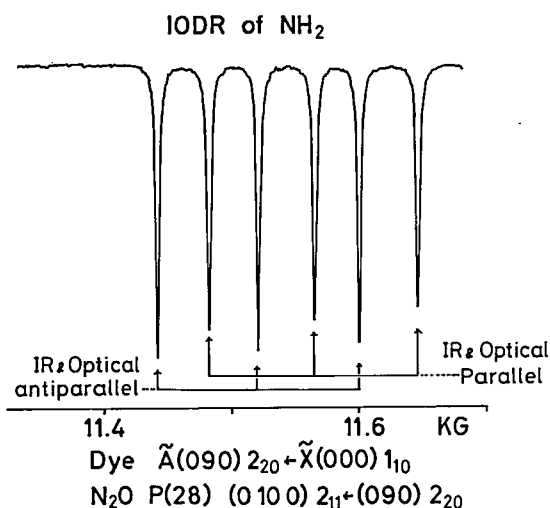


Figure 1. Infrared optical double resonance signal of NH_2 . The double resonance signal was observed as changes in fluorescence intensities, when the infrared transition in \tilde{A} , $(0, 10, 0) 2_{11} - (0, 9, 0) 2_{20}$, was saturated by an N_2O P(28) laser. The \tilde{A} $(0, 9, 0) 2_{20} - \tilde{X}$ $(0, 0, 0) 1_{10}$ transition was pumped by a dye laser, and fluorescence thus induced from the upper level was monitored.

II-A-11 Microwave Spectrum of the SF Radical

Yasuki ENDO, Shuji SAITO, and Eizi HIROTA

In 1969 Carrington et al.¹⁾ detected the SF radical in $X^2\Pi_{3/2}$ in the gas phase for the first time using electron paramagnetic resonance spectroscopy. The molecular constants they reported were later improved by Amano and Hirota²⁾ using zero-field microwave spectroscopy. Molecular parameters of a $^2\Pi$ molecule could, however, be completely specified only after high-resolution spectra not only of $^2\Pi_{3/2}$ but also of $^2\Pi_{1/2}$ are observed and analyzed. For SF it has been difficult to identify spectra of $^2\Pi_{1/2}$, because they show small Zeeman effects and are thus difficult to be discriminated against spectra of other molecules (e.g. SF_2) present in reaction mixtures. We thus redesigned our cell so that the magnetic field up to 60 G may be applied. We generated SF directly in the glow discharge cell using a mixture of OCS (10 mTorr) and CF_4 (35 mTorr). As shown in Figure 1, the magnetic field of 60 G is just enough to split the $J = 4.5 - 3.5$ transitions into two groups of Zeeman components. Thus the transitions of $J = 3/2 - 1/2$ to $J = 11/2 - 9/2$ were measured, and simultaneously the observation of $^2\Pi_{3/2}$ spectra was made more complete.

The least-squares analysis of the observed spectra gave molecular constants listed in Table I. The Table also shows how much the uncertainty in the spin-orbit coupling constant affects A_D (the centrifugal distortion term of the A constant) and b (a hyperfine structure constant). It is interesting to note that the Λ -doubling constant α_p is anomalously small. This result suggests that $^2\Sigma^+$ and $^2\Sigma^-$ states contributions are nearly cancelled. The Fermi contact term, which is equal to $b + c/3$, is 105(5) MHz. When the orbital which the unpaired electron occupies is a pure p orbital, $(c + 3d)/3$

Table I. Molecular Constants of SF in $X^2\Pi_1$ (MHz)^a

A_D	1.4171 (31) { ∓ 3.3 } ^b	$a + (b + c)/2$	428.39 (11)
		$a - (b + c)/2$	535.65 (39)
B_0	16 576.913 0 (44)	b	211.(13) { ∓ 14 } ^b
D_0	0.029 215 (92)	d	589.78 (80)
α_p	-1.706 (20)	a	482.02 (21)
		c	-318 (13) { ∓ 14 } ^b

^a Values in parentheses denote 2.5 times standard errors and apply to the last digits of constants.

^b The spin-orbit coupling constant A was assumed to be $-387 \pm 25 \text{ cm}^{-1}$ [see Ref. 1]. Values in { } correspond to the uncertainty $\pm 25 \text{ cm}^{-1}$ in A. The signs should be taken in the same order.

should be equal to a . In fact, $(c + 3d)/3$ is 483.6(76) MHz, close to a of 482.02(21) MHz. The spin density on the fluorine nucleus is also obtained to be 15%.

References

- 1) A. Carrington, G. N. Currie, T. A. Miller, and D. H. Levy, *J. Chem. Phys.* **50**, 2726 (1969).
- 2) T. Amano and E. Hirota, *J. Mol. Spectrosc.* **45**, 417 (1973).

SF RADICAL

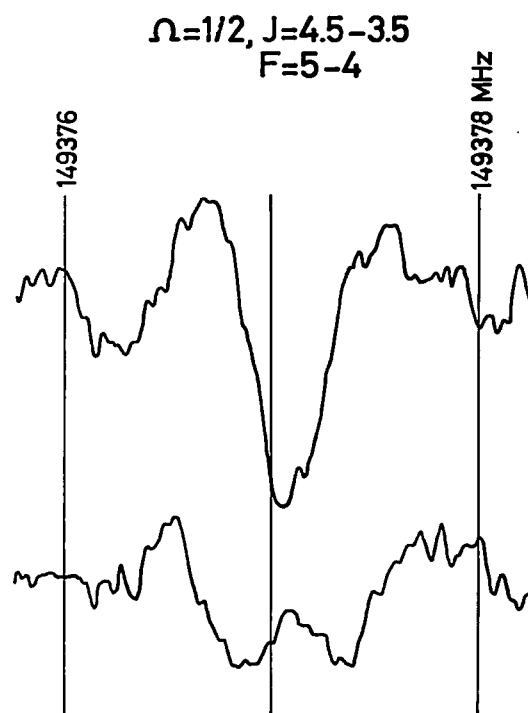


Figure 1. The $J = 4.5 - 3.5$, $F = 5 - 4$ transition of SF in $^2\Pi_{1/2}$. The lower trace was recorded with a magnetic field of about 60 G.

II-A-12 Microwave Spectrum of the ClSO Radical

Shuji SAITO, Yasuki ENDO, and Eizi HIROTA

We have already investigated $\text{HSO}^{1)}$ and $\text{FSO}^{2)}$ by microwave spectroscopy, and the ClSO radical, which was studied in the present work, is the third molecule of the XSO series. However, little has been known about ClSO. Wayne and Radford³⁾ observed a number lines by far-infrared laser magnetic resonance, but they have not made assignment for them because of complexities of the spectra.

We generated ClSO directly in a 3.5 m long glow-

discharge cell using a mixture of S_2Cl_2 (15 mTorr) and O_2 (10 mTorr) with 10 mA discharge current. A small magnetic field was found useful in picking paramagnetic lines from among other diamagnetic lines.

The molecular constants obtained are summarized in Table I. If the ClSO angle is assumed to be 107.8° , the S-O and S-Cl bond lengths are calculated to be 1.418 Å and 2.090 Å, respectively.

References

- 1) See II-A-1.
- 2) Y. Endo, S. Saito, and E. Hirota, *J. Chem. Phys.*, to be published.
- 3) F. D. Wayne and H. E. Radford, private communication.

Table I. Molecular Constants of the ClSO Radical (MHz)

A	32 819.3	a_F	26.4
B	4 553.2	T_{aa}	-19.0
C	3 992.4	T_{bb}	-10.9
Δ^a	0.191	T_{cc}	29.8
ϵ_{aa}	-787.8	χ_{aa}	-7.8
ϵ_{bb}	-78.8	χ_{bb}	3.3
ϵ_{cc}	4.4	χ_{cc}	4.5

^a In $\text{amu } \text{\AA}^2$

II-A-13 Diode Laser Spectroscopy of the HO_2 ν_2 Band

Keiichi NAGAI and Yasuki ENDO

Johns et al.¹⁾ observed the lowest vibration-rotation band (ν_3) of HO_2 by infrared laser magnetic resonance spectroscopy. However, no other vibrational data have been reported, except that Smith and Andrews²⁾ and Jacox and Milligan³⁾ observed fundamental bands for eight isotopic species of HO_2 trapped in low-temperature Ar matrices. Yamada⁴⁾ has recently observed the ν_1 band of HO_2 in the gas phase by using a difference-frequency laser, and the present work reports the observation and analysis of the ν_2 band.

The HO_2 radical was generated directly in a multiple-reflection discharge cell using a mixture of allyl alcohol (150 mTorr) and O_2 (350 mTorr) diluted with He to 1.5 Torr. Both Zeeman and source modulation were employed. About 31% of the region 1370 to 1416 cm^{-1} was scanned. Wavelength calibration was made by observing spectra of CHF_3 , which in turn were measured by our high-precision wavelength meter.⁵⁾ Of 153 observed lines 148 lines were assigned. But 137 lines were included in the least-squares analysis. The ground-state parameters were fixed to values

obtained by microwave spectroscopy and by far-infrared laser magnetic resonance spectroscopy.

References

- 1) J. W. C. Johns, A. R. W. McKellar, and M. Riggall, *J. Chem. Phys.* **68**, 3957 (1978).
- 2) D. W. Smith and L. Andrews, *J. Chem. Phys.* **60**, 81 (1974).
- 3) M. E. Jacox and D. E. Milligan, *J. Mol. Spectrosc.* **42**, 495 (1972).
- 4) See II-A-15.
- 5) K. Nagai, K. Kawaguchi, C. Yamada, K. Hayakawa, Y. Takagi, and E. Hirota, *J. Mol. Spectrosc.*, in press.

Table I. Molecular Constants of HO₂ in the ν_2 State^a

A	628 299.8 (37)	ϵ_{aa}	-53 033.5 (98)
B	33 469.3 (50)	ϵ_{bb}	-473.5 (39)
C	31 480.5 (51)	ϵ_{cc}	10.3 (33)
Δ_N	0.1189 (24)	Δ_K^s	30.92 (73)
Δ_{NK}	3.427 (49)	Δ_{NK}^s	0.68 (24)
Δ_K	156.15 (34)		
δ_N	0.0190 (31)	$\tilde{\nu}_0$	1391.7534 (3)
δ_K	3.6 (25)		
H_{KN}	0.0074 (26)		
H_K	0.1466 (91)		
h_N	[0.000045] ^b		

^a In MHz, except for $\tilde{\nu}_0$ (band origin) which is given in cm⁻¹. Values in parentheses denote standard errors and apply to the last digits of constants.

^b Assumed.

II-A-14 Dye Laser Excitation Spectroscopy of SiH₂

Tetsuo SUZUKI and Shuji SAITO

In the course of searching for SiH₃, Dubois et al.¹⁾ observed the $\tilde{A}^1B_1 - \tilde{X}^1A_1$ band of SiH₂, and the observation was later extended to higher ν_2' states.²⁾ Milligan and Jacox³⁾ have reported vibrational as well as ultraviolet spectra of SiH₂ in low-temperature Ar matrices. We started the present work to extract more detailed information on SiH₂.

To observe SiH₂ spectra we used the reaction of CF₄ discharge products with silane in a fluorescence cell, which emitted very strong chemiluminescence. Therefore, we had used narrow band-pass filters, which, for example, transmitted only (010) \rightarrow (010) emission when we excited the (010) \leftarrow (000) transition. The best fluorescence signal was obtained when the partial pressure of SiH₄ was 5 mTorr in a total pressure of 200 mTorr. We thus observed fluorescence signals at 15 533 and 16 393 cm⁻¹, which, according to Dubois et al., correspond to (000) \leftarrow (000) and (010) \leftarrow (000) bands, respectively. The 17 275 cm⁻¹ region,

where we expect to observe (020) \leftarrow (000), was covered by much stronger HCF spectra, but later by replacing CF₄ with SF₆ we could confirm the presence of spectra. The spectra observed in the three regions consist of weak lines (70 such lines, for example, in the 16 350 to 16 436 cm⁻¹ region) overlapped by several much stronger lines. Weak lines could be identified, in most part, with the aid of the results by Dubois et al. On the other hand, strong lines are more difficult to interpret. They appeared only in the three regions, but did not in other regions we scanned. We resolved these strong fluorescence signals into several components using a 25 cm monochromator; the first group of components appeared at the frequency lower than the excitation line by 1003 to 1006 cm⁻¹, that is, by the bending frequency in the lower state, $\tilde{\nu}_2''$, and the second group of components further by 977 \pm 988 cm⁻¹. These observations strongly suggest that strong lines are also due to SiH₂.

References

- 1) I. Dubois, G. Herzberg, and R. D. Verma, *J. Chem. Phys.* **47**, 4262 (1967); I. Dubois, *Canad. J. Phys.* **46**, 2485 (1968).
- 2) I. Dubois, G. Duxbury, and R. N. Dixon, *J. Chem. Soc., Faraday Trans. II* **71**, 799 (1975).
- 3) D. E. Milligan and M. E. Jacox, *J. Chem. Phys.* **52**, 2594 (1970).

II-A-15 The HO₂ ν_1 Band Observed by a Difference-Frequency Laser

Chikashi YAMADA and Yasuki ENDO

As described in II-A-13 no gas phase vibrational spectra have been reported on the HO₂ ν_1 band. Pine¹⁾ has recently developed an infrared light source in the region 2.2 μ m to 4 μ m, by mixing outputs of an argon-ion laser and a dye laser in a non-linear element (LiNbO₃). We used a similar source in the present experiment. Unfortunately our Ar⁺ laser is unstable in both frequency and output power. Therefore, we employed N₂O bands as references.²⁾ We could thus observe Q branches with K = 1 \leftarrow 2, 0 \leftarrow 1, 1 \leftarrow 0, and 2 \leftarrow 1, and also 'R₁(N) with N = 1 to 5 and 'P₀(N) with N = 16 to 18. A least-squares analysis gave the following constants as preliminary results: A' = 586 673.6 (34.6), B' = 33 657.7 (0.8), C' = 31 701.4 (1.1), $\epsilon_{aa}' = -46 029$ (94), $\epsilon_{bb}' = -291$ (11), [ϵ_{cc}' : not determined], and $\tilde{\nu}_0 = 3436.2072$ (0.0008), all in MHz, except $\tilde{\nu}_0$ which is given in cm⁻¹. Values in parentheses denote one standard errors. Ground-state parameters were fixed to values already determined precisely by other methods, and centrifugal distortion constants in the ν_1 state were all assumed to be the same as those in the ground state.

References

- 1) A. S. Pine, *J. Opt. Soc. Amer.* **64**, 1683 (1974); *J. Mol. Spectrosc.* **54**, 132 (1975); *J. Opt. Soc. Amer.* **66**, 97 (1975).
- 2) C. Amiot and G. Guelachvili, *J. Mol. Spectrosc.* **51**, 475 (1974).

II-A-16 Laser Excitation Spectroscopy of the Singlet Methylene Produced by UV Photodissociation of Ketene

Nobukimi OHASHI (*Kanazawa Univ.*), Shuji SAITO, Tetsuo SUZUKI, and Eizi HIROTA

Because of its importance in various fields, the methylene has been a subject of many spectroscopic investigations, and it is now established that its ground electronic state is a 3B_1 state accompanied by a low-lying metastable state, \tilde{a}^1A_1 , although the separation $\tilde{a} - \tilde{X}$ is still under controversy. Herzberg and others¹⁾ observed and analyzed the $\tilde{b}^1B_1 - \tilde{a}^1A_1$ band, and we started the present work to improve their results by using a technique of dye laser excitation spectroscopy, and, if possible, to extract some information on the separation between the \tilde{a} and \tilde{X} states.

We could successfully generate CH_2 in the \tilde{a} state by photolyzing ketene with a cw UV multiline output of 1.6 W from an Ar^+ laser (SP 171-17). The peak absorption of ketene is slightly shifted (330 nm) from the laser frequency. Only the output power at 334 nm, which was about 20% of the total in the UV region, is effective for the photolysis of ketene. However, we could detect the following transitions as laser excitation spectra: for $\tilde{b}^1B_1(0, 14, 0) - \tilde{a}^1A_1(0, 0, 0)$ at 16 800 to 17 000 cm^{-1} , 19 lines were observed and assigned to 3P_1 , 3Q_1 , 3R_1 , 1R_1 , and 3P_3 branches, whereas for the $(0, 13, 0) - (0, 0, 0)$ band of the same electronic transition at 15 850 to 16 500 cm^{-1} nine rotational lines of 1Q_0 , 1R_0 , 3P_2 , and 1R_2 branches were recorded. It was found imperative to closely superimpose the ultraviolet laser beam on the dye laser beam which was used to excite fluorescence. Interference filters were found particularly useful in reducing scattered ultraviolet light.

Reference

- 1) G. Herzberg, *Proc. Roy. Soc. A* **262**, 291 (1961); G. Herzberg and J. W. C. Johns, *Proc. Roy. Soc. A* **295**, 107 (1966).

II-A-17 Diode Laser Spectroscopy of the FSO ν_1 Band

Yasuki ENDO and Keiichi NAGAI

We have recently completed analyzing microwave spectra of FSO in the ground and ν_3 states.¹⁾ We tried to estimate the force constants using centrifugal distortion constants and inertia defects obtained from the observed rotational spectra. Although we could obtain good results for the bending mode (ν_3), almost no information was provided for the $S=O$ (ν_1) stretching mode. Therefore, we aimed, in the present work, at high resolution spectroscopy of the ν_1 band using a diode laser as a source.

As in our microwave work we generated FSO by the reaction of OCS (40 mTorr) with products of a microwave discharge in an O_2 (50 mTorr)/ CF_4 (100 mTorr) mixture, except that He was added to 400 mTorr to protect surfaces of mirrors. This method of generation was found more efficient than AC discharges in the cell. Zeeman modulation was employed. The region 1216 cm^{-1} to 1230 cm^{-1} was scanned with many mode gaps, and 47 transitions thus observed were subjected to a least-squares analysis. The ground-state parameters were fixed to the microwave data. Preliminary molecular constants thus obtained are listed in Table I.

Reference

- 1) Y. Endo, S. Saito, and E. Hirota, *J. Chem. Phys.*, to be published.

Table I. Molecular Constants of FSO in the ν_1 state (MHz)^a

A	38 468.20 (42)	$\bar{\nu}_0$	1217.16475 (48) ^b
B	9 317.0 (10)		
C	7 483.5 (12)	ϵ_{aa}	-346.22 (37)
Δ_K	0.863 8 (27)	$\epsilon_{bb} + \epsilon_{cc}$	30.40 (46)

^a Values in parentheses denote one standard deviation and apply to the last digits of constants. The following parameters were fixed to the ground-state values: Δ_N , Δ_{NK} , δ_N , and $\epsilon_{bb} - \epsilon_{cc}$.

^b In cm^{-1} .

II-B Microwave Spectroscopy of Non-polar Molecules

Most non-polar molecules are of high symmetry and thus play important roles in the theory of molecular structure. It is therefore very unfortunate that we cannot apply microwave spectroscopy to them, which is known to provide most accurate data on molecular structure. However, recent advances in theory and experiment of molecular spectroscopy have made it possible to observe weak rotational transitions in molecules which are normally classified as non-polar molecules. The observation is based upon the small dipole moments which are induced by one of three following mechanisms: (1) degenerate vibration, (2) centrifugal distortion, and (3) isotopic substitution. The present project is based upon the last mechanism. At present, we know little about the origin of induced dipole moments, but once spectral lines are observed, we obtain detailed information not only on molecular structure but also on other important properties.

II-B-1 Microwave Spectra of Deuterated Ethylenes: Molecular Structure and Intra-molecular Potential Function

Eizi HIROTA, Yasuki ENDO, Kazuhiro YOSHIDA¹⁾ (*Sophia Univ.*), Shuji SAITO, and Katsunosuke MACHIDA (*Kyoto Univ.*)

The C = C bond length in ethylene has been chosen as a standard in the discussion of molecular structure. We therefore aimed at determining the ethylene structure as precisely as possible. To this purpose we have improved rotational constants of three deuterated species, which we measured previously, by observing additional transitions.

The improved constants are listed in Table I. For CH₂ = CD₂, however, we could not have determined the Δ_K constant, because of the a-type selection rules; the errors in other parameters thus included those due to ±20% uncertainty in the assumed Δ_K, in addition to the fitting errors (2.5σ). By correcting for small centrifugal distortion terms and also for harmonic terms of vibration-rotation constants α, we converted the A, B, and C constants in Table I to A_z, B_z, and C_z, and calculated the r_z structure using them. We took into account isotopic effects only for r_z (C – H). The results are summarized in Table II.

Note

1) IMS Graduate Student from Sophia Univ. for 1977 - 79.

Table I. Rotational Constants and Centrifugal Distortion
Constants of Deuterated Ethylenes (MHz)^a

	CH ₂ = CD ₂	CH ₂ = CHD	cis-CHD = CHD
A	97 496.7 (18)	120 093.521 (70)	99 667.262 (89)
B	25 675.260 (44)	27 470.737 (26)	25 417.208 (41)
C	20 268.791 (40)	22 297.745 (14)	20 199.073 (24)
Δ _J	0.032 73 (57)	0.039 04 (53)	0.035 9 (12)
Δ _{JK}	0.191 5 (28)	0.180 4 (45)	0.117 (11)
Δ _K	[1.224] ^b	2.116 4 (34)	1.458 9 (63)
δ _J	0.007 88 (13)	0.008 405 (63)	0.008 649 (98)
δ _K	0.206 (22)	0.243 8 (43)	0.196 6 (66)

^a Values in parentheses denote 2.5 standard errors, except for CH₂ = CD₂ for which they include those due to ±20% uncertainty in Δ_K, and apply to the last digits of constants.

^b Assumed.

Table II. r_z Structure of Ethylene^a

r _z (C = C)	1.33986 (69) Å
r _z (C – H)	1.08591 (67) Å
θ _z (CCH)	121.208 (47) ^o
r _z (C – H) – r _z (C – D)	0.00128 (12) Å

^a Values in parentheses denote one standard error in the least-squares fitting.

II-B-2 Microwave Spectra of Deuterated Ethanes: Internal Rotation Potential and r_z Structure

Eizi HIROTA, Yasuki ENDO, Shuji SAITO, and J. L. DUNCAN (*Univ. of Aberdeen*)

It is now well-known that rotational spectra of one isotopic species in one torsional state are not sufficient to determine the potential function to the CH_2 group internal rotation in the molecule. In fact, our previous data on CH_3CHD_2 in the ground state have provided a linear relationship between the first two Fourier coefficients V_3 and V_6 of the potential function.¹⁾ Furthermore, intramolecular vibrations may make the potential barrier slightly different for different isotopic species. To clarify these points, we have measured and analyzed microwave spectra of CH_3CHD_2 in the first excited torsional state and of $\text{CH}_3\text{CH}_2\text{D}$ and $\text{CD}_3\text{CH}_2\text{D}$ in the ground states.

By combining the $v = 0$ and $v = 1$ spectra of CH_3CHD_2 we determined V_3 and V_6 to be 2.8618 (80) and 0.0196 (66) kcal/mole, respectively, as shown in Figure 1. We found that the effective value of V_3 changes linearly with the number of deuterium atoms substituted; the slope we obtained is -0.010 kcal/mole/D atom, which may be compared with -0.017 kcal/mole/D atom, obtained by Kirtman et al.²⁾ from calculations on C_2H_6 and C_2D_6 . Therefore, the effective V_3 in C_2H_6 is estimated to be 2.882 kcal/mole with an uncertainty of 0.010 kcal/mole.

We also investigated $\text{CH}_2\text{DCH}_2\text{D}$ and, in fact, found rotational spectra which correspond to those of the gauche form. This is probably one of the most direct evidences for the staggered conformation in ethane. The rotational constants we thus obtained for four isotopic species were used to calculate the r_z structure shown in Table I, which should replace earlier results of Ref.³⁾

References

- 1) E. Hirota, S. Saito, and Y. Endo, *J. Chem. Phys.* **71**, 1183. (1979).
- 2) B. Kirtman, W. E. Palke, and C. S. Ewig, *J. Chem. Phys.* **64**, 1883 (1976).
- 3) J. L. Duncan, D. C. McKean, and A. J. Bruce, *J. Mol. Spectrosc.* **74**, 361 (1979).

Table I. r_z Structure of Ethane^a

$r_z(\text{C}-\text{C})$	1.5351 (1) Å
$r_z(\text{C}-\text{H})$	1.0940 (2) Å
$\theta_z(\text{CCH})$	111.17 (1)°
$r_z(\text{C}-\text{H}) - r_z(\text{C}-\text{D})$	0.0012 (2) Å
$\theta_z(\text{CCH}) - \theta_z(\text{CCD})$	0.040 (10)°
$r_z(\text{C}-\text{C}) - r_z(^{13}\text{C}-\text{C})$	0.00015 (10) Å
$\delta r_z(\text{C}-\text{C})/\text{D atom}$	$[-5 \times 10^{-5}]_{\text{assumed}}$

^a Values in parentheses denote one standard deviation in the least-squares fitting.

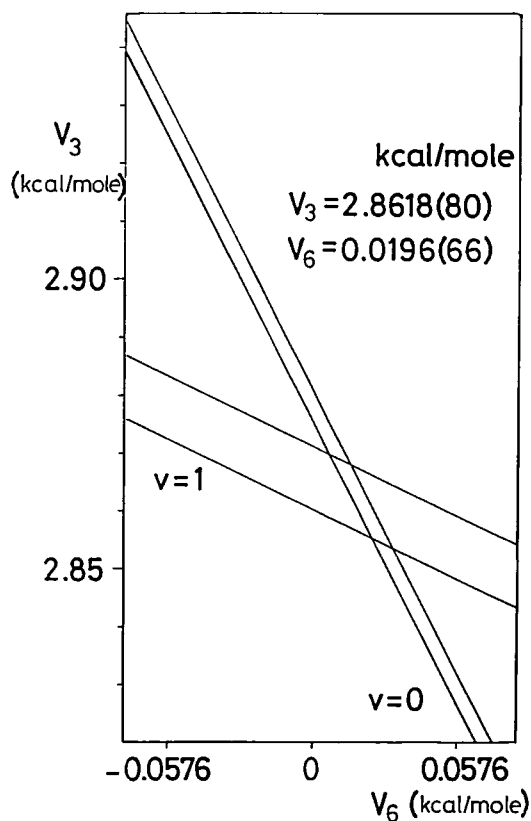


Figure 1. Relationship between V_3 and V_6 of CH_3CHD_2 .

II—C Development of New Instruments for High Resolution Spectroscopy

The scope of researches is limited by capabilities of instruments. This is particularly true for spectroscopic investigations of simple molecules, one of the main problems the Division is interested in. When we repeat investigations using spectrometers of similar performance, we will obtain almost identical results. It is therefore very urgent for us to always maintain our research facilities at levels of performance as high as possible. High precisions with which we determine molecular parameters often unravel new aspects of molecular properties that have not been known before. Needless to say, high sensitivity will supply us with fundamentally new information on molecular systems we are investigating. Along with these efforts to improve our facilities and with their applications to more interesting problems, we should try to develop methods that are based upon something new. This project obviously premises not only detailed knowledge on molecules under investigations, but also that connecting with related fields. Various kinds of technical problems are to be solved. In this sense joint researches including collaboration with Development Workshop are indispensable. Developments of Instruments that are thus brought about will open new research areas in the field of molecular science.

II-C-1 Computer-Aided Diode Laser Spectroscopy

Keiichi NAGAI and Yasuki ENDO

Infrared spectrum is often very rich, and it takes time to read out line wavenumbers from recorder charts. Therefore, an interface was developed between an infrared diode laser spectrometer and a YHP 2113 mini-computer, which was already installed and has been used to control a microwave spectrometer.

The wavenumber of an absorption line is normally determined in reference to (a) standard line(s), with the aid of fringes obtained from an etalon. Therefore, we need to determine the line position relative to peaks of fringes. Three kinds of data, the sample spectrum, the reference spectrum, and fringe pattern, are thus stored on 3×500 matrices, and two such matrices are processed at the same time on CPU, which determines line positions in reference to fringe peaks (see Figure 1). About 100 points are normally allocated to one fringe separation (FSR), which corresponds roughly to 0.01 cm^{-1} . Smoothing could be done for both absorption spectrum and fringe pattern. Line positions can be determined only for cases where the line is recorded as a second derivative (or a similar lineshape) and no serious overlapping takes place. The signal-to-noise ratio could be improved by accumulating signals.

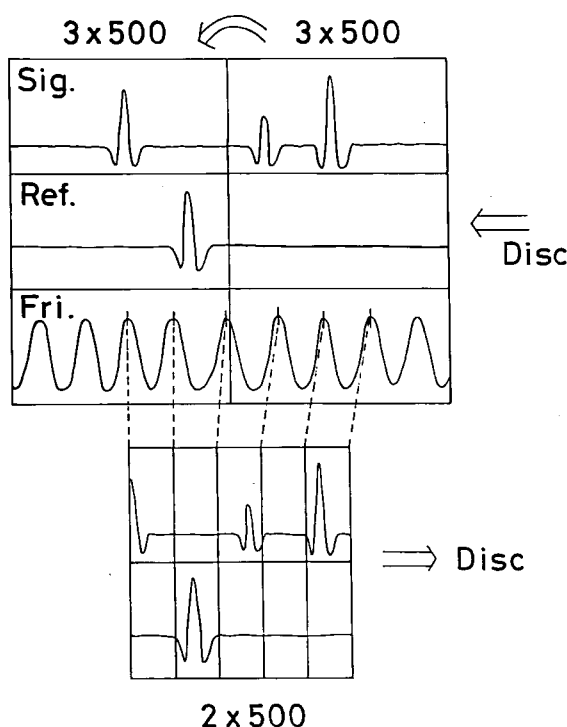


Figure 1. Two 3×500 matrices, stored on a disc, are processed on CPU, and both sample spectrum and reference spectrum are measured in the unit of FSR of an etalon. The central part of the spectrum, which is thus calibrated, is given in a 2×500 matrix and may be stored on a disc.

II-C-2 A Near-Infrared Diode Laser Spectrometer

Chikashi YAMADA and Eizi HIROTA

Near-infrared regions have attracted little attention of spectroscopists, because molecular spectra are rather sparse there. Spectroscopic techniques have also been less developed in this region than in other regions. It is, however, to be noted that the metastable states of a few important molecules may be detected by near-infrared absorptions from the ground states, and high vibrational states may also be explored in similar ways. Because these states are expected to play important roles in various fields of molecular science, we are setting up a near-infrared diode laser spectrometer which is sensitive enough to detect weak absorptions such as those mentioned above.

Fortunately, recent developments in laser communication are producing laser diodes of high performance in the near-infrared region. We have tested a Hitachi HLP 1400 diode; it oscillates at room temperature, delivering an output power of 6.5 mW at 816 nm, when a current 120 mA (twice the threshold current) is fed. Single mode oscillation continues for 5 to 7 cm^{-1} before the mode hops. The output beam was found definitely polarized. We are developing a temperature-control unit which will make it possible to use diodes in wider wavelength regions. So far we observed a few absorption lines of the $\text{NO}_2 \tilde{A} - \tilde{X}$ band; the linewidth we obtained, about 1000 MHz, is a little larger than the Doppler width 670 MHz, probably because of instability in current and temperature. However, as Table I shows, near-infrared diodes are superior in quality to infrared diodes in many respects.

Table I. Comparison of Near-Infrared and Infrared Diode Lasers

	Near-Infrared	Infrared
Composition	III-V Group diodes GaAlAs (0.8 μm) InGaAsP (1.3 μm) InP/InGaAsP (1.5 μm) InGaAsSb/AlGaAsSb (1.8 μm)	IV-VI Group diodes PbSnTe (6 ~ 30 μm) PbGeTe (4 ~ 6 μm) PbSSe (4 ~ 8 μm) PbSnSe (8 ~ 30 μm)
Temperature	-200 ~ +50°C	-260 ~ -200°C
Mode	single (or nearly single)	multiple
Polarization	definite	indefinite
Threshold	50 ~ 100 mA	~ 500 mA
Modulation sensitivity	5 MHz/ μA	0.2 MHz/ μA
Temperature dependence of osc. frequency	90 MHz/mK	10 MHz/mK
Mode width	> 5 cm^{-1}	0.3 ~ 4 cm^{-1}
Output	5 ~ 15 mW	< 1 mW

II—D Development of New Instruments for Condensed Phase Spectroscopy

We started our molecular dynamic group by constructing a few instruments necessary for executing our projects. They are a light scattering spectrometer for intensity measurement, a light scattering spectrometer for band-shape measurement, and a dual thermal lensing spectrometer for the measurement of intensity distributions of highly excited vibration spectra.

II-D-1 Light Scattering Spectrometer for Intensity Measurement

Tadashi KATO and Tsunetake FUJIYAMA

The light source is a He-Ne laser (NEC GLG 5800) which produces 50 mW power at 632.8 nm. The laser beam is irradiated on a sample cell ($16 \times 15 \times 12 \text{ mm}^3$) made of quartz. The scattered light is led

into a piezoelectrically driven Fabry-Perot interferometer (Burleigh RC 110). Light emerging from the interferometer is focused by a telescope lens into a pinhole. The central spot of the interferometer ring is then detected by a photomultiplier (HTV R-649). The photomultiplier signal is amplified, discriminated, and then, put into a multichannel analyzer (Canberra Series 30) by which the spectra are averaged over many times. In order to eliminate the axial drift of the interferometer cavity and maintain the parallelism of the two mirrors, the stabilization system (Burleigh DAS 10, RC 43) is used.

The mirror spacing of the interferometer is continuously variable from 0.1 mm to 150 mm. Therefore, the free spectral range (FSR) is variable from 50 cm^{-1} to 0.033 cm^{-1} . The finesse is about 20 for $\text{FSR} = 1\text{ cm}^{-1}$ and about 60 for $\text{FSR} = 25\text{ cm}^{-1}$.

The signal to noise ratios of the observed spectra (averaged for about 15 min) for ordinary molecular liquids were about 20. The spectra were observed for the systems: benzyl alcohol-carbon tetrachloride, phenol-carbon tetrachloride, acetone-water, dimethyl sulfoxide-water, and poly- γ -methyl-L-glutamate-1,2-dichloroethane.

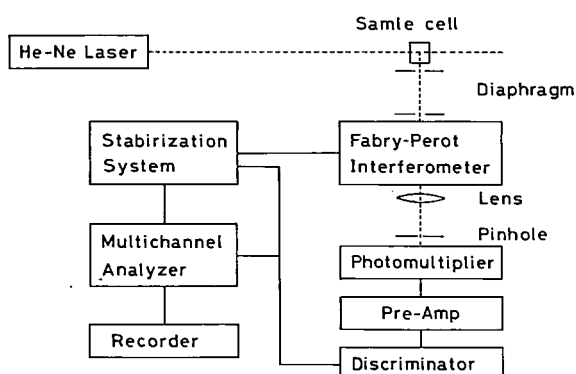


Figure 1. Block diagram of the light scattering spectrometer.

II-D-2 Light Scattering Spectrometer for Line-Shape Measurement

Nobuyuki ITO¹⁾ (Tokyo Metropolitan Univ.) and Tsunetake FUJIYAMA

A schematic diagram of the light scattering spectrometer constructed in this laboratory is shown in Figure 1.

Optical System: The light source is an argon ion laser (Spectra-Physics model 165-09) which produced 0.1-1 W power at 488 nm. The scattering

angle θ is varied by a combination of the adjustable mirrors (M_1 and M_2). The incident light is focused into a sample cell ($12 \times 15 \times 16\text{ mm}^3$) made of fused quartz. The temperature drift of sample is less than $\pm 0.5\text{ K}$ within the temperature range of 273-373 K.

Electric System: The R-374 (HTV) photomultiplier tube (PM) is operated at 840 V at room temperature. The photocurrent is amplified by a factor of about 400 by a preamplifier and autocorrelated by a 400 channel correlation and probability analyzer (KANOMAX SAI-43A). The computed time-autocorrelation function of the photocurrent is then displayed on an oscilloscope and recorded on an X-Y recorder. At the same time the autocorrelation function is transferred in digital form from the correlator to a micro-computer (Sharp MZ-80C).

By the use of this spectrometer, we can observe the correlation functions for the samples whose scattering intensity is larger than $\sim 10^{-6}\text{ cm}^{-1}$ (in Rayleigh ratio) and whose correlation time is longer than $\sim 2\text{ }\mu\text{s}$.

The spectra for those systems have been observed: binary solutions of tert-butyl alcohol-water, 2-butoxyethanol-water, carbon disulfide-acetone, aqueous agarose gel, and 12 hydroxyoctadecanoic acid-benzene gel.

Note and Reference

- 1) IMS Graduate Student from Tokyo Metropolitan Univ. for 1980 -
- 2) N. Ito, T. Kato, and T. Fujiyama, *Bunko Kenkyu*, 29, 106 (1980).

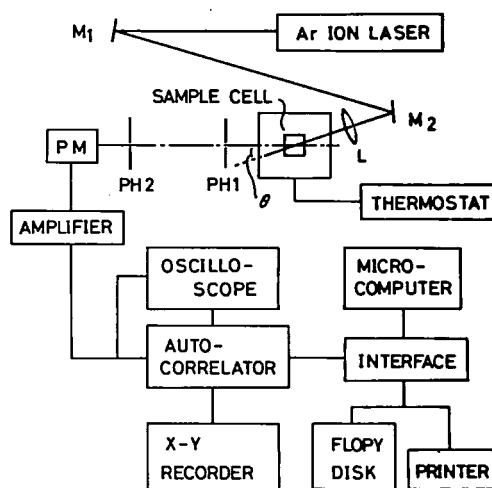


Figure 1. Block diagram of the light beating spectrometer.

II-D-3 Dual-beam Thermal Lensing Spectrometer

Shiaki HYODO¹⁾ (Tokyo Metropolitan Univ.) and Tsunetake FUJIYAMA

The dual-beam thermal lensing spectrometer constructed in this laboratory is shown schematically in Figure 1. The heating beam from a tunable flash lamp excited dye laser (Chromatix CMX-4) is incident on the beam splitter (SP). The most of the power is led to the sample and the remainder is used for the power monitoring. The monitoring beam is reflected by a mirror (M1) and interference filter (IF1) after being passed through the pinhole (PH2, $400\mu\text{m}\phi$) and is focused by a lens (L1) just before the sample cell. The probe laser beam from the He-Ne laser (NEC GLG105) passes collinearly with the heating beam through the sample cell. The heating beam is, then, separated from the probe beam by the prism and the interference filter (IF2). The probe laser beam is deivered by the thermal lensing effect and the intensity at the center of the probe beam is detected by the detector (Hamamatsu TV S874-18L). The intensity of the probe beam is amplified and integrated by a box-car integrator (NF BX530A). At the same time, the intensity of the heating beam for the power monitoring is integrated by another box-car integrator. The out-put powers of these box-car integrators are recorded on a 2-pen x-t recorder (Rikendenshi SP-H3C) simultaneously.

Figure 2 shows the absorption spectrum of C-H stretching vibration ($\nu = 6$) for liquid benzene. Absorption coefficients of 1×10^{-1} can be detected by this system with the resolution of about 3 cm^{-1} .

Note

1) IMS Graduate Student from Tokyo Metropolitan Univ. for 1980 -

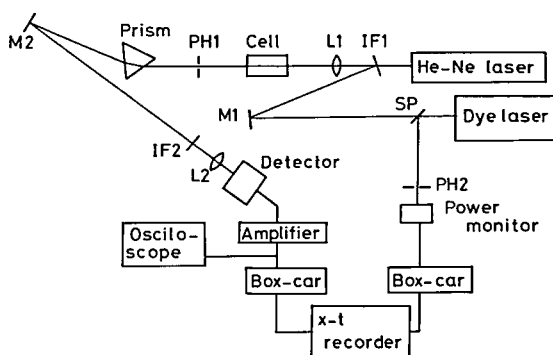


Figure 1. Block diagram of dual-beam thermal lensing spectrometer.

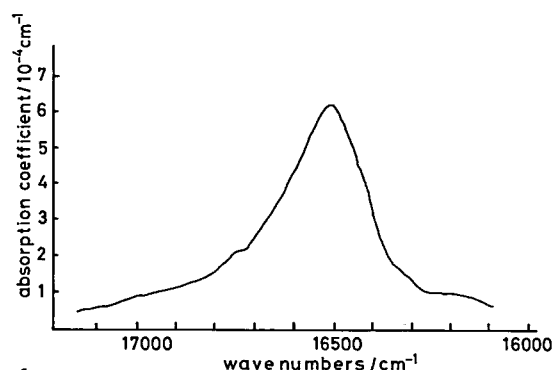


Figure 2. Absorption spectrum of C-H stretching vibration for liquid benzene ($\nu = 6$).

II—E Local Structure Formations in Solutions

The space-time correlation between the positions and between the orientations of different molecules are useful information for understanding the mixing state of solutions from a molecular view point. Coherent visible light scattering experiments afford information about these correlations in the form of fluctuations in the semimacro-regions. Mean-square amplitudes and time correlations of concentration fluctuations can be obtained by observing the Rayleigh line intensity and the Rayleigh line shape, respectively. Based upon these observations, the local structure formations can be discussed from the view points of the spacial correlations between the positions of different molecules and the velocity correlations between different molecules.

II-E-1 Light Scattering Study of Local Structures in Solutions

Mean Association Numbers and Concentration Fluctuation for Alcohol-Carbon Tetrachloride Systems.

Tadashi KATO, Toru NAKANISHI (Tokyo Metropolitan Univ.), and Tsunetake FUJIYAMA

[Bull. Chem. Soc. Jpn., 53, 2173 (1980)]

Light scattering spectra were observed for carbon tetrachloride solutions of methanol, ethanol, and n-propanol. The Rayleigh intensities were reduced to concentration fluctuation values. The observed concentration dependence of the concentration fluctuation was analyzed by using two distinct models: an ideal associated complex (IAC) model¹⁻⁴⁾ and polymer chain (PC) model. In the IAC model, a group of hydrogen-bonded alcohol molecules is treated as a complex whose size is independent of the association number, l . In the PC model, on the other hand, the group of hydrogen-bonded molecules is treated as a linear polymer whose length is proportional to l . It was shown that the PC model can explain both the concentration fluctuation and the heat of mixing data while the IAC model cannot be applied to the present systems in the sense that it cannot explain the heat of mixing data. The mean association number obtained by the IAC model, however, was clarified to be useful parameter for describing the relation between the concentration fluctuation and the special correlation of microscopic density.⁵⁾

References

- 1) K. Iwasaki, M. Tanaka, and T. Fujiyama, *Bull. Chem. Soc.* **49**, 2719 (1976).
- 2) K. Iwasaki, Y. Katayanagi, and T. Fujiyama, *Bull. Chem. Soc. Jpn.* **49**, 2988 (1976).
- 3) T. Kato, S. Hyodo, and T. Fujiyama, *Bull. Chem. Soc. Jpn.* **82**, 1010 (1978).

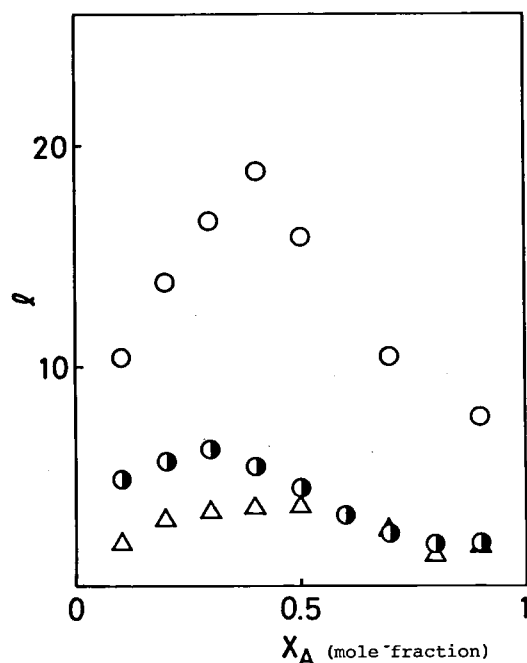


Figure 1. Mean Association Number Obtained for the IAC Model: (○) methanol, (●) ethanol, and (△) n-propanol.

- 4) T. Fujiyama and M. Tanaka, *Bull. Chem. Soc. Jpn.* **51**, 1655 (1978).
- 5) T. Kato, T. Nakanishi, and T. Fujiyama, *Bull. Chem. Soc. Jpn.* **53**, 2173 (1980).

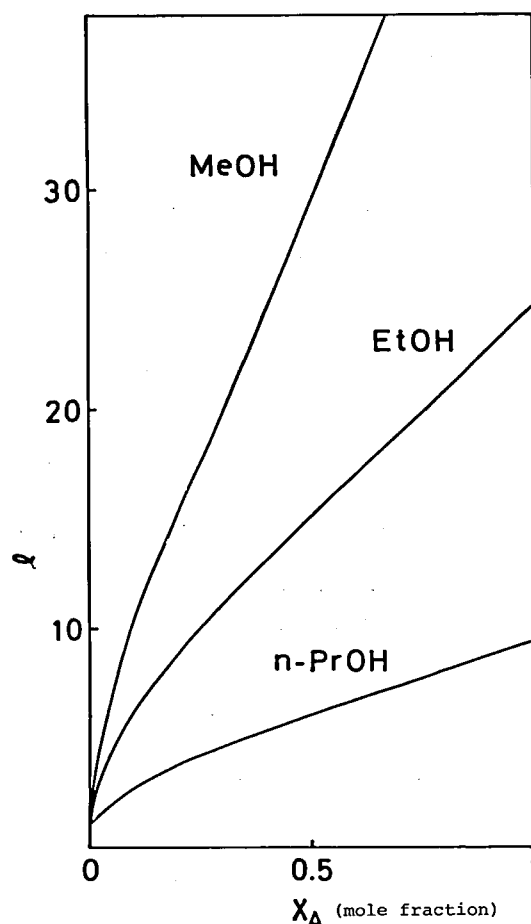


Figure 2. Mean Association Numbers Obtained for the PC Model.

II-E-2 Light Scattering Study of Local Structures in Solutions. Cooperative Translational Motion of Alcohol Molecules in Carbon Tetrachloride Solutions.

Tadashi KATO, Nobuyuki ITO¹⁾ (Tokyo Metropolitan Univ.), and Tsunetake FUJIYAMA

[*Bull. Chem. Soc. Jpn.*, **53**, 2167 (1980)]

The concept of a "moving unit" — a group of molecules which move together for the time much longer than the velocity autocorrelation time, τ — was introduced in order to obtain information about cooperative translational motions of

molecules in associated solutions. The mutual diffusion coefficient was theoretically expressed in terms of the self diffusion coefficients and the number of molecules which form a moving unit. The theoretical results were applied to the study of the mutual diffusion coefficients for methanol-carbon tetrachloride and ethanol-carbon tetrachloride solutions measured by the light scattering spectrometer.²⁾ It was shown that the mean number of alcohol molecules which constitute a moving unit is much smaller than the mean association number of alcohol,³⁾ especially in the high concentration range of alcohol. This indicates that the hydrogen-bonded polymer of alcohol molecules cannot move without changing the polymer shape within the time τ .

The number of molecules which constitute a moving unit was compared with the mean association number which was obtained for the ideal associated complex model.³⁾ It has been shown that the ideal associated complex model is practically useful for the determination of a "moving unit" in associated solutions.

Note and References

- 1) IMS Graduate Student from Tokyo Metropolitan Univ. for 1980 -
- 2) N. Ito, T. Kato, and T. Fujiyama, *Bunko Kenkyu* **29**, 106 (1980).
- 3) T. Kato, N. Ito, and T. Fujiyama, *Bull. Chem. Soc. Jpn.* **53**, 2167 (1980).

II—F Intensity Distributions of Vibration Spectra

The detailed features of vibration spectra of the low pressure gas are completely determined by the structure of an isolated molecule. The vibration spectra of the liquid, on the other hand, may be affected by intermolecular interactions to some extent, although the strength of the chemical bond is much stronger than that of the intermolecular interactions. Therefore, we must consider the effects of intermolecular interactions in order to explain the spectral behaviours of the liquid samples.

Convesely speaking, intensity and band-shape measurements can be useful method for understanding the molecular behaviour in the condensed phases. In the present project, we focus our attention on the asymmetric feature of infrared absorption bands and the depolarization degree of Raman lines.

II-F-1 Shapes of the ν_1 Band of Liquid Chloroform and Intermolecular Interaction

Tetsuo SUZUKI, Yumiko K. TSUTSUI, and
Tsunetake FUJIYAMA

[*Bull. Chem. Soc. Jpn.*, **53**, 1931 (1980)]

The infrared absorption spectrum for the ν_1 fundamental of chloroform or chloroform-d shows strong asymmetry, with a remarkable tailing on the high frequency side. The observed band-width of the ν_1 fundamental of chloroform-d is significantly narrower than that of chloroform.

The asymmetric band profile of the ν_1 fundamental was successfully resolved into three symmetric band profiles. Being taken account of the band parameters obtained for the gas and the crystalline phases together with the concentration dependence of the relative intensities of these resolved bands, it has been concluded that there exist two different types of chloroform molecules in pure liquid chloroform. One is a molecule which

interacts with another molecule, and the other is a non-interacting molecule. The isotope effect on the width of the ν_1 band, on the other hand, can be explained in terms of the difference in the reduced mass.

The present result is essentially different from the previous works on the band parameter studies of the ν_1 band of liquid chloroform¹⁻⁶⁾ in a sense that the inhomogeneity of line-width is emphasized in the present study.

References

- 1) W. G. Rothschild, G. J. Rosasco, and R. C. Livingston, *J. Chem. Phys.*, **64**, 282 (1976).
- 2) L. C. Rosenthal and H. L. Strauss, *J. Chem. Phys.*, **64**, 282 (1976).
- 3) C. Brobeck, I. Rossi, Nguyen-Van-Thanh, and A. Ruoff, *Mol. Phys.*, **32**, 71 (1976).
- 4) J. Schroeder, V. H. Schiemann, and J. Jonas, *Mol. Phys.*, **34**, 519 (1977).
- 5) A. Moradi-Araghi and M. Schwartz, *J. Chem. Phys.*, **68**, 5548 (1978).
- 6) J. Schroeder, V. H. Schiemann, and J. Jonas, *J. Chem. Phys.*, **69**, 5479 (1978).

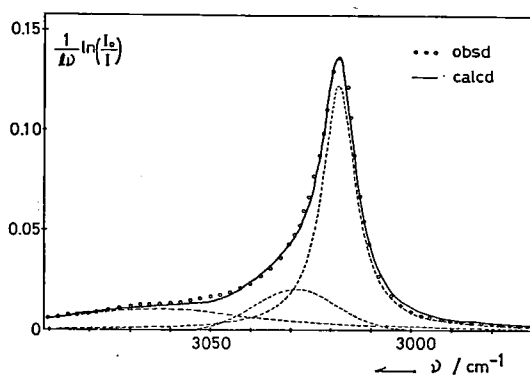


Figure 1. Observed (circles) and calculated (real line) spectra for the ν_1 band of CHCl_3 .

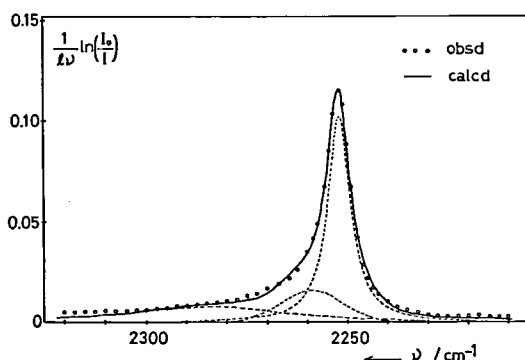


Figure 2. Observed (circles) and calculated (real line) spectra for the ν_1 band of CCl_4 .

II-F-2 Fluctuation of Local Field and Depolarization Degree of the ν_1 Line of Carbon Tetrachloride.

Shiaki HYODO¹⁾ (Tokyo Metropolitan Univ.) and
Tsunetake FUJIYAMA

[*Bull. Chem. Soc. Jpn.*, **53**, (1980)]

It has been established that the depolarization degree of Raman scattering, ρ , is expressed in terms of a Raman scattering tensor, $\bar{\alpha}'$, as

$$\rho = 3\gamma^2 / (45\bar{\alpha}^2 + 4\bar{\gamma}^2)$$

$$\text{where } \alpha = \frac{1}{3} (\alpha'_{xx} + \alpha'_{yy} + \alpha'_{zz})$$

$$\gamma^2 = \frac{1}{2} [(\alpha'_{yy} - \alpha'_{zz})^2 + (\alpha'_{zz} - \alpha'_{xx})^2 + (\alpha'_{xx} - \alpha'_{yy})^2]$$

Therefore, the depolarization degree ρ should be exactly zero, if the relation, $\alpha'_{xx} = \alpha'_{yy} = \alpha'_{zz}$, holds. The ν_1 Raman line of carbon tetrachloride is the very case of this, because the vibration belongs to an a_1 symmetry of a tetrahedral molecule. But it has never been observed to be zero: the most reliable value at present is $\rho = 0.0039 \pm 0.0002$ which is reported by Murphy et al.²⁾ In the present study, the depolarization degree of a molecule having a Td symmetry was expressed in terms of the mean square fluctuation of the local field which is felt by a molecule in the condensed phase. By the use of the mean square amplitude values observed by the X-ray diffraction method,³⁾ the depolarization degree of liquid carbon tetrachloride was calculated to be 0.0026, which agrees well with the observed value. This beautiful agreement, in turn suggests us the possibility of determining the magnitude of the thermal displacement of component molecules in the condensed system by observing depolarization degree of liquid samples. This line of approach is going to be extended to the solution systems.

Note and References

- 1) IMS Graduate Student from Tokyo Metropolitan Univ. for 1980 -
- 2) W. F. Murphy, M. V. Evans, and P. Bender, *J. Chem. Phys.* **47**, 1836 (1967).
- 3) K. Nishikawa and Y. Murata, *Bull. Chem. Soc. Jpn.* **52**, 293 (1979).

II—G Double Resonance Spectroscopy Using a Tunable Diode Laser

Lasers provide us with a variety of nonlinear spectroscopic techniques for gas phase molecular spectroscopy with ultra-high resolution and ultra-high sensitivity. One of such techniques, laser-microwave double resonance, is a useful method for, a) assignments of complicated absorption spectra, b) microwave spectroscopy of excited molecules, c) observation of nearly forbidden microwave transitions such as pure rotational transitions of nonpolar molecules, and d) investigation of state-to-state relaxation processes. In the infrared region, this technique has been applied to many molecular systems using fixed frequency lasers or semitunable lasers. However, in order to apply the technique, in general, to molecular systems of interest in spectroscopy, it is highly desirable to use a tunable laser in double resonance. The purpose of this project is to establish the experimental technique of infrared- microwave double resonance using a tunable diode laser, and to apply it to actual molecular systems in the whole infrared region.

II-G-1 Pure Rotational Spectrum of CF₄ in the $\nu_3 = 1$ State

Michio TAKAMI (*Inst. Phys. Chem. Res. and IMS*)

[*J. Chem. Phys.* **71**, 4164 (1979);
ibid **73**, (1980) in press]

Molecules with tetrahedral symmetry have a small vibrationally-induced dipole moments in their triply-degenerate vibrational states. In this work, pure rotational spectrum of CF₄ allowed by such induced dipole moment was investigated in the $\nu_3 = 1$ vibrational state by infrared-radiofrequency and infrared-microwave double resonance. A tunable diode laser was used as an infrared pumping radiation source. The observed pure rotational transitions were those among the tetrahedral fine structure splittings in the radiofrequency region, and those between the different Coriolis sublevels in the microwave region. So far 176 radiofrequency and 117 microwave transitions have been observed by double resonance with 100 kHz resolution. The observed spectrum revealed that one of the Coriolis sublevels, $R = J - 1$ state, was perturbed by the $2\nu_4$ state, which was about 20 cm^{-1} below the ν_3 state. From the transitions measured in the $R = J + 1$ and J Coriolis sublevels, tensor and scalar constants of the excited state were determined. The double resonance measurement made it possible to assign many vibration-rotation lines in the ν_3 Q-branch spectrum where a large number of infrared absorption lines were heavily overlapped within a narrow wavelength interval. From the analysis of Q-branch spectrum, accurate rotational and tensor constants in the ground vibrational state were determined. The determined constants are

summarized in Table I.

Table I. Molecular constants of CF₄.

$\nu_3 = 1$ state		
tensor constants		
α_{224}	-0.750 0 (3)	MHz
F_{134}	0.012 47 (6)	"
D_{044}	0.000 144 (4)	"
G_{244}	-0.000 120 (2)	"
G_{246}	0.000 077 2 (9)	"
H_{044}	$-0.043 (3) \times 10^{-6}$	"
H_{066}	$0.033 9 (14) \times 10^{-6}$	"
scalar constants		
B	5 720.52 (5)	MHz
α_{220}	3.92 (7)	"
ζ_3	0.808 08 (2)	"
ν_3	1 283.7191 (10) cm^{-1}	
Ground state		
B_0	5 731.631 (10)	MHz
D_{044}	0.000 136 7 (15)	"

II-G-2 Dipole Moment and Pure Rotational Transitions of SiH₄ and GeH₄ in the $\nu_3 = 1$ Vibrational State

Michio TAKAMI (*Inst. Phys. Chem. Res. and IMS*)

Infrared-radiofrequency double resonance using a tunable diode laser was applied also to investigate the pure rotational spectra of SiH₄ and GeH₄ in the $\nu_3 = 1$ vibrational state. Vibrationally-induced dipole moments in the ν_3 excited states of these molecules were found to be of the order of 0.02 D from their infrared Stark spectra. So far three radiofrequency transitions among the tetrahedral fine structure splittings of SiH₄ have been observed. More extensive double resonance measurement in SiH₄ and GeH₄ is in progress.

II—H Large Amplitude Intra-Molecular Motions

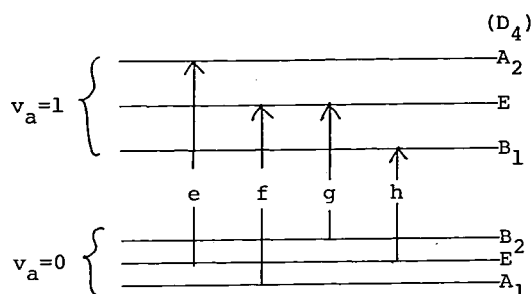
The subject of this study is a molecular distortion, whose amplitude is much greater than that of the usual molecular vibration, but which does not yet cause a decomposition of the molecule. Such a distortion takes place in the course of an internal rotation, inversion, and isomerization reaction of a molecule. High resolution infrared spectroscopy provides useful pieces of information on the detailed itinerary of a travel of a molecule from one equilibrium conformation to another and the amount of energy required in such a travel. For example, every vibrational level (v) of the hydrazine molecule splits into three sublevels because of the inversion motions of the two amino groups. The wavefunction $\psi_{vj}(\eta)$ associated to each of these sublevels represents a unique distribution of the probability with which any given η (inversion) coordinate occurs. An effective rotational constant A_{vj} derived from an infrared analysis is taken as the rotational constant $A(\eta)$ of the distorted molecule averaged over the all possible η values with the weight given by $|\psi_{vj}(\eta)|^2$. A number of A_{vj} values should, therefore, form a set of data for obtaining $A(\eta)$, and this is considered to be a valuable piece of information of the geometry of the molecule distorted along η .

II-H-1 Diode Laser Spectroscopy of Hydrazine — NH_2NH_2

Masamichi TSUBOI, Yoshiaki HAMADA, and Naoki TANAKA (*Faculty of Pharmaceutical Science, Univ. of Tokyo and IMS*)
Kentarou KAWAGUCHI, Chikashi YAMADA, Keiichi NAGAI, and Eizi HIROTA

Antisymmetric wagging band ($v_a = 1 \leftarrow 0$, 1020-860 cm^{-1}) and two twisting bands (1200-1350 cm^{-1}) of hydrazine, NH_2NH_2 , have been examined by the use of tunable infrared diode lasers (Laser Analytics LS-3). J-structures of ten Q-branch clusters in the former band and J-structures of nine Q-branch clusters in the latter two bands have been analyzed. Peak position of each line has been determined with a precision of about 0.0005 cm^{-1} by the use of etalon fringes, CO_2 or OCS standard

lines, and a high-precision λ meter. Some of the rotational constants and other parameters were determined. It has been found, in addition, that the inversion splitting becomes smaller with increasing J and with increasing K , both in the $v_a = 0$ state (shown by f-g) and $v_a = 1$ state (shown by e-h). An explanation is given for this finding.



II—I Production of Highly Excited Atoms from Molecules

Tamotsu KONDOW (*Univ. of Tokyo and IMS*), Tsutomu FUKUYAMA (*National Institute for Environmental Studies*), Shigeru OHSHIMA (*Univ. of Tokyo*), and Kozo KUCHITSU (*Univ. of Tokyo*)

Highly excited Rydberg atoms, i.e. atoms with very large principal quantum numbers (say $n \leq 50$), are produced in the gas phase by electron impact on atoms or molecules. One of the electrons (Rydberg electron) in such an atom is very weakly bound to the ion core, and consequently, this atom behaves like an assembly of two nearby independent particles: the Rydberg electron and the ion-core. In addition, its radiative lifetime is as long as μs or even ms , depending on its principal quantum

number.¹⁾ Therefore, a highly excited Rydberg atom is a long-lived species of high electronic energy and is a potential source of novel chemical reactions. In fact, its reaction with a molecule sometimes resembles that of a free electron with a molecule, while in other cases the reaction is similar to an ion-molecule reaction.²⁾

The purpose of the present project is to investigate the mechanisms of formation and reaction of highly excited Rydberg atoms by

producing them through an electron-impact dissociation of a variety of molecules. The experiment is based on the crossed molecular- and electron-beam scheme. The distributions of the kinetic energy and the principal quantum numbers of the high Rydberg atoms ejected from the molecule are measured as a function of the ejection angle.

Figure 1 shows a schematic diagram of the apparatus, which consists of a molecular beam source, a low energy electron gun, a field ionizer and a detector for highly excited Rydberg atoms (HIERA detector), and a mass spectrometer. The latter four devices are installed in a rotatable chamber so that the angular distribution of the high Rydberg atoms can be measured. In order to make an intense and monoenergetic molecular beam, a nozzle beam source was constructed. A supersonic beam is formed through a nozzle with an opening diameter of 50 or 90 μm . It was found to produce a nitrogen beam of about $3 \times 10^{17} \text{ s}^{-1} \text{ sr}^{-1}$ at a stagnation pressure of 1000 Torr. The effective divergence angle of the beam was about 3° . An electron gun of modified Simpson-Kuyatt type was employed to form the Rydberg atoms. A trip of LaB₆ or TaC was mounted on a hairpin filament in the gun so as to increase the electron emission. An electron current of $10^{-5} \sim 10^{-4} \text{ A}$ was obtained in the energy range of 5 ~ 100 eV. A test electron gun was placed in front of a field ionizer. It was used to monitor the intensity of the molecular beam

reaching the ionizer and to ensure that the HIERA detector and its circuits were operating properly. The test gun produced a rectangular electron beam of 10^{-4} A . The field ionizer consists of two parallel electrodes separated by 3 mm. Highly excited atoms of different principal quantum numbers are discriminated by changing an electrostatic voltage applied between these electrodes. The HIERA detector is composed of a plate and a grid facing each other and a channel plate multiplier mounted behind the grid. Highly excited Rydberg atoms are ionized almost completely when a voltage of 6 kV is applied between the plate and the grid. The product ions are collected by the channel plate multiplier.

Since highly excited atoms are produced by impact of pulsed electrons and ionized by the HIERA detector, the distributions of time of flight and principal quantum numbers can be measured simultaneously. A block diagram of electronic circuits for these measurements is shown in Figure 2. By introducing test signals the whole circuits were found to operate properly. Measurements are being carried out on the highly Rydberg nitrogen atoms produced from a nitrogen molecular beam excited by electrons of 50 eV and 50 μA .

References

- 1) R. F. Stebbings, *Adv. Atom. Mol. Phys.*, **15**, 77 (1979).
- 2) H. Hiraishi, T. Kondow, T. Fukuyama and K. Kuchitsu, *J. Phys. Soc. Jpn.*, **46**, 1628 (1979); *ibid.*, *Chem. Phys. Lett.*, **66**, 9 (1979).

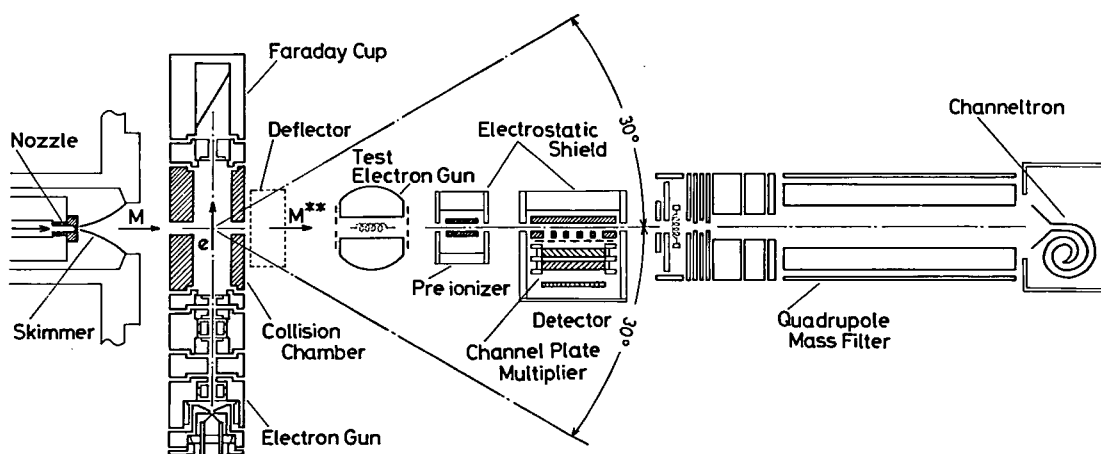


Figure. 1 A schematic diagram of the apparatus

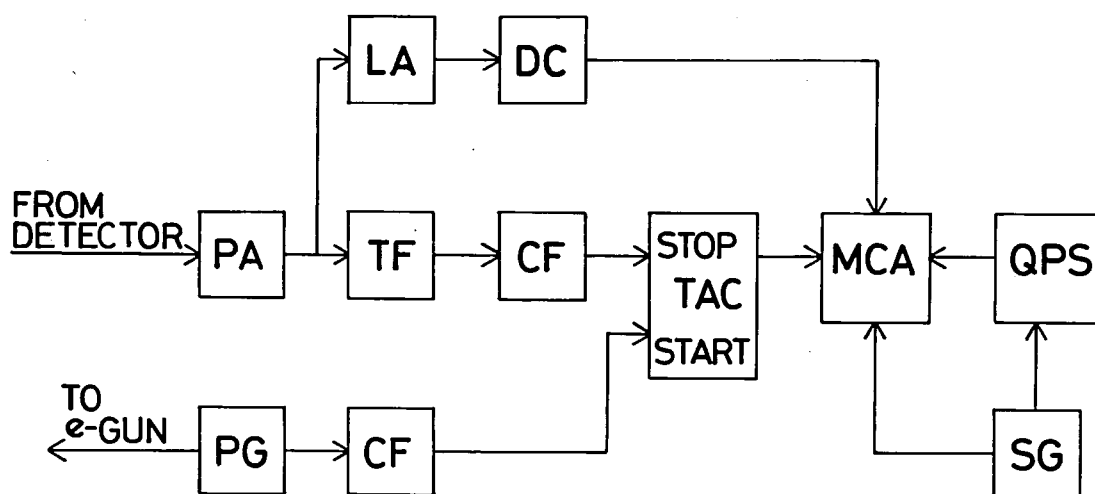


Figure 2. A block diagram of the detector circuits.

PA preamplifier
 LA linear amplifier
 DC discriminator
 TF timing filter amplifier
 CF constant fraction discriminator
 TAC time-to-amplitude converter

MCA multichannel analyzer
 QPS quadrupole power supply for mass spectrometer
 SG sawtooth generator
 PG pulse generator

RESEARCH ACTIVITIES III

Division of Electronic Structure

III—A Primary Photochemical Reactions of Organic Compounds

III-A-1 Direct Measurement of the Reaction Rate for cis \rightarrow trans Photoisomerization of Stilbene.

Minoru SUMITANI, Nobuaki NAKASHIMA, and Keitaro YOSHIHARA

[*Chem. Phys. Lett.*, **68**, 225 (1979)]

Rate constants are reported for cis-trans isomerization of stilbene, obtained by monitoring fluorescence generated by two consecutive picosecond light pulses. The main reaction is shown to occur in the singlet manifold via perpendicular singlet state with a lifetime shorter than a few picoseconds.

III—B Electronic Structures of Excited States

III-B-1 Laser Flash Photolysis of Benzene. II. Laser-Induced Cluster Formation in Gas Phase.

Nobuaki NAKASHIMA, Haruo INOUE, Minoru SUMITANI, and Keitaro YOSHIHARA

[*J. Chem. Phys.*, in press]

Gaseous benzene of 21 torr (about 1/4 of the saturated vapor pressure) was excited by a KrF excimer laser with an emission at 248 nm. The absorption immediately after excitation is assigned to an $S_n \leftarrow S_1$ transition. Three peaks are observable quite similar to the solution spectrum.¹⁾ With a rise time of several tens of nanoseconds appears a broad spectrum of a transient species (Tx) as a shoulder around 225 nm. In the presence of oxygen (720 torr) Tx is produced immediately after excitation. Tx is completely quenched by cis-2-butene.

A depletion of gaseous benzene was observed in the time-resolved spectra (Figure 1). The depletion is accompanied by an appearance of broad absorptions at lower wave length region. The quantum yield of fluorescence and of isomerization upon excitation around 248 nm is known to be 0.09 and 0.07, respectively. Thus the quantum yield of the formation of Tx must be less than or equal to 0.84. The absorption intensity of the species due to a broad absorption and Tx are proportional to that of the $S_n \leftarrow S_1$ absorption and the laser intensity.

A formation of the benzene mist was observed

visually. The relation between the appearance of broad absorption in the nanosecond time scale and the formation of a mist is under investigation.

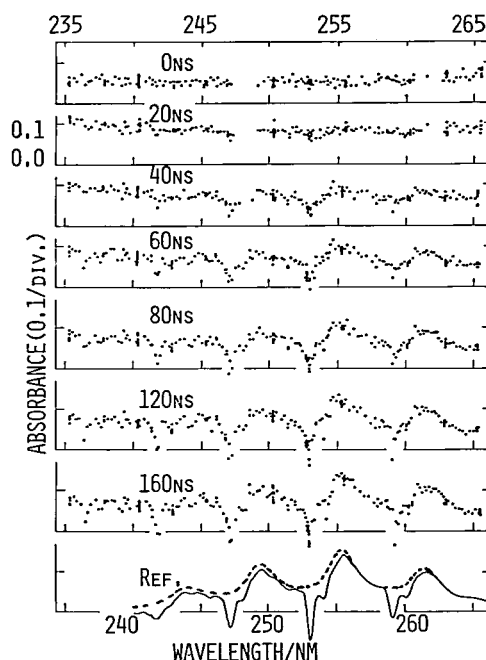


Figure 1. Time-resolved transient absorption spectra of gaseous benzene at 21 torr. Delay times are from the peak of the laser pulse. Ref. (· · · ·) absorption spectrum of benzene in chloroform; (—), difference (solution-gas) spectrum.

Reference

- 1) N. Nakashima, M. Sumitani, I. Ohmine, and K. Yoshihara, *J. Chem. Phys.*, **72**, 2226 (1980).

III-B-2 Laser Flash Photolysis of Benzene. III. $S_n \leftarrow S_1$ Absorption of Gaseous Benzene.

Nobuaki NAKASHIMA, Haruo INOUE, Minoru SUMITANI, and Keitaro YOSHIHARA

[*J. Chem. Phys.*, in press]

Gaseous benzene was excited by a KrF excimer laser and a transient absorption was observed in the region between 210 and 930 nm. The $S_n \leftarrow S_1$ absorption spectrum is assigned with time-resolved spectroscopy and with its effects on foreign gas. Three peaks have been found and are assigned as follows: 545 nm ($^1E_{1u}$, $f \sim 0.003$), 400 nm (1^1E_{2g} , $f \sim 0.02$), and 267 nm (2^1E_{2g} , $f \sim 0.08$). The observed energies above the ground state are 7.8 eV for the 1^1E_{2g} state and 9.4 eV for the 2^1E_{2g} state. Spectral shapes become sharper and each peak shifts to shorter wavelengths compared with those in cyclohexane solution. The results suggest that the 2^1E_{2g} has a valence character. Other differences between the solution and gas spectra are discussed.

III-B-3 Time-resolved Measurements of Electron and Energy Transfer of Rhodamine B Monolayer on Surface of Organic Crystals.

Nobuaki NAKASHIMA, Keitaro YOSHIHARA, and Frank WILLIG

[*J. Chem. Phys.*, in press]

Fluorescence decays of a monolayer of rhodamine B on single crystals of anthracene, phenanthrene, and naphthalene have been measured for the first time with a picosecond laser and a streak camera. The fluorescence decays were not single exponentials. Two different decay characteristics have been observed corresponding to an exo- and endo-energetic electron transfer reaction between excited dye and substrate. The short decay of 35 ± 7 ps on an anthracene crystal is explained by the electron-transfer kinetics from anthracene to excited rhodamine B. In the cases of naphthalene and phenanthrene, the electron transfer reaction becomes endo-energetic and slower. The decays within several tens of picoseconds are analysed in terms of two-dimensional Förster-type energy transfer to quencher sites where dyes are suggested to be in contact with each other. In connection to this phenomenon, the concentration quenching of the fluorescence of rhodamine B in aqueous solution was elucidated in terms of the Förster-type energy transfer to the nonfluorescent dimer leading to a nonexponential decay.

III-B-4 Biphotonic Ionization of 8-Anilino-1-Naphthalenesulfonate in Polar solvents

Hiroki NAKAMURA, Jiro TANAKA (*Nagoya Univ.*), Nobuaki NAKASHIMA, and Keitaro YOSHIHARA

The photonization of 8-anilino-1-naphthalene-sulfonate in polar solvents occurs through a biphotonic process, proved by ns flash photolysis. A transient absorption of a charge transfer to solvent (CTTS) state is found with ~ 10 ns lifetime. The CTTS state is shown to be an intermediate of the photoionization process.

III-B-5 Picosecond Time-Resolved Fluorescence Studies of Intramolecular Heteroexcimers

Masahito MIGITA, Tadashi OKADA, Noboru MATAGA (*Osaka Univ.*), Nobuaki NAKASHIMA, Keitaro YOSHIHARA, Yoshiteru SAKATA, and Soichi MISUMI (*Osaka Univ.*)

[*Chem. Phys. Lett.*, **72**, 229 (1980)]

Intramolecular heteroexcimer formation processes in the excited state of $p - (CH_3)_2N - C_6H_4 - (CH_2)_3 - (9\text{-anthryl}) (A_3)$ as well as $p - (CH_3)_2N - C_6H_4 - (CH_2)_3 - (1\text{-pyrenyl}) (P_3)$ in hexane and 2-propanol have been investigated by means of picosecond time-resolved fluorescence measurements.

III-B-6 Picosecond Laser Spectroscopy of Intramolecular Heteroexcimer Systems. I. Time-Resolved Fluorescence Studies of $p - (CH_3)_2NC_6H_4 - (CH_2)_n - (9\text{-Anthryl})$, $p - (CH_3)_2NC_6H_4 - (CH_2)_n - (1\text{-Pyrenyl})$ Systems and 9,9'-Bianthryl

Masahito MIGITA, Tadashi OKADA, Noboru MATAGA (*Osaka Univ.*), Yoshiteru SAKATA, Soichi MISUMI (*Osaka Univ.*), Nobuaki NAKASHIMA, and Keitaro YOSHIHARA

In order to elucidate the details of elementary processes of photochemical charge transfer and heteroexcimer formation processes, and also in order to compare the obtained results with those of transient absorption spectral measurements, we have examined the following intramolecular heteroexcimer systems by means of ps time-resolved fluorescence measurements with a mode-

locked Nd: YAG laser and a streak camera: $p - (\text{CH}_3)_2\text{NC}_6\text{H}_4 - (\text{CH}_2)_n - (9\text{-anthryl})$ ($n=0, 1, 2, 3$), $p - (\text{CH}_3)_2\text{N} - \text{C}_6\text{H}_4 - (\text{CH}_2)_n - (1\text{-pyrenyl})$ ($n=1, 2, 3$) and 9,9'-bianthryl. Effects of methylene chain length, solvent polarity as well as viscosity upon the intramolecular charge transfer processes have been clearly demonstrated. It is concluded that molecules with a sandwich configuration in the ground state are not recognized in both of $n=3$ compounds and it takes a few ns for the heteroexcimer formation in hexane because of an extensive conformation change necessary to take sandwich configuration. Both of conformation

change and solvent reorientation are involved in the heteroexcimer formation processes in polar solvents, and the heteroexcimer formation becomes faster with increase of solvent polarity and with decrease of solvent viscosity. Moreover, two-step conformation changes are observed in the case of the heteroexcimer formation of $n=3$ compound in polar solvents, i.e. a heteroexcimer with loose structure is formed at first, which is followed by a structural change to the one of sandwich type. In strongly polar solvent, acetonitrile, formation of heteroexcimer is very fast, occurring within the time-resolution of the picosecond apparatus.

III—C Studies on Transient Phenomena in biology

III-C-1 Picosecond Fluorescence Lifetime of the Coenzyme of D-Amino Acid Oxidase

Nobuaki NAKASHIMA, Keitaro YOSHIHARA, Fumio TANAKA (*Mie Nursing College*), Kunio YAGI (*Nagoya Univ.*)

[*J. Biol. Chem.*, **255**, 5261 (1980)]

Conformational difference surrounding the coenzyme, FAD, of D-amino acid oxidase [D-amino acid: O_2 oxidoreductase (deaminating), EC 1.4.3.3.] between its monomeric and dimeric forms were examined by observing fluorescence of FAD. The fluorescence lifetime of the coenzyme was measured directly with a mode-locked Nd:YAG laser and a streak camera in picosecond region. The values of lifetime of FAD fluorescence in the monomer and dimer were 130 ± 20 ps and 40 ± 10 ps, respectively. The relative quantum yield of the fluorescence of FAD combined with the protein to that of free FAD depended on the concentration of the enzyme; it was higher at lower concentration. Comparing the lifetime with relative quantum yield of FAD combined with the protein, it is concluded that the fluorescence is quenched mostly by a dynamic process. These results indicate that the distance between the isoalloxazine nucleus and a quencher is nearer in the dimer than in the monomer.

III-C-2 Picosecond Transit Behavior of the Reaction-Center Particles of Photosystem I Isolated from Spinach Chloroplast. I. Decay Characteristics of Excited Chlorophylls

Akira NAMIKI, Nobuaki NAKASHIMA, Keitaro YOSHIHARA, Isamu IKEGAMI (*Teikyo Univ.*)

Transient behavior in the reaction center particles of photosystem I isolated from spinach chloroplasts was studied by absorption and fluorescence spectroscopy on a picosecond time scale. Immediately after an intense excitation ($\text{ca. } 5 \times 10^{16}$ photons/ cm^2), a marked depletion of the absorption peak was observed. In both absorption and fluorescence, the recovery of the ground state and the decay of the excited state were found to be consist with a fast component (~ 25 ps) and slow component (~ 1.0 ns) for the reaction center particles. Only one slow component (~ 1.0 ns) was observed in photosystem I particles. After changing the redox state of the reaction center, the fast component was ascribed to the efficient energy quenching process of the nearest neighbour antenna chlorophylls by the reaction center.

III-C-3 Picosecond Transient Behavior of the Reaction-Center Particles of Photosystem I Isolated from Spinach Chloroplast. II. Energy Transfer and Electron Transfer at Weak Light Excitation

Keiji KAMOGAWA, Nobuaki NAKASHIMA, Keitaro YOSHIHARA, and Isamu IKAGAMI (*Teikyo Univ.*)

Primary process of photosynthesis in picosecond time scale was investigated with highly enriched reaction center particles of photosystem I prepared from spinach chloroplasts. Spectral changes were observable even under the condition of a low intensity excitation, one photon for a reaction center. In contrast to the results under intense excitation, the flash absorption spectra showed only a slight decay of the main bleaching band at 676 nm and a remarkable variation of the band

feature as time proceeded. The most characteristic change was an appearance of a new band in the 700 nm region. It was almost accomplished within 50 ps and the new band did not decay even at 8 ns. In a chemically oxidized sample, $P700^+ - X$, the main bleaching decayed without any spectral change. These observations indicate that the excitation

transferred from antenna chlorophylls to P700 and subsequently P700 was oxidized resulting $P700^+$ in a stable form. Kinetic analysis showed that the charge separation proceeds with a time constant of ca. 30 ps. An absorption appeared around 750 nm during a few tens of picoseconds and is assigned to an $S_n - S_1$ absorption of P700.

III—D Solar Energy Conversion by Using Photocatalytic Effects of Semiconductors —Decomposition of Water and Hydrogen Evolution—

III-D-1 Photocatalytic Decomposition of Gaseous Water over TiO_2 and TiO_2-RuO_2 Surfaces

Tomoji KAWAI and Tadayoshi SAKATA

[*Chem. Phys. Lett.*, 72 87 (1980)]

The photocatalytic decomposition of water over semiconductor powder is an attractive way to convert solar into chemical energy. The advantages over electrochemical cell are that no electrical connection is required and the effective surface area of the catalyst can be increased easily.

Hg-lamp radiation leads to the continuous production of hydrogen and oxygen from gaseous water at room temperature. The rate of hydrogen evolution per 100 mg TiO_2-RuO_2 and 20 hours was 11 micromole at a steady state.

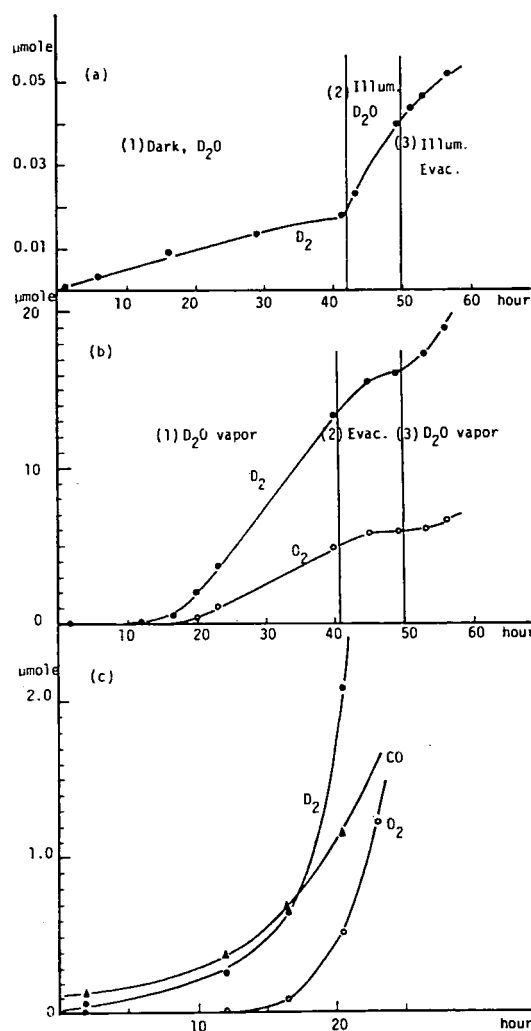
III-D-2 Photocatalytic Decomposition of Water by Solar Energy. Hydrogen Evolution, CO_2 Fixation on Powdered Semiconductors and their Mechanisms with Pulsed Laser-Dynamic Mass Technique

Tomoji KAWAI and Tadayoshi SAKATA

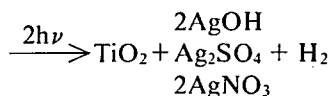
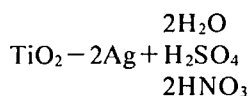
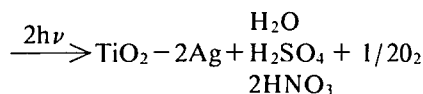
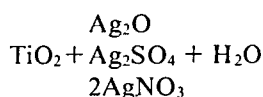
[*Proceedings of 7th Int. Cong. Catalysis*, B38 (1980)]

Since simultaneous evolution of hydrogen and oxygen from water is not desirable, we have developed a method to produce hydrogen and oxygen separately using TiO_2-Ag/Ag^+ catalyst powder. In this two step photodecomposition of water, we could successfully produce H_2 and O_2 separately in time, as follows;

Figure 1. (a) The amount of D_2 evolved against the reaction time at room temperature on a reduced TiO_2 catalyst prepared



by irradiation in the presence of CO gas (100 Torr) for 10 h to form CO_2 ; (1) in dark, with saturated D_2O vapor, (2) under irradiation with D_2 vapor, (3) under irradiation without D_2O vapor. Heat-treated reduced surfaces show similar behaviour, although the amount of D_2 produced is dependent on the period and temperature of the heat treatment. (b) The amount of D_2 and O_2 evolved during irradiation against the reaction time on TiO_2-RuO_2 catalyst (TiO_2 : 80 mg, RuO_2 : 20 mg) at room temperature; (1) with saturated D_2O vapor, (2) without D_2O vapor, (3) with D_2O vapor. (c) Expansion of (b) to show the early stage of the reaction.



III-D-3 Photocatalytic Hydrogen Production from Liquid Methanol and Water.

Tomoji KAWAI and Tadayoshi SAKATA

[*J.C.S. Chem. Comm.*, **694** (1980)]

Hydrogen production from methanol and water is an attractive process, since methanol can be used

Since the band gap of TiO_2 is in the UV region (3eV), sun light cannot be used efficiently. We report the results of H_2 evolution from water, which is efficiently driven by the visible light by using inorganic semiconductors (CdS , GaP , Ag_2S and Fe_3O_4) and EDTA as an electron donor.

Table I. H_2 evolution from water with EDTA by visible light

Photocatalyst	H_2 (μmol)
CdS	9.8
GaP	4.4
Ag_2S	0.03
Fe_3O_4	22.0

* CdS = 400 mg, GaP , Ag_2S , Fe_3O_4 = 700 mg

*reactant: H_2O (l) = 40 mol EDTA = 250 mg

*10 hr irradiation

as a fuel in the form of hydrogen gas, a clean fuel in the hydrogen energy system. This reaction has been carried out thermally in the vapor phase at temperatures above 250°C using a catalyst such as Fe_2O_3 . We report here that H_2 is highly efficiently produced at room temperature from liquid CH_3OH and H_2O using a TiO_2 powder photocatalyst mixed with metal (Pt , Pd), metal oxide (RuO_2) or Rhodium complex.

Table I. H_2 production from CH_3OH (10 ml) and H_2O (10 ml) on various supported TiO_2 photocatalysts. 500 W Xe-lamp, 10 hour irradiation.

Photocatalyst	H_2 (mmol)/10 hr	Quantum yield at $\lambda = 380 \text{ nm}$
TiO_2	0.27	3.2%
$\text{RuO}_2/\text{TiO}_2/\text{Pt}$	5.2	44.0
TiO_2/Pt	4.6	40.0
TiO_2/Pd	2.2	19.0
$\text{RuO}_2/\text{TiO}_2$	0.37	4.0
$\text{TiO}_2/[\text{Ph}_3\text{P}]_3\text{Rh (I) Cl}$	0.49	4.2
$\text{TiO}_2 + \text{MV}$, $\text{Pt}/\text{Al}_2\text{O}_3$	0.99	8.6

^a Photocatalyst = 300 mg, Pt : 5wt %, Pd : 5wt %, RuO_2 : 10wt %, $[\text{Ph}_3\text{P}] \text{ Rh (I) Cl}$: 10wt %, M.V. (methylviologen): 20 mg, Pt (3wt %)/ Al_2O_3 : 20 mg

III-D-4 Conversion of Carbohydrate into Hydrogen Fuel by a Photocatalytic Process

Tomoji KAWAI and Tadayoshi SAKATA

[*Nature* **286** 474 (1980)]

Most green plants synthesize carbohydrates,

such as sugar, starch or cellulose, from water and carbon dioxide. We show a new route for the conversion of carbohydrates into hydrogen (a clean fuel in the hydrogen energy system), taking advantage of the photocatalytic process. We found that the irradiation of the carbohydrates in the presence of water and a $\text{RuO}_2/\text{TiO}_2/\text{Pt}$ photocatalyst powder leads to the efficient

production of hydrogen gas. This new process is expressed as equation (1) together with the

photosynthesis of carbohydrates by green plants eq. (2).

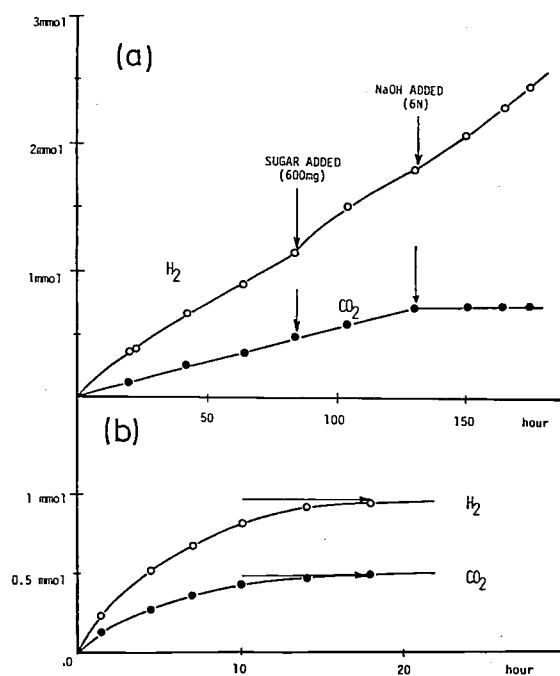
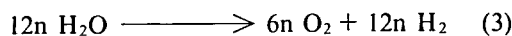
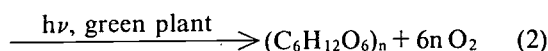
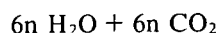
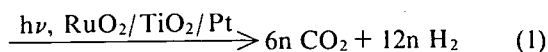
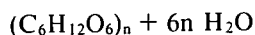


Figure 1. (a) H₂ and CO₂ evolution from sugar in water versus the irradiation time. Experimental conditions: sugar (600 mg), H₂O (40 ml), RuO₂/TiO₂/Pt (300 mg), 500 W Xe irradiation. Additional sugar (600 mg) and NaOH (9.6 g) were put into the solution at 85 and 130 hours after the start of the reaction, respectively.

(b) H₂ and CO₂ production with the irradiation time from a small amount of sugar. Experimental conditions: 500 W H₂-ultrahighpressure lamp, sugar (13 mg), H₂O (40 ml), RuO₂/TiO₂/Pt (150 mg). Arrows (—>) indicate the estimated amounts of H₂ and CO₂ which are produced from 13 mg of sugar according to eq. (1).



Here, (C₆H₁₂O₆)_n represents sugar (saccharose) (n = 2), starch (n ≈ 100) or cellulose (n ≈ 1000 to 5000) after hydrolysis.

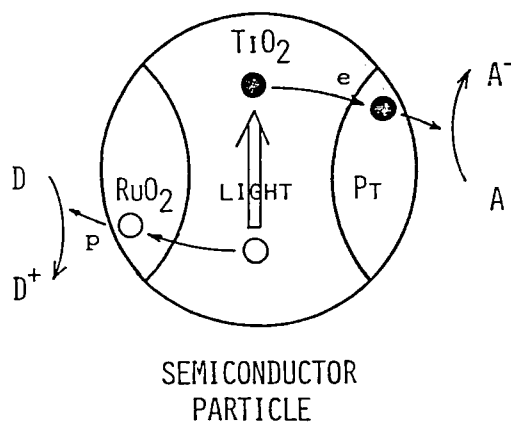


Figure 2. A schematic figure of the RuO₂/TiO₂/Pt particle. ○: hole (p) in the valence band of TiO₂, ●: electron (e) in the conduction band. A and D represent acceptor and donor, respectively, of electrons in the solution. In reaction (1), carbohydrate and proton in the solution play the roles of D and A, respectively.

Table I. H₂ and CO₂ evolution from water and sugar, starch or cellulose on the RuO₂/TiO₂/Pt photocatalyst suspended in neutral water and 6N NaOH solution, irradiated by 500 W Xe lamp. The rates of gas evolution represent the values at 50 hours after the beginning of the irradiation.

Reactant	H ₂ (μmol/20 hr)	CO ₂ (μmol/20 hr)	Quantum Yield at λ = 380 nm
Sugar + H ₂ O	280	133	1.2%
Starch + H ₂ O	204	96	0.8
Cellulose + H ₂ O	70	42	0.3
H ₂ O	4	/ ^a	0.02
Sugar + 6N NaOH	341	/	1.5
Starch + 6N NaOH	320	/	1.3
Cellulose + 6N NaOH	244	/	1.0
Sugar + H ₂ O with TiO ₂ Catalyst	2	1.2	/

^a Oxygen (1.6 μmol/20 hr) was simultaneously evolved.

^b Experimental conditions: Sugar (600 mg), Starch (120 mg), Cellulose (120 mg)
RuO₂/TiO₂/Pt photocatalyst (300 mg)
H₂O (40 ml), 6N NaOH aqueous solution (40 ml)

III-D-5 Hydrogen Production from Biomass and Water by Photocatalytic Reactions

Tadayoshi SAKATA and Tomoji KAWAI

Total photosynthetic production on the earth is estimated to be 5×10^{10} ton/year, expressed as carbon. A huge amount of energy, 6 – 10 times as much as the total energy demand of mankind, is stored every year through the photosynthetic activity of green plants and some bacteria. Its utilization to produce fuels has been proposed by a number of people. The production of methane or ethanol by fermentation of biomass or the extraction of hydrocarbons from some special plants such as heavea and *Euphoriba lathyris* have been considered. We report a new method of hydrogen production from biomass such as wood, cotton, grasses and seaweed by using photocatalytic reactions of a powdered semiconductor suspended in water. This method is a very simple one and has some advantages over fermentation in which some delicate procedures such as temperature control and sterilization are indispensable.

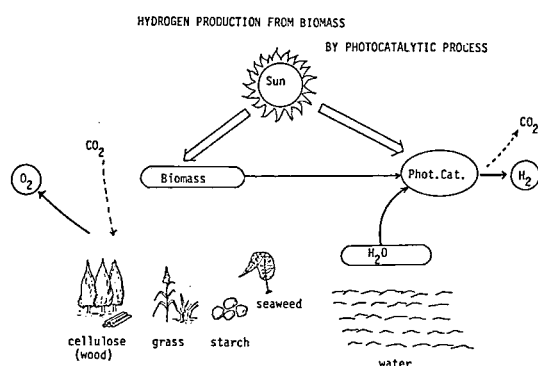
Table I. Photocatalytic Hydrogen Production from Biomass

	H ₂ (μmol/10h)	Q.Y. at 380 nm
Cotton (Cellulose)	200	1.5%
Starch	170	1.3
Sweet potato	378	2.8
Wood (Cherry)	148	1.1
Grass (White Dutch clover)	142	1.1
Lignin	77	0.6
Fatty oil	212	1.6
Seaweed	166	1.2
Human urine	228	1.7

Photocatalyst: Pt (4%)/TiO₂

Light source: 500W Xe lamp

5N NaOH



III-D-6 Heterogeneous Photocatalytic Production of Hydrogen and Methane from Ethanol and Water

Tadayoshi SAKATA and Tomoji KAWAI

Ethanol as a fuel has been attracting attention because of the expected exhaustion of petroleum in the near future. In several countries such as Brazil and the USA, they are beginning to utilize ethanol as a fuel for automobiles. And its mass production has been planned from biomass fermentation in expectation of increasing demand.

Thus the utilization and reforming of ethanol is of current interest. We found that the band gap irradiation of TiO₂ photocatalyst suspended in an ethanol-water mixture can produce hydrogen, methane and acetaldehyde at room temperature. When the surface of the photocatalyst was modified with various metals, metal oxides or metal-complexes, the quantum yield of hydrogen production was increased remarkably, amounting to 38% for Pt-TiO₂. Besides the increase of reactivity, this surface modification was found to bring about a sensitization effect, causing hydrogen to be evolved even by sub-band gap irradiation.

The main reaction path is considered to be as follows.

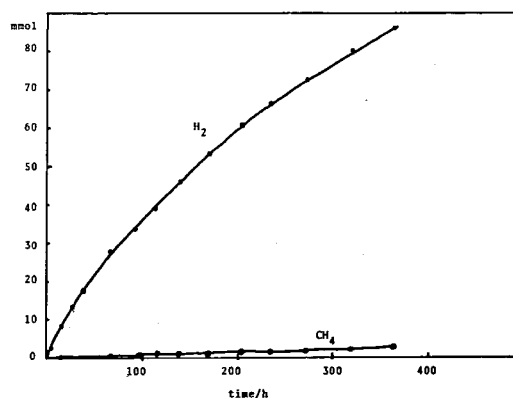
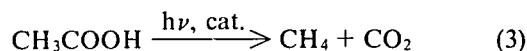
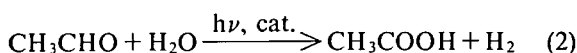
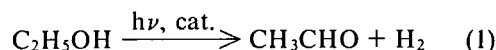


Figure 1. H₂ and CH₄ evolution from ethanol and water versus the irradiation time. Experimental conditions: ethanol (15 mL), H₂O (15 mL), Pt/TiO₂ (300 mg), 500W Xe irradiation.

Table I Hydrogen production from C₂H₅OH (15 mL) and H₂O (15 mL) on various supported TiO₂ photocatalysts (300 mg)^a and the quantum yields under monochromatic irradiation at 380 nm.

Photocatalyst	H ₂ (mmol) ^a	Quantum Yield ^d at 380 nm (%)
TiO ₂	0.11	0.8
Ir (CO) (PPh ₃) ₂ Cl/TiO ₂ ^b	0.31	2.3
(PPh ₃) ₃ RhCl ₃ /TiO ₂ ^c	0.60	4.5
Pd/TiO ₂	0.65	4.9
Ni/TiO ₂	0.87	6.5
Rh/TiO ₂	2.50	19.0
Pt/TiO ₂	5.08	38.0

^a 500W Xe lamp; irradiation for 10h.

^b Chlorocarbonyl bis (triphenylphosphine) iridium (I)

^c Chlorotris (triphenylphosphine) Rh (I)

^d The experimental error of quantum yields is within 10% of each value.

III-D-7 Photocatalytic Reaction of Benzene, Naphthalene and Coal with Water

Kazuhito HASHIMOTO, Tomoji KAWAI and Tadayoshi SAKATA

It is well known that benzene is stable even under irradiation. Our experiments demonstrate that benzene is decomposed by the photocatalytic reaction with water using Pt/TiO₂ or Pt/TiO₂/RuO₂ with the band-gap radiation of TiO₂ (400 nm). By using the same method, other aromatic compounds and fossil fuel such as coal, oil sand and pitch were found to react with water to form carbon dioxide and hydrogen. Table I shows hydrogen production from various organic compounds and water under UV illumination with a 500 W Xe lamp. One of the most efficient reactions for the hydrogen production is methanol and water system, in which the amount of hydrogen production exceeds 1.5 m mol per 10 hours and the quantum yield of hydrogen production is 50%. The decomposition of aromatic compounds is difficult as compared with that of alcohols, especially in neutral aqueous solutions. The hydrogen production rate, however, is increased remarkably by adding NaOH to the solutions, and the rate is scarcely dependent on the kind of aromatic compounds; the hydrogen production rate for small aromatic compounds like benzene is almost equal to that of highly polymerized compounds like coal. Figure 1 shows the temperature dependence of the hydrogen production rate from coal and water. The observed rate at 100°C is about five times as much as that at 25°C. This result seems to indicate the existence of dark reactions.

In practical application, two problems are left to be solved. One is to increase the reaction efficiency more than 10 times, and the other is to develop a

small band-gap semiconductor which is stable and can absorb a visible light. If one could succeed in solving these problems, this new photocatalytic reaction would become one of the most efficient methods for gasifications of solid or liquid fossil fuels.

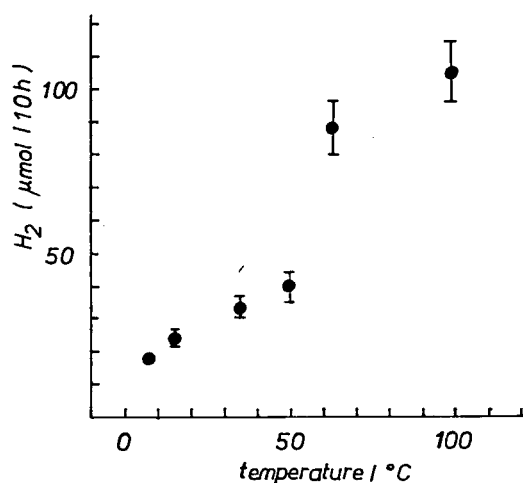


Figure 1. Temperature dependence of the hydrogen production rate from coal and water by using Pt/TiO₂ as a photocatalyst.

Table I. The amount of hydrogen production from various organic compounds. [μ mol / 10 hours]

Reactant	Neutral aq. soln.	Alkaline aq. soln
Benzene	55	200
Naphthalene	10	90
Coal	15	170
Oil sand	0	100
(Methanol)	13900	—
(Ethanol)	5500	—
(Sugar)	280	340

III-D-8 Luminescence of $\text{Ru}(\text{bipy})_3\text{Cl}_2$ Adsorbed on Semiconductor or Insulator

Takashi KAJIWARA (*Toho Univ.*), Kazuhito HASHIMOTO, Tomoji KAWAI and Tadayoshi SAKATA

We have studied the hydrogen production from water and, or organic compound by using semiconductors. However, most semiconductors which are stable under irradiation in electrolyte solution have wide band-gaps; they work efficiently only with UV light. For extending the absorbing range, dye sensitization would be one of the most probable methods. To develop a new method for solar energy conversion based on dye sensitization, we studied the dynamical properties of the excited state of $\text{Ru}(\text{bipy})_3\text{Cl}_2$ adsorbed on powdered semiconductors (TiO_2 , SnO_2 , —) or insulators (SiO_2 , ---) by using n sec pulsed dye laser as a exciting light source. The luminescence of $\text{Ru}(\text{bipy})_3\text{Cl}_2$ was found to be influenced strongly, depending on the kind of substrate material.

(1) *Insulator* The luminescence of $\text{Ru}(\text{bipy})_3\text{Cl}_2$ on SiO_2 is composed of two exponential decay components, a fast one of 260 ns decay time and a slow one of 1.1 μs at liquid N_2 temperature, whereas that of $\text{Ru}(\text{bipy})_3\text{Cl}_2$ in solution exhibits a single exponential decay. This result seems to indicate the existence of two different adsorbing sites.

(2) *Semiconductor* The luminescence of $\text{Ru}(\text{bipy})_3\text{Cl}_2$ on TiO_2 and SnO_2 is composed of two different kinds of components. One is the very fast component which decays in a exciting pulse range (10 ns). The other is a slow component which decays exponentially versus a square root of time.

The fast decay is considered to be caused by the quenching process due to the electron transfer from the excited dye to semiconductor (anodic photocurrent).

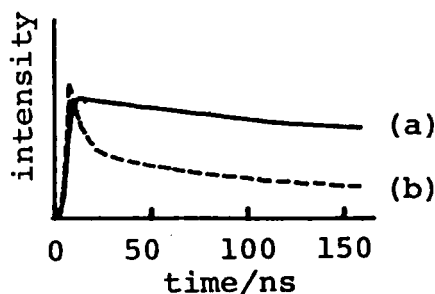


Figure 1. Initial decay of luminescence from $\text{Ru}(\text{bipy})_3\text{Cl}_2$ adsorbed on SiO_2 (a) and TiO_2 (b) powder at liquid N_2 temperature.

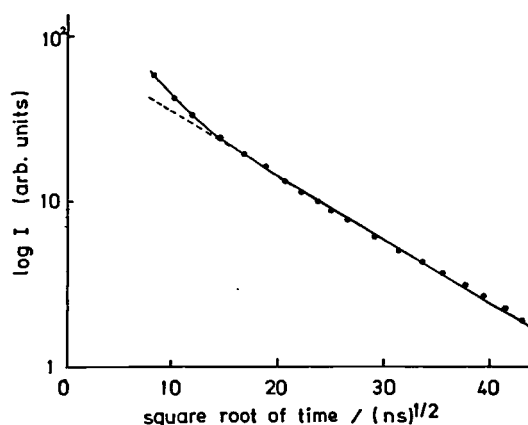


Figure 2. Semilogarithmic plot of luminescence intensity versus a square root of time for $\text{Ru}(\text{bipy})_3\text{Cl}_2$ adsorbed on SnO_2 powder at liquid N_2 temperature.

III—E Study of Elementary Processes in Chemical Reaction

The purpose of the project is to perform a detailed study on the reactivity of molecules in vibrationally and/or electronically excited states and on the distribution of energy among the internal states of reaction products. A crossed molecular beam apparatus was constructed for the purpose of studying the effect of laser irradiation and product internal energy distribution under the collision-free condition. With a quadrupole mass spectrometer and the laser-induced fluorescence technique, the molecular beam apparatus will be a powerful tool in clarifying the elementary chemical reaction mechanism.

III-E-1 Construction of Crossed Molecular Beam Apparatus

Iwao NISHIYAMA and Ichiro HANAZAKI

An atomic collision technique using a molecular beam is a powerful mean for the study of chemical reaction under a collision free condition. Detailed

and clear information for the dynamics of chemical reaction can be obtained by combining the technique with sensitive detection methods such as mass spectrometry and recently developed laser spectroscopy. We have designed and constructed a crossed molecular beam apparatus in order to study the internal and translational energy distribution of products and/or effects of internal energy excitation of a reactant on a chemical reaction.

The vacuum chamber and pumping system are shown in Figure 1. This apparatus has two sets of nozzle-beam sources crossed at right angles with each other. Each beam source is divided into two chambers, each can be evacuated differentially by two oil-diffusion pumps. A supersonic nozzle (50 μm in diameter) and a skimmer (500 μm in diameter) are set in the chamber evacuated by a 3500 ls^{-1} oil-diffusion pump. This chamber, flange-fitted to the main chamber, can be removed easily along a slide rail. A nozzle to skimmer distance can be varied from 0 to 30 mm. Main chamber (collision chamber) is a stainless steel cylinder with dimensions about 910 mm ϕ \times 750 mmH, and can be evacuated to 8×10^{-8} Torr by 3500 ls^{-1} oil-diffusion pump. The chamber has optical windows for the purpose of introducing laser light. Pulsed IR and visible/UV lasers are used for the excitation of reactants and detection of products. A quadrupole mass filter (Extranuclear Labs) is installed in the chamber and differentially pumped by two ion pumps in order to reduce a background signal.

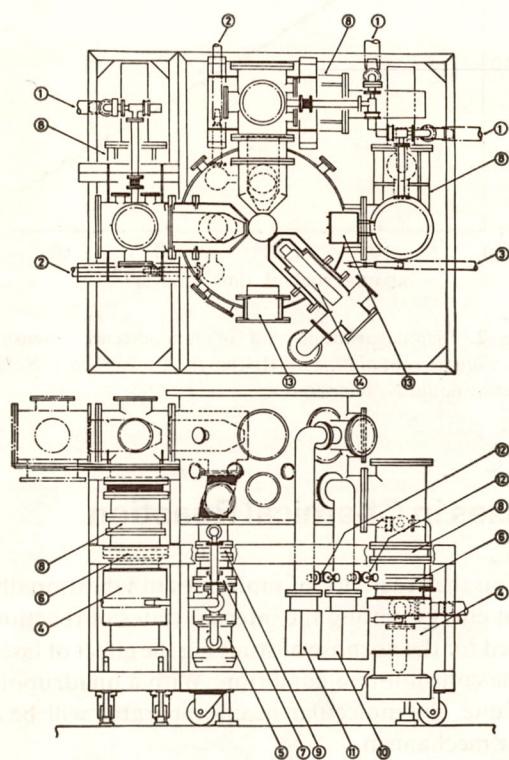


Figure 1. Crossed molecular beam apparatus: (1) to rotary pump; 950 lmin^{-1} , (2) *do.*; 360 lmin^{-1} , (3) *do.*; 180 lmin^{-1} , (4) oil diffusion pump; 3500 ls^{-1} , (5) *do.*; 1400 ls^{-1} , (6) water cooled baffle; 10 inches, (7) *do.*; 6 inches, (8) gate valve; 12 inches, (9) *do.*; 6 inches, (10) ion pump; 64 ls^{-1} , (11) *do.*; 32 ls^{-1} , (12) to sorption pump, (13) cold trap, (14) quadrupole mass filter.

III-E-2 Formation of Chlorine Atom by Infrared Multiphoton Dissociation of Trichloroethylene under the Molecular Beam Condition

Iwao NISHIYAMA and Ichiro NANAZAKI

Multiphoton dissociation process of molecules induced by an intense IR laser radiation has been received much attention and widely studied. The process is observed for many kinds of molecules if the absorption band coincides with the laser wavelength, and if the molecule has sufficiently high state density. However, most of experiments reported so far were made under the gas cell condition where collisional processes and secondary chemical reactions may be cooperative. It seems to be important to study the process under the molecular beam condition for the purpose of clarifying what are the primary products and whether the process can be observed under a collision-free condition.

IR multiphoton dissociation of trichloroethylene was investigated under the collision-free condition. Sample gas was introduced through a multichannel capillary to the collision chamber. Radiation of CO_2 TEA laser (Lumonics 203) was introduced through a ZnSe window set on the bottom flange of the vacuum chamber and focused by a Ge lens (focal length; 12 cm) into the sample beam. The product was detected by a quadrupole mass filter (Extranuclear Labs) with a pulse counting system. Signals were accumulated by a signal averager (NIC 1170). Figure 1 shows the time-of-flight spectrum of chlorine atom produced upon irradiation of trichloroethylene with the 10.6 μm P (20) line. Isotope of chlorine ($m/e = 37$) was also observed with the intensity ratio of the natural abundance. Other fragments were not observed because of low signal-to-noise ratio. The apparatus is now being improved to obtain a better S/N ratio.

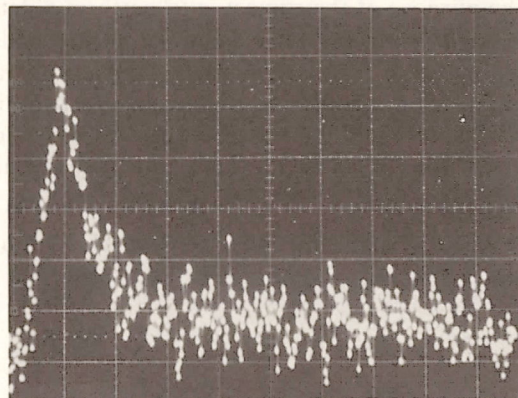


Figure 1. Time-of-flight spectrum of chlorine atom ($m/e = 35$) produced by the multiphoton dissociation of trichloroethylene: ordinate; 64 counts div^{-1} , abscissa; 250 μs div^{-1} .

III—F Chemical Reactions Through Highly Excited Vibrational States

The nature of highly excited vibrational states has been a subject of increasing interest in the last decade. On the one hand, we are interested in their fundamental dynamical behaviour, especially the vibrational energy transfer and the coupling between the highly excited vibrational mode and the chemical reaction channel. On the other hand, a possibility seems to arise to control the chemical reaction by pumping the highly excited vibrational states. In this project, we have studied infrared multiphoton dissociation of vapor-phase molecules by observing the emission from the reaction products and also by observing the photon absorption with the optoacoustic technique. In addition we have recently started to study the chemical reaction induced by the laser excitation of "local mode", which may lead to realization of the channel-selective chemical reaction through the vibrational excitation.

III-F-1 Infrared Multiphoton Dissociation of Ammonia: Laser Energy and Pressure Dependence of the Emission from NH and NH₂

Ichiro HANAZAKI, Kazuo KASATANI,* and Keiji KUWATA* (*Osaka Univ.)

[*Chem. Phys. Letters*, **75**, 123 (1980)]

Ammonia is known to produce electronically excited fragments, NH (³Π_i) and NH₂(²A₁), upon irradiation with an intense infrared radiation. We have constructed a TEA CO₂ laser based on the Rogowski-type electrode configuration and UV preionization, and measured the laser energy and sample pressure dependences of the emission energy from these two kinds of excited species. Upon irradiation with the 10.6 μm P (20) laser line, both emissions were found to obey an Arrhenius-type relation where the vibrational temperature is proportional to the square-root of the laser energy.

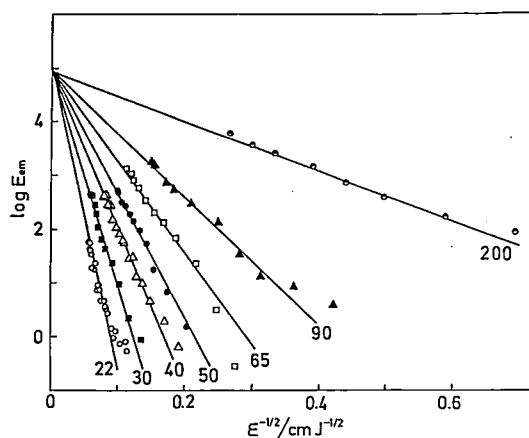


Figure 1.

In Figure 1 illustrated is the laser pulse energy dependence of the emission energy from NH₂(²A₁) measured at 620 nm (numbers in the figure are pressure in Torr). Similar results were obtained for the 0-0 band emission of NH (³Π_i) observed at 336 nm. Writing the relation as

$$E_{em} \propto \exp(-A/\epsilon^{1/2}),$$

parameter A was found to be proportional to the reciprocal of the sample pressure, as illustrated in Figure 2. These results indicate that the multiphoton dissociation occurs through highly excited vibrational mode(s), the distribution of which is likely Boltzmann-type. The laser energy and sample pressure dependences reflect the collision-assisted multiphoton absorption mechanism. The independence of the emission energy at infinitely high laser energy (see Figure 1) can be interpreted as the result of rapid quenching of the emitting states.

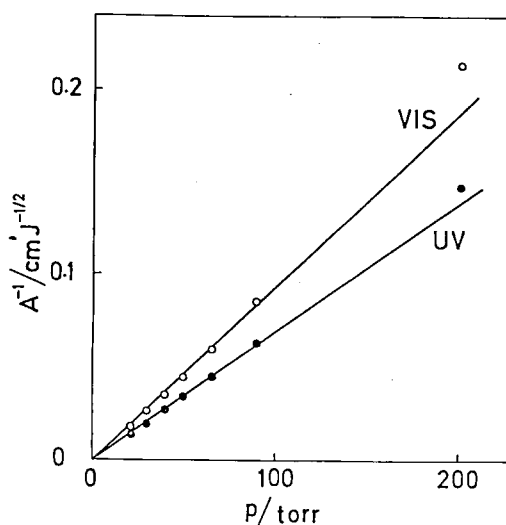


Figure 2.

III-F-2 Infrared Multiphoton Dissociation of Ammonia (II): Optoacoustic Measurement of Vibrational Distribution

Ichiro HANAZAKI, Susumu KUWABARA, Iwao NISHIYAMA, Kazuo KASATANI* and Keiji KUWATA* (*Osaka Univ.)

Optoacoustic measurement was performed on the infrared multiphoton excitation of ammonia at pressures of 0.5 ~ 90 Torr. The laser fluence range from $1 \mu\text{Jcm}^{-2}$ to 1kJcm^{-2} could be covered by employing both collimated and focused conditions. Part of the results is shown in Figure 1 (numbers in the figure are sample pressure in Torr), where $\langle n \rangle$, number of absorbed photons/molecule, was estimated by calibrating the optoacoustic signal with respect to the absorption coefficient obtained from the measurement of light transmission. Similar result was obtained for higher fluence by focusing the laser beam with a germanium lens ($f=12 \text{ cm}$). In both cases, $\langle n \rangle$ increases linearly with ϵ , the laser fluence, at lower fluences, then reaches a pressure-dependent threshold fluence, after which $\langle n \rangle$ increases approximately as $\epsilon^{1/2}$. In the latter region, $\langle n \rangle$ at a fixed ϵ increases linearly with increasing sample pressure.

The pressure and fluence dependences of the emissions from $\text{NH}_2(^2\text{A}_1)$ and $\text{NH}(^3\Pi)$ reported previously may be interpreted on the basis of the present results; *i.g.*, the dissociation occurs through vibrational mode(s) which has a Boltzmann-like distribution. The vibrational temperature is determined by the collision-assisted multiphoton absorption and excitation mechanism to be proportional to $\epsilon^{1/2}$ and to the sample pressure. Putting

$$skT_v = h\nu\langle n \rangle$$

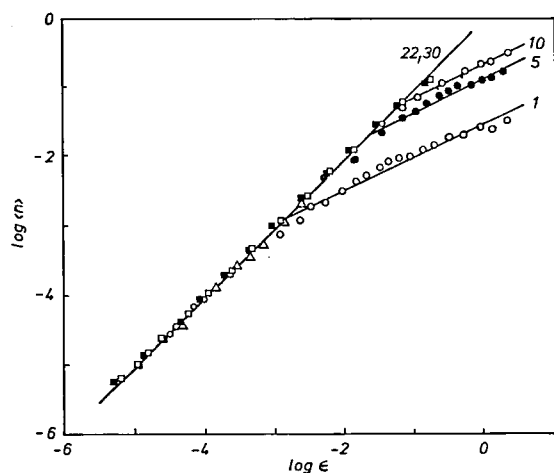


Figure 1.

where T_v is the vibrational temperature and s is the number of active vibrational modes, we can estimate s by comparing the result with the Arrhenius plot of the emission energy. The result $sE_A = 185 \text{ kcal/mol}$ is approximately equal to the activation energy E_A of the dissociation $\text{NH}_3 \rightarrow \text{NH}_2(^2\text{A}_1)$, indicating that a single mode (presumably of the lowest frequency) has high T_v and active in the multiphoton dissociation.

III-F-3 State-selective Chemistry in the Electronic Ground State

Ryoichi NAKAGAKI and Ichiro HANAZAKI

Chemical reactions induced by state-selective laser irradiation will provide us detailed knowledge about reaction kinetics and mechanism. It is possible to induce non-thermal chemical reactions in the electronic ground manifold by employing tunable lasers which permit a direct single-photon excitation into highly excited vibrational levels.* It should be noted that the state-selective chemical reaction is expected to be realized both in the gas phase and in the condensed phase. Recently we measured the C-H overtone spectra of pure liquid

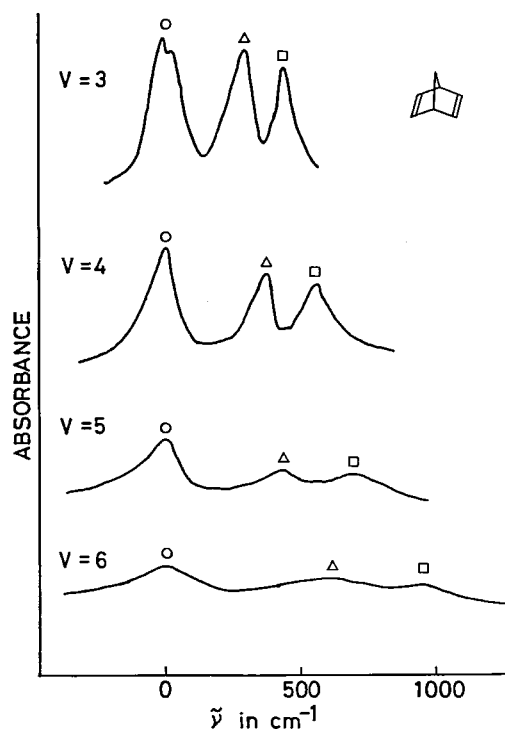


Figure 1. The C-H overtone spectra of BCH. Bands with ○, Δ, and □ are assigned as double bond CH, methylene CH₂, and bridge-head CH stretching vibrations, respectively. V designates the vibrational quantum number of the C-H stretching.

[2,2,1]-bicycloheptadiene (BCH) by means of conventional absorption spectroscopy (Figure. 1). Photolysis study of BCH and construction of sensitive photoacoustic detection system are in progress.

* Higher overtone spectra of the X-H (X = C, N, and O) stretching vibrations have been extensively studied from theoretical and experimental point of view.

III—G Study on Photochemical Processes Related to Planetary Space Chemistry

Molecular processes in planetary space proceed under various kinds of extreme physical conditions, such as ultra high vacuum, very low or high temperature and strong uv radiation. Recent developments of the vacuum and laser technology, however, have made laboratory experimental approach for those processes possible.

Comet is one of the most interesting objects among the solar planets, since it is considered to preserve materials including volatiles of the protosolar nebula. Recent studies have drawn attention to the similarity between the molecular processes thought to be taking place in comets and the reactions in the primitive earth simulation experiments where assumed atmospheres (mixtures of CH₄, NH₃, H₂O and H₂) were subjected to prolonged electric discharge. In these points, knowledge of the physical and chemical properties of comets is crucial to our understanding of the origin of life as well as the early history of the solar system. Rocket-ultraviolet observations brought the informations to permit quantitative analysis of the composition and structure of comets. The interpretation of these observations requires a knowledge of the photochemical properties of the potential parent molecules and an understanding of the nature of the free radicals observed in comets.

In this project, we are also studying the photochemical processes expected to occur in an oxidizing atmosphere composed mainly of CO₂ and CO.

III-G-1 "A Ultra-High-Vacuum, Pulsed Molecular Beam Apparatus for the Study of Electronically Excited Cometary Molecules"

Hisanori SHINOHARA, Norio OKADA, Nobuo MIZUTANI, and Nobuyuki NISHI

We have set up a ultra-high-vacuum, pulsed molecular beam apparatus which can investigate UV photodissociative reactions by measuring both mass and emission spectra of the recoiling photofragments.

A overall schematic of the apparatus is shown in Figure 1. Vacuum housing are machined from 304 stainless steel, and all vacuum seal are copper gasketed except for metal sealed [Helicoflex: pure aluminum (1050) O-ring with an elastic core (Inconel 750)] optical windows bakable to 300°C. The vacuum system consists of three mutually orthogonal axes: a laser beam axis, a molecular beam axis, and a quadrupole mass filter axis. Liquid nitrogen (or helium) cryopumping in the

system is accomplished by concentric traps. Typical pressures in the reaction chamber after one hour photolysis are $5 \times 10^{-8} \sim 10^{-9}$ Torr depending on molecular beam flux, gas condensibility, etc. The photofragments which scatter into the mass filter must pass through a buffer chamber orifice (6 mm) and then through a detector chamber orifice (3.5 mm). The mass spectrometer (Extranuclear Corp.) is enclosed in the detection chamber which is maintained at a pressure of 10^{-9} Torr by a 110 l/s turbo molecular pump and cryogenic pumping.

Pulsed supersonic molecular beam is generated by a commercially available electric fuel injector for an automobile engine with some modifications. Supersonic molecular beams of CS₂ and acrolein (C₂H₃CHO) were photolyzed by a pulsed ArF excimer laser at 193 nm (Lumonics TE-861). Figure 2 shows the time-of-flight spectra of CS and C₂ fragments resulting from photoyses of CS₂ and acrolein, respectively. C₂ fragment, observed in comets, may stem directly from parent acrolein molecule.

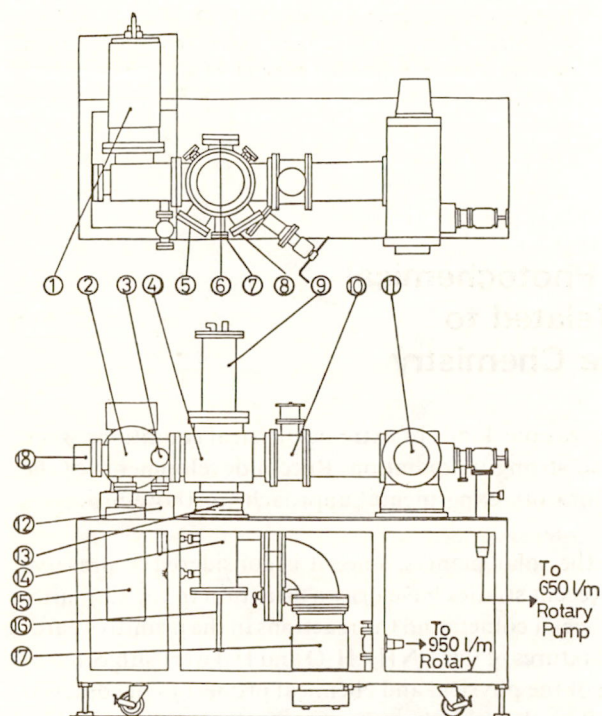


Figure 1. Schematic of apparatus. The three stage differentially pumped vacuum chamber is illustrated.

- 1 unit pump (1500 l/s)
- 2 detector chamber ($\sim 10^{-10}$ torr)
- 3 titanium sublimation pump
- 4 reaction chamber ($1 \times 10^{-9} \sim 10^{-10}$ torr)
- 5, 6, 7, 8 optical window
- 9 reaction chamber liquid nitrogen (helium) trap
- 10 UHV valve
- 11 turbo molecular pump (400 l/s)
- 12 ion pump (16 l/s)
- 13 gate valve
- 14 nozzle chamber (1×10^{-7} torr)
- 15 soaption pump (or 100 l/s turbo molecular pump and 2" diffusion pump 100 l/s)
- 16 sample inlet
- 17 6" diffusion pump (1500 l/s)
- 18 quadrupole mass spectrometer

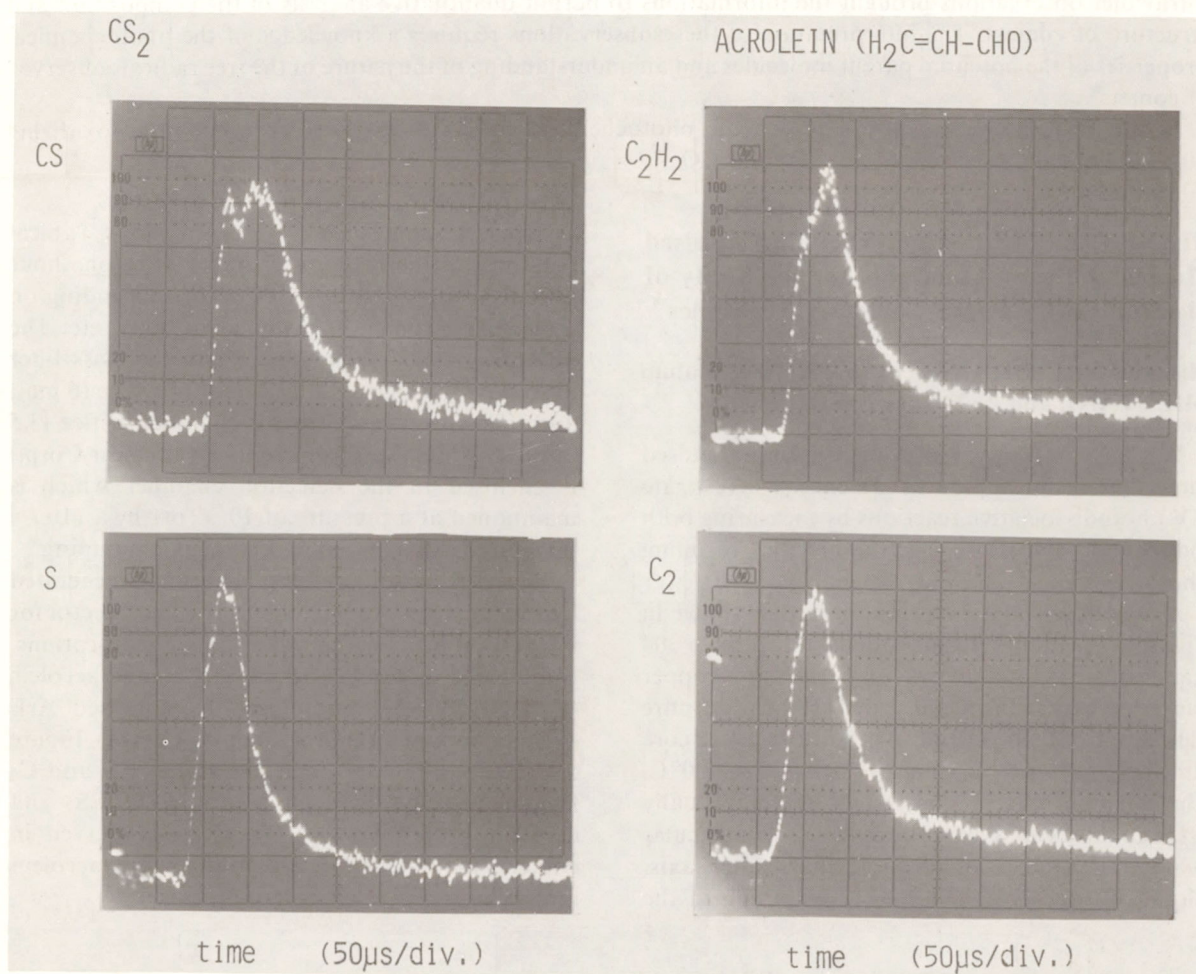


Figure 2. Time of flight spectra of fragment species from photofragmentations of CS_2 and acrolein.

III-G-2 Photochemical Conversion from Methylamine to Hydrogencyanide with an ArF Laser at 193 nm.

Nobuyuki NISHI, Hisanori SHINOHARA and Ichiro HANAZAKI

[*Chem. Phys. Letters*, 73, 473 (1980)]

Very recently, Gardner and McNesby¹⁾ have demonstrated that vacuum uv photolysis of methane and ammonia mixtures results in copious formation of methylamine. Comets contain ammonia and, possibly, methane as primitive components. Radio observations gave evidence for the presence of HCN and CH₃CN in reasonable amount.

ArF laser irradiation on methylamine vapor induces emission due to the excited radicals of NH, CN, CH and NH₂. The spectrum in uv and visible region is shown in Figure 1. The most striking feature is the appearance of the CN ($B^2\Sigma \rightarrow X^2\Sigma$) emission. The NH ($A^3\Pi_i \rightarrow X^3\Sigma^-$) emission is very strong, but the fluorescence due to NH ($c^1\Delta$), which

appears strongly in the steady light photolysis at 123.6 nm, could not be observed. The double logarithmic plots of the emission intensity vs. laser power gave the slope values of 2.0, 1.5 and 1.6 for the CN, NH and CH emissions, respectively.

Absorption of two photons of ArF laser light corresponds to 12.8 eV which is well above the ionization potential of methylamine (8.97 eV). The observations of the doublet CN and the triplet NH suggest the dissociations from super excited state which yield more than three fragments. After 3600 shot irradiation, methylamine was found to be converted to 70% of HCN and 6% of CH₃CN by the high resolution mass analysis. Apart from the reaction of the CN radical, one of the most possible intermediates yielding HCN is methylenimine which is generated by the reaction of the small photofragments with methylamine. We concluded that a super-excitation can easily produce cyanogen compounds from methylamine.

Reference

- 1) E. P. Gardner and J. R. McNesby, *J. Photochemistry*, 13, 353 (1980).

LASER PHOTOFRAGMENTATION OF CH₃NH₂ AT 193 nm

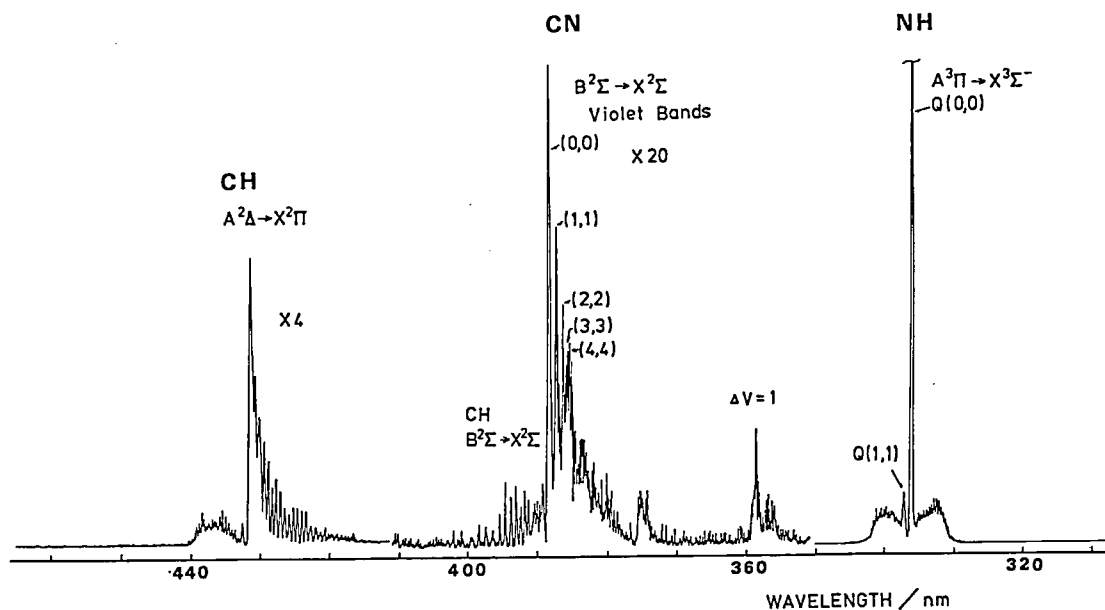


Figure 1. Fluorescence spectrum upon the ArF laser photolysis of methylamine (UV and visible region).

III-G-3 Excited State Dynamics and Quenching Rates for NH ($A^3\Pi_i$) Radical

Nobuyuki NISHI, Hisanori SHINOHARA and Ichiro HANAZAKI

ArF laser photolysis of methylamine produces the $A^3\Pi_i$ state of NH radical selectively. Analysis of the rotational population shows non-Boltzmann distribution with its maximum around the level of $N' = 10$. No obvious spin polarization was observed. The vibrational temperature is found to be low, because the intensity of the (1,1) band is very weak.

A Stern-Volmer plot of $1/\tau_f$ (τ_f ; fluorescence life time) versus methylamine pressure gives a radiative lifetime of 545 ± 65 ns for NH ($A^3\Pi_i$). This value is the longest one among the values reported so far. The slope yields a quenching rate constant of $(5.5 \pm 0.1) \times 10^{-10}$ cm³ molecule⁻¹s⁻¹. Table I summarizes the quenching constants of NH with CO, CH₄, C₂H₄ and CH₃OH. All of the values for NH ($A^3\Pi_i$) in the table are very large corresponding to the hard sphere collision rates estimated from the classical theory. The $A^3\Pi_i$ state is quenched in almost every collision with gases. It is concluded that the main quenching process is not the spin state conversion of the $A^3\Pi_i$ to $a^1\Delta$ in contrast to the case of NH ($c^1\Pi$) but, possibly, the formation of strong complexes with those gases.

Table I. Quenching rates of NH $A^3\Pi_i$, $c^1\Pi$ and $a^1\Delta$ with various gases.

Reactions	Rates (cm ³ molecule ⁻¹ sec ⁻¹)
NH $A^3\Pi_i$ + CO	7.1×10^{-11}
NH $c^1\Pi$ + CO	5×10^{-10} ^a
NH $A^3\Pi_i$ + CH ₄	9.4×10^{-11}
NH $a^1\Delta$ + CH ₄	1.2×10^{-11} ^b
NH $A^3\Pi_i$ + C ₂ H ₄	3.4×10^{-10}
NH $a^1\Delta$ + C ₂ H ₄	3.8×10^{-11} ^b
NH $X^3\Sigma^-$ + C ₂ H ₄	10^{-14}
NH $A^3\Pi_i$ + CH ₃ OH	3.7×10^{-10}
NH $A^3\Pi_i$ + CH ₃ NH ₂	5.5×10^{-10}

^a H. Okabe, *J. Chem. Phys.*, **49**, 2726 (1968).

^b J. R. McDonald, R. G. Miller and A. P. Baranavski, *Chem. Phys.*, **30**, 133 (1978).

^c D. W. Cornell, R. S. Berry and W. Lwowski, *J. Am. Chem. Soc.*, **88**, 544 (1966).

III-G-4 ArF Laser Photolysis of Cometary Molecules —Product Analysis by a High Resolution Mass Spectrometer—

Nobuyuki NISHI and Hisanori SHINOHARA

Ammonia and methyl alcohol have been known as cometary molecules since their microwave transitions were found in comet Kohoutek (1973f). Laser photolyses of these molecules have been investigated by using an ArF laser which can provide excitation energies of 6.39 and 12.78 eV through one photon and two photon processes, respectively. A low ionization voltage of 20 V was applied for the high resolution mass analyses in order to prevent undesirable fragmentations by the electron impact. Ammonia was converted to nitrogen molecule and hydrogen azide. The mass spectrum of photolyzed methyl alcohol was composed of complicated signals. Main products were H₂CO, C₂H₅OH, C₂H₄ and CO. Furthermore, acetonitrile and formamide were formed in the mixture of 450 mTorr of ammonia and 1.6 Torr of CH₃OH. The amount of CH₃CN was as much as that of H₂CO. A prominent peak appears at the mass number of 75, which corresponds to glycine. When NH₃ was added still more to the same pressure of CH₃OH, the yields of HCN, CH₃NH₂ and CH₃CN were enhanced notably. The emissions due to diatomic radicals of CH, OH and NH were observed in the reaction cell suggesting that intricate fragmentation and recombination reactions occur to yield new molecules of biological importance.

III-G-5 Vacuum Ultraviolet Laser Photolysis of Carbon Suboxide —Emissions from Electronically Excited Atomic and Diatomic Carbons—

Masayuki UMEMOTO, Hisanori SHINOHARA, Nobuyuki NISHI and Ryoichi SHIMADA (*Kyushu Univ.*)

Carbon suboxide (C₃O₂) is believed to play very important roles not only in the atmospheric chemistry on Mars but also in the primary process of chemical evolution.

Emissions due to electronically excited fragments of C, ^{*}C₂^{*} and CO^{*} have been observed upon irradiation of a ArF laser at 193 nm. The spectra are shown in Figure 1. The C₂ ($d^3\Pi_g \rightarrow a^3\Pi_u$) Swan band system exhibits a similar structure to that observed in the high pressure electric discharge

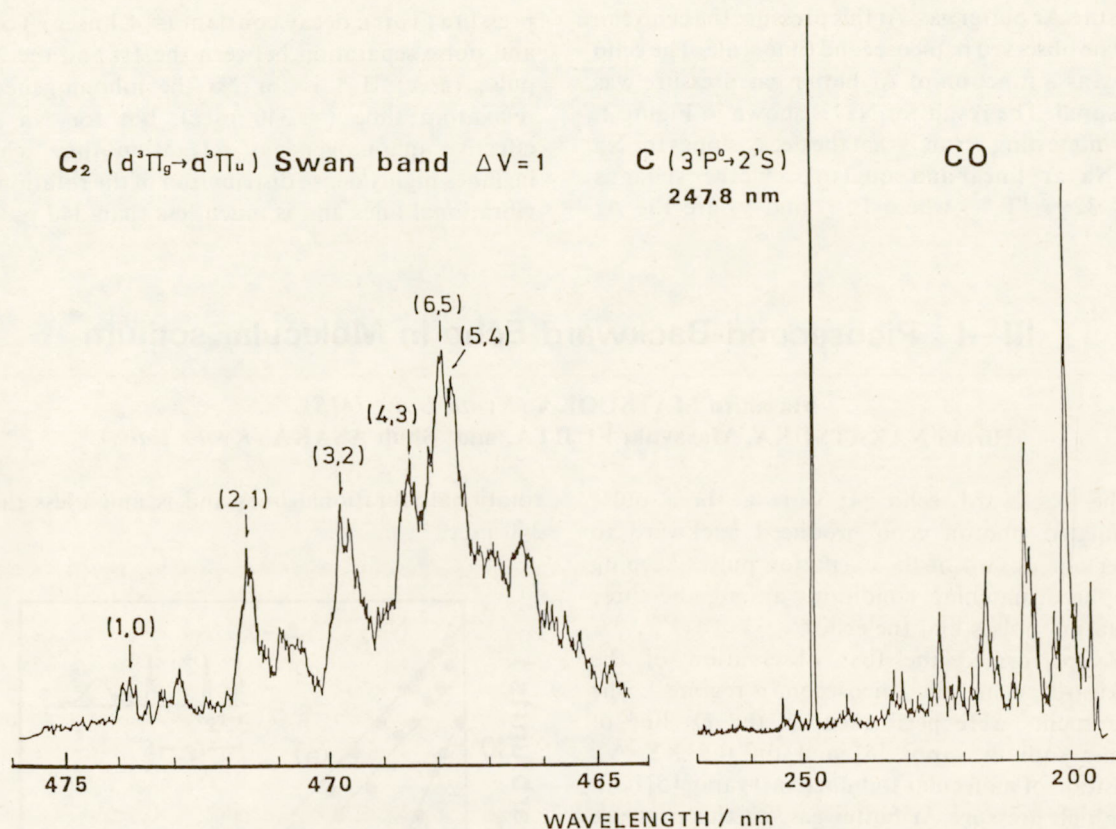


Figure 1. Emission spectra upon the ArF laser photolysis of C_3O_2 . Pressure were kept at 500 and 700 mTorr for the visible and the uv spectra, respectively, by using a flow control valve and a capacitance manometer (MKS Baratron type 221).

or ArF laser photolysis of carbon monoxide. However this emission is observable below 100 mTorr in this system. The lifetime, extrapolated to zero pressure, of $5.8 \pm 1.8 \mu s$ is twenty times as long as that of the normal Swan band emission. Appearance of this "high pressure band" in the low pressure photolysis of C_3O_2 seems to suggest that the C_2 emission seen in the high pressure electric discharge of CO is not formed from three body collisions.¹⁾ The rise and decay of the carbon emission at 247.8 nm are observed as short as the

laser pulse whose width is about 10 ns. Irradiation of a KrF laser at 248 nm induced another carbon emission at 193 nm resulting from the $3^1P^o \rightarrow 2^1D$ transition. It is confirmed that the carbon emissions are not from CO produced by the photolysis of C_3O_2 but directly from C_3O_2 through the two photon excitation to a super-excited state.

Reference

- 1) A. R. Fairbairn, *Proc. R. Soc. (London) Ser. A* **312**, 207 (1969).

III—H "Single Vibronic Level Fluorescence Spectroscopy"

Yasuo UDAGAWA, Yoko MOCHIZUKI, Koji KAYA (Tohoku Univ.),
Isamu SUZUKA (Nippon Univ.), and
Mitsuo ITO (Tohoku Univ. and IMS)

The backward echo is a three pulse stimulated photon echo produced backward to either one or two of the excitation pulses keeping the phase matching conditions among the three excitation pulses and the echo.

We performed the first observation of the backward echo in picosecond regime. The experiments were performed on the D_1 line of atomic sodium vapor and on the $X\Sigma-A\Sigma$ transition of molecular sodium (Na_2) vapor both with high

pressure Ar buffer gas. At this pressure the echo can only be observed in picosecond time scale. The echo decay as a function of Ar buffer gas pressure was measured. The result for Na₂ is shown in Figure 1. One interesting result is that the decay slopes for Na and Na₂ are linear and equal to each other so far as $P \ll 32\gamma\tau_2/T_2^{*2}$, where P , γ and τ_2 are the Ar

pressure (Torr), decay constant ($= 4.1 \text{ nsec} \cdot \text{Torr}$), and pulse separation between the 1st and the 2nd pulse (nsec). T_2^* is for Na the inhomogeneous relaxation time ($= 340 \text{ psec}$), but for Na₂ an effective inhomogeneous relaxation time which includes highly dense distribution of the rotational-vibrational lines and is much less than 340 psec.

III—I Picosecond-Backward Echo in Molecular sodium

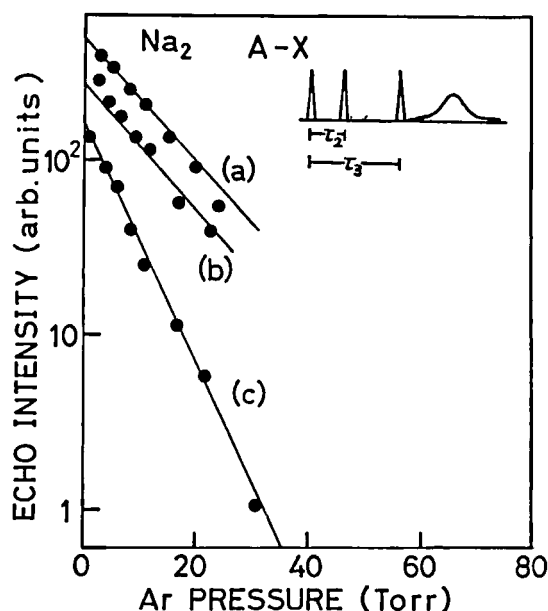
Masahiro MATSUOKA (*Kyoto Univ. IMS*),

Hiroki NAKATSUKA, Masayuki FUJITA, and Shuji ASAKA (*Kyoto Univ.*)

The backward echo [1–3] is a three pulse stimulated photon echo produced backward to either one or two of the excitation pulses keeping the phase matching conditions among the three excitation pulses and the echo.

We performed the first observation of the backward echo in picosecond regime. The experiments were performed on the D₁ line of atomic sodium vapor [4] and on the X Σ –A Σ transition of molecular sodium (Na₂) vapor [5] both with high pressure Ar buffer gas. At this pressure the echo can only be observed in picosecond time scale. The echo decay as a function of Ar buffer gas pressure was measured. The result for Na₂ is shown in Figure 1. One interesting result is that the decay slopes for Na and Na₂ are linear and equal to each other so far as $P \ll 32\gamma\tau_2/T_2^{*2}$, where P , γ and τ_2 are the Ar pressure (Torr), decay constant ($= 4.1 \text{ nsec} \cdot \text{Torr}$), and pulse separation between the 1st and the 2nd pulse (nsec). T_2^* is for Na the inhomogeneous relaxation time ($= 340 \text{ psec}$), but for Na₂ an effective inhomogeneous relaxation time which includes highly dense distribution of the

rotational-vibrational lines and is much less than 340 psec.



RESEARCH ACTIVITIES IV

Division of Molecular Assemblies

IV—A Photoelectric and Optical Properties of Organic Solids in Vacuum Ultraviolet Region

The analysis of photoelectron and also absorption spectra in vacuum ultraviolet region gives a reliable and quantitative information about the electronic properties of the organic solids — simple, charge-transfer and also polymeric materials —. We have started to observe the photoelectron spectra of fairly small organic compounds by means of an ultra-high vacuum photoelectron spectrometer equipped with temperature control system.

IV-A-1 Polarization Energies of Organic Solids Determined by Ultraviolet Photoelectron Spectroscopy

Naoki SATO, Kazuhiko SEKI and Hiroo INOKUCHI

We have been studying the energy structures of organic solids using ultraviolet photoelectron spectroscopy. We notice that the peak positions of the solid photoelectron spectra coincide well with those of the gas phase ones except a shift on the energy scales, which is called the relaxation shift R_+ , and that the peak widths of the solid spectra are broader than those of the gas phase ones. There are few experimental works concerning with these problems studied systematically.

The polarization energy, P_+ , is defined as $I_g - I_s$, where I_g and I_s are the ionization potentials in the

gas and solid phases, respectively. It corresponds to the electrostatic stabilization energy of the photoionized molecules by the polarization of surrounding molecules in the solid. As I_s we take the threshold ionization energy I_s^{th} and the adiabatic ionization energy I_g^a for I_g . They should reflect the bulk energy states rather than the surface ones, in interpretation of band widths of the photoelectron spectra in the solid state.

The values of P_+ are collected in Table I for a few tens of organic compounds with some aromaticity. We notice that P_+ 's of condensed polycyclic aromatic hydrocarbons are quite similar, about 1.7 eV. For other compounds, we found a large variation of P_+ ranging 0.9 – 3.0 eV. These data will be elucidated by the energy balance among the molecular polarizability, the molecular packing and some intermolecular interaction in the solid state.

Table I. The Polarization Energies of Organic Solids Determined by Ultraviolet Photoelectron Spectroscopy

Compound	I_g^a/eV	$I_s^{\text{th}}/\text{eV}$	P_+/eV
benzene	9.17*	7.58*	1.6
naphthalene	8.12*	6.4	1.7
anthracene	7.36*	5.70	1.7
naphthacene	6.89*	5.10	1.8
pentacene	6.58*	4.85	1.7
chrysene	7.51*	5.8	1.7
benz [a] anthracene	7.38*	5.64	1.7
naphth [2,1-a] anthracene	7.2*	5.45	1.8
dibenz [a,h] anthracene	7.35*	5.55	1.8
picene	7.5*	5.7	1.8
triphenylene	7.81*	6.2	1.6
pyrene	7.37*	5.8	1.6
perylene	6.90*	5.2	1.7
benzo [ghi] perylene	7.12*	5.4	1.7

coronene	7.25*	5.52	1.7
violanthrene A	6.42	4.86	1.6
<i>p</i> -terphenyl	7.9	6.1	1.8
benz [<i>a</i>] indeno [1,2,3- <i>cd</i>] azulene	6.84	5.0	1.9
benzo [<i>c</i>] phenanthrene	7.6*	6.2	1.4
tetrabenz [<i>a,cd,j,lm</i>] perylene	6.58	5.3	1.2
9,10-diphenylanthracene	7.05*	5.85	1.2
bianthryl	7.2*	5.9	1.3
rubrene	6.41	5.3	1.1
tetrathianaphthacene (TTN)	6.07	4.4	1.7
tetrathiafulvalene (TTF)	6.4*	5.0*	1.4
dimethylTTF (DMTTF)	6.00	5.1	0.9
tetramethylTTF (TMTTF)	6.03	4.9	1.1
dibenzoTTF (DBTTF)	6.68	4.4	2.3
hexachlorobenzene (HCB)	8.98	7.3	1.6
hexabromobenzene (HBB)	8.80	7.1	1.8
hexaiodobenzene (HIB)	7.90	5.9	2.0
<i>p</i> -chloranil (CA)	9.74	8.1	1.6
<i>p</i> -bromanil (BA)	9.59	7.4	2.2
<i>p</i> -iodanil (IA)	8.58	5.6	3.0
tetracyanoquinodimethane (TCNQ)	9.5*	7.4	2.1
tetracyanonaphthoquinodimethane (TNAP)	8.5	6.0	2.5

*By other workers.

IV-A-2 Ultraviolet Photoelectron Spectroscopy of Aliphatic Hydrocarbon Solid Films

Kazuhiko SEKI and Hiroo INOKUCHI

Photoelectron spectra were measured for 7 aliphatic hydrocarbons and tetramethylsilane solid films deposited onto substrate cooled by liquid nitrogen. The light source with He I ($h\nu = 21.2$ eV), Ne I (16.8 eV) and Ar I (11.7 eV) radiation was already reported.¹⁾ The photoelectron spectrometer was newly constructed one with a base pressure of about 10^{-8} Pa. All the compounds except hexane gave photoelectron spectra showing valence band (VB) structure. This is in contrast to the case of *n*-C₃₆H₇₄,²⁾ whose spectra showed conduction band (CB) features at $h\nu \leq 21.2$ eV. As an example, the spectra of neopentane is shown in Figure 1. The gas and solid phase photoemission thresholds I_g^a and I_s^{th} and their difference (polarization energy) P_+ are listed in Table I. One can see that aliphatic hydrocarbons have a little smaller P_+ (~ 1.5 eV) than aromatic ones (~ 1.7 eV, see IV-A-1). Judging from the magnitude of P_+ , the compounds for which electron affinity was reported negative also give threshold energies corresponding not VB \rightarrow CB excitation of electrons, but to VB \rightarrow vacuum level one.

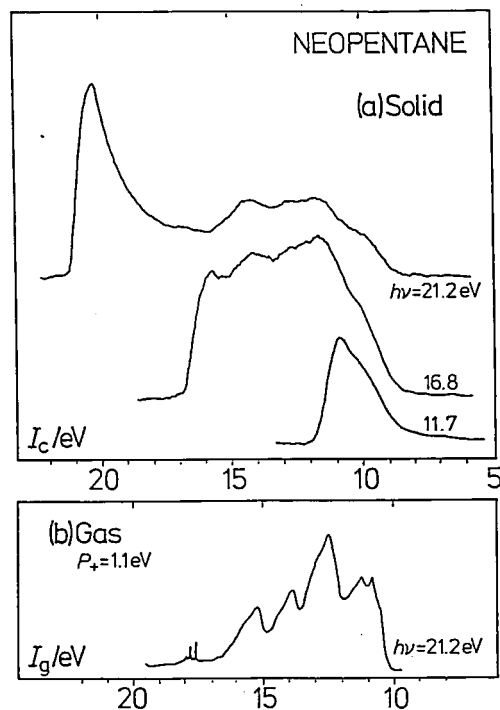


Figure 1. Photoelectron spectra of neopentane in solid (a) and gas (b) phases.

Table I. Photoelectron emission thresholds of solid and gas phases and their differences.

Compound	I_s^{th} /eV	I_g^{th} /eV	P_+ /eV
Hexane	8.55	10.24	1.6 ₉
2,2-Dimethylbutane	8.8	10.28	1.5
3-Methylpentane	8.86	10.15	1.2 ₉
Neopentane	8.74	10.2	1.5
Tetramethylsilane	8.23	9.79	1.5 ₆
Cyclohexane	8.22	9.76	1.5 ₄
Methylcyclohexane	8.28	9.4	1.1
1-Hexene	7.58	9.36	1.7 ₈

References

- 1) K. Seki, N. Sato and H. Inokuchi, *IMS Ann. Rev.*, 65 (1978).
- 2) K. Seki, S. Hashimoto, N. Sato, Y. Harada, K. Ishii, H. Inokuchi and J. Kanbe, *J. Chem. Phys.*, 66, 3644 (1977).

IV-A-3 Photoelectron Spectroscopy of 2,2-Diphenyl-1-picrylhydrazyl (DPPH) and 2,2-Diphenyl-1-picrylhydrazine (DPPH₂)

Kazumichi NAKAGAWA,¹⁾ Naoki SATO, Kazuhiko SEKI and Hiroo INOKUCHI

Solid-phase photoelectron spectra of solution-vaporized films of DPPH (see Figure 1(a)) which is a typical free radical and those of 2,2-diphenyl-1-picrylhydrazine (see Figure 1(b) and called as DPPH₂ hereafter) which is a parent molecule of DPPH were measured using the retarding type photoelectron spectrometer reported elsewhere.²⁾ Observed spectra are shown in Figure 2. Gas-phase spectra of DPPH₂ were measured by Perkin-Elmer spectrometer PS-18. Ionization threshold energy I_{th} determined are listed in the Table I. Spectra of DPPH-DPPH₂ mixed films were also measured. Ionization potentials of them are plotted in Figure 3.

The value of polarization energy $P_+ \equiv I_g^{\text{th}} - I_s^{\text{th}}$ of DPPH₂ is 1.0 eV, which is much smaller than that of typical aromatic compound ($P_+ = 1.7$ eV).³⁾ This result implies that non-bonding electrons of nitrogen atoms which contribute to the first ionization peak are localized at N-N part of the molecule and the N-N part separated by phenyl and picryl groups may give smaller polarization energy. Simillar small P_+ values were observed for some aromatic molecules having large substituent.³⁾

Continuous change of I_s^{th} shown in the Figure 3 and remarkable change of I_s^{th} within $0 < X < 0.4$ show that mixing occurs uniformly and that molecular interaction between DPPH-DPPH₂ has larger contribution to P_+ than DPPH-DPPH₂ interaction.

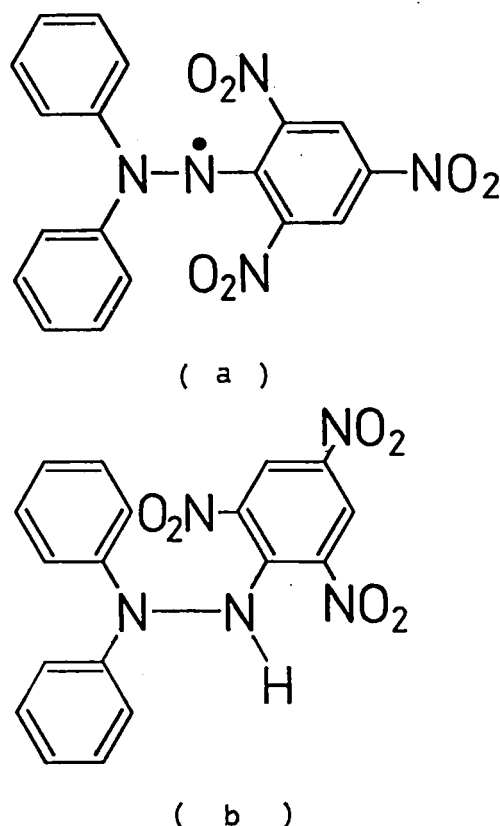


Figure 1. (a) 2,2-Diphenyl-1-picrylhydrazyl (DPPH) and (b) 2,2-Diphenyl-1-picrylhydrazine (DPPH₂).

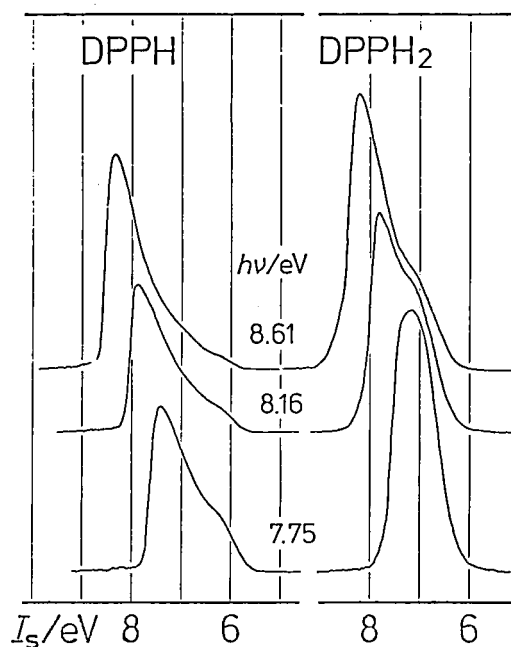
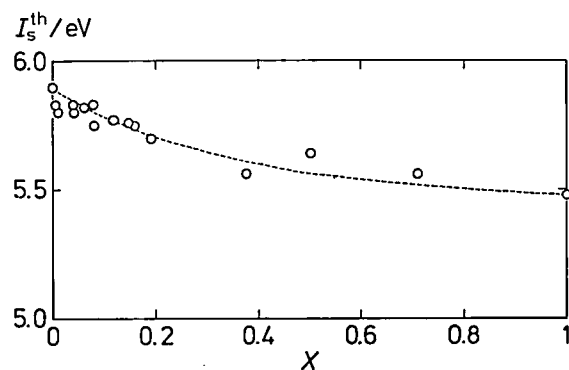


Figure 2. Photoelectron spectra of DPPH and DPPH₂. Spectra obtained with 8.61, 8.16 and 7.75 eV UV light are shown.

Table I. Threshold ionization energy $I_{th}^{a)}$

	I_g^a/eV	I_s^a/eV
DPPH	—	5.5 ± 0.1
DPPH ₂	6.9 ± 0.1	5.9 ± 0.1

^{a)} Signs g and s show gas- and solid-phase, respectively.

**Figure 3.** Threshold ionization energy I_s^{th} of $(\text{DPPH})_x(\text{DPPH}_2)_{1-x}$.

Note and References

- 1) present address: Dept. Pure Appl. Sci., Univ. of Tokyo.
- 2) T. Hirooka, K. Tanaka, K. Kuchitsu, M. Fujihira, H. Inokuchi and Y. Harada, *Chem. Phys. Lett.*, **18**, 390 (1973).
- 3) see IV-A-1.

IV-A-4 Anisotropic Vacuum UV Absorption Spectra of Oriented Polyacrylonitrile Films

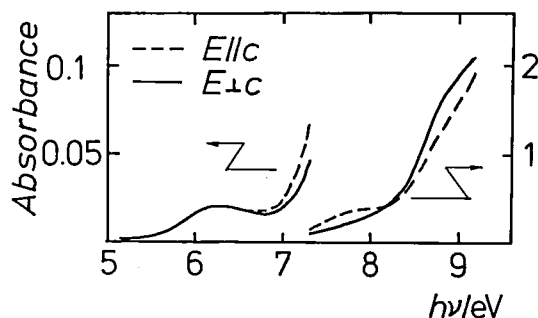
Shimpei HASHIMOTO (*Japan Synthetic Rubber Co.*), **Kazuhiko SEKI**, **Naoki SATO** and **Hiroo INOKUCHI**

As a part of our study of the electronic properties of elongated polymer films,¹⁾ we measured the anisotropic vacuum uv spectra of polyacrylonitrile (PAN) films oriented by uniaxial elongation. Onari²⁾ reported the absorption spectrum of non-oriented PAN film without an assignment for the features in it. The films cast from *N,N*-dimethylformamide solution were elongated 3 to 5 times. Polarized IR spectra showed the CN bond is predominantly oriented perpendicular to the direction of elongation, which was found to correspond to the *c* axis of the crystalline part of the polymer. Vacuum uv spectra were measured with the apparatus already reported.³⁾ Figure 1 shows the spectra obtained for films of 130 and 800 nm thick, with *c* parallel and perpendicular to the electric vector of the light *E*. The results are

summarized in Table I. Considering the discussion of other workers for PAN and related compounds, we assigned these features as shown in Table I.

Table I. Polarization and assignment of features in the polarized absorption spectra.

$h\nu/\text{eV}$	polarization	assignment
6.3	isotropic	forbidden $\pi^* \leftarrow \pi (^1\Sigma^- \leftarrow ^1\Sigma^+, ^1\Delta \leftarrow ^1\Sigma^+)$
7.8	$\parallel c$	$\pi^* \leftarrow n(^1\Pi \leftarrow ^1\Sigma^+)$
≥ 9	$\perp c$	$\pi^* \leftarrow \pi (^1\Sigma^+ \leftarrow ^1\Sigma^+)$, $\sigma^* \leftarrow \sigma$

**Figure 1.** Polarized absorption spectra of elongated polyacrylonitrile films (800 nm thick for $h\nu \geq 7.3$ eV and 130 nm thick for $h\nu \leq 7.3$ eV). The ordinate is normalized to the absorbance of a film of 100 nm thickness.

References

- 1) S. Hashimoto, S. Hino, K. Seki and H. Inokuchi, *Chem. Phys. Lett.*, **40**, 279 (1976); S. Hashimoto, K. Seki, N. Sato and H. Inokuchi, *Rep. Progr. Polym. Phys. Jpn.*, **21**, 375, 379 (1978); **22**, 439, 443 (1979).
- 2) S. Onari, *J. Phys. Soc. Jpn.*, **26**, 500 (1969).
- 3) S. Hashimoto, K. Seki, N. Sato and H. Inokuchi, *IMS Ann. Rev.*, **67** (1978).

IV-A-5 Ultraviolet Photoelectron Spectra of Tetrahalogeno-*p*-benzoquinones and Hexahalogenobenzenes in the Solid State

Naoki SATO, **Kazuhiko SEKI** and **Hiroo INOKUCHI**

[*J. Chem. Soc., Faraday Trans. II* in press.]

The electronic structures of tetrahalogeno-*p*-benzoquinones and hexahalogenobenzenes ($\text{C}_6\text{X}_4\text{O}_2$ and C_6X_6 ; X = Cl, Br and I) in the solid state were studied using ultraviolet photoelectron spectroscopy. The spectra of the iodocompounds suggest that their conduction band structures are different from those of the other compounds. We have plotted the obtained ionization potentials

against the ionization potentials of the substituent halogen atoms in Figure 1. The ionization potential of $C_6I_4O_2$ solid is unusually small (see Table I). Its polarization energy is 3.0 eV, which is the largest value observed for organic solids. The crystal structure of $C_6I_4O_2$ shows that the $O \cdots I$ interatomic distance between adjacent molecules is shorter than the sum of the van der Waals radii of the two atoms,¹⁾ which suggests the existence of some charge-transfer interaction should also contribute to the large polarization energy of $C_6I_4O_2$.

Table I. Ionization Potentials and Polarization Energies of $C_6X_4O_2$ and C_6X_6 (X = Cl, Br and I)

	X	I_a^h /eV	I_a^v /eV	I_g^h /eV	I_g^v /eV	P_a /eV	R_v /eV
$C_6X_4O_2$	Cl	8.1	8.8	9.74	9.84	1.6	1.1
	Br	7.4	8.0	9.59	9.72	2.2	1.7
	I	5.6	—	8.58	—	3.0	—
C_6X_6	Cl	7.3	8.2	8.98	9.38	1.6	1.1
	Br	7.1	7.8	8.80	9.0	1.8	1.2
	I	5.9	6.5	7.90	8.09	2.0	1.6

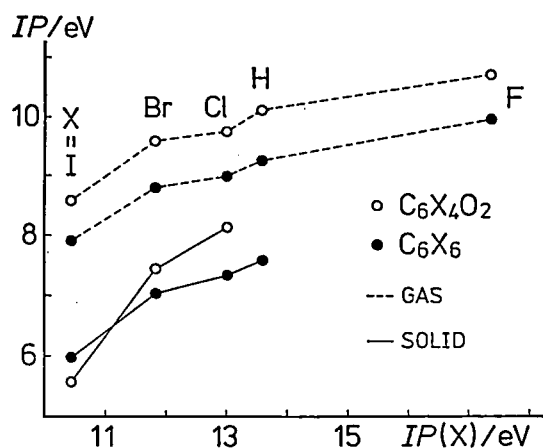


Figure 1. Plot of ionization potentials of the compounds against the ionization potentials of the substituent atoms. O, $C_6X_4O_2$; ●, C_6X_6 ; (---) gas phase; (—) solid state.

References

- 1) H. Kobayashi, T. Danno and I. Shirotani, *Bull. Chem. Soc. Jpn.*, **47**, 2333 (1974).
- 2) I. Shirotani, A. Onodera, Y. Kamura, H. Inokuchi and N. Kawai, *J. Solid State Chem.*, **18**, 235 (1976).

IV-A-6 Polarization Energies of Tetra-thiafulvalene Derivatives

Naoki SATO, Hiroo INOKUCHI and Ichimin SHIROTANI (Univ. of Tokyo)

Ultraviolet photoelectron spectroscopic studies were carried out on dimethyl-(DM-), tetramethyl-(TM-) and dibenzo-(DB-) derivatives of tetra-thiafulvalene (TTF) in gaseous and solid states. For most of organic compounds photoelectron spectra in the two phases coincide well each other except some energy shift, the relaxation shift R_v , and broadening of the bands in solid phase spectra.¹⁾ In the case of DBTTF, the spans of the two highest energy bands are different between the two phases, which is shown in Figure 1 and agrees with the previous result by Nielsen.²⁾

In Table I the energy values of the TTF derivatives are determined by the present work and are compared with those of a few related compounds. In this table, the superior a, th and v represent the adiabatic, threshold and vertical

Table I. Energy Values of TTF Derivatives and Related Compounds

Compounds	I_a^h /eV	I_a^v /eV	P_a /eV	I_g^h /eV	I_g^v /eV	R_v /eV	ϕ /eV
TTF	6.4*	5.0*	1.4	6.92*	5.7*	1.2	4.5*
DMTTF	6.00	5.1	0.9	6.34	5.9	0.4	4.4
TMTTF	6.03	4.9	1.1	6.38	5.8	0.6	4.5
DBTTF	6.68	4.4	2.3	7.03	5.1	1.9	4.1
Tetrathia-naphthalene	6.07	4.4	1.7	6.22	5.2	1.0	4.0
Naphthalene	6.89*	5.10	1.8	7.01*	5.68	1.3	4.4
Anthracene	7.36*	5.70*	1.7	7.47*	6.5*	1.0	4.3

ϕ ; work function. *By other workers.

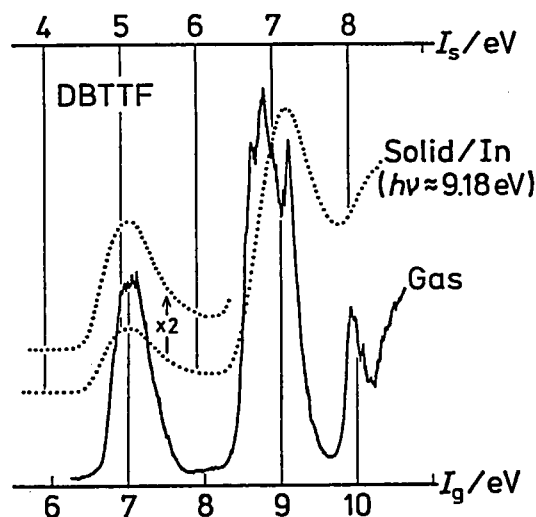


Figure 1. Comparison of the two highest energy bands of photoelectron spectra of DBTTF between the two phases. The span between the first and second bands of the solid phase spectra is about 0.2 eV larger than that of the gas phase spectrum.

ionization potentials, respectively. The polarization energy P_+ is defined as $I_g^a - I_s^{th}$. The methyl substitution looses the tight packing of TTF skeletons, which reduces P_+ values of DMTTF and TMTTF. On the other hand, P_+ of DBTTF, 2.3 eV, is the largest among the electron donor-type compounds, as far as we know. In this case, the

addition to aromatic rings to TTF skeleton causes the increase of molecular polarizability.

References

- 1) W. D. Grobman and E. E. Koch, "Photoemission in solids II", eds. L. Ley and M. Cardona, Springer, Berlin, 1979.
- 2) P. Nielsen, *Solid State Commun.*, **26**, 835 (1978).

IV—B Photoconduction in Organic Solids

We have started to observe a photoconduction of organic semiconductors by means of ultra-high vacuum photocoduction apparatus (UHV-PCA). The photoconductive phenomena depend very strongly on purity, crystallinity and also surface states of solid specimens. In cooperation with joint research group and also Chemical Materials Center, a workshop for the purification and sample preparation of organic materials, especially polycyclic aromatic compounds, was arranged.

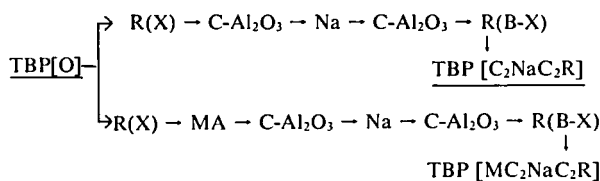
IV-B-1 Purification of Tetrabenzo[*a,cd,j,l*m]perylene

Satoshi IWASHIMA (*Meisei Univ.*), Hitoshi HONDA (*Meisei Univ.*), Junji AOKI (*Toho Univ.*), Gunzi SAITO, Naoki SATO, Hiroo INOKUCHI and Tadashi SUGAWARA

Tetrabenzoperylene (TBP) was synthesized by self-condensation reaction of benzanthrone in the mixture of copper powder, zinc chloride, and sodium chloride at 220°C. The crude product (TBP [0]) contaminated with the starting materials, violanthrene B, isoviolanthrene B, and other unknown materials was purified by conventional methods.¹⁾ The purification process is shown in Table I.

TBP thus purified shows no peaks due to benzanthrone, violanthrene B, isoviolanthrene B by the analysis with high pressure liquid chromatography (HPLC) (μ -porasil, benzene-hexane (1:9), flow rate 1.0 ml/min and μ -bondapak C₁₈, methanol, flow rate 1.0 ml/min, Waters Associates Inc). However, TBP[MC₂NaC₂R] contains considerable amount of unknown impurity, the retention time of which is very close to that of TBP on HPLC analysis. Also TBP[C₂NaC₂R] contains several impurities with a trace of amount each. With the aid of gel permeation chromatography (Jaigel-H (2H, 1H), chloroform, 14 recycles, Japan Anal. Ind. Co. LC-09), the impurities in TBP[C₂NaC₂R] were removed except one which shows almost the same retention time with TBP on HPLC. In order to obtain highly purified TBP, preparative HPLC is now undertaken.

Table I. Purification Process of Tetrabenzo[*a,cd,j,l*m]-perylene



- C-Al₂O₃ : Column chromatography (activated carbon and activated alumina)
 Na : Treatment with diethylene glycol and metallic sodium
 MA : Treatment with maleic anhydride
 R(X) : Recrystallization (Extraction) from xylene
 R(B-X) : Recrystallization from benzene and then from xylene

Reference

- 1) S. Iwashima, H. Honda, J. Aoki and H. Inokuchi, *Mol. Cryst. Liq. Cryst.*, **59**, 207 (1980).

IV-B-2 Detrapping of Charge Carriers by Singlet Excitons in Naphthalene Single Crystal

Kazumichi NAKAGAWA,¹⁾ Masahiro KOTANI (*Gakushuin Univ.*) and Hisashi TANAKA (*Gakushuin Univ.*)

[To be published in *Phys. Stat. Sol. (b)*]

The detrapping of charge carriers by singlet excitons in naphthalene crystal was investigated at 300K. Singlet excitons were generated homo-

geneously in the bulk of the crystal by two-photon absorption and the detrapped charges were observed as pulsed photocurrent. From the waveform and the effect of the pulse to pulse interval the amount and the spatial distribution of trapped, as well as detrapped, charges were determined. The bimolecular rate constant for the detrapping was found to be $(8 \pm 6) \times 10^{-10} \text{ cm}^3 \text{ s}^{-1}$. The result indicates that, in naphthalene crystal, the

probability of the detrapping reaction is high, close to the diffusion limit, whereas that of the singlet-singlet annihilation is lower.^{2,3)}

Note and References

- 1) Present address: Univ. of Tokyo.
- 2) S. Fujiwara, T. Nakayama and N. Itoh, *Phys. Stat. Sol. (b)*, **78**, 519 (1976).
- 3) H. Auweter, A. Braun, U. Mayer and D. Schmid, *Z. Naturforsch.*, **34a**, 761 (1979).

IV—C Reduction Kinetics and Electron Transport Behavior of Cytochrome c_3

The reduction mechanism of cytochrome c_3 was analysed directly from the observation of $\text{Fe}^{3+}/\text{Fe}^{2+}$ ratio by means of Mössbauer effect. And also, unusual electrical behaviors of ferrocyanochrome c_3 are being studied as a function of temperature and ambient pressure.

IV-C-1 Kinetics of Cytochrome c_3 Reduction with Hydrogenase: A Mössbauer Effect Study

Megumi UTUNO (*Univ. of Tokyo*), Kazuo ÔNO (*Univ. of Tokyo*), Keisaku KIMURA, Hiroo INOKUCHI, and Tatsuhiko YAGI (*Shizuoka Univ.*)

[*J. Chem. Phys.*, **72**, 2264 (1980)]

An electron transfer process was studied in cytochrome c_3 in the presence of a small quantity of hydrogenase using the Mössbauer effect. The concentration ratio of ferri- and ferro-form was determined by the ratio of the Mössbauer spectrum area of ferri- to ferro-form a_3/a_2 . The plot of $\ln [a_3/(a_2 + a_3)]$ vs time, shown in Figure 1, is linear. A redox reaction of cytochrome c_3 catalyzed by hydrogenase is known to obey the first order rate law in aqueous solution. A time differential equation of ferri-form rate is described as follows:

$$da_3/dt = -ka_3$$

in which k is the rate constant. The solid line in Figure 1 shows a plot of this equation with $k = 3.2 \times 10^{-5} \text{ s}^{-1}$ which is in good agreement with the experimental data.

Since there is a large excess of cytochrome c_3 in this system, most of the cytochrome c_3 cannot have a hydrogenase molecule as a nearest neighbor and consequently, cannot be directly affected by the catalytic action of the hydrogenase. Therefore, the reduction of cytochrome c_3 indicates that there exists both intra and intermolecular transfer of electrons even in the solid phase.

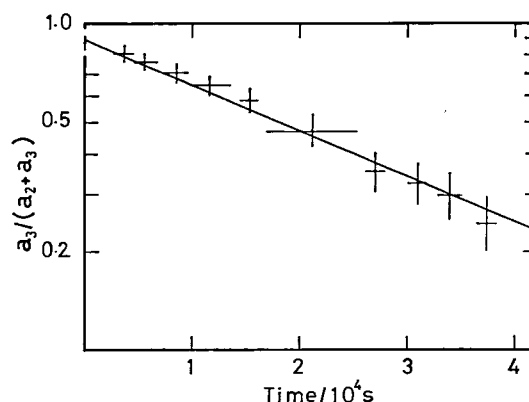


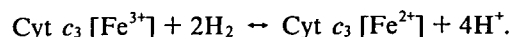
Figure 1. Concentration ratio of ferri-form (cytochrome c_3) as function of time.

IV-C-2 Electrical Conductivity of an Anhydrous Cytochrome c_3 Film as a Function of Temperature and Ambient Pressure

Yusuke NAKAHARA (*Tech. College of Miyakonojo*), Keisaku KIMURA, Hiroo INOKUCHI, and Tatsuhiko YAGI (*Shizuoka Univ.*)

[*Chem. Phys. Lett.*, **73**, 31 (1980)]

Cytochrome c_3 undergoes a reversible oxidation-reduction with molecular hydrogen with the action of hydrogenase [hydrogen: ferricytochrome c_3 oxidoreductase ECl.12.2.1] even in the solid state:¹⁾



Cytochrome c_3 works as an electron carrier in the redox system of sulfate bacteria, *Desulfovibrio*. This electron carrier, cytochrome c_3 , was isolated from *d. vulgaris*, Miyazaki, and was purified. The complete amino-acid sequence of this tetra-hemoprotein has already been determined.

We observed the D. C. resistivity of amorphous film of cytochrome c_3 , in the course of its oxidoreduction, as a function of temperature and ambient pressure. Table I collects the resistivity

data of several protein solids. Among them, we find the value of ferrocyclochrome c_3 appears to be extremely low, 57 Ωcm at 268 K. Further, increasing the pressure of hydrogen gas (as a reducing agent) caused a drastic decrease of resistivity. The minimum value was 8 Ωcm under the hydrogen pressure of 200 kPa.

This unusual behavior and extremely low resistivity found in cytochrome c_3 is discussed in connection with its molecular properties.

Table I. Electrical Resistivity of Solid Proteins

Material	Activation Energy $\Delta E/\text{J}\cdot\text{mol}^{-1}$	Resistivity $\rho(303\text{K})/\Omega\text{cm}$	$\rho_0/\Omega\text{cm}$
Lysozyme	—	$> 10^{14}$	—
Ribonuclease	—	$> 5 \times 10^{14}$	—
Trypsin	—	$> 10^{14}$	—
Myoglobin	1.5×10^4	3.6×10^{10}	1.2×10^8
Cytochrome c			
oxid. ^{a)}	1.3×10^5	6.1×10^{16} ^{a)}	1.6×10^{-5}
oxid.	$5.8 \times 10^4(323 - 358\text{K})$	3.1×10^{11} ^{a)}	4.0×10^1
red.	$5.8 \times 10^4(283 - 333\text{K})$	3.1×10^9	4.0×10^{-1}
Cytochrome c_3			
oxid.	$1.6 \times 10^5(293 - 343\text{K})$	2.3×10^{12}	5.4×10^{-16}
red.	$3.7 \times 10^5(233 - 268\text{K})$	5.7×10^1 ^{b)}	2.5×10^{-70}

^{a)} The resistivity at 303 K by the extrapolation with ΔE and ρ_0 .

^{b)} Value at 268 K.

IV—D Chemistry and Physics of Graphite Intercalates

Electronic properties of graphite-alkalimetal and graphite-metalhalide are being studied continuously in relation to their electronic structures by the measurements of the conductivity, the superconductivity, the magneto-resistance, NMR, ESR and the Raman scattering. We have introduced novel graphite specimen, graphite filament prepared from graphite in argon flame, as host material to make the intercalates.

IV-D-1 Graphite Filaments and Their Alkalimetal Intercalation Compounds

Mizuka SANO (*Univ. of Electro-Communications and IMS*), **Naoki SATO**, **Hiroo INOKUCHI**, **Koshiro TORIUMI**, and **Shohei TAMURA** (*Univ. of Tokyo*)

A new type of "carbon filaments", about 20 cm long and 7 μm in diameter each, were grown by heating purified graphitic material in argon plasma generated in d.c. arc. The filaments were converted into softer filaments on heating at 3000 or at 3400 $^\circ\text{C}$, which are to be referred to 'graphite filaments'.

The filaments have cylindrical shapes of smooth surface with circular cross-section. From the X-ray diffraction and the electron diffraction of a narrow

beam (1 μm in diameter, 50 keV) incident upon a single filament grazingly, it is evident that the filament consists of the concentric stacking of graphitic layer planes, all the individual c -axes being perpendicular to the filament axis.

The longitudinal electrical resistivities are 1300, 660, and 610 $\mu\Omega\text{cm}$ at 300 K for carbon, graphite-3000, and graphite-3400 filaments, respectively, and increase monotonously with decreasing temperature down to 4.2 K. The carbon filament showed positive and the graphite filament showed negative transverse magnetoresistance in the whole range of 120 kOe at 1.7 and 4.2 K.

The graphite filaments intercalated with K, Rb, or Cs possess the resistivity of 23 ~ 25, and 28 ~ 30 $\mu\Omega\text{cm}$ (300 K) at the 1st and the 2nd stage, respectively, with metallic temperature dependence. A golden K-graphite filament turned blue

and its resistivity reached $36 \mu\Omega\text{cm}$, when hydrogen was introduced to the filament. This change is quite similar to that found for K-grafoil compound.^{1,2)}

References

- 1) M. Sano and H. Inokuchi, *Chem. Lett.*, **1979**, 405.
- 2) M. Sano, H. Inokuchi, M. Kobayashi, S. Kaneiwa and I. Tsujikawa, *J. Chem. Phys.*, **72**, 3840 (1980).

IV-D-2 Raman Scattering from Graphite Intercalated with FeCl_{3-y}

Kentaro OHHASHI (*Kyoto College of Pharmacy*), Ikuji TSUJIKAWA (*Kyoto Univ.*) and Hiroo INOKUCHI

Intercalation compounds of graphite are classified according to their state, n , (the number of graphite layers between nearest intercalant layers). Recent studies of Raman spectra on graphite- FeCl_3 have shown the stage dependence of the frequencies in the vicinity of 1600cm^{-1} .¹⁻³⁾ We found the stage changes in the reheating process of graphite- FeCl_{3-y} compounds by observation of the changes of Raman spectra before and after reheating, one example of which is shown in Figure 1. For the stage change of the $n = 2$ compound (with a minor fraction of $n = 1$) to the $n = 3$ one (with a minor fraction of $n = 2$), we propose the model⁴⁾ consisting of two steps as shown in Figure 2. It was found from our data that the $n = 3$ compound could be produced below some threshold fraction of $n = 1$ in the $n = 2$ compound.

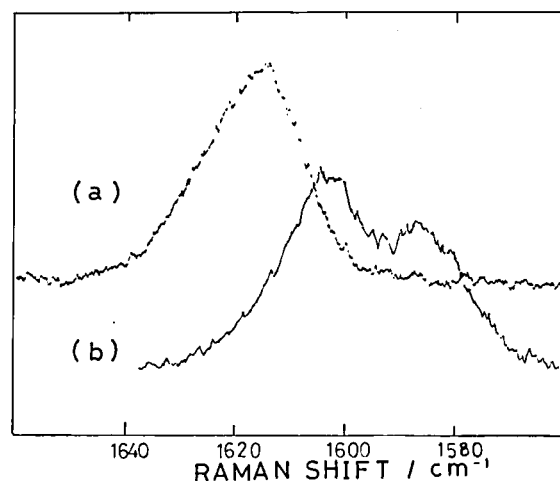


Figure 1. Raman spectra at room temperature before and after reheating of the graphite- FeCl_{3-y} compound. (a) before reheating: stage-1 30%, stage-2 70%, $y = 0.45$ (b) after reheating: stage-2 10%, stage-3 90% $y = 0.55$.

On the other hand, we determined y -value *i.e.* FeCl_2 content from measurement of Mössbauer spectra. We are attempting to make clear whether there is or not a correlation between FeCl_2 content and the degree of charge transfer from carbon to intercalant. Such a charge transfer has been observed by electrical resistivity measurements.⁵⁾

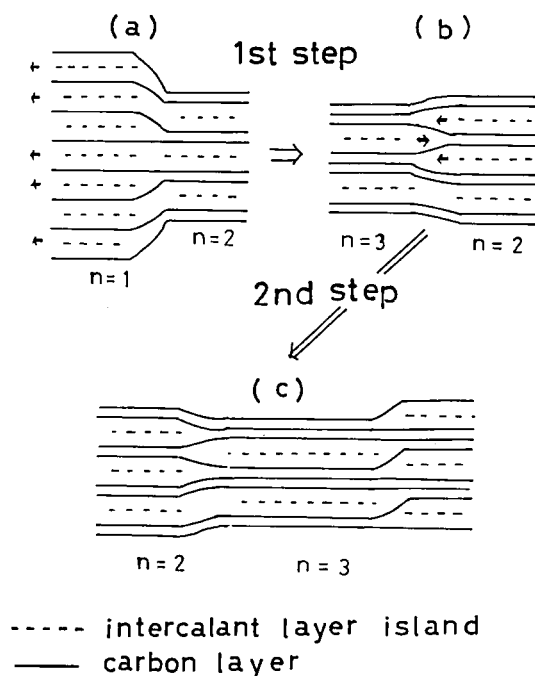


Figure 2. The model of the stage change in the reheating process from the stage 2 compound (with a minor fraction of stage 1) to the stage 3 compound (with a minor fraction of stage 2). (a) desorption of intercalant from the periphery of the stage 1 compound (b) interlayer migration of intercalant islands (c) domain structure of the stage 3 compound with a minor fraction of stage 2.

References

- 1) N. Caswell and S. A. Solin, *Solid State Comm.*, **27**, 961 (1978).
- 2) C. Underhill, S. Y. Leung, G. Dresselhaus and M. S. Dresselhaus, *Solid State Comm.*, **29**, 769 (1979).
- 3) K. Ohhashi, I. Tsujikawa and H. Inokuchi, *Ann. Rev. IMS*, **100** (1979).
- 4) G. Schoppen, H. Meyer-Spache, L. Siemsglüss and W. Metz, *Mat. Sci. and Eng.*, **31**, 115 (1977).
- 5) K. Ohhashi, S. Shimotori, I. Tsujikawa and H. Inokuchi, to be published in *Synthetic Metals*, (1980).

IV—E Organic Metals

Since the discovery of highly electrically conducting charge transfer complexes and anion-radical salts of tetracyanoquinodimethane (TCNQ), several proposals have been forwarded to design new 'organic metals'.¹⁾ Some of the criteria for achievement of the metallic state are as follows.

1. The component molecule which is responsible for electron transport should be flat in the neutral and ionic state. 2. The donor and acceptor molecules must form segregated stacks. 3. The spacing between component molecules in the segregated stacks must be uniform. 4. Unpaired electrons on the donor and/or acceptor molecules must be present in the complex. 5. Incomplete charge transfer. 6. Minimal on site Coulomb repulsion energies.

Obviously the achievement of the metallic state in these systems is a complicated interplay of many factors. However, under certain circumstances one may abstract and discuss one criterion exclusively. In order to design and predict other systems which are likely to yield highly conducting complexes, we will elucidate these requirements for 'organic metals'.

Reference

1) A. F. Garito and A. J. Heeger, *Acc. Chem. Res.*, **7**, 232 (1974), J. B. Torrance, *ibid.*, **12**, 79 (1979).

IV-E-1 Requirements for an 'Organic Metal'

Gunzi SAITO and John P. FERRARIS (*Univ. of Texas at Dallas*)

[*Bull. Chem. Soc. Jpn.*, **53**, 2141 (1980)]

Current theories on the origin of high electrical conductivity in 'organic metals' emphasize the need for incomplete charge transfer as well as segregated stacks of donor and acceptor molecules and uniform spacing within the stacks. We examine 61 of the complexes based on tetrathiafulvalene and TCNQ together with their various derivatives and analogues in terms of partial charge transfer. We chose this series because only an examination of a series with similar structure can minimize the so called size and shape effect considerably. In Figure 1 and 2 respectively are tabulated the structures of the donor and acceptor molecules considered here along with their first electrochemical half-wave potentials, ($E_1(D)$ for $D \rightarrow D^+ + e$; $E_1(A)$ for $A + e \rightarrow A^-$). Conductivity results obtained from several literatures are plotted in Figure 3. Those complexes in the upper left of the figure have small $E_1(D) - E_1(A)$ values and favor the completely charge transferred ionic state. Those on the lower right favor the nonionic state. In general, complexes displaying substantial electrical conductivity fall between the two lines on the graph; partial charge transfer state. Therefore, to the degree our approximation is accurate, related combinations with the redox potential, $-0.02 \leq E_1(D) - E_1(A) \leq 0.34V$ have a high possibility of being 'organic metals', where $0.24 \leq E_1(D) \leq 0.53V$ and $-0.02 \leq E_1(A) \leq 0.65V$.

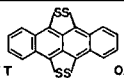
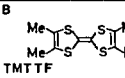
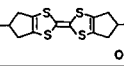
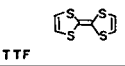
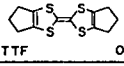
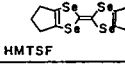
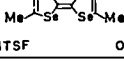
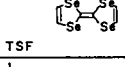
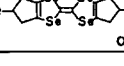
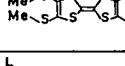
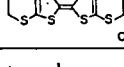
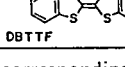
A  TTT 0.24	B  TMTTF 0.27
C  0.30	D  TTF 0.31
E  HMTTF 0.33	F  HMTSF 0.41
G  TMTSF 0.44	H  TSF 0.44
I  0.48	J  0.50
K  0.53	L  DBTTF 0.53

Figure 1. Electron donors with corresponding electrochemical half-wave potentials.

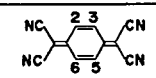
		
a 2,5-(CN) ₂ 0.65	b F ₄ 0.53	c 2,5-(Br) ₂ 0.41
d 2,5-(Cl) ₂ 0.41	e 2,5-(I) ₂ 0.35	f 2,5-(F) ₂ 0.33
g Br 0.29	h Cl 0.29	i F 0.26
j 2,5-Cl, Me 0.26	k 2,5-Br, Me 0.26	l 2,5-I, Me 0.25
m TCNQ 0.14	n Me 0.12	o 2,5-(ⁱ Pr) ₂ 0.12
p 2,5-(Et) ₂ 0.11	q 2,5-(Me) ₂ 0.10	r 2,5-OEt, SMe 0.08
s OMe 0.07	t 2,5-(OMe) ₂ -0.01	u 2,5-OMe, OEt -0.02

Figure 2. Electron acceptors with corresponding electrochemical half-wave potentials.

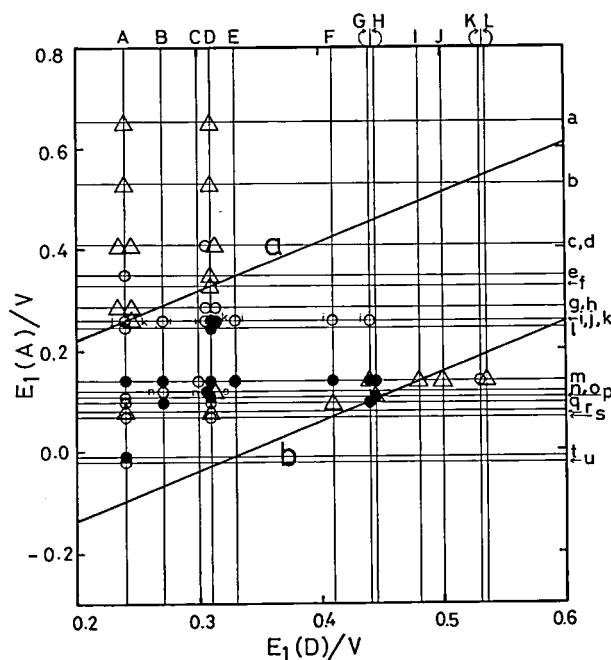


Figure 3. Conductivity of complexes plotted as $E_1(A)$ vs. $E_1(D)$.
 Δ = insulators or semiconductors; \circ = highly conducting in compaction studies; \bullet = 'organic metals.'

IV—F Studies of Ion-Molecule Reactions by a Threshold Electron-Secondary Ion Coincidence Technique

The knowledge of the microscopic reaction cross sections for evolution of a system in a single reactant quantum state (translational, rotational, vibrational, and electronic) to a single product quantum state is essential for a complete understanding of a chemical reaction. In neutral-neutral reactions, the access to this "state-to-state" cross sections has been made possible by the advent of new technique, such as molecular beams and lasers, which prepare and probe these states. Ion-molecule reactions, on the other hand, afford different approaches toward this microscopic cross sections since ions can readily be prepared in various internal states in the initial ionization processes, such as photoionization, and the emitted photoelectrons provide information on the distribution among these states.

In this project, we are studying state-selected ion-molecule reactions by the use of a photoionization technique which utilizes the threshold photoelectron-secondary ion coincidence. The technique allows direct determination of $\sigma_i(i,v)$, namely, the reaction cross section as a function of the internal and collisional energies of reactants. The selection of electronic, vibrational, rotational, and fine-structure states are possible by this technique.

IV-F-1 Determination of Separate Reaction Cross Sections for the Two Spin-Orbit States $\text{Ar}^+(^2P_{3/2}, ^2P_{1/2})$

Kenichiro TANAKA, Tatsuhisa KATO, Jean DURUP (Univ. of Paris-Sud and IMS), and Inosuke KOYANO

[*J. Chem. Phys.* 73, 586 (1980)]

Utilizing the threshold electron-secondary ion coincidence technique which we have developed

recently,¹⁾ the reaction cross sections of the individual spin-orbit states $\text{Ar}^+(^2P_{3/2}, ^2P_{1/2})$ in the reaction



have been determined directly as a function of collision energy E_{CM} in the range from 0.05 to 0.50 eV.

Experimental results are summarized in Figure 1, from which several interesting aspects of this reaction are immediately apparent. The cross

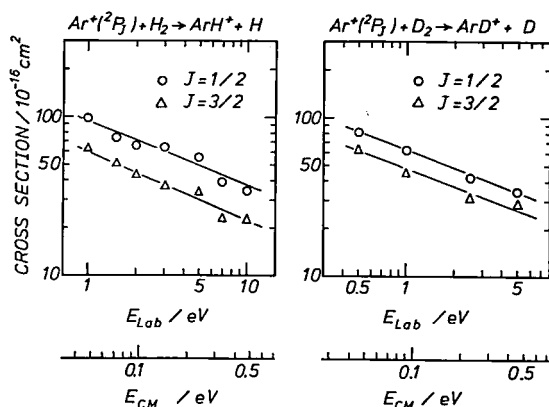
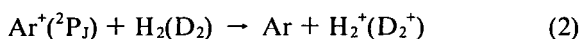


Figure 1. State-selected cross sections for reaction (1) as a function of the collision energy.

sections for the reactions with H_2 are about 1.5 times larger for $^2P_{1/2}$ than for $^2P_{3/2}$ and this ratio is independent of the collision energy within the range studies here. The ratio for the reactions with D_2 , on the other hand, is about 1.3, apparently smaller than that for the reactions with H_2 , and is again independent of the collision energy.

Charge transfer channels



have also been investigated and it has been found that the cross sections are more than 5 times larger for the $^2P_{1/2}$ state than for the $^2P_{3/2}$ state in the case of the H_2 reaction, whereas they are almost the same for the two states in the case of the D_2 reaction.

Reference

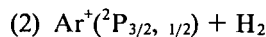
- 1) K. Tanaka and I. Koyano, *IMS Ann. Rev.*, 73 (1978); I. Koyano and K. Tanaka, *J. Chem. Phys.*, 72, 4858 (1980).

IV-F-2 Theoretical Studies of the State Selected Reaction $Ar(^2P_{3/2}, ^2P_{1/2}) + H_2(D_2) \rightarrow ArH^+ (ArD^+) + H(D)$

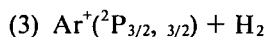
Jean DURUP (*Univ. of Paris-Sud and IMS*),
Tatsuhisa KATO, Kenichiro TANAKA, and
Inosuke KOYANO

In order to understand the experimental results on the title reaction (given in the preceding section (IV-F-1)), we have developed a reaction model which takes spin-orbit coupling into account and performed a theoretical calculation of the cross sections.

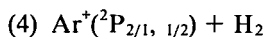
Spin-orbit coupling mixes the $2^2A'$, $3^2A'$, and $1^2A''$ states which evolve from the reactant state $Ar(^2P) + H_2$ (in the general C_s configuration) to form new states (2), (3), and (4):



$$\frac{1}{\sqrt{6}} [2(2^2A') + (3^2A') + i(1^2A'')]$$

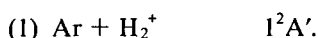


$$\frac{1}{\sqrt{2}} [(3^2A') + i(1^2A'')]$$



$$\frac{1}{\sqrt{3}} [-(2^2A') + (3^2A') + i(1^2A'')].$$

None of them, however, correlate directly with the product state $ArH^+ + H$. The charge transfer state $Ar + H_2^+$ has the $^2A'$ symmetry ($1^2A'$) and this state correlates with the product state which also has the $^2A'$ symmetry:

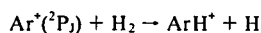


Thus the essence of the theory is to investigate couplings between state (1) and each of states (2), (3), and (4). In calculating, it has been assumed that the coupling is dependent only on the $2^2A'$ component of the latter states.¹⁾ Landau-Zenner type transition probabilities have been calculated as a function of the intermolecular distance R using the potential energy surfaces calculated by Baer and Beswick.²⁾ It has been assumed that the product $ArH^+ + H$ is produced only when the system approaching with impact parameter smaller than the Langevin critical value b_0 undergoes transition.

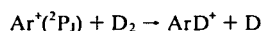
Results for the reactive channel are summarized in Table I. It is seen that fairly good agreement with experiment is obtained concerning the cross section ratios $\sigma(1/2)/\sigma(3/2)$.

References

- 1) S. Chapman and R. K. Preston, *J. Chem. Phys.*, 60, 650 (1974).
- 2) M. Baer and J. A. Beswick, *Phys. Rev.*, A19, 1559 (1979).

Table I. Comparison of the Cross Section $\sigma(1/2)/\sigma(3/2)$ 

$E_{\text{CM}}(\text{eV})$	$\sigma(1/2)/\sigma(3/2)$	
	(Exptl.)	(Model)
0.048	1.59	1.29
0.095	1.53	1.27
0.238	1.65	1.29
0.476	1.48	1.32

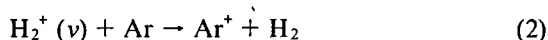
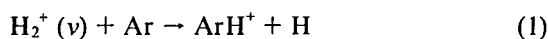


$E_{\text{CM}}(\text{eV})$	$\sigma(1/2)/\sigma(3/2)$	
	(Exptl.)	(Model)
0.046	1.29	1.50
0.091	1.38	1.49
0.227	1.35	1.50
0.455	1.21	1.56

IV-F-3 Direct Observation of Enhanced Charge-transfer Cross Sections at Near-Resonance: $\text{H}_2^+(\nu) + \text{Ar} \rightarrow \text{Ar}^+ + \text{H}_2$

Kenichiro TANAKA, Tatsuhisa KATO, and Inosuke KOYANO

Vibrational energy dependence of the cross sections for the reactions



has been examined by using a **TESICO** technique.¹⁾ Reaction (1) is exoergic by 1.30 eV for H_2^+ in $\nu=0$, while reaction (2) is endoergic by 0.33 eV for H_2^+ in $\nu=0$ and becomes exoergic for $\nu \geq 2$.

Figure 1 summarizes the results obtained for $\nu = 0 - 4$ of the reactant H_2^+ ion at a fixed collision energy of 0.77 eV. As can be seen from the figure, it is clearly shown that while the cross section of reaction (1) is almost independent of the vibrational states, the cross section of reaction (2) is dramatically enhanced at $\nu = 2$. Reaction (2) with H_2^+ in $\nu = 2$ has a near-resonant channel



where the exoergicity is only 16 meV and the Franck-Condon factor for the $\text{H}_2(\nu=0) - \text{H}_2^+(\nu=$

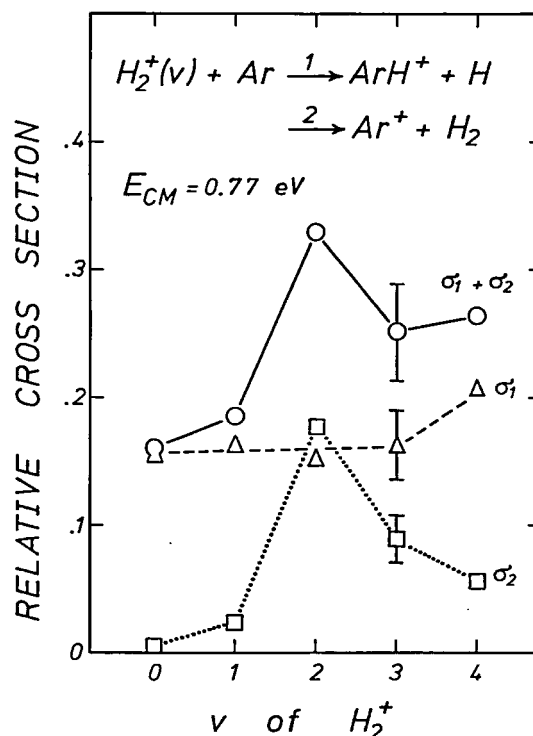


Figure 1. Relative cross section for the reaction of H_2^+ with Ar to form ArH^+ (1) and Ar^+ (2) as a function of vibrational quantum number of H_2^+ , obtained at the collision energy of 0.77 eV.

2) transition has a favorable value. The large cross section observed in reaction (2) at $\nu = 2$ can be explained by assuming that reaction (2) proceeds via this near-resonant channel.

More detailed investigation of this reaction, covering wider range of collision energies, and similar calculations to those described in IV-F-2 are in progress.

Reference

- 1) I. Koyano and K. Tanaka, *J. Chem. Phys.*, **72**, 4858 (1980).

IV-F-4 Calculation of Ion Trajectory and Potential Mapping for TEPSICO Ion Optics.

Tatsuhisa KATO, Jean DURUP (*Université Paris-Sud and IMS*), Kenichiro TANAKA, and Inosuke KOYANO

In **TEPSICO** apparatus,¹⁾ a multi-element electrostatic lens system is used for producing nearly monoenergetic low-energy ion beams. The system is based upon the design of Gustafsson and Lindholm,²⁾ as modified by Herman *et al.*,³⁾ and consists of a set of circular (with circular apertures) and semicircular metal plate electrodes for decelerating and focussing ions. In an attempt to find an optimum operating condition for this lens

system theoretically, we have performed a calculation of the potential distribution along the system and the trajectories of ions moving subject to these potentials.

The potential distributions were obtained by solving the Laplace equation

$$\nabla^2 v = 0 \quad (1)$$

numerically in the following manner. The space between electrodes in the lens system was divided into small cubes by a three dimensional grid with a constant interval h . The potential at any grid point (I,J,K) was computed under a given initial and boundary conditions using the equation

$$V(I,J,K) = (V(I+1,J,K) + V(I-1,J,K) + V(I,J+1,K) + V(I,J-1,K) + V(I,J,K+1) + V(I,J,K-1))/6.$$

The procedure was iterated until a consistent set of $V(I,J,K)$ was obtained. The motions of a charged particle on the potential surfaces so obtained were then solved. An example of the ion trajectory obtained with $h = 0.1$ mm is shown in Figure 1.

From the results of these calculations, we find that

- (1) several optimum sets of voltages are possible for a given configuration of electrodes,
- (2) the condition which we have chosen empirically is very close to one of the optimum conditions,
- (3) the number of electrodes of the system can be reduced without reducing the performance.

References

- 1) K. Tanaka and I. Koyano, *IMS Ann. Rev.*, 73 (1978).
- 2) F. Gustafsson and E. Lindholm, private communication to J. B. Hasted (cited in *Atomic and Molecular Processes*, edited by D. R. Bates, Academic, London, 1962, p. 705).
- 3) Z. Herman, J. D. Kerstetter, T. L. Rose, and R. Wolfgang, *Rev. Sci. Instr.*, 40, 538 (1969).

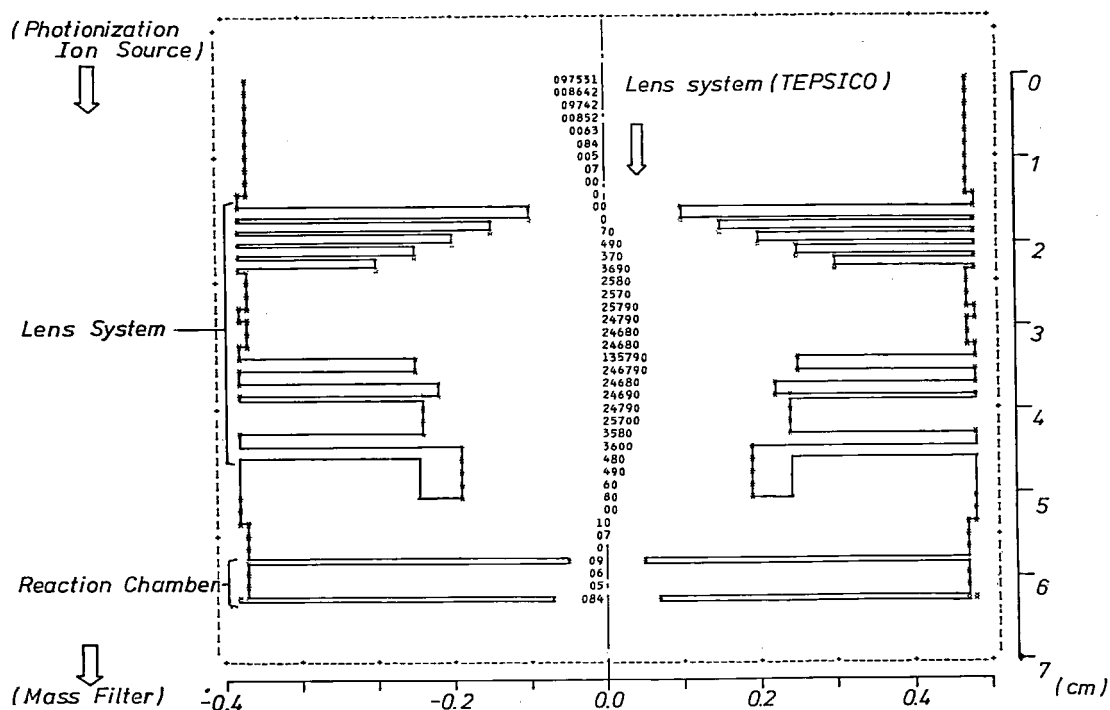


Figure 1. An example of calculated ion trajectories. Ions are injected with incident energy of 2.0 eV from the top to be focussed at the entrance of the reaction chamber.

IV—G Photoionization Processes in Small Molecules

Kenichiro TANAKA, Tatsuhisa KATO and Inosuke KOYANO

Two techniques have generally been used for the study of molecular photoionization processes, *i. e.*, measurements of photoionization efficiency curves (PIEC) and photoelectron spectra (PES). While PIEC yields a wealth of information on the ionization processes and energy levels of ions and neutral molecules, difficulty is often encountered with this technique when autoionization obscures the step structure of the curve. In such a situation, we often resort to PES which provides precise locations of ionic states and transition probabilities to these states. However, ionic states that can be studied by the ordinary (constant wave-length) PES are largely limited to the states which combine with the ground state of the parent molecule with favorable Franck-Condon factors.

Another type of photoelectron spectroscopy is the threshold electron spectroscopy which uses a

variable wave-length light source and detects only the zero kinetic energy photoelectrons (threshold electrons). In this method, ionic states which are not favored by direct ionization are often observed through autoionization, since threshold electrons are produced if an autoionizing state has the same energy as one of the ionic states and the autoionizing transition between them is allowed by selection rules.

In this project, we study photoionization processes in small molecules by simultaneous measurements of photoionization efficiency curves and threshold electron spectra. An apparatus which incorporates these two complementary techniques has been constructed and diatomic molecules H_2 , N_2 , O_2 , and CO have been studied so far. Several triatomic and tetra-atomic molecules are also being investigated.

IV—H Studies of Formation and Destruction Mechanisms of Interstellar Molecules

Hideo YAMAZAKI (*Tokyo Inst. of Tech.*), Kenichiro TANAKA and Inosuke KOYANO

Recent discoveries of a large variety of molecules, including complex organic ones, in interstellar space of our galaxy stimulated not only astrophysicists but also chemists to wonder and investigate how these molecules were formed under the physical conditions prevailing in interstellar space. Among several mechanisms which have been proposed, the gas-phase and grain surface molecular synthesis models are most intriguing to chemists. The only promising gas phase models seem to be those involving ion-molecule reactions, since rates of most neutral reactions are not sufficiently large at interstellar temperatures because of the activation energies required.

In this project, we are carrying out non-steady-

state calculations of the abundance of these molecules based on an ion-molecule reaction model. Several computational methods have been tried to solve more than 200 coupled rate equations numerically over the time scale as long as 10^{14} seconds. Emphasis is placed on the interpretation of larger molecules with more than five atoms, including the recently detected $n = 5, 7$ and 9 members of the HC_nN series, and on the prediction of the abundance of molecules which have not yet been detected owing to the lack of dipole moment. Results indicate that the gas phase ion-molecule reaction model is indeed capable of explaining the abundance of the observed molecules (see also *IMS Ann. Rev.*, 77 (1978), 104 (1979)).

IV—I Spectroscopy and Chemical Dynamics using Supersonic Nozzle Beams

The usefulness of supersonic nozzle beams has increasingly been recognized in both spectroscopy and chemical dynamics. The capability of cooling internal degrees of freedom of molecules and the possibility of producing various kinds of molecular clusters are important properties of the technique. In this project, we aim at high resolution absorption and Raman spectroscopy, dynamical studies of cluster reactions, and their combinations, utilizing the above properties of supersonic nozzle beams.

IV-I-1 Construction of a Molecular Beams Apparatus for Spectroscopic and Dynamical Studies

Yuji MORI (*Tokyo Inst. of Tech. and IMS*),
Kenichiro TANAKA, Tatsuhisa KATO and
Inosuke KOYANO

For the above purpose, we have constructed a molecular beams apparatus which incorporates a supersonic nozzle beam source, a mass-selected ion beam source, and a mass spectrometric detector which can be rotated around the scattering center. It is also designed so as to allow high resolution absorption and Raman spectroscopy of internally cooled molecules using various types of lasers. The whole view of the apparatus is shown in Figure 1.

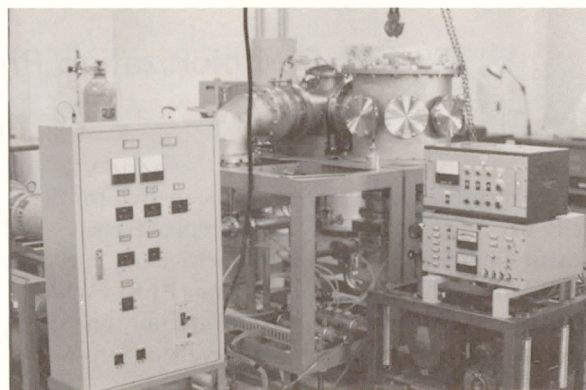


Figure 1. Whole view of the apparatus.

IV—J Several Topics in HeI Photoelectron Spectroscopy

Molecular photoelectron (PE) spectroscopy with HeI resonance line is now a well-established technique to determine ionization potentials of valence electrons, and during the last decade it has been employed for a variety of PE studies associated with electronic structures of organic and inorganic molecules in the gas phase. There still remain many interesting subjects to be studied by HeI PE spectroscopy. Firstly, we are now in position to compare HeI spectra systematically on the basis of *ab initio* SCF MO calculations for many fundamental organic molecules. It seems quite appropriate to compile a handbook which covers HeI spectra of many kinds of fundamental organic compounds together with *ab initio* MO assignments. Secondly, an application of HeI PE spectroscopy to skewed compounds and rotational isomers, combined with *ab initio* calculations, is also interesting from a molecular structural point of view. If HeI spectra are measured in higher resolution, this field will much expand. Thirdly, quantitative measurements of PE intensities are important from analytical and theoretical points of view, so that it is desirable to establish a method of reliable PE intensities. Intensity-defined PE spectra may be quite useful for analytical purposes. On the other hand, PE band intensities are closely related to partial photoionization cross sections associated with specific ionic states

IV-J-1 Systematic Assignments of HeI Photoelectron Spectra of 100 Fundamental Organic Compounds

Katsumi KIMURA, Shunji KATSUMATA
(*Hokkaido Univ.*), Yohji ACHIBA, Tomoko
YAMAZAKI (*Hokkaido Univ.*) and Suehiro
IWATA
(*Inst. Phys. Chem. Res. and IMS*)

Photoelectron spectroscopy with HeI 584Å resonance line is now a well-established physico-chemical technique to determine ionization potentials up to 21.22 eV.¹⁾ During the past several years, HeI photoelectron spectra of many fundamental organic compounds in the gaseous phase have been measured by the authors under similar experimental conditions.²⁾ It is most ideal that HeI spectra of many series of compounds

measured under the same experimental conditions are systematically compared and spectral assignments are made on the basis of *ab initio* calculations with the same degree of approximations.

In order to make systematic assignments for our HeI spectra, we have recently carried out *ab initio* SCF MO calculations (4-31G) for about 100 fundamental organic compounds as well as *ab initio* CI calculations (6-31G) for the ionic species of about 20 typical ones. The series of the compounds studied are summarized in Table I. Results of the *ab initio* calculations have been compiled together with the 200 HeI photoelectron spectra in a handbook.³⁾

Table I. The series of organic compounds studied

1. Very simple molecules	2. Saturated hydrocarbons
3. Unsaturated hydrocarbons	4. Alkyl halides
5. Chloro-methanes and -ethanes	6. Alkyl alcohols
7. Alkyl thioalcohols	8. Amines
9. Ethers and thioether	10. XCH_2CH_2Y type compounds
11. Skew compounds	12. Alkyl aldehydes
13. Chloroacetaldehydes	14. Acetyl halides
15. Ketones	16. Glyoxals
17. Alkyl acids	18. Anhydrides
19. Nitro-alkanes	20. Cyano-alkanes
21. Thioformamide	22. Cyano-alkanes
23. Miscellaneous	

References

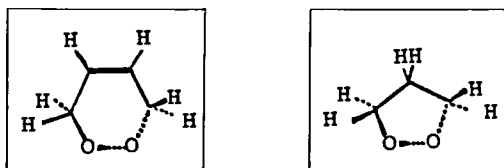
- 1) D. W. Turner *et al.*, "Molecular Photoelectron Spectroscopy. A Handbook of He 584Å Spectra", Interscience, London (1970).
- 2) K. Kimura *et al.*, Monograph Series of the Res. Inst. of Appl. Elect. (Hokkaido Univ.) No. 25 (1978).
- 3) To be published from Center for Academic Publications Japan.

IV-J-2 Cyclic Peroxides: Dihedral Angle around the Peroxide Bond by Microwave and Photoelectron Spectroscopic Studies

Toshihiko KONDO*, Mitsutoshi TANIMOTO*, Masakatsu MATSUMOTO*, (*Sagami Chem. Res. Center), Katsunori NOMOTO, Yohji ACHIBA and Katsumi KIMURA

[*Tetrahedron Lett.*, **21**, 1649 (1980)]

A recent photoelectron (PE) study of several peroxides by Coughlin *et al.*¹⁾ has suggested a linear relationship between the ionization potential separation (ΔI) of the two oxygen nonbonding orbitals and the dihedral angles (ϕ) around the peroxide bond, that was estimated from Dreiding models. For 3,6-dihydro-1,2-dioxin (1) and 1,2-dioxolane (2),



our microwave study has revealed that $\phi = 80 \pm 2^\circ$ and $50 \pm 2^\circ$, respectively. On the other hand, we have also obtained a HeI PE spectrum of 1, as shown in Figure 1, and indicated on the basis of *ab initio* SCF MO calculations (4-31G) that ΔI does

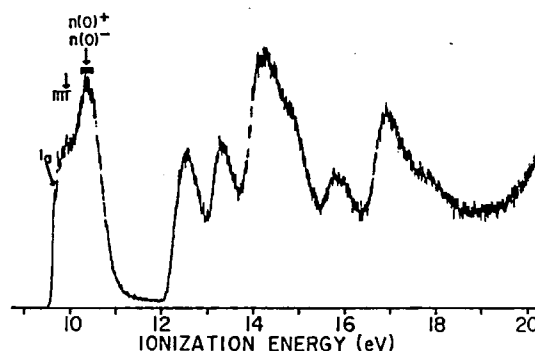


Figure 1. HeI photoelectron spectrum of compound 1.

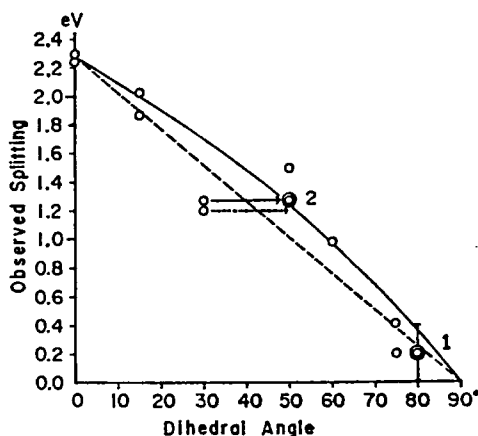


Figure 2. Observed ionization potential splitting (ΔI) against the dihedral angle (ϕ) for cyclic peroxides. Open circles and the broken line indicate the data of Coughlin *et al.*,¹⁾ while double circles show the present results.

not exceed 0.4 eV. For 2, it is already known that $\Delta I = 1.27$ eV.¹⁾ From the present work it has been concluded that the linear relationship of Coughlin *et al.*¹⁾ shown by a broken line in Figure 2 should be slightly modified as shown by a solid curve.

Reference

- 1) D. J. Coughlin, R. S. Brown and R. G. Salomon, *J. Am. Chem. Soc.*, **101**, 1533 (1979).

IV-J-3 Automatic Data-Processing System for Photoelectron Intensity Measurements

Yohji ACHIBA, Noriyoshi KAKUTA*, Koshiro MIYAHARA* (*Hokkaido Univ.) and Katsumi KIMURA

Recently we have proposed a method of using a HeI photoelectron (PE) spectrometer for determining partial photoionization cross sections of molecules at 58.4 nm.^{1,2)} This method may be applicable to future SOR researches, if an appropriate automatic data-processing system is introduced. Since the method uses a binary mixture of a standard and a sample gas, the determination of mole fractions is one of laborious processes. In order to reduce experimental errors introduced in the determination of mole fractions and relative PE intensities, we have constructed a microcomputer

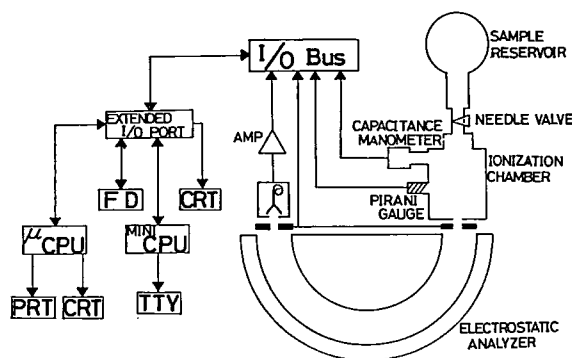


Figure 1. A block diagram of microcomputer based data-processing system for photoelectron intensity measurements. μ -CPU: NEC COMPO BS/80 microcomputer, mini-CPU: YHP 2109B minicomputer (32K), PRT: Printer, FD: Flexible disk CRT: Monitoring display, TTY: Keyboard printer.

based data-processing system whose block diagram is illustrated in Figure 1. It has been found that with this system the standard errors in the mole fraction determination are reduced down to about 5%. An example of pressure measurements is shown in Figure 2. Furthermore, the use of the computer controlled scanning system has been found very efficient in the determination of relative PE intensity measurements.

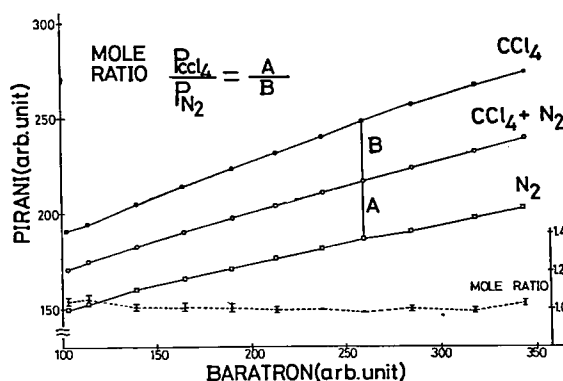


Figure 2. Plots of Baratron and Pirani outputs measured in the ionization chamber for a binary mixture of carbon tetrachloride and molecular nitrogen as well as the component gases. The mole ratio of CCl_4 to N_2 in the sample reservoir was 1.0:2.2, whereas the resulting mole ratio in the ionization chamber is nearly 1:1 (A:B). The broken line shows a trend of experimental mole ratios obtained at various different pressures.

References

- 1) K. Kimura, Y. Achiba, M. Morishita and T. Yamazaki, *J. Electron Spectrosc.*, **15**, 269 (1979).
- 2) N. Kakuta, Y. Achiba, K. Miyahara and K. Kimura, *Abstracts of the 41st Ann. Meeting of Chem. Soc. of Japan*, 161 (1980).

IV—K Studies of Molecular Complexes and Clusters by Hel Photoelectron Spectroscopy

Various inter-molecular species such as van der Waals molecules, hydrogen bonded species and electron-donor-acceptor (EDA) complexes in the gaseous phase are interesting species to be studied by HeI photoelectron spectroscopy, because changes in MO energies by the formation of such species can be directly studied on the basis of ionization potentials of valence electrons. It is difficult however to detect such inter-molecular species in ordinary photoelectron measurements, since the concentration is too low to detect. In order to obtain a measurable density of such a species, it is necessary to introduce a supersonic molecular beam in a photoelectron spectrometer with a high-speed pumping system. The gaseous EDA complex of $(\text{CH}_3)_2\text{O}$ with BF_3 has recently been studied by a HeI photoelectron spectrometer which we previously constructed at Hokkaido University, a gas inlet system of effusive nozzle type being used. On the other hand,

in order to measure a more weakly bound inter-molecular species, we have newly designed and constructed a HeI photoelectron spectrometer with a high-speed pumping system and a supersonic molecular beam source. The construction of this apparatus has almost been completed.

IV-K-1 Photoelectron Spectroscopic Study of EDA Complex of $(\text{CH}_3)_2\text{O}$ with BF_3 in the Gas Phase

Katsunori NOMOTO, Yohji ACHIBA and Katsumi KIMURA

Using a nozzle-type gas inlet system, we have successfully measured a HeI photoelectron (PE) spectrum due to complex formation of $(\text{CH}_3)_2\text{O}$ with BF_3 in the gas phase for the first time. The apparatus used here is the same as used previously in the PE study of the dimers of formic acid and acetic acid.¹⁾ A glass nozzle of 0.1 mm in diameter was used.

A HeI PE spectrum of the complex is shown in Figure 1, together with those of its components and their mixture. New bands appearing in the complex formation are indicated by solid lines in Figure 1. Since the geometry of this complex is already known,²⁾ we have also carried out *ab initio* MO calculations (4-31G). From the present work it has been concluded that 1) the calculated Koopmans theorem IPs agree fairly well with the observed IPs, and 2) the complex formation raises the oxygen nonbonding IP by 1.98 eV, while it reduces the fluorine nonbonding IP by 1.2 eV.

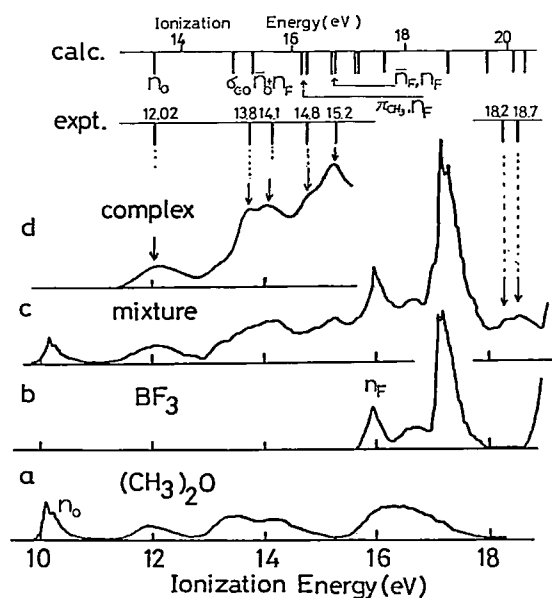


Figure 1. HeI photoelectron spectra of (a) $(\text{CH}_3)_2\text{O}$, (b) BF_3 , (c) a mixture of a and b, and (d) the difference spectrum due to the EDA complex. A comparison of ionization potentials between experiment and *ab initio* (Koopmans theorem) calculation.

References

- 1) K. Nomoto, *Doctoral Thesis* (Hokkaido University, 1979).
- 2) S. Shibata and K. Iijima, *Chem. Lett.*, 29 (1977).

IV-K-2 Construction of a New Photoelectron Spectrometer for Studying Molecular Complexes and Clusters in the Gas Phase

Shinji TOMODA, Kenji SATO, Yohji ACHIBA and Katsumi KIMURA

The extension of molecular photoelectron (PE) spectroscopy to a wide variety of weakly bound inter-molecular species (van der Waals molecules, hydrogen bonded species, EDA complexes, etc.) in the gas phase is expected to give direct information on ionization potentials of these species and excited states of the ionized species. Recently, van der Waals molecules of some rare gas atoms have been studied by HeI PE spectroscopy, by using a supersonic molecular beam source.¹⁾

In order to study various types of inter-molecular species we have newly designed and constructed a PE spectrometer with a high-speed pumping system. The apparatus consists of 1) a main vacuum chamber containing a hemispherical electron analyzer (21 cm in diameter), 2) an ionization chamber containing an electrostatic lens system and a HeI resonance source, 3) a supersonic nozzle beam source, and 4) a detector system. A schematic drawing of this apparatus and its photographic picture are shown in Figures 1 and 2, respectively. Eliminating the components of earth's magnetic field, we have just observed usual PE spectra of some testing samples. Final adjustment of the apparatus is now going on.

Reference

- 1) P. M. Dehmer and J. L. Dehmer, *J. Chem. Phys.*, **67**, 1774 (1977); *ibid.*, **68**, 3462 (1978); *ibid.*, **69**, 125 (1978).

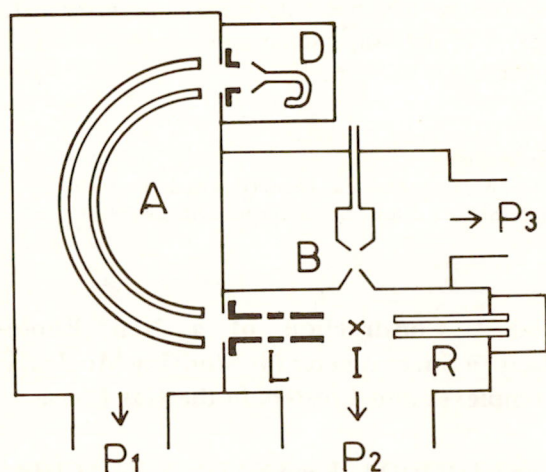


Figure 1. A schematic drawing of the molecular-beam photoelectron spectrometer.

A: Hemispherical electron energy analyzer, B: Supersonic nozzle beam source, D: Channel electron multiplier detector, I: Ionization region, L: Electrostatic lens system, P₁: Oil diffusion pump (6"), P₂: Oil diffusion pump (10"), P₃: Turbomolecular pump, R: HeI resonance lamp.

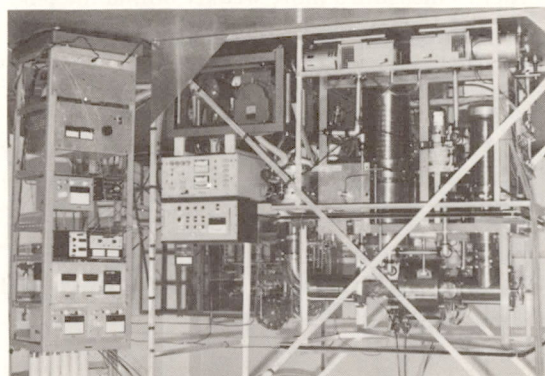


Figure 2. A photographic picture of the apparatus.

IV—L Photoelectron-Mass Spectroscopy of Multiphoton Ionization

In this project, a new attempt is made to combine molecular photoelectron spectroscopy with recently developed multiphoton-ionization spectroscopies using a tunable dye laser, in order to obtain more direct informations about electronically excited states as well as to study their electronic structures. Since state-selected molecular ions may be possibly produced by using a multiphoton ionization technique with a tunable dye laser, the photoelectron-mass spectroscopy will also become a powerful experimental method for studying dissociation processes of molecular ionized species.

IV-L-1 Construction of an Apparatus for Studying Multiphoton Ionization Electron and Mass Spectroscopy

Yohji ACHIBA, Kosuke SHOBATAKE and Katsumi KIMURA

An apparatus has been designed and is near completion to study multiphoton ionization using a mass spectrometer and an electron spectroscopic technique. The apparatus consists of three chambers as shown in Figure 1. A molecular beam is produced in Part 1 which is evacuated by an oil diffusion pump with a backing mechanical booster pump. The main chamber (Part 2) is pumped by an oil diffusion pump with a liquid nitrogen trap and a water baffle. Since most of the beam molecules through a skimmer are pumped out differentially by a beam catcher (Part 3), the reaction area may be

kept below 1×10^{-6} Torr under normal operating condition. Part 3 is evacuated by an oil diffusion pump and connected with a quadrupole mass spectrometer for characterization of the molecular beam.

A time-of-flight electron analyzer and a quadrupole mass filter are hold on the side ports of the main chamber. Each of the port is differentially pumped by a turbo molecular pump. A pulsed Nd-YAG pumped dye laser (Quanta-Ray, DCR-PDL1) is introduced through the bottom window of the main chamber to irradiate the molecular beam at the center of the main chamber. Adjustment and a series of test run are now under way.

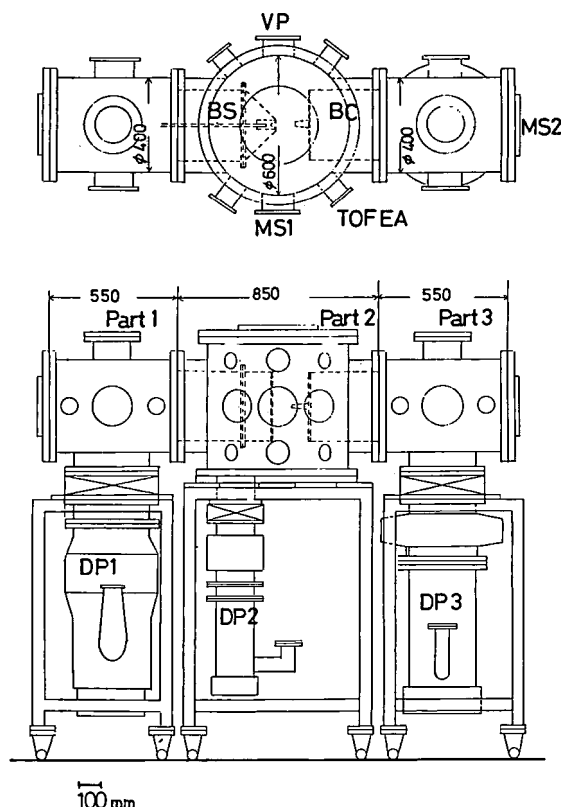


Figure 1. A schematic drawing of the apparatus of multiphoton electron and mass spectroscopy. BS: Beam source, BC: Beam catcher, MS1: Quadrupole mass filter, TOFEA: Time-of-flight electron analyzer, VP: Viewing port, MS2: Quadrupole mass spectrometer for characterization of the molecular beam, DP1: Oil diffusion pump (5,000 l/s), DP2: Oil diffusion pump (1,500 l/s), DP3: Oil diffusion pump (3,500 l/s).

IV—M Production, Characterization, and Spectroscopic Studies of Molecular Complexes and Clusters

There are several techniques to investigate the physics and chemistry of molecular complexes and clusters. One of the most powerful techniques for the production of such weakly bound compounds is the supersonic expansion of a high pressure gas through a small nozzle hole, by which one can obtain a very large number of exotic complexes. However, the identification and characterization of these complexes is difficult because of its weak bonding character.

In the present project we plan to develop new types of supersonic beam sources to investigate the UV, VUV and IR absorption spectroscopy, laser induced fluorescence spectroscopy and electron bombardment and multiphoton ionization mass spectroscopy of van der Waals complexes, molecular complexes and clusters. Then we plan to characterize these complexes by using these spectroscopic means.

We pay a great interest in finding what would happen after a weakly bound molecular complexes are brought to vibrationally and/or electronically excited states and to obtain the information on the predissociation dynamics of these molecules in relation to the intermolecular potential between the component molecules.

IV-M-1 Construction of an Apparatus for Molecular Beam Chemistry

Kiyohiko TABAYASHI and Kosuke SHOBA – TAKE

A multipurpose molecular beam machine for studying “molecular beam chemistry” is under

construction. The basic design is that of Yuan Lee¹⁾ which enables us to produce, characterize, and carry out the spectroscopic studies of molecular complexes and clusters by a molecular beam technique.

References

- 1) Y. T. Lee *et al.*, *Rev. Sci. Instrum.*, **40**, 1402 (1969).

RESEARCH ACTIVITIES V

Division of Applied Molecular Science

V—A Nature and Its Chemical Consequences of Interaction Between Benzene Rings in Bridged Aromatic Compounds

We continued our efforts in delineating the mechanism of the interaction between the aromatic rings in a fixed three dimensional framework. As a chemical consequence of the excitonic interaction between the three benzene rings held at an angle of 120° each other, triptycenes undergo photochemical bridging between the benzene rings to give the monocentric diradical species, i.e., carbene and nitrene, due to one of the bridgehead atoms. Bridging regioselectivity with respect to the bridgehead substituents has now been disclosed. As an interesting property in the ground state, electrical conductivity measurements have been carried out for the EDA complex of a strong π -donor. The rates of electron hopping between two quinone rings have been measured for some polytritycenespolyquinones.

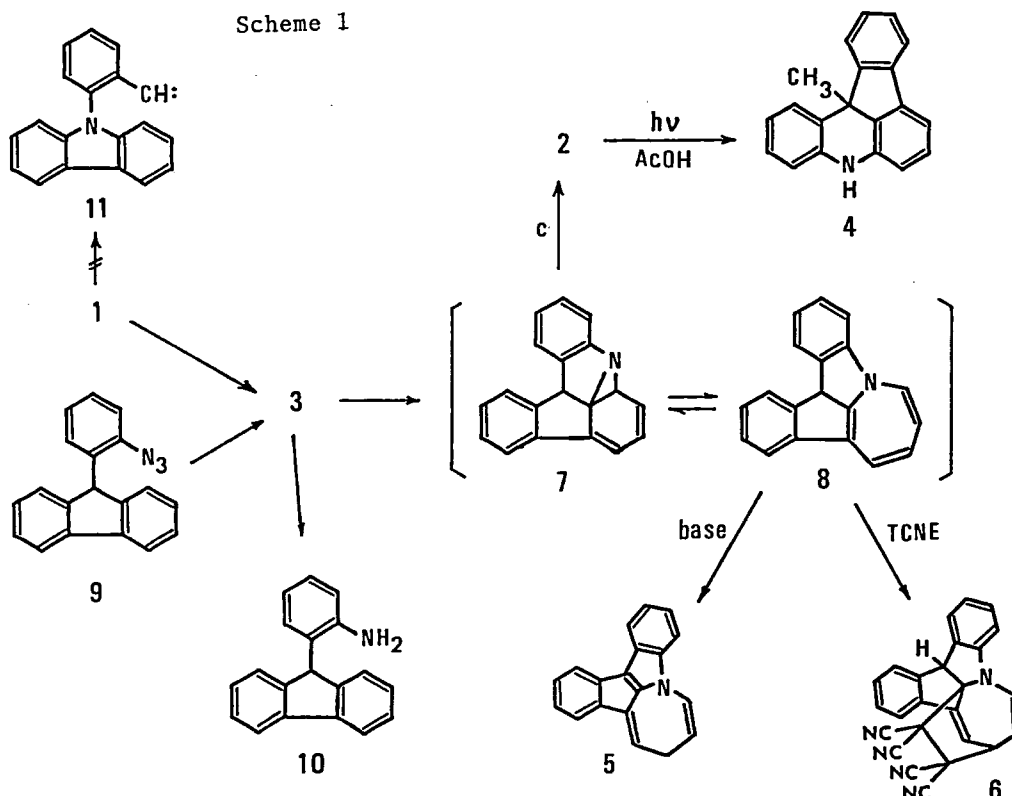
V-A-1 Formation of *o*-(9-Fluorenyl)phenyl-nitrene in the Photoisomerization of 1-Azatriptycene

Tadashi SUGAWARA and Hiizu IWAMURA

[*J. Am. Chem. Soc.*, in press]

When irradiated with a low-pressure mercury lamp in acetic acid, azatriptycene **1** underwent photorearrangement as described by Witting and

Steinhoff¹ to give indeno-acridine **2** which was now found to be converted to 12b-methyl-5,12b-dihydro derivative **4** on further irradiation. In dilute methanolic sodium methoxide, indeno-azepinoindole derivative **5** was obtained in 69% yield. In acetonitrile in the presence of TCNE, the 1H-azepine was isolated as the 2,5-adduct **6**. *o*-(9-Fluorenyl)aniline **10** was obtained as a product of the triplet manifold of the reactions. The results are fully indicative of the formation of *o*-(9-fluorenyl)-phenylnitrene **3** followed by internal addition to



give azanorcaradiene **7** from which products **2**, **5** and **6** can be derived depending on the different modes of the cleavage of the aziridine ring. Nitrene **3** was generated unambiguously from the corresponding azide **9** to give the similar results as those of **1** (Scheme 1). Formation of **3** from **1** was detected by ESR spectroscopy; the characteristic intense X,Y transition of the triplet nitrene **3**

appeared at 6820 G and had the zero field splitting parameters of $D \approx 1.0$ and $E = 0.0 \text{ cm}^{-1}$ (Figure 1). The high bridging selectivity at the nitrogen end of the *o*-benzeno moieties of **1** should be noted.

Reference

- 1) G. Wittig and G. Steinhoff, *Justus Liebigs Ann. Chem.*, 676, 21 (1964).

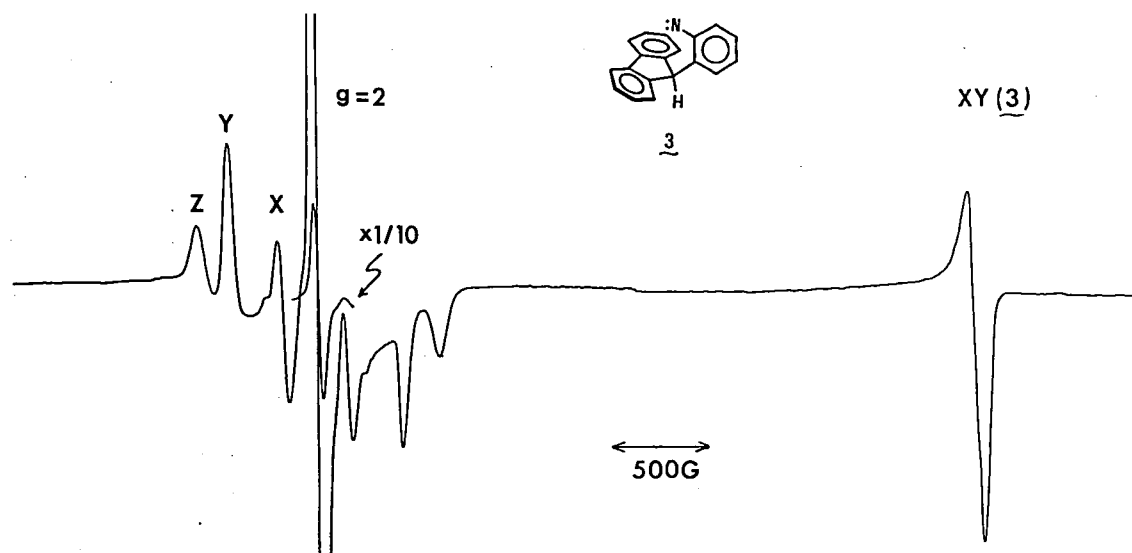


Figure 1. ESR spectra obtained on irradiating **1** in methylcyclohexane glass at 4.2K. The klystron frequency was 9.30 GHz and the $g = 2$ region of the spectra showed a strong signal due to the adventitious formation of free radicals.

V-A-2 Contrasting Photochemical Bridging Regioselectivity in Bridgehead-Substituted 9,10-Etheno- vs. 9,10-(*o*-Benzeno)-9,10-dihydroanthracenes

Michiko IWAMURA (*Toho Univ.*), Hideyuki TUKADA (*Univ. of Tokyo*), and Hiizu IWAMURA

[*Tetrahedron Lett.*, in press]

A comparative study has been carried out on the photoisomerization of a series of the title compounds. There are two possible termini capable of competitive π - π bringing in the excited states of these molecules (Scheme 1 and 2). The bridging regioselectivity obtained from the product analyses

is given in Table 1. The results are quite contrasting in that path b prevails in the ethenoanthracenes whereas bridging takes place almost always at the end of the *o*-benzeno moieties near to the substituent in triptycenes. The selectivity in the former system can be interpreted in terms of the relative stability of the initially formed cyclopropyldicarbonyl diradicals A' and B'. The product-developing step cannot be associated with these diradicals in the triptycene photoisomerization but with a later stage on the excited state energy surface of the rearrangement. Since most of the substituents can stabilize the radical and carbenic centers when directly attached, either an alternative diradical C which may come later in the course of the rearrangement or a concerted cheletropic elimination of the monocentric diradicals is proposed as responsible for the product-forming step in the triptycene photo-rearrangement.

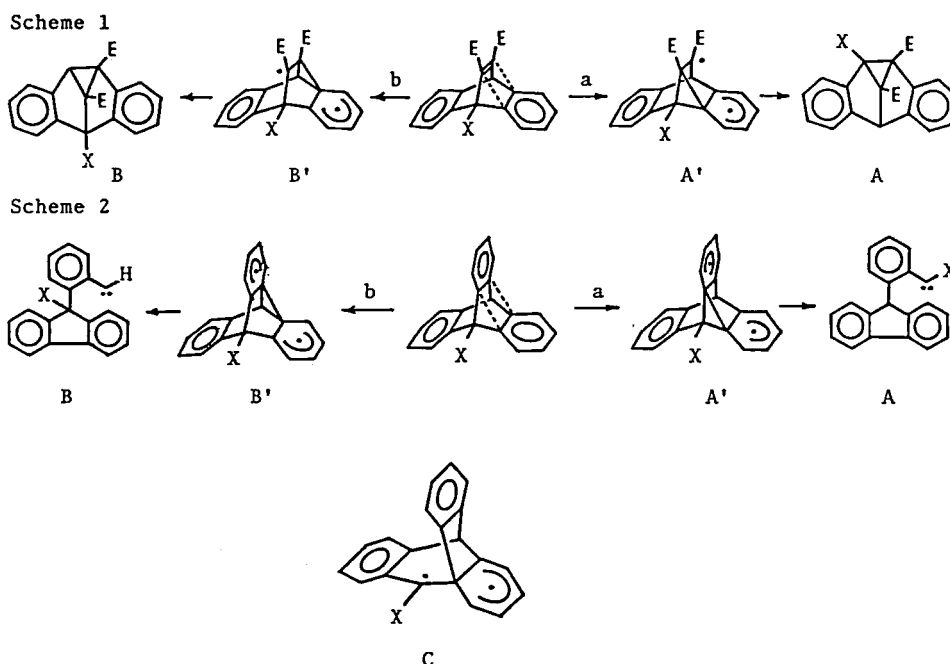


Table I. Bridging Regioselectivity for Typical Di- π -methane and Triptycene Photorearrangements

X	Ethenoanthracene		o-Benzoanthracene	
	path a	path b	path a	path b
OCH ₃	0	100 %	100 ^a	0 %
OAc	0	100		
OCOPh	0	100	100 ^a	0
CH ₃	29	71	21	79
(CH ₃) ₂ CH	23	77		
(CH ₃) ₃ C	0	100	0	100
Br	0	100	100	0
Ph	100	0	100	0
Ac	29	71	100 ^a	0
CHO	12	88	100	0
NO ₂	0	100		

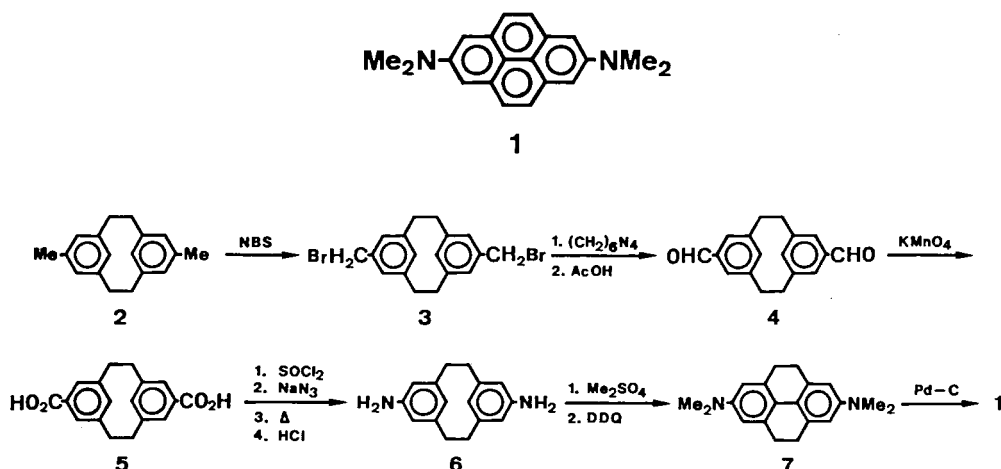
a) H. Iwamura and K. Yoshimura, *J. Am. Chem. Soc.*, **96**, 2652 (1974); H. Iwamura and H. Tukada, *Tetrahedron Lett.*, 3451 (1978); Y. Kawada, H. Tukada and H. Iwamura, *ibid.*, **21**, 181 (1980).

V-A-3 Synthesis of 2,7-Bis(dimethylamino)-pyrene and the Electrical Conductivity of Its CT Complex with TCNQ

Yoshiteru SAKATA (*Univ. of Osaka and IMS*),

As a new potentially powerful π -donor for organic metals, we synthesized 2,7-bis(dimethylamino) pyrene **1** via 6 steps from **2** including unique transannular reaction of [2.2]metacyclophane as shown in the Scheme. Total yield of **1** was 3.9% based on **2**.

1 forms a 1:1 CT complex with TCNQ as dark blue fine needles. The electrical conductivity of the complex, measured on a polycrystalline sample, was *ca.* $10^{-2} \text{ ohm}^{-1} \text{ cm}^{-1}$ at room temperature. The measurements of the temperature-dependent conductivity on a single crystal are now in progress.



V-A-4 Radical Anions of 9,10-Dihydro-9,10-[1',2']-benzenoanthracene-1,4,5,8-tetraone

Glen A. RUSSELL, N. K. SULEMAN (*Iowa State Univ.*), Hiizu IWAMURA, Takahiko OOSUMI¹⁾, and O. W. Webster (*Dupont and Co.*)

The formation of radical ions upon reduction of title bisquinone **1** has been investigated in CH₃CN and (CH₃)₂SO solutions by ESR spectroscopy. Electrolytic reduction at Hg or Pt of **1** gave initially the 1 : 4 : 6 : 4 : 1 pentet of Figure 1a ($a^H = 1.10$ G, $g = 2.00506$ in (CH₃)₂SO). This species does not have the electron delocalized over both rings because cooling the CH₃CN solution resulted in selective line broadening of the second and fourth peaks. The hydrogen atoms of the bisquinone rings of **1**^{•-} are time-averaged by electron migration for which an energy barrier of $\Delta H^\ddagger = 6.2$ kcal mol⁻¹ ($\Delta S^\ddagger = -7$ e.u.) was calculated. Continued electrolysis of **1** gave the diradical dianion in which the singlet-triplet energy separation (J) is much smaller than a^H and no appreciable electron-electron dipolar broadening is observed. More extensive electrolytic or chemical reduction of **1** led to radical trianion

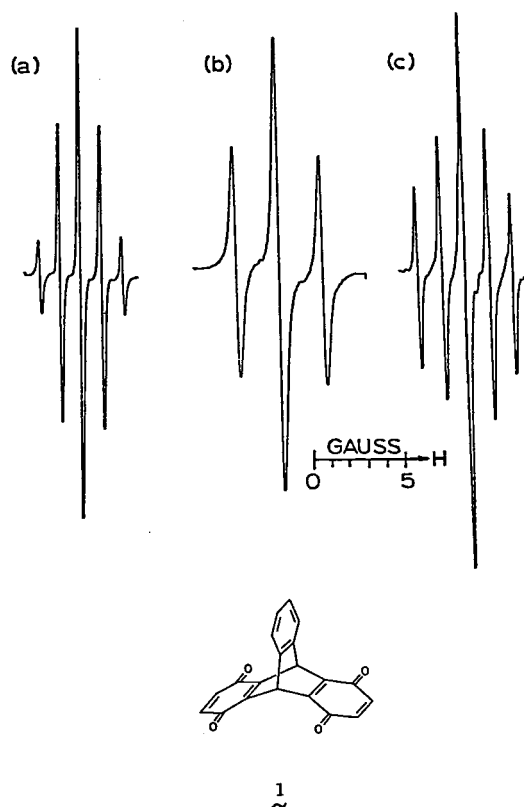


Figure 1. Radical anions derived from triptycene bisquinone **1** in CH₃CN: (a) **1**^{•-}, (b) **1**^{2•-}, (c) **1**^{3•-} containing a trace of **1**^{2•-} (shoulders in center and high field peak).

with $a^H = 1.30$ G and $g = 2.00495$ in (CH₃)₂SO (Figure 1c). From the line broadening ΔH^\ddagger for electron jump was calculated to be 3.7 kcal mol⁻¹ ($\Delta S^\ddagger = -24.3$ e.u.). More extensive solvation for **1**^{3•-} is concluded.

Note

1) IMS Graduate Student from Ehime Univ. for 1979.

V-A-5 Syntheses, Structures, and Redox Reactions of 5,18; 7,16; 9,14-Tris(*o*-benzeno)heptacene-1,4,6,8,10,13,15,17-octaones

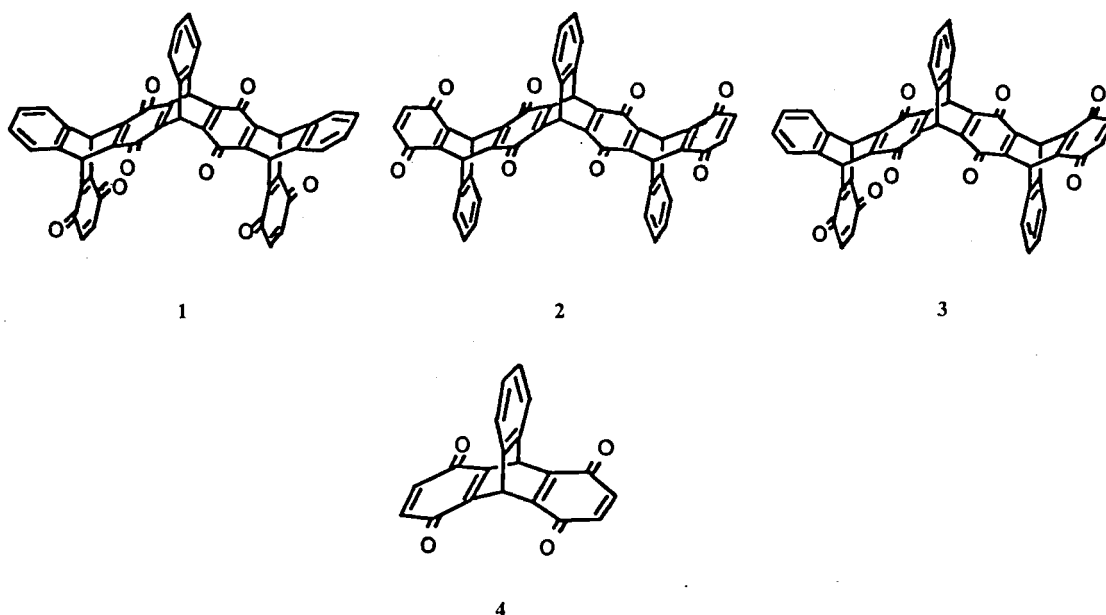
Yoshinori NISHIZAWA, Takehiko OOSUMI,¹⁾ and Hiizu IWAMURA

Three isomeric title polyquinones **1**, **2** and **3** and the lower analogs have been prepared to delineate the interaction between the acceptor rings on the polytritycene framework. Base-catalyzed isomerization of the Diels-Alder adducts from the triptycenebisquinone **4**² and 1,4-dimethoxyanthracene followed by oxidation with Ce(IV) ions gave desired **1**, **2** and **3**.

ESR spectra due to mono-anion radicals of these quinones except for **4** (see V-A-4) showed only unresolved singlets, indicating that the unpaired electron should reside not in the outer quinone rings but in the inner ones. The results are reasonably interpreted in terms of the electron-withdrawing effect of the outer quinone rings. The half-wave reduction potentials of these quinones measured in acetonitrile are in accordance with these interpretations.

References

- 1) IMS Graduate Student from Ehime Univ. for 1979.
- 2) H. Iwamura and K. Makino, *J. Chem. Soc., Chem. Commun.*, 720 (1978); *IMS Ann. Rev.*, 107 (1979).



V -B Stereochemical Consequences of the Non-bonded Interaction in Overcrowded Molecules

We have been interested for some time in the unexpectedly high potential energy barrier to rotation around the single bond in overcrowded molecules. In triptycenes the barriers can be high enough to bring the rotation around the bond extending out of the bridgehead carbons to a halt. Rotational isomerism was now found to be an important factor to be considered in interpreting a rather complex ESR signals in the spin-trapping experiments. In contrast to these high rotational barriers due to high non-bonded interaction, the idea of geared rotation has been put forward to explain the unexpectedly fast rotation in apparently congested molecules. One of the most dramatic demonstrations of the conformational mobility in overcrowded molecules has now been obtained by bis(1-triptycyl) ether.

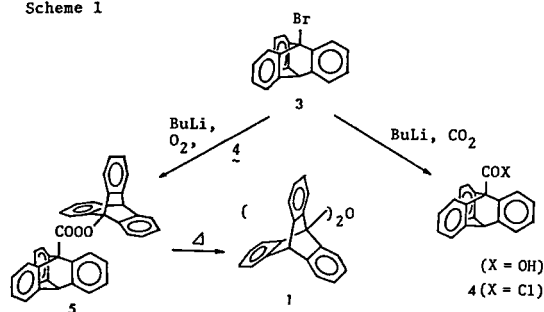
V-B-1 Unconventional Synthesis and Conformational Flexibility of Bis(1-triptycyl) Ether

Yuzo KAWADA and Hiizu IWAMURA

[*J. Org. Chem.*, **45**, 2547 (1980)]

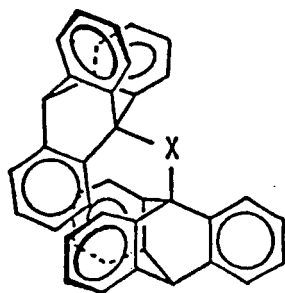
Unexpectedly high conformational flexibility in overcrowded molecules is often associated with the geared rotation of two parts of the molecule. As one of the most dramatic demonstration of these effects, the title compound was prepared. 1-Triptycyl-lithium prepared from 1-bromotriptycene (**3**) and butyllithium was allowed to react with oxygen followed by treatment with 1-triptycenecarbonyl chloride (**4**) to give 1-triptycyl 1-triptyceneperoxydicarboxylate (**5**) in 49% overall yield. When decomposed at 130 — 150°C in perfluorodecalin, the peroxyester gave bis(1-triptycyl) ether, **1**, colorless solid, mp 470°C, in quantitative yield (Scheme 1).

Scheme 1



The conventional reaction of di-(9-anthryl)-methane with benzyne gave di-(1-triptycyl) methane, **2**, mp 416°C. Both **1** and **2** gave rather simple ¹H and ¹³C NMR spectra which correspond to a structure with six benzene rings being equivalent. Since the ground state of these molecules is considered to have C₃ symmetry and to be degenerate six-fold, the observed spectral pattern can be rationalized only in terms of a rapid interconversion among the degenerate conformers. No sign of restricted rotation around the

bridgehead-to-oxygen or -to-methylene bond was manifest in the NMR spectra of these two di-(1-triptycyl) derivatives taken at temperatures down to -94°C .



- 1 (X = O)
2 (X = CH₂)

V-B-2 Rotational Barriers in Bisadducts of 1-Cyano-1-methylethyl radicals with Nitrones and Nitroso Compounds

Michiko IWAMURA (*Toho Univ.*), Morimatsu KATO^H,¹⁾ and Hiizu IWAMURA

[*Org. Magn. Reson.*, 13, 1905 (1980)]

The temperature-dependent ^1H NMR spectra (Figure 1 and 2) have been measured for the bisadducts **2a** and **3** of 1-cyano-1-methylethyl radicals with α -phenyl-*N*-benzyl nitron and nitrosobenzene, respectively. A free energy of activation of $\Delta G^{\ddagger} = 15.0 \sim 15.4$ kcal/mol at $24 \sim 45^{\circ}\text{C}$ has been obtained for **2a** by applying the Eyring equation to the rate constants at the coalescence points of the methyl signals. The line shapes due to four methyl signals exchanging between two sites of equal population have been simulated by calculation to give activation enthalpy of 12.5 kcal/mol and the corresponding entropy of -9.4 e.u. for **3**. As the inversion barriers at pyramidal nitrogens of hydroxylamine derivatives should be lowered in *N*-phenyl derivative because of conjugation, the rate process which is responsible for the observed temperature-dependent NMR spectra can be assigned to

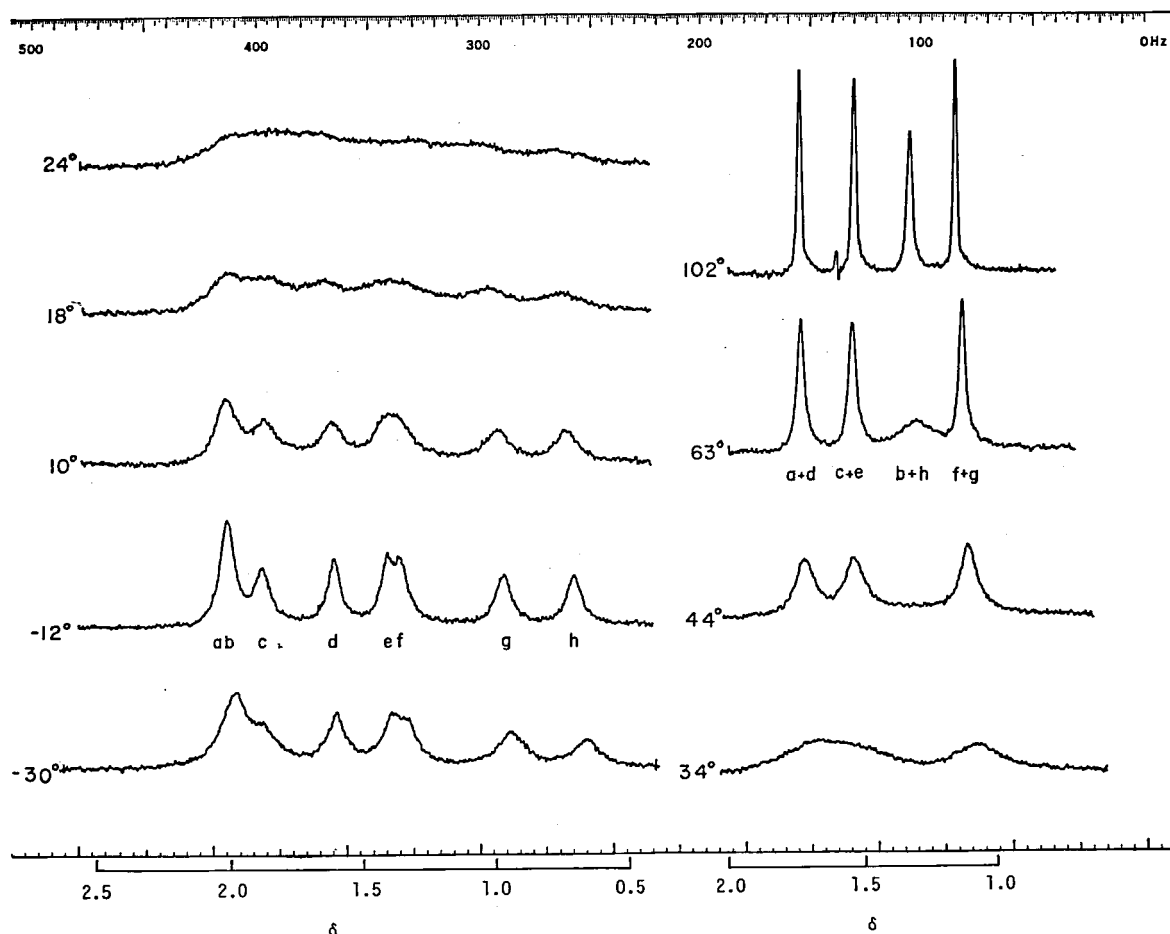


Figure 1. ^1H (60 MHz) NMR spectra due to the methyl groups in trisubstituted hydroxylamine **2a** as a function of temperature.

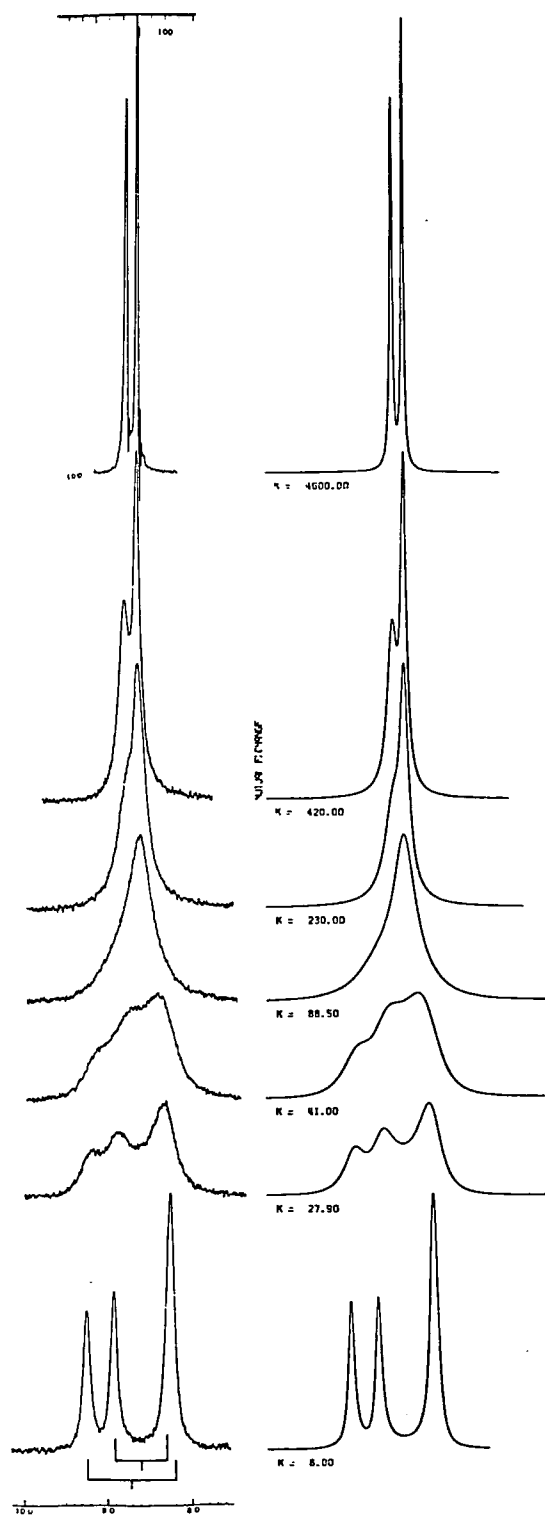
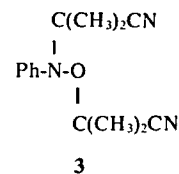
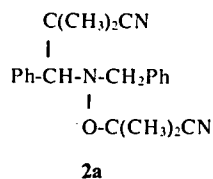


Figure 2. Observed (left) and simulated (right) temperature dependent ^1H NMR (the methyl part only) for a solution of bisadduct 3 in 1,1,2,2-tetrachloroethane.

restricted rotation around one of the skeletal C-N-O-C bonds. Relevance of the results to the conformations of nitroxides derived from the spin trapping method using α -phenyl-*N*-*t*-butylnitrone and nitroso spin traps is discussed.

Note

1) IMS Graduate Student from Nagoya Inst. of Tech. for 1978—1980.



V-B-3 Out-Of-Plane Deformation of a Benzene Ring Incorporated in Cyclophanes

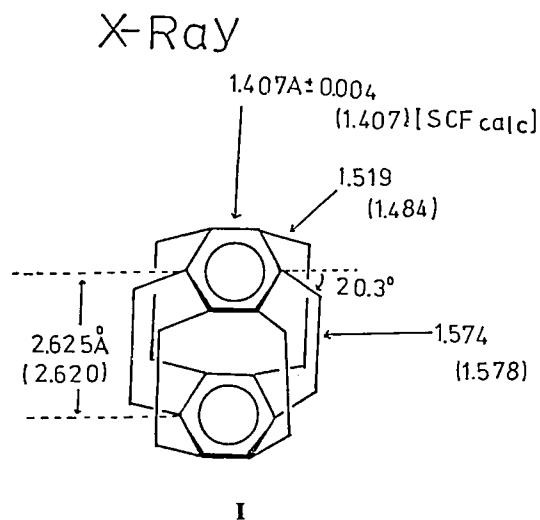
Hiizu IWAMURA, Morimatsu KATOH,¹⁾ and Hiroshi KIHARA (*Hagi Women's Junior College*)

[*Tetrahedron Lett.*, **21**, 1757 (1980)]

The elucidation of the chemical bonding in the deformed benzene rings is an important key to a thorough understanding of chemistry of cyclophanes. In order to evaluate the deformation of the apparently planar benzene ring in superphane, we have carried out the semiempirical and the *ab initio* SCF MO calculations for the C_6H_6 molecule fixed in a geometry simulating the experimental structure of superphane (**I**). The ring is considered to be bowl-shaped and the π -orbitals are not perpendicular to the ring plane but are deflected by *ca.* 10° (Figure 1). As a result, the ring is found to be

Note

1) IMS Graduate Student from Nagoya Inst. of Tech. for 1978—1980.



strained by $20.5 \text{ kcal mol}^{-1}$ in reference to the heat of formation of the regular benzene molecule with D_{6h} symmetry. The value is more than twice as large as those ($6 - 9 \text{ kcal mol}^{-1}$) of the boat benzene in a number of [2.2] paracyclophanes (II), slightly larger than those ($11 - 15 \text{ kcal mol}^{-1}$) of the chair

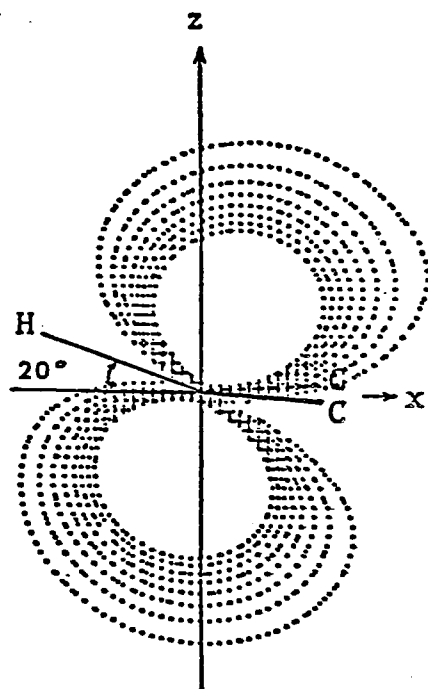


Figure 1. π -Electron distribution in the mirror plane passing through the ring carbon of the bowl-shaped benzene.

benzene (III), and comparable to those ($17 - 20 \text{ kcal mol}^{-1}$) of the boat benzene in [2.2] paracyclophanes and of the skew benzene ring found in the middle ring of multiply-layered [2.2] paracyclophanes (IV). Whereas destabilization of the deformed benzene rings has its origin mostly in poorer π -bonding, deformation of the σ -framework is found to be responsible for the strain in the bowl-shaped benzene ring (Figure 2).

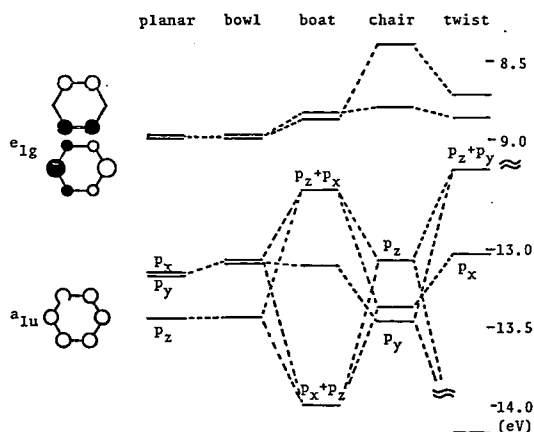


Figure 2. MO correlation diagrams of the higher occupied orbitals as the benzene ring deforms out-of-plane. Note that three p_z orbitals are not destabilized as we go from the planar to bowl shaped benzenes.

V—C Structural Studies by Means of NMR of Other Nuclei

NMR structural studies with the aid of nuclei other than routine ^1H , ^{13}C , ^{19}F and ^{31}P have been carried out. After optimizing the experimental conditions for the measurement on a Varian FT-80A spectrometer of samples with the natural abundance (0.037%) ^{17}O , we measured chemical shifts for more metal carbonyls and some hydropyrans and found a couple of interesting empirical rules which would be of use as a measure of the carbene reactivity and the anomeric effect, respectively. ^{35}Cl NMR studies on ion-pairing of electrolytes in mixed solvents have just started in collaboration with Professor Fujiyama's group.

V-C-1 ^{17}O NMR Chemical Shifts of Tungsten Carbonyl Carbene Complexes. An Independent Experimental Measure for the Moss Reactivity Parameter m_{CXY} of Carbene :CXY

Yuzo KAWADA and Hiizu IWAMURA

Recently Moss proposed with considerable success a unifying theory on the reactivities of electrophilic, ambiphilic and nucleophilic carbenes.¹ The essence of the theory is contained in parameter

m_{CXY} which increases as we go from electrophilic (<1) through ambiphilic (~ 1.5) to nucleophilic (>2) carbenes. The parameter is given experimentally by the least-square slope of $\log(k_i/k_{\text{isobutene}})_{\text{CXY}}$ vs. $\log(k_i/k_{\text{isobutene}})_{\text{CCl}_2}$ for the olefin triad $\text{Me}_2\text{C} = \text{CMe}_2$, $\text{Me}_2\text{C} = \text{CH}_2$ and *trans*- $\text{MeCH} = \text{CHMe}$ and is found to follow eq. 1 in which σ^+_R and σ_I are the Taft substituent constants. The experimental determination of the m_{CXY} parameters is limited up to $m_{\text{CF}_2} = 1.48$ and the method is operationally impossible to apply for carbenes with higher nucleophilicity.

$$m_{\text{CXY}} = -1.10 \sum_{\text{X,Y}} \sigma_{\text{R}}^+ + 0.53 \sum_{\text{X,Y}} \sigma_{\text{I}} - 0.31 \quad (1)$$

We have found that the ^{17}O NMR chemical shifts for the carbonyl group trans to the carbene ligand in $(\text{OC})_5\text{W}:\text{CXY}$ correlate nicely with the m_{CXY} parameter, providing an independent experimental measure for the latter constants of a wide variety of carbenes, especially of nucleophilic ones.

Reference

- 1) R. A. Moss, M. Fedorynski, and W.-C. Shieh, *J. Am. Chem. Soc.*, **101**, 4736 (1979).

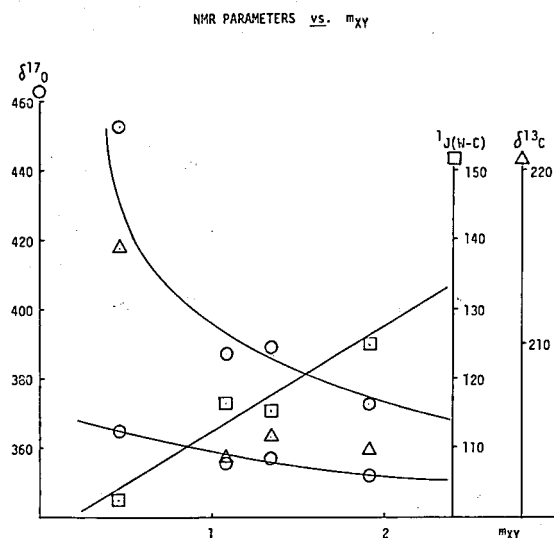


Figure 1. NMR parameters for $(\text{OC})_5\text{W}:\text{CXY}$ vs. the reactivity constants m_{CXY} .

V-C-2 The Anomeric Effect in 2-Alkoxytetrahydropyrans As Revealed by the ^{17}O NMR Chemical Shifts

Ronald D. MCKELVEY,¹⁾ Yuzo KAWADA, Tadashi SUGAWARA, and Hiizu IWAMURA

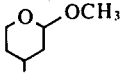
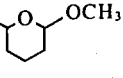
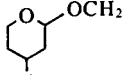
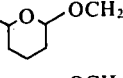
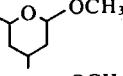
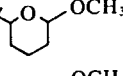
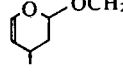
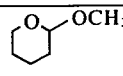
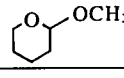
The anomeric effect is the preference of axial over equatorial C_1 electronegative substituents in pyranose rings. In view of the demand for a facile method in determining the pyranose ring conformations, we have examined the ^{17}O NMR chemical shifts for several pairs of 2-

alkoxytetrahydropyrans in toluene and found that both the ring and 2-alkoxy oxygens resonate at higher field in the axial 2-alkoxy than in the equatorial epimers (Table I). The axial conformation is considered to be stabilized by donation from the axial lone pair of the ring oxygen into the COR anti-bonding orbital. Increase of shielding of the ring oxygen with the stronger electron-withdrawal by the axial OR cannot be explained by increase in the mean inverse cube of the 2p electron radius $\langle r^{-3} \rangle_{\text{oxygen}}$ nor in the orbital terms $[Q_{\text{AA}} + \sum Q_{\text{AB}}]$ in the Karplus-Pople expression of the paramagnetic screening.² Increase in the effective excitation energy ΔE is concluded to be a dominant factor in the paramagnetic screening term.

References

- 1) IMS Invited Foreign Scholar 1980.
- 2) M. Karplus and J. A. Pople, *J. Chem. Phys.*, **38**, 2803 (1963).

Table I. ^{17}O NMR Chemical Shifts for 2-Alkoxytetrahydropyrans Referenced to Water (ppm)

	isomer	ring oxygen	alkoxy oxygen
	cis	48.8	31.8
	trans	38.5	24.6
	cis	73.7	33.1
	trans	59.5	23.3
	cis	50.6	62.1
	trans	78.5	43.8
	cis	81.0	60.4
	trans	67.1	55.0
	cis	74.1	25.8
	trans	59.9	23.9
	cis	74.9	33.9
	trans	52.2	23.1
	cis	101.5	62.2
	trans	105.3	62.4
		42.3	23.1
		44.0	56.1

V-D Spin-state Variations among Nickel(II) Complexes Containing Macrocyclic Ligands

We are continuing studies on spin-state variations among nickel(II) complexes containing macrocyclic ligands. Nickel(II) ion and tetradentate macrocyclic ligands (L) form a number of complexes of the type NiLX_2 , X = anion or solvent, which either are four coordinate diamagnetic complexes or six coordinate complexes having a triplet ground state. Changes from paramagnetism to diamagnetism or *vice versa* are often brought about by apparently trivial changes in the macrocyclic ligands, anions, and/or solvents. In some cases, the paramagnetic and diamagnetic forms of the same compound can be isolated. The behaviors of such systems in solid and solution states have been investigated.

V-D-1 The Role Played by Water in Spin-state Variations among Nickel(II) Halide Complexes Containing 7R(S),14S(R)- 5,5,7-12,12,14-Hexamethyl-1,4,8,11-tetraazacyclotetradecane

Tasuku ITO and Koshiro TORIUMI

[Acta Cryst., B36 (1980) in press]

Nickel(II) halide (Cl^- , Br^- , and I^-) and the title macrocyclic ligand form low-spin four coordinate complexes having a singlet ground state, $[\text{NiL}]\text{X}_2 \cdot 2\text{X}_2\text{O}$, and high-spin six coordinate complexes having a triplet ground state, $[\text{NiX}_2\text{L}]$. These complexes are interconvertible. In the solid states, the low-spin complexes are dihydrates, whereas the high-spin complexes are anhydrides. The occurrence of the spin state variation is invariably associated with the presence or the absence of water. Of particular interest is the fact that water molecules are not involved in coordination, although water has considerable coordinating ability for a nickel(II) ion. The crystal and molecular structures of $[\text{NiCl}_2\text{L}] \cdot 2\text{CHCl}_3$, $[\text{NiL}]\text{Cl}_2 \cdot 2\text{H}_2\text{O}$, $[\text{NiL}]\text{Br}_2 \cdot 2\text{H}_2\text{O}$ (*P* $\bar{1}$ and *Pcab* forms), and $[\text{NiF}_2\text{L}] \cdot 5\text{H}_2\text{O}$ have been determined by single crystal X-ray diffraction. Figure 1 shows the dispositions of water and halide ion in the vicinity of the nickel(II) ion which lies on a center of symmetry in each compound. In the crystals of $[\text{NiL}]\text{Cl}_2 \cdot 2\text{H}_2\text{O}$ and $[\text{NiL}]\text{Br}_2 \cdot 2\text{H}_2\text{O}$, water mole-

cules and halide ions are located above the hydrogen atoms of N-H groups and involved in hydrogen bonds. The water and the halide ion are further hydrogen-bonded to each other, forming "hydrogen-bonded chelate ring" of the type shown in 1. The formation of such specific hydrogen-bonds should be responsible for the failure of water in coordination and the spin-state variations.

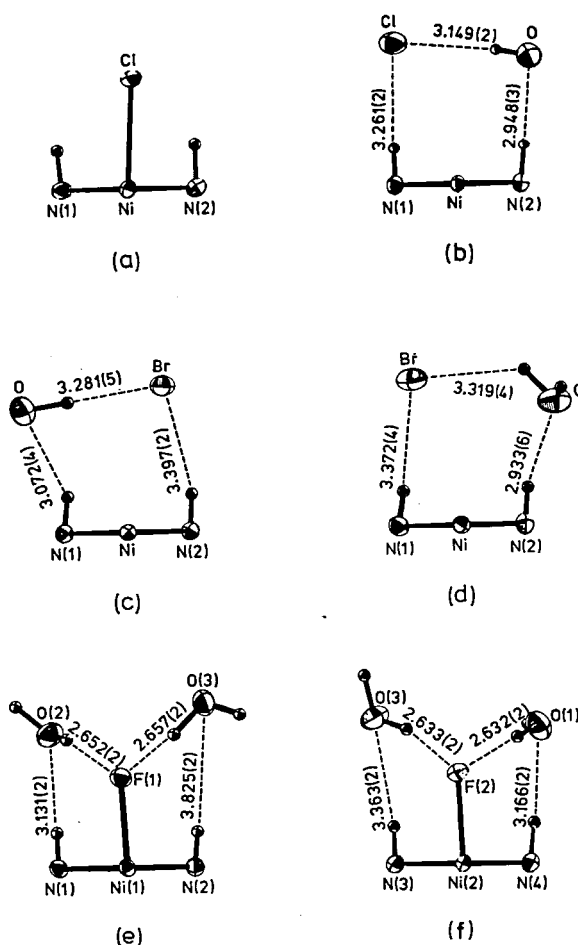
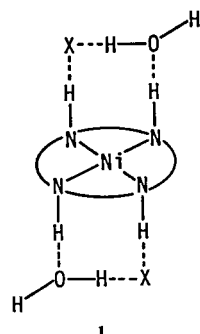


Figure 1. Dispositions of water and halide ion in the vicinity of nickel(II), and hydrogen-bond distances (Å): (a) $[\text{NiCl}_2\text{L}] \cdot 2\text{CHCl}_3$; (b) $[\text{NiL}]\text{Cl}_2 \cdot 2\text{H}_2\text{O}$; (c) $[\text{NiL}]\text{Br}_2 \cdot 2\text{H}_2\text{O}$ (*P* $\bar{1}$ form); (d) $[\text{NiL}]\text{Br}_2 \cdot 2\text{H}_2\text{O}$ (*Pcab* form); (e) and (f) $[\text{NiF}_2\text{L}] \cdot 5\text{H}_2\text{O}$.

V-D-2 Dehydration Associated with High-spin to Low-spin Conversion of 5,5,7,12,12,14-Hexamethyl- 1, 4, 8, 11 - tetraazacyclotetra - decanenickel(II) Halide Dihydrate

Tasuku ITO, Yukie TSUTSUMI,* Yukio HIRATSUKA,* Katsura MOCHIZUKI,* and Masatoshi FUJIMOTO* (* Hokkaido Univ.)

[Bull. Chem. Soc. Jpn., in press]

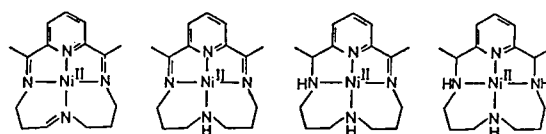
The title compounds, orange, low-spin four-coordinate complexes, $[\text{NiL}]\text{X}_2 \cdot 2\text{H}_2\text{O}$ ($\text{X} = \text{Cl}^-$, Br^- , I^- for *meso*-L and $\text{X} = \text{Cl}^-$, Br^- for *rac*-L) were found to be converted, upon dehydration by heating in the solid state, to violet, high-spin six-coordinate complexes, $[\text{NiX}_2\text{L}]$. The enthalpies of the dehydration reactions were determined by Differential Scanning Calorimetry. The enthalpy values are significantly larger than those usually found for dehydration reactions of coordination compound hydrates and can be compared to those for dehydration reactions of many simple inorganic hydrates, even though the present complexes bear large organic ligands. In the crystals of $[\text{Ni}(\text{meso-L})]\text{X}_2 \cdot 2\text{H}_2\text{O}$ ($\text{X} = \text{Cl}^-$ and Br^-), water molecules are disposed above the hydrogen atoms of N-H groups and are involved in strong hydrogen-bonds, forming "hydrogen-bonded chelate rings" (V-D-1). Waters of crystallization are not involved in coordination, even though water has high coordinating ability for Ni^{2+} . These situations are reflected in the enthalpy values found in this study.

V-D-3 Spin-state Equilibria of the Nickel(II) Complexes of 2,12-Dimethyl-3,7,11,17-tetraazabicyclo[11.3.1]heptadeca- 1(17),2,11,13,15-pentaene Analogs in Water

Katsura MOCHIZUKI,* Masatoshi FUJIMOTO,* Haruko ITO** and Tasaku ITO (* Hokkaido Univ., ** Nagoya Univ.)

[Bull. Chem. Soc. Jpn., 53, 2535(1980)]

Spin-state equilibria between a singlet low-spin and a triplet high-spin species of the title complexes (Figure 1) in water were investigated by means of electronic spectra. The equilibrium constants and the thermodynamic parameters, ΔH and ΔS , were evaluated from detailed analyses of the temperature dependence of the electronic spectra. The values are shown in Table I. The electronic spectra of the singlet and the triplet species were determined from the same analyses.



[Ni(L-2H)]²⁺ [Ni(L)]²⁺ [Ni(L+2H)]²⁺ [Ni(L+4H)]²⁺

Figure 1. Structures of studied complexes

Table I. Equilibrium Constants^a and Thermodynamic Parameters

	<i>K</i>	<i>T</i> /K	$\frac{\Delta H}{10^4 \text{ J mol}^{-1}}$	$\frac{\Delta S}{\text{J mol}^{-1} \text{ K}^{-1}}$
$[\text{Ni}(\text{L}+4\text{H})](\text{ClO}_4)_2^b$	0.31 ₂	299.4	2.02	77.0
$[\text{Ni}(\text{L}+4\text{H})](\text{ClO}_4)_2^c$	0.45 ₉	299.4	2.04	74.9
$[\text{Ni}(\text{L}+2\text{H})](\text{ClO}_4)_2$	0.55 ₆	299.3	2.16	77.0
$[\text{Ni}(\text{L})](\text{ClO}_4)_2$	3.99 ₆	299.3	2.12	59.4
$[\text{Ni}(\text{L}-2\text{H})](\text{ClO}_4)_2$	0.59 ₃	299.3	2.32	82.0

a $K = [\text{triplet}]/[\text{singlet}]$. b α -C-*meso* isomer. c C-*rac* isomer.

V—E Structure Determination of New or Chemically Interesting Coordination Compounds by X-ray Diffractometry

V-E-1 Crystal and Molecular Structure of a Silver(II) Complex with a Macrocyclic Ligand

Tasaku ITO, Koshiro TORIUMI, and Haruko ITO (Nagoya Univ.)

One dominant characteristic of macrocyclic ligands is the stability which they impart to the

resulting metal complexes. In some cases, compounds of metal ions in unusual oxidation states have been obtained. One example of stabilization of macrocyclic complexes with unusual oxidation states is found with silver(II). The crystal and molecular structure of 1,4,8,11-tetraazacyclotetradecanesilver(II) perchlorate has been studied by single crystal X-ray analysis. The

complex crystallizes in the triclinic space group $P\bar{1}$ with cell dimensions $a = 8.647(2)$, $b = 8.794(2)$, $c = 8.056(1)$ Å, $\alpha = 67.26(1)$, $\beta = 117.53(1)$, $\gamma = 122.92(1)^\circ$, and $Z = 1$. The structure was solved to give an $R = 0.026$ for 3851 reflexions with $|Fo| > 3\sigma(|Fo|)$. Figure 1 shows a perspective drawing of the structure. The silver sits on a center of symmetry and is surrounded by a square-planar array of nitrogen atoms at an average distance of 2.158(2) Å. Weak axial interactions with perchlorate oxygens result in distorted octahedral coordination in which Ag-O is 2.788(2) Å. The Ag-N distances are significantly larger than a "natural radius" of a hole of the macrocyclic ligand. The silver is accommodated very tightly in the hole.

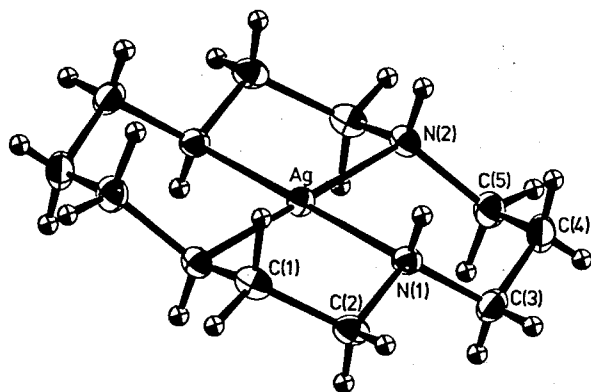


Figure 1.

V-E-2 Optical Resolution of 7*R*(*S*),14*R*(*S*)-5,5,7,12,12,14 - Hexamethyl - 1,4,8,11 - tetraazacyclotetradecanenickel(II) Ion and the Absolute Configuration of the (+)₅₈₉-Isomer

Haruko ITO (Nagoya Univ.), Junnosuke FUJITA (Nagoya Univ. and IMS), Koshiro TORIUMI, and Tasuku ITO

Several unsuccessful attempts have been reported on the optical resolution of the title complex, $[\text{NiL}]^{2+}$. In this study, we have succeeded in the optical resolution, using $[\text{NiL}]\text{Br}_2$ and sodium *d*-tartrate. The CD spectra of four- and six-coordinate complexes containing the (+)₅₈₉- or (−)₅₈₉- isomers have been studied. In order to determine the absolute configuration of (+)₅₈₉- $[\text{NiL}]^{2+}$, a single crystal X-ray analysis has been carried out on $[\text{Ni}_2\text{L}_2(d\text{-tart})(\text{H}_2\text{O})](\text{ClO}_4)_2 \cdot 2\text{H}_2\text{O}$, which is a less-soluble diastereoisomer obtained in a process of the optical resolution. Crystal data are: monoclinic, $P2_1$, $a = 17.568(3)$, $b = 11.482(2)$, $c = 13.272(2)$ Å, $\beta = 102.59(1)^\circ$ and $Z = 4$. The final R -index was 0.046. Figure 1 shows a perspective view of the diastereomer. The resolving agent, *d*-tartrate, is coordinated to two nickel(II) ions, giving a dimer of $[\text{NiL}]^{2+}$. The absolute configurations of the asymmetric carbon atoms are all *S*, whereas those of the asymmetric nitrogen atoms are all *R*.

V-E-3 The Crystal and Molecular Structure of *meso*-1,4,7,10,13,16-Hexaazacyclooctadecanecobalt(III) Chloride

Yuzo YOSHIKAWA*, Koshiro TORIUMI, Tasuku ITO, and Hideo YAMATERA* (*Nagoya Univ.)

The title compound is a first example of a *meso*-isomer of an inert complex with a cyclic hexadentate ligand. The crystal and molecular structure of the compound was determined by single crystal X-ray diffractometry. The crystals are rhombohedral with space group $R\bar{3}$, $a = 9.298(1)$ and $c = 16.851(2)$ Å, and $Z = 3$, in hexagonal setting. The structure was refined by block-

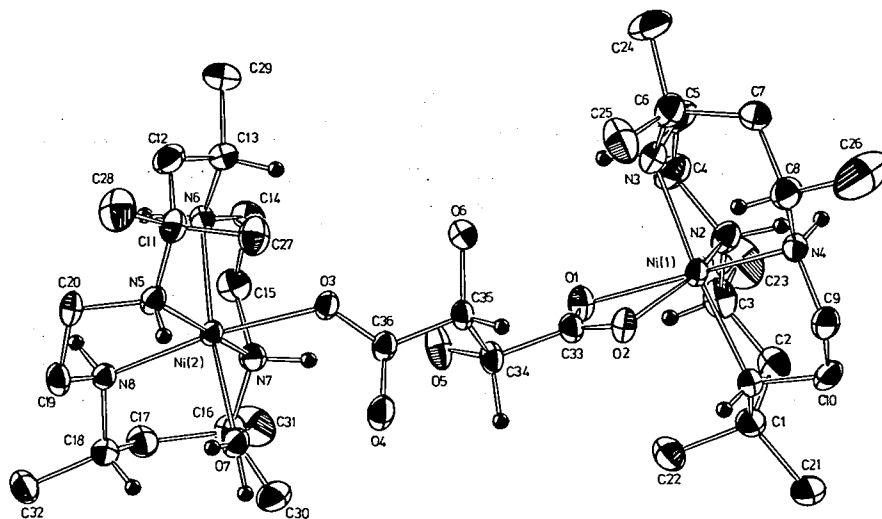


Figure 1.

diagonal least squares method to give a final R value of 0.021 for 952 independent reflexions. A perspective drawing of the complex cation is shown in Figure 1. The complex ion has S_6 symmetry. The results of conformational analysis for the complex ion were well compared to the structure observed in the crystal.

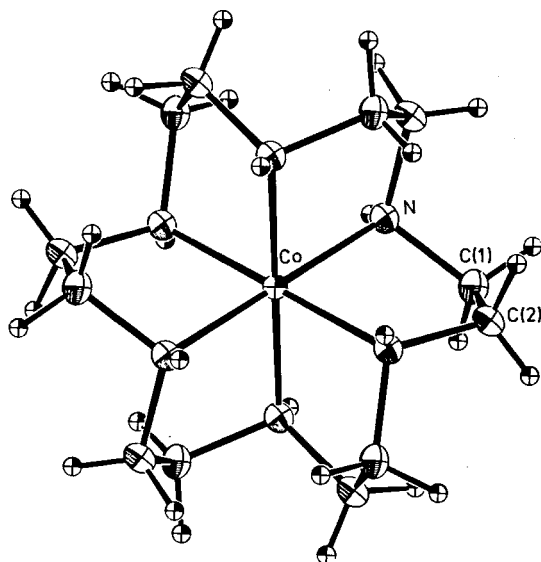


Figure 1.

V-E-4 The Crystal and Molecular Structure of *trans*-Dichloro-*bis*-(+)-*S,S-trans*-1,2-diaminocyclopentane)cobalt(III) Chloride Hydrogen Chloride Dihydrate, *trans*-[CoCl₂(+cptn)₂]Cl·HCl·2H₂O

Masafumi GOTO,* Kyoko OHTA,* Koshiro TORIUMI and Tasuku ITO (* Nagoya City Univ.)

Crystals of the title compound are orthorhombic, space group $P2_22_1$, $a = 9.571(2)$, $b = 24.541(3)$, $c = 8.412(2)$ Å and $Z = 4$. The crystal structure has been refined to give an R value of 0.044 for 2666 observed reflexions collected by X-ray diffractometry. As shown in Figure 1, the complex cation has approximately D_2 symmetry. The cobalt atom is surrounded by the four nitrogen atoms of two +cptn ligands in an approximate plane with the average Co-N distance of 1.979(3) Å and by two chlorine atoms occupying axial positions with an average separation from cobalt of 2.257(2) Å. The previously reported anomalous solution CD behavior of the title complex arises from the strain present at the bridgehead carbons of the +cptn chelate rings.

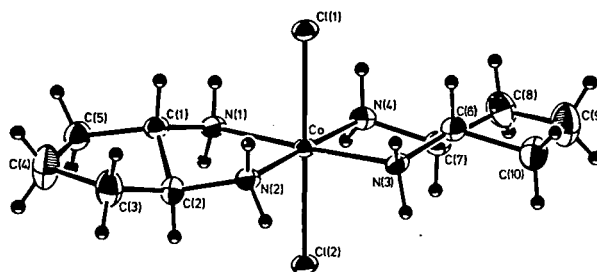


Figure 1.

V—F Preparation and Stereochemistry of Metal Complexes Containing Aminophosphine Chelate Ligands

V-F-1 Preparation and Circular Dichroism of Dichloro-(*S*)-2-(butylphenyl-phosphinomethyl)pyrrolidine-palladium(II) ([PdCl₂L]) and Its Related Complexes, and the Absolute Configuration of [PdCl₂L] Determined by X-Ray Analysis

Isamu KINOSHITA(Nagoya Univ.), Kazuo KASHIWABARA(Nagoya Univ.), Junnosuke FUJITA(Nagoya Univ. and IMS), Takashi YAMANE(Nagoya Univ.), Hitoshi UKAI(Nagoya Univ.), and Tamaichi ASHIDA(Nagoya Univ.)

[Bull. Chem. Soc. Jpn., 52, 1413(1979)]

(*S*)-2-(Butylphenylphosphinomethyl)pyrrolidine (L) was prepared from (*S*)-proline via four main reaction steps. A pair of diastereomers of the PdCl₂L complex, the isomerism of which comes from chiral configuration of the phosphorus atom, crystallized in different forms (needle and blocks), which were separated by hand picking. The molecular structure and absolute configuration of one (block) of the dichloro complexes was determined by X-ray analysis. Crystallographic data are; $P2_12_12_1$, $Z = 4$, $a = 13.576(4)$, $b = 16.351(3)$, $c = 3.041(2)$ Å, and $R = 7.8\%$ for 1659 reflections. The Pd atom has a distorted square planar coordination of four donor atoms. The Pd-Cl bond distance *trans* to Pd-P, 2.367 Å, is longer

than that trans to Pd-N, 2.296 Å. The absolute configuration of the coordinated phosphorus atom was determined to be *R* by assuming *S* configuration for the asymmetric carbon atom of the aminophosphine. The circular dichroism spectra of the diastereomers and their related complexes were compared with one another.

V-F-2 Preparation and Resolution of the *fac*-*Tris*(2-aminoethyl-dimethylphosphine)cobalt(III) Complex and the Absolute Configuration of Its (+)₅₈₉-Isomer Determined by X-Ray Analysis

Isamu KINOSHITA(Osaka City Univ.), Kazuo KASHIWABARA(Nagoya Univ.), Junnosuke FUJITA(Nagoya Univ. and IMS), Keiji MATSUMOTO(Osaka City Univ.), and Shun'ichiro OOI(Osaka City Univ.)

A new lemon-yellow *fac*-[Co{NH₂CH₂CH₂P(CH₃)₂}₃]Br₃·3H₂O was prepared by the reaction of *cis*-[CoCl₂(en)₂]Cl (en = ethylenediamine) with the phosphine ligand in *N,N*-dimethylformamide under nitrogen atmosphere, and resolved into enantiomers by SP-Sephadex column chromatography using 0.2 mol/dm³ sodium (+)₅₈₉-tartratoantimonate(III) as an eluent. The crystal structure of the (+)₅₈₉-isomer was determined by X-ray diffraction. The crystal data are; orthorhombic, *P*2₁2₁2₁, *a* = 26.501(8), *b* = 9.573(4), *c* = 10.081(5) Å, *Z* = 4 *D*_c = 1.73, *D*_m = 1.73 gcm⁻³. The three phosphorus atoms are arranged in the facial manner and the absolute configuration is Δ. The chelate ring are of the λ-gauche conformation and hence the complex ion can be designated as the *lel*₃ structure, although the NCCP torsion angles (44.3~53.3°) are smaller than those of 1,2-diamine chelate complexes of cobalt(III) (~55°). The

complex shows two absorption bands at 23700 cm⁻¹ (ε = 474) and 30200 cm⁻¹ (ε = 229) assignable to the first and the second absorption bands, respectively. The energy difference between these two bands is considerably smaller than that of [Co(en)₃]³⁺.

V-F-3 Optical Resolution of 2-Aminoethylbutylphenylphosphine and the Absolute Configuration Assigned on the Basis of Circular Dichroism Spectra of Its Palladium(II) Complexes

Isamu KINOSHITA(Osaka City Univ.), Kazuo KASHIWABARA(Nagoya Univ.), and Junnosuke FUJITA(Nagoya Univ. and IMS)

[Bull. Chem. Soc. Jpn., 53, in press]

2-Aminoethylbutylphenylphosphine was resolved by preparing a pair of diastereomers, (a) and (b) of the (+)₅₈₉-di-μ-chlorobis-[(*S*)-*N,N*-dimethyl-α-phenylethylamine-2C,N]dipalladium(II) complex. The diastereomers were easily separated by solubility difference in benzene. The optically active free aminophosphine can be obtained from (a) and (b) by treating with sodium cyanide in water. The absolute configuration of the chiral phosphorus atom of the ligand can be assigned by comparing the circular dichroism spectrum of its dichloro palladium(II) complex with those of a pair of diastereomers of [PdCl₂{(*S*(C))-2-(butylphenylphosphinomethyl)pyrrolidine}] of known absolute configuration.¹⁾ The aminophosphine obtained from the less soluble diastereomer, (a) is the (*R*)-configuration.

Reference

- 1) I. Kinoshita, K. Kashiwabara, J. Fujita, T. Yamane, H. Ukai and T. Ashida, Bull. Chem. Soc. Jpn., 52, 1413(1979).

V—G Chiral Recognition in Catalytic Hydrogenation of α-Acylaminoacrylic Acids by Cationic Rhodium(I) Complexes of Chiral Aminophosphines Derived from (*R,R*)-1,2-Cyclohexanediamine or (*R*)-1,2-Propanediamine

Kazuo KASHIWABARA(Nagoya Univ.), Kazuhiro HANAKI(Nagoya Univ.), and Junnosuke FUJITA(Nagoya Univ. and IMS)

[Bull. Chem. Soc. Jpn., 53, 2275(1980)]

Four chiral diphosphines, (*R,R*)-1,2-bis[*N*-methyl(diphenylphosphino)amino]cyclohexane, (*R,R*)-1,2-bis[(diphenylphosphino)amino]cyclohexane, (*R*)-1,2-bis[(diphenylphosphino)amino]propane were prepared from the corresponding optically active diamines. The cationic 1,5-cyclooctadiene rhodium(I) complexes with these diphosphines act as effective homogeneous catalysts for the effective hydrogenation of α -acylaminoacrylic acids. The optical yields and the absolute configuration of the products depend on the kind of diphosphine ligands. The (*R,R*)-1,2-bis[*N*-methyl(diphenylphosphino)amino]cyclohexane complex catalyst yields *N*-benzoyl-(*S*)-leucine, *N*-benzoyl-(*S*)-phenylalanine, and *N*-acetyl-(*S*)-phenylalanine in 94, 92, and 89% e.e., respectively. The other three catalysts are less effective (6~74% e.e.). The aminophosphine complexes with methyl groups on the nitrogen atoms always give (*S*)-amino acids, those with no methyl group (*R*)-amino acids. Such a difference in the chiral recognition was discussed on the basis of circular dichroism spectra and Dreiding molecular models of the rhodium(I) complexes.

RESEARCH ACTIVITIES VI

COMPUTER CENTER

VI—A Theoretical Investigations of Metalloporphyrins and Charge-Transfer Complexes by the Ab Initio SCF MO Method

Metalloporphyrins and charge-transfer complexes are interesting polyatomic systems because of their complicated electronic structure and because of their catalytic function. Heme, chlorophyll, and flavin are prominently important as an active center of energy conversion processes in biological systems. In this project the electronic structure and the fundamental functions are studied for several complexes by performing ab initio MO computations.

VI-A-1 Potential Energy Surfaces for Out-of-Plane Movement of Fe Ion in Fe-Porphine

Shigeru OBARA and Hiroshi KASHIWAGI

In the deoxygenation of hemoglobin Fe cation goes out of porphyrin plane together with the change from low-spin to high-spin. Study of the potential energy surface for the out-of-plane movement of Fe in Fe-porphine is of fundamental importance to elucidate catalytic functions of hemoproteins.

We have carried out ab initio LCAO SCF MO calculations of Fe-porphine with an extended basis set consisting of 184 CGTO's by the use of the JAMOL3 program. The distance between Fe and the porphine plane is changed from 0.0 to 1.2 a.u. Calculated potential energy surfaces are found to be classified into two groups in their shape. In typical low- and intermediate-spin states, the minimum point is at the porphine plane. On the other hand, in high-spin states the surface is almost flat from 0.0 to 0.4 Å. In high-spin states Fe ion is easy to move. The position of Fe would be determined by the interaction between an axial ligand and Fe or porphyrin as discussed by Olafson et al.¹⁾ In order to elucidate the origin of the difference in shape, potential energy surfaces of 1E_g and 3E_g are also calculated, which have the same configuration $(d_{xy})^2 (d_{\pi})^3 (d_{x^2-y^2})^1$. Their shape resembles that of the high-spin states, although the configuration of 1E_g and 3E_g is similar to that of the lowest 3E_g , $(d_{xy})^2 (d_{\pi})^3 (d_{z^2})^1$. This result leads to a conclusion that the shape of the potential energy surface depends on the electron occupation of the $d_{x^2-y^2}$ orbital but does not on the spin multiplicity itself.

Reference

- 1) B. D. Olafson and W. A. Goddard III, *Proc. Natl. Acad. Sci. USA*, 74, 1315(1977).

VI-A-2 Theoretical Analysis of Mössbauer Spectra of Fe-Porphines

Shigeru OBARA and Hiroshi KASHIWAGI

Many Mössbauer experiments have been performed on hemes. The observed isomer shift (IS) and quadrupole splitting (QS) have a strong relation to the oxidation and spin state of heme.¹⁾ Theoretical analysis of Mössbauer spectra is useful to elucidate the electronic structure of heme.

The ground state of Fe-porphyrins without axial ligands is still controversial. Their ground state has been considered as $^3A_{2g} (d_{xy})^2 (d_{\pi})^2 (d_{z^2})^2$ or $^3E_g A (d_{xy})^2 (d_{\pi})^3 (d_{z^2})^1$ from various experiments. We have tried to confirm the assignment by a theoretical analysis of Mössbauer spectra.

Ab initio LCAO SCF MO calculations on FeP(Py)CO, FeP, and FeP(Py) are carried out with basis sets consisting of 241, 184, and 223 CGTO's, respectively, by the use of the JAMOL3 program. The total energy and the observable quantities of Mössbauer experiment are calculated. In low- and high-spin complexes, the sign and direction of the principal component of electric field gradient (EFG) tensor and the asymmetry parameter η are in good agreement with experiments. We determined three empirical parameters in the formulas of IS and QS by using observed IS and QS of the low- and high-spin complexes. The lowest triplet state of FeP is $^3A_{2g}$ and the second lowest is $^3E_g A$. Calculated QS values of both states do not agree with the experimental.²⁾ The energy of the lowest 3E_g state comes close to that of $^3A_{2g}$ by performing a

ligand field CI. The ${}^3E_g B (d_{xy})^1(d_{\pi})^3(d_{z^2})^2$ function mixes with the ${}^3E_g A$ by about 10% of weight. The change of QS is examined for the mixing of ${}^3E_g A$ and ${}^3E_g B$ by using the SCF wavefunctions. At 20% mixing of ${}^3E_g B$, the calculated QS coincides with the observed. The calculated sign, direction, and η of EFG also agree with the experimental data.²⁾

References

- 1) Y. Maeda, *J. de Phys. Colloque C2*, supplement, 514(1979).
- 2) J. P. Collman et al., *J. Am. Chem. Soc.* **97**, 2676(1975).

VI-A-3 Ab Initio MO Study of Charge Transfer Complexes, Benzene + TCNE and Naphthalene + TCNE

Yoshitaka WATANABE,* Kichisuke NISHIMOTO,* and Hiroshi KASHIWAGI (* Osaka City Univ.)

It has been pointed out that the ab initio MO method based on STO-3G minimal basis set is not appropriate for the calculations of charge transfer complexes. In order to investigate the charge transfer interaction, one must use an extended basis set, such as the 4-31G basis set. However, the ab

initio MO calculation of large supermolecules, for example, flavin + tryptophan, is very laborious. The charge transfer interaction between aromatic systems mainly comes from the π -electron interaction. Therefore, one approach is to use a split basis set for π -orbital and STO-3G for σ -one's. In order to examine whether this approach does work or not, we calculate the systems of benzene + TCNE and naphthalene + TCNE which have been studied experimentally in detail. By the use of JAMOL3 we carried out MO calculations based on semiorthogonalized orbitals with the following basis sets; (1) STO-3G (2) STO-3G π -split (3) 4-31G. Experimental geometries are used for benzene, naphthalene and TCNE. The geometry of supermolecule is shown in Figure 1. Each counter molecule is assumed to be parallel to each other with intermolecular distance of 3.298 Å. As seen from Table I, STO-3G π -split gives a comparable result with the 4-31G.

As a conclusion, STO-3G π -split is as suitable as the 4-31G for the ab initio MO calculation of the charge transfer complex. With this basis set we are carrying out the calculations of the stacking interaction between flavin and tryptophan, flavin and tyrosine, which play an important role in the oxidation-reduction reaction of biochemical systems.

Table I. (1) Benzene + TCNE and (2) naphthalene + TCNE complexes. (Intermolecular distance $R = 3.298$ Å)

Basis set	geometry		threshold ^a		binding energy (Kcal/mole)	dipole moment (Debye)	gross charge on TCNE
			δ_1^b	δ_2^b			
(1)	STO-3G	C_{2v} A form	1×10^{-4}	1×10^{-8}	0.027	0.1987	0.006
	STO-3G π -split	C_{2v} A form	1×10^{-4}	1×10^{-8}	-2.237	0.4288	0.018
		C_{2v} B form	1×10^{-4}	1×10^{-8}	-2.176	0.4292	0.018
		C_s C form	1×10^{-4}	1×10^{-8}	-0.616	0.2472	0.008
		C_{2v} A form	1×10^{-3}	1×10^{-6}	3.345	0.4366	0.018
	4-31G	C_{2v} A form	1×10^{-4}	1×10^{-8}	-2.617	0.7995	0.028
	Experiment				-6.6 ^d	-3.34 ^e	
(2)	STO-3G π -split	C_s	1×10^{-3}	1×10^{-6}	-4.228	0.7753	0.026
	Experiment				-7.67 ^d	-4.06 ^e	1.28 ^e

^a Y. Osanai and H. Kashiwagi, *Int. J. Quantum Chem.* **17**, 1031(1980).

^b a threshold for $|S^{ij}|$.

^c a threshold for $(ij|ij)$.

^d In vapor.

^e In solution (CCl₄).

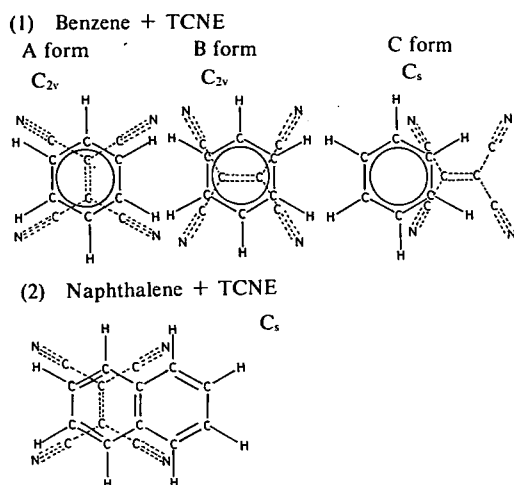


Figure 1. The geometries of benzene + TCNE and naphthalene + TCNE complexes

VI-A-4 Ab Initio SCF Calculation of Chlorophyll

Unpei NAGASHIMA (*IMS Graduate Student 1980- from Hokkaido Univ.*) and Hiroshi KASHIWAGI

In the primary process of the photosynthesis in green plants, chlorophyll functions in two important capacities, i) as an antenna chlorophyll which absorbs the light energy, and ii) as a reaction center chlorophyll which traps energy transferred from the antenna chlorophyll and induces electron transfer. It has been pointed out that a reaction center consists of a chlorophyll dimer. The structure of the dimer is still controversial. Shipman's model¹⁾ (Figure 1) is the most reasonable among several models from the experimental viewpoint, since the model well fits to the facts that an unpaired electron is spread equally over two chlorophyll molecules in the dimer cation, and that the carbonyl group of the chlorophyll ring is related to a hydrogen bond.

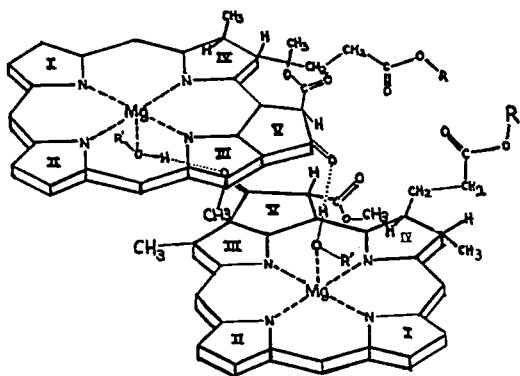


Figure 1. The Shipman's model for a chlorophyll dimer.

Our purpose of this investigation is to inspect the electronic structure of the reaction center and the adequacy of the Shipman's model from the viewpoint of molecular orbital theory. SCF calculations of the ground and ionic state of chlorophyll monomer have been carried out with a basis set of single zeta quality by using the JAMOL3 program.

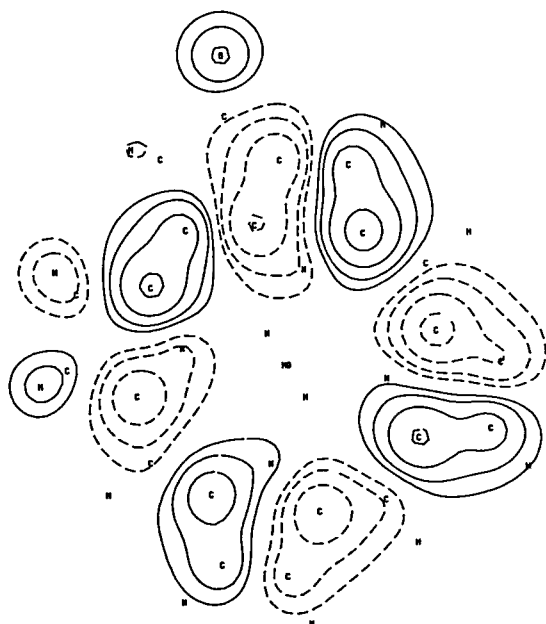


Figure 2. Contour map for the highest occupied molecular orbital (HOMO) of chlorophyll monomer. Contours are constructed for a plane 1.2 a.u. above the molecular plane.

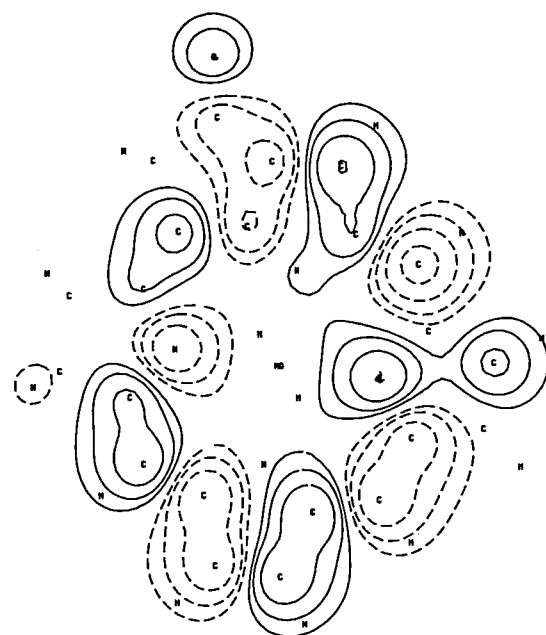


Figure 3. Contour map for the lowest unoccupied molecular orbital (LUMO) of chlorophyll monomer. Contours are constructed for a plane 1.2 a.u. above the molecular plane.

The highest occupied (HOMO) and the lowest unoccupied molecular orbital (LUMO) of the monomer are shown in Figure 2 and 3, respectively. When two molecules are piling up on each other as Figure 1, the HOMO and LUMO overlap well with each other from the phase relation in the region of rings III and V. This fact suggests that the model structure is stabilized by the π - π interaction

between two molecules. The phase relation between HOMO's of two chlorophylls is essentially same as the HOMO-LUMO relation in that region, which contributes to the stabilization of the dimer cation.

Reference

- 1) L. L. Shipman, T. M. Cotton, J. R. Norris and J. J. Katz, *Proc. Natl. Acad. Sci. USA.*, **73**, 1791(1976).

VI—B Implementation of On-Line QCLDB System

Masahumi TOGASHI (*Hokkaido Univ.*), Yoshihiro OSAMURA (*Osaka city Univ.*)
 Shinichi YAMABE (*Nara Univ. of Education*), Fumihiko HIROTA (*Shizuoka Univ.*)
 Haruo HOSOYA (*Ochanomizu Univ.*), Suehiro IWATA (*Institute of Physical
 and Chemical Research*), Shigeru OBARA, Hiroshi KASHIWAGI, Keiji MOROKUMA,
 Kiyoshi TANAKA (*Hokkaido Univ.*), and Kimio OHNO (*Hokkaido Univ.*)

The quantum chemistry literature data base (QCLDB) contains literatures concerning ab initio computations of atomic and molecular electronic structures. Approximately 2000 literatures published in January 1977-December 1979 have been collected from nineteen internationally well-known core journals. The printout service of QCLDB has been available over a year at the IMS Computer Center and at the Hokkaido University Computing Center.

Recently an on-line QCLDB system has been implemented on the HITAC M-200H computers. The system is set up on the basis of the data base management system ORION of Hitachi. In the on-line QCLDB compounds, journals, and authors can be used as keywords to search for literatures on a TSS-terminal.

LOW TEMPERATURE CENTER

VI—C A Cryostat for AC Magnetic Susceptibility Measurements

Kenichi IMAEDA, Toshiaki ENOKI, and Hiroo INOKUCHI

The feature of AC magnetic susceptibility measurement method is to be able to measure both the real part χ' and the imaginary part χ'' of magnetic susceptibility simultaneously without an external magnetic field. We can get informations about superconducting transitions and cooperative phenomena of magnetic moments etc. from AC magnetic susceptibility measurements. A schematic view of our cryostat is given in Figure 1. It has a variable temperature sample chamber with heater. The measurable temperature region is from about 1.3K to 200K. Three sample holders with a standard sample, an unknown sample and nothing are suspended with silk threads. They rotate by revolving a turntable and one of them is always in

the center of the cryostat where we can measure. The search coil system consists of 17696 turns primary one and 6956 turns secondary one. A half of the secondary coil is wound in the opposite sense to the other to cancel an induced electromotive force in the absence of the sample. We are planning to measure the magnetic property of violathrone-B which is paramagnetic because of the free radical resulting from detaching a hydrogen atom from a peripheral carbon of the tetrahedral type of bonding.¹⁾

Reference

- 1) T. Maekawa, *Bull. Chem. Soc. Japan*, **42**, 2631(1969).

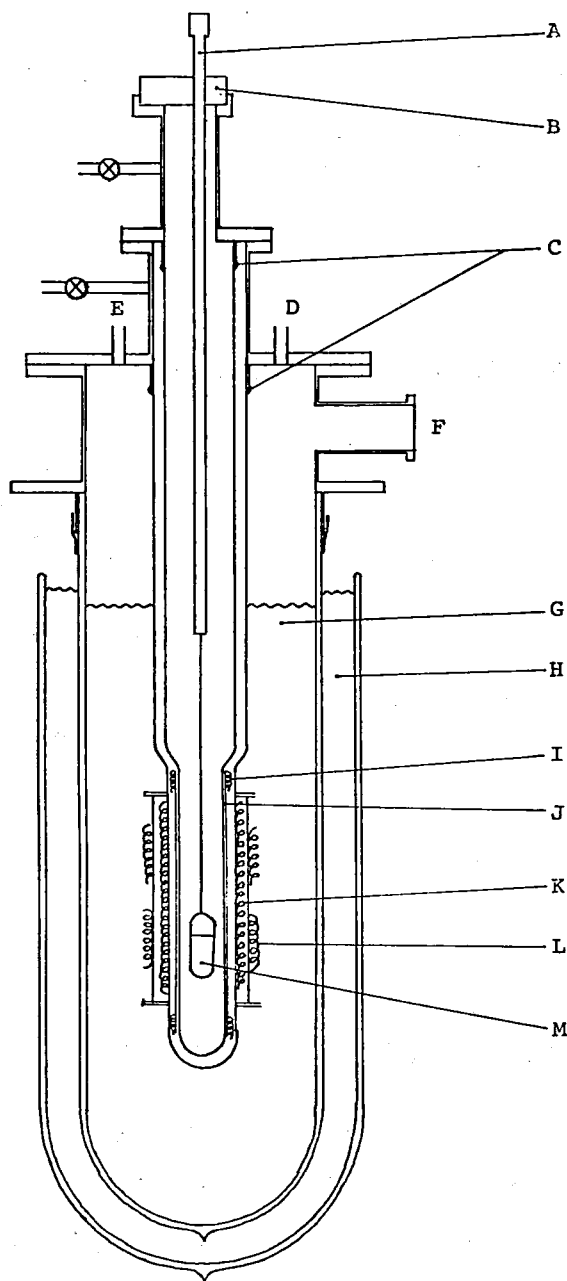


Figure 1. Schematic view of a cryostat. A-adjusting rod for the position of sample, B-turntable, C-cover seal, D-liq. He inlet, E-He gas outlet, F-pumping port, G-liq. He, H-liq. N₂, I-heatr, J-

copper pipe, K-primary coil, L-secondary coil, M-sample holder.

VI—D Solid State Properties of Complexes between Polycyclic Aromatic Hydrocarbons and Alkali-metals

VI-D-1 The Solid State Properties of Triphenylene-Potassium Complexes in Hydrogen Atmosphere

Toshiaki ENOKI and Hiroo INOKUCHI

The electrical resistivity and electron paramagnetic resonance are investigated for two

triphenylene-potassium complexes with different compositions, $\text{TpK}_{1.46}$ and $\text{TpK}_{0.87}$, in hydrogen atmosphere. $\text{TpK}_{1.46}$ shows a two stage absorption process of hydrogen, consistent with the hydrogen-deuterium exchange reaction previously presented.¹⁾ At the first stage, we find the enhancement of the electrical conductivity and the spin concentration, that is suggested hydrogen molecules are

dissociated into atoms in the complex crystal. We consider the dissociated hydrogen atoms react with the complex into hydride at the second stage, that causes to lower the conductivity and the spin concentration. In the case of $\text{TpK}_{0.87}$, we have a one stage absorption process. The introduction of hydrogen does not cause so much enhancement of the conductivity, while the spin concentration gets lowered in all time course of the absorption. The absorbed hydrogen is regarded to react directly with the complex molecule into hydride without the creation of the dissociated hydrogen state. The difference of the absorption process between the two complexes is due to the different ability of the electron transportation in the complexes.

Reference

- 1) K. Kimura and H. Inokuchi, *J. Catal.* **29**, 49(1973).

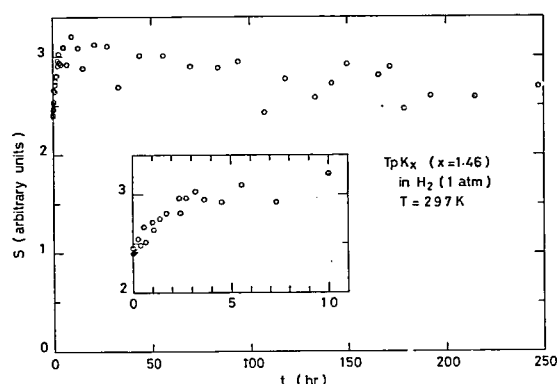


Figure 1. Time dependence of the spin concentration for $\text{TpK}_{1.46}$ just after the introduction of hydrogen gas.

VI-D-2 Electrical and Magnetic Properties of Triphenylene-Potassium Complexes

Toshiaki ENOKI and Hiroo INOKUCHI

The resistivities and the absorptions of ESR are investigated as a function of temperature for

triphenylene-potassium complexes with different compositions, $\text{TpK}_{0.87}$ and $\text{TpK}_{1.46}$. $\text{TpK}_{0.87}$ is a semiconductor with the resistivity at room temperature ρ_{rt} of $4 \times 10^4 \Omega\text{cm}$ and the activation energy E_a of 0.50 eV, while $\text{TpK}_{1.46}$ has ρ_{rt} of $8 \times 10^2 \Omega\text{cm}$ and E_a of 0.14 eV. We have a sharp Lorentzian absorption of ESR with the line width of 1.2G for $\text{TpK}_{0.87}$ at room temperature. As temperature goes down, it splits into two lines reflecting two

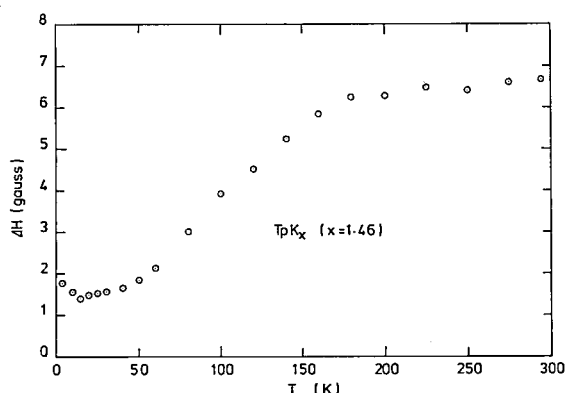


Figure 1. Temperature dependence of the line width for $\text{TpK}_{1.46}$.

inequivalent sites, and finally, these show inhomogeneous broadening below 15K. For $\text{TpK}_{1.46}$, ESR absorption shows a faintly asymmetric Lorentzian shape with the width of about 5.6G at room temperature. The intensity exhibits the depression of the spin concentration at low temperatures, while, the line width, remaining almost constant above about 180K, decreases to have a minimum around 10K and grows up below lower temperature as the lowering of temperature as shown in Figure 1. We conjecture these facts are caused by the development of antiferromagnetic short range order.^{1,2)}

References

- 1) M. Date, *J. Phys. Soc. Japan* **11**, 1016(1956).
- 2) R. R. Bartkowski, M. J. Hennessy, B. Morosin and P. M. Richards, *Solid. State. Commun.* **11**, 405(1972).

VI—E X-ray Study of Partially Oxidized Derivative of Magnus Green Salt

Ryozo KUBOTA (*Kyoto Univ.*), Toshiaki ENOKI
and Ikuji TSUJIKAWA (*Kyoto Univ.*)

In order to investigate one-dimensional metallic compounds, we take the partially oxidized

derivative of Magnus Green Salt (MGS), which has the formula $\text{Pt}_6(\text{NH}_3)_{10}\text{Cl}_{10}(\text{HSO}_4)_4(\text{MGSPoS})$

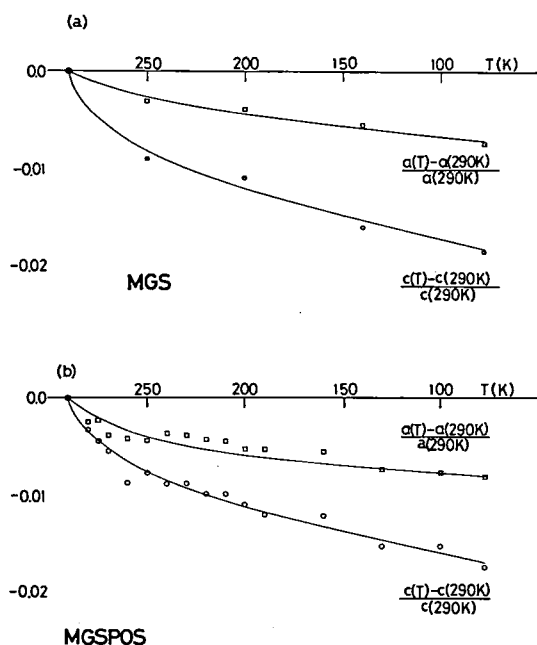


Figure 1. Temperature dependence of the lattice parameter *a* and *c*. (a) is for MGS and (b) for MGSPoS

with the Pt average valence of +2.33. Thermal analysis by DSC leads to the existence of a glassy state in MGSPoS below ~200K, and heat capacity measurements by a.c. and adiabatic methods support this. From d.c. electrical conductivity measurements, it is shown that in MGSPoS, two metal-semiconductor transitions take place at about 220K and about 280K. In order to examine these transitions and the glassy state from the structural point of view, we measured the X-ray

powder patterns of MGS and MGSPoS at various temperatures between 77.3K and 290K. As shown in Figure 1, in MGS, the contraction of the lattice constant *c* (// Pt chain) is three times larger than that of *a* (⊥ Pt chain). In MGSPoS, however, the contraction of *c* is only about twice of that of *a*. This

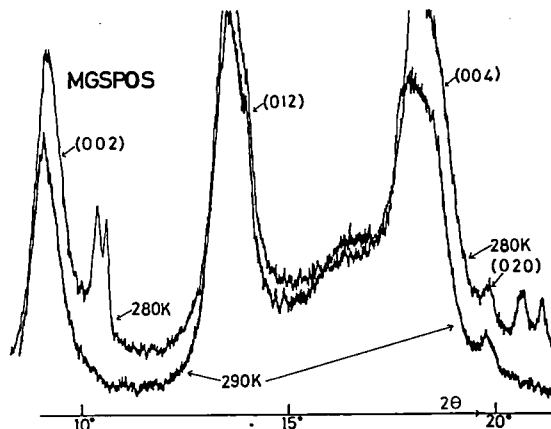


Figure 2. X-ray patterns of MGSPoS at 280K and 290K

small contraction of *c* in MGSPoS compared to that in MGS is perhaps ascribed to the large size of substituting ligand HSO_4^- . Though there is no drastic change in lattice constants at the transition temperatures, X-ray patterns of MGSPoS change drastically between 280K and 290K as shown in Figure 2. This indicates a structural transition which may correspond to the metal-semiconductor transition at about 280K. Details of the structural transition are now under investigation.

CHEMICAL MATERIALS CENTER

VI—F Synthesis of a New Atropisomeric Diphosphine Ligand and its Use in Rh(I)-Catalyzed Asymmetric Hydrogenation of α -Acylaminoacrylic Acids

Akira MIYASHITA, Arata YASUDA, Hidemasa TAKAYA,
Toshiaki SOUCHI,* and Ryoji NOYORI* (*Nagoya Univ.)

2,2'-Bis(diphenylphosphino)-1,1'-binaphthyl (BINAP) (**1**), an axially dissymmetric bis(triaryl)-phosphine which possesses many interesting structural characteristics, was synthesized in optically pure form.^{1,2)} This time, we have extensively studied the asymmetric hydrogenation of α -acylaminoacrylic acids catalyzed by its Rh(I) complexes.

Two kinds of Rh complexes (*S*)-**3** and (*S*)-**4** were produced when (*S*)-**2** in methanol was exposed to hydrogen (eq 1). The major complex (*S*)-**3**, purified by recrystallization from methanol, serves as an highly excellent catalyst for the asymmetric hydrogenation of prochiral α -acylaminoacrylic acids or esters as shown in Table I.

The ^{31}P NMR spectroscopy of the chiral Rh

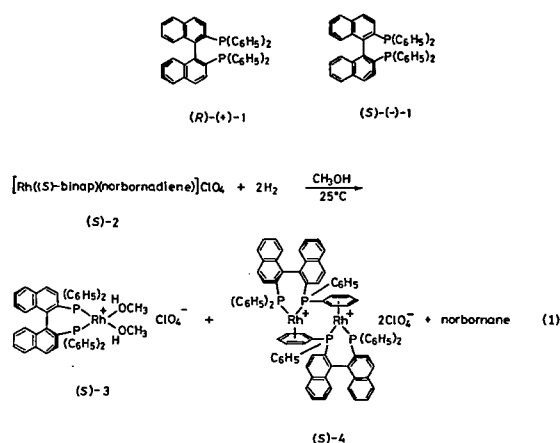


Table I. Asymmetric Hydrogenation of α -acylaminoacrylic Acids Catalyzed by the Rh-BINAP complex.^a

substrate	config. of BINAP	% yield	% ee (config.)	substrate	config. of BINAP	% yield	% ee (config.)
$\begin{array}{c} \text{H} \\ \diagdown \\ \text{C} = \text{C} \begin{array}{l} \diagup \text{COOH} \\ \diagdown \text{NHCOPh} \end{array} \\ \diagup \text{Ph} \end{array}$	(S)	96	96 (R)	$\begin{array}{c} \text{H} \\ \diagdown \\ \text{C} = \text{C} \begin{array}{l} \diagup \text{COOH} \\ \diagdown \text{NHCOPh} \end{array} \\ \diagup \text{Ph} \end{array}$	(S)	97	79 (R)
$\begin{array}{c} \text{H} \\ \diagdown \\ \text{C} = \text{C} \begin{array}{l} \diagup \text{COOH} \\ \diagdown \text{NHCOPh} \end{array} \\ \diagup \text{Ph} \end{array}$	(R)	97	100 (S)				
$\begin{array}{c} \text{H} \\ \diagdown \\ \text{C} = \text{C} \begin{array}{l} \diagup \text{COOH} \\ \diagdown \text{NHCOPh} \end{array} \\ \diagup \text{Ph} \end{array}$	(S)	98	71 (R) ^b				
$\begin{array}{c} \text{Ph} \\ \diagdown \\ \text{C} = \text{C} \begin{array}{l} \diagup \text{COOH} \\ \diagdown \text{NHCOPh} \end{array} \\ \diagup \text{H} \end{array}$	(R)	93	87 (R) ^c	$\begin{array}{c} \text{H} \\ \diagdown \\ \text{C} = \text{C} \begin{array}{l} \diagup \text{COOH} \\ \diagdown \text{NHCOPh} \end{array} \\ \diagup \text{H} \end{array}$	(S)	97	98 (R)
$\begin{array}{c} \text{H} \\ \diagdown \\ \text{C} = \text{C} \begin{array}{l} \diagup \text{COOH} \\ \diagdown \text{NHCOPh} \end{array} \\ \diagup \text{Ph} \end{array}$	(S)	99	84 (R)	$\begin{array}{c} \text{H} \\ \diagdown \\ \text{C} = \text{C} \begin{array}{l} \diagup \text{COOH} \\ \diagdown \text{NHCOPh} \end{array} \\ \diagup \text{H} \end{array}$	(S)	97	67 (R)
$\begin{array}{c} \text{H} \\ \diagdown \\ \text{C} = \text{C} \begin{array}{l} \diagup \text{COOMe} \\ \diagdown \text{NHCOPh} \end{array} \\ \diagup \text{Ph} \end{array}$	(S)	98	93 (R)				
$\begin{array}{c} \text{H} \\ \diagdown \\ \text{C} = \text{C} \begin{array}{l} \diagup \text{COOMe} \\ \diagdown \text{NHCOPh} \end{array} \\ \diagup \text{Ph} \end{array}$	(R)	97	92 (S)				

^a H₂ 3—4 atm; substrate/cat. = 100—150; solvent, C₂H₅OH.

^b H₂ 50 atm.

^c Solvent, THF.

References

- 1) H. Takaya, T. Souchi, A. Yasuda, and R. Noyori, *IMS Ann. Rev.*, 92(1978).

- 2) K. Toriumi, T. Ito, and H. Takaya, *IMS Ann. Rev.*, 118(1979).

VI—G Selective 1,4-Addition of Diethylaluminum Benzenethiolate to Vinyloxiranes. Stereoselective Synthesis of Allylic Alcohols

Arata YASUDA, Mikio TAKAHASHI (*Nagoya Univ.*), and Hidemasa TAKAYA

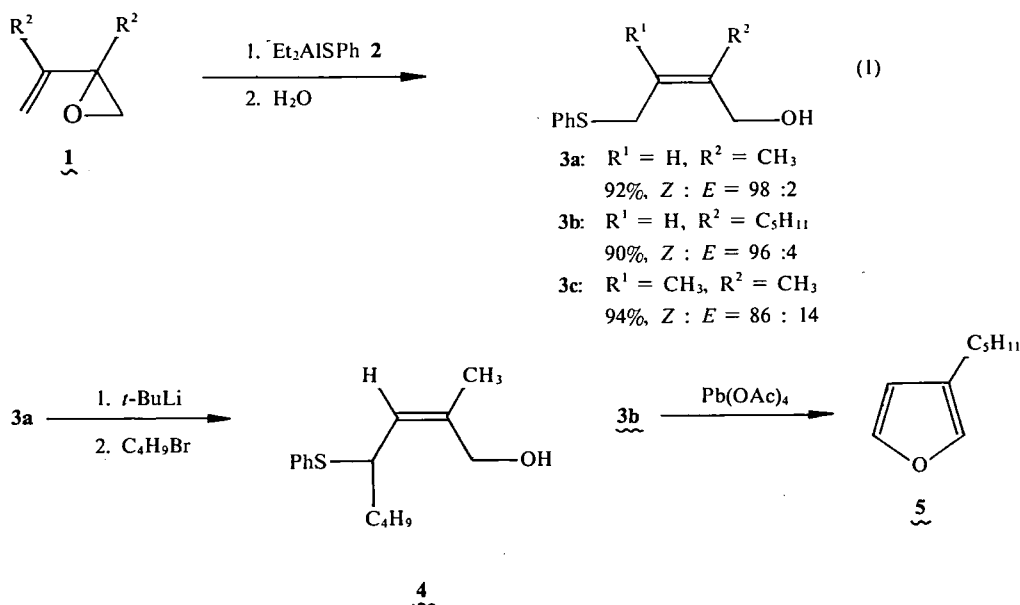
Oxiranes are often used as starting materials for natural product synthesis because of their ready accessibility and high reactivity. We have developed a new synthetic route to Z isomer of 4-phenylthio-substituted allylic alcohols **3** by selective 1,4-addition of dialkylaluminum benzene-

complex (*S*)-**3** in methanol with (*Z*)- α -acetamidocinnamic acid showed that only one of two possible diastereomers exists in the solution, which indicates that the ability of enantioface differentiation of the catalyst is almost complete. The ³¹P NMR measurements also revealed that depending on the reaction conditions the catalytic hydrogenation system contains a variety of catalysts and coordination complexes which behave differently in enantioface differentiation. In order to attain high optical yield, therefore, it is requisite to make an effort to control the conditions so that a selected catalyst possessing high chiral recognition ability is specifically created.

thiolate (**2**) to vinyloxiranes **1**. Some representative results are shown in eq 1. The carbanion derived from **3a** and *t*-BuLi can easily be alkylated by alkylbromide such as butylbromide to give allylic alcohol **4** in good yield with retention of olefin configuration. The compound **3b** can also be

converted to furan derivative **5** by the treatment with lead tetraacetate. Thus the compound **3** has

potential utility as starting materials for synthesizing useful organic compounds.



VI—H Organometallic Synthesis by Use of Transition Metal Vapors

Akira MIYASHITA and Hidemasa TAKAYA

The use of transition metal atoms in organometallic synthesis is of much recent interests because of the high chemical potential of the individual metal atoms. The metal atom technique allows us the direct synthesis of a number of interesting and unstable organometallic compounds. We have constructed a metal atom reactor,

an apparatus designed first by K. J. Klabunde. Our attention is mainly focused on the developments of new routes to various kinds of organometallic compounds which play important roles as reactive intermediates in many catalytic processes of recent interests.

DEVELOPMENT WORKSHOP

VI—I Design Study of UVSOR (Ultraviolet Synchrotron Orbital radiation) Light Source

Makoto WATANABE, Akira UCHIDA, Takeshi KATAYAMA*
and Katsuhide YOSHIDA** (* Univ. of Tokyo, ** Univ. of Tokyo and IMS)

An electron storage ring dedicated to ultraviolet synchrotron orbital radiation research of molecular science and related fields has been designed. This is a 600 MeV storage ring, the injector of which is a 600 MeV synchrotron with a 12 MeV linac. The photons in the 10 — 2000 Å region are mainly

utilized. Since the storage ring is dedicated to synchrotron radiation (SOR) research, it has been designed so as to have advantages of small emittance and small beam size in the bending sections, and so that the wigglers can be installed at long straight sections, where the dispersion

function is 0 and the horizontal beam divergence is small. One bunch operation for producing pulsed light (width ~ 0.5 nsec, interval ~ 170 nsec) is possible. The ring is composed of eight bending magnet sections, and four long and four short straight sections. From one bending section, two outlets of the SOR are available. To each outlet, two optical instruments will be attached, the details of which will be described in "Large Scale Research

Equipments". In both long and short straight sections, two doublets of quadrupoles are installed. The electrons are injected from the inner side of the ring into one long straight section. The remaining three long straight sections are reserved for an RF cavity and two wigglers. A preliminary test of ultrahigh vacuum system was made as part of the "Special Research Project".

VI—J Designing of a High-Speed Image Processor and its Use for Picosecond Time-Resolved Spectroscopy

Yoshihiro TAKAGI, Minoru SUMITANI, and Keitaro YOSHIHARA

Time-resolved spectroscopy is often important for the study of picosecond dynamics of excited states in molecules. As a means for spectroscopy measurements the use of TV camera and microcomputer has been developed in many laboratories. We have designed a microcomputer-based high-speed image processor for picosecond time-resolved spectroscopy which is combined with a streak camera. A block diagram of the construction is shown in Figure 1. A video signal of the streak image was sampled, integrated, digitized,

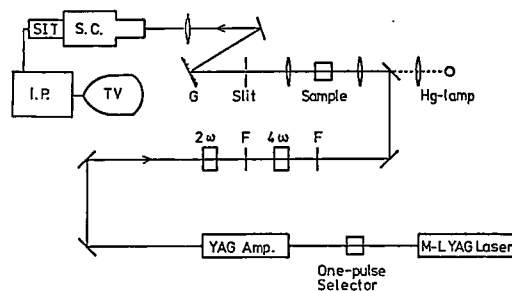


Figure 2. Schematic diagram of the experimental set-up for time-resolved emission spectroscopy. G: grating, F: filter, S.C.: streak camera, SIT: TV camera, and I.P.: image processor.

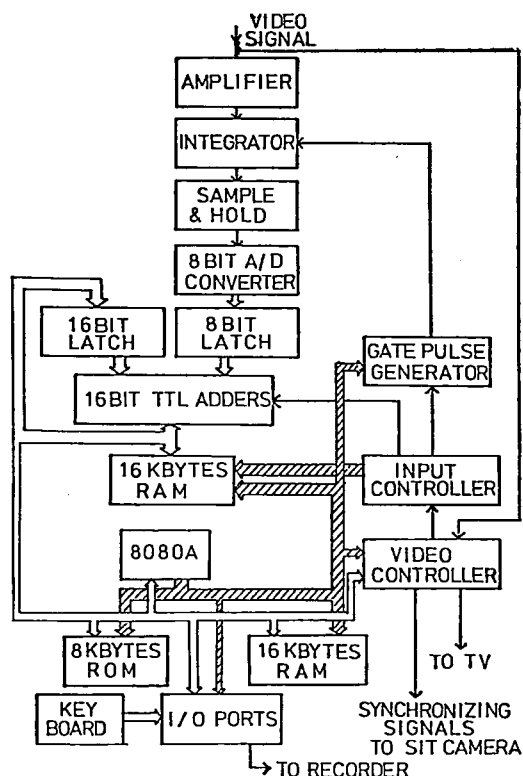


Figure 1. Hardware block diagram of the image processor.

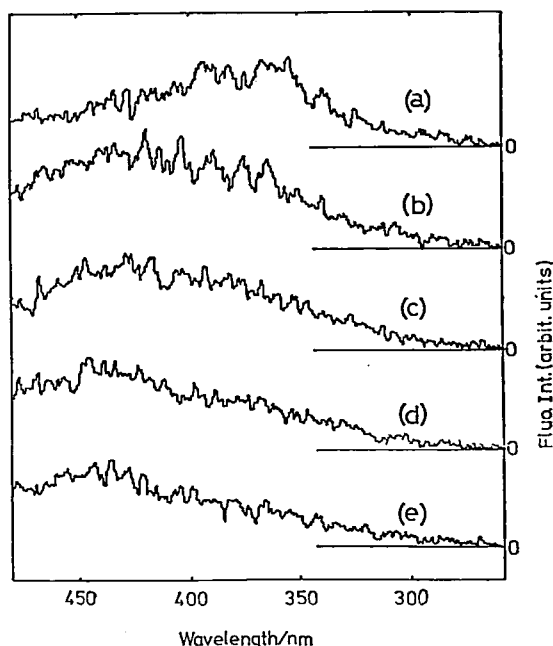


Figure 3. Time-resolved fluorescence spectra of DMABN in acetonitrile at every block of time interval. (a) 0—45ps, (b) 60—105ps, (c) 120—165ps, (d) 180—225ps, and (e) 240—285ps.

and then stored into IC memories. The data of up to 32 channels sampled from the streak image can be simultaneously acquired. A microprocessor contained in the image processor gives some corrections to the data and displays it graphically on a TV screen. Processing speed is as high as to repeat the data acquisition by 1 Hz, which has made the efficiency of the measurement greatly increase.

Using the image processor time-resolved emission spectra of p-dimethylaminobenzonitrile (DMABN) excited by a mode-locked YAG laser have been obtained and a remarkable spectral

change in the picosecond domain has been found. Figure 2 shows a block diagram of the arrangement for the measurement of the time-resolved emission spectra. Figure 3 is a recorder trace of the spectra of DMABN in acetonitrile. A clear spectral shift to the longer wavelength with time appears which suggests us that there exist two isomers in the excited state of DMABN and one of which corresponding to the longer wavelength band has a polarity much larger than the other and stabilized due to the interaction with the polar solvent.

RESEARCH FACILITIES

Computer Center

The Computer Center began its service in January 1979 with two HITAC M-180 computers. One of them was replaced by a HITAC M-200H in April 1980. M-200H and M-180 have a processing capacity of over 10 and 4 million instructions per second, respectively. Both of the processors use 32 bit words and are essentially IBM-compatible at both the hardware and software levels. They have 12 and 4 mega byte main memory, 7150 and 3340 mega byte disk memory, respectively, and other I/O devices. The computers are used not only by the research staff at IMS but also by the staff at nearby National Institutes as well as by scientists outside the Institutes in the related fields. As of March 1980 the number of project groups was 180 consisting of 338 users. In the twelve month period ending March 1980, 155, 980 jobs were processed with 6494 hours of the CPU time.

Unattended operation of the Computer Center at night and on holidays has been carried on since September 1979, using the automated operation system developed by the Center and Hitachi Ltd. the hardware consists of many sensors (smoke, heat, water, temperature, humidity, and earthquake), alarm systems, and automatic fire extinguishers. The software returns preassigned responses to operator calls from the system. The system sends alarms and terminates itself, airconditioners and the power supply in an emergency. It can also automatically stop the operation or freeze running jobs when preassigned conditions are satisfied. The system has been providing an uninterrupted, unmanned week long service.

A program library for molecular science has been established under a unique library management system, with which users can search on their TSS terminal whereabouts and guides of wanted programs. Many programs have already been registered and are being used frequently. All of the QCPE programs has been obtained and will be so on the continued basis. An arrangement has been made to introduce programs supported by the National Resource for Computation in Chemistry at Berkeley, Calif.

In June 1979 the center began its service of QCLDB (Quantum Chemistry Literature Data Base), a file of references of ab initio molecular orbital calculations. Users now can search for references on their TSS-terminal under ORION, a data base management system supported by Hitachi. References can be found using keywords such as compounds, journals, and authors. (See section VI-B.)



TSS-Terminal Room



Open I/O Room

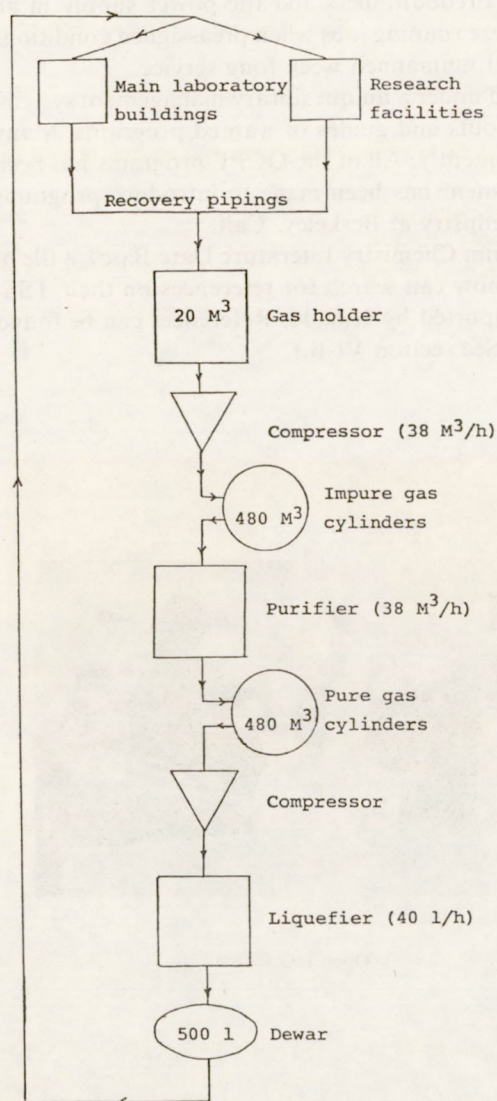
Low Temperature Center

Low Temperature Center supplies coolants such as liquid nitrogen and liquid helium. The staff of this center also develops cryogenic techniques in close cooperation with research divisions and other centers.

The center building (1430m², 2 stories and 1 basement) was completed in March 1979. It consists of three machine rooms, ten laboratories, a machine shop and also a control room for a helium liquefaction and recycling system. The floor and the walls of the machine rooms for compressors and kinney vacuum pumps were separated from the rest of the building to avoid the propagation of mechanical vibrations of the heavy machines.

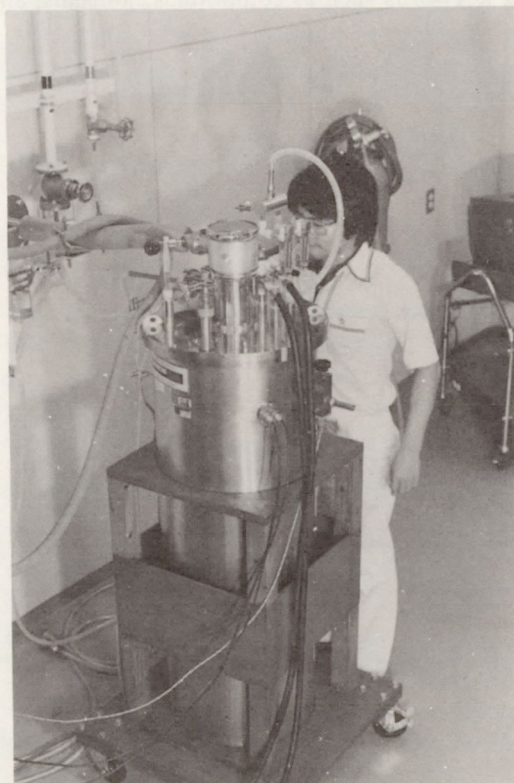
The laboratories are to be equipped with spectroscopic, magnetic and calorimetric instruments for low temperature measurements. Seven laboratories are located at basement in order to keep a well regulated environment. Especially, one of them is the shielded room where the attenuation rate of electromagnetic disturbance is 80 dB. One can use two Kinney vacuum pumps in the laboratories when he experiments below 4.2K.

A helium liquefier (CTI-1410) with capacity of 40 l/h runs to supply liquid helium to research groups. Main laboratory building and research facilities are equipped with the recycling pipings for helium gas. Helium gas used by experiments is recovered to Low Temperature Center and purifies up to 99.99% purity. The flowsheet of the helium liquefaction system is as follows:



Major equipments are:

Helium Liquefier	CTI 1410
Helium Purifier	OSAKA SANSO UIO-1394-5
Cold Converter of Liquid Nitrogen	OSAKA SANSO CO-3
Helium Leak Detector	ULVAC DLMS-33
Rare Gas Purifier	BOC MK-3
Optical Measurement Cryostat	OXFORD 204
12T Superconducting Magnet	IGC MIDI-BRUTE-120
5T Superconducting Magnet	VMC SM-5075Q



12T Superconducting Magnet

Chemical Materials Center

The chemical materials center plays an important role in the preparation of chemical substances in IMS. The scientists and technicians of this facility carry out works on synthesis and purification of organic and inorganic compounds and preparation of single crystals. They develop new synthetic procedures to obtain interesting substances in pure forms and in large quantities. They also carry out their own researches on synthesis of new interesting chemicals, developments of new selective chemical transformations, elucidation of reaction mechanisms, and application of new methodologies to analysis of materials (see Research Activities VI-F ~ H). They participate in taking charge of and disposition of waste chemicals and solvents. The Center building was completed in March 1978. Piping works were completed and laboratory apparatuses were sufficiently equipped. The stockroom stores more than five hundred chemicals and solvents. Hot water enough for experiments is supplied by solar energy collectors equipped on the roof of the building.

Major equipments are:

Gas Chromatograph-Mass Spectrometer

NMR Spectrometer

High Performance Liquid Chromatographs

Inert Atmosphere Glove Box

CO₂TEA Laser

Infrared Spectrometer

Instrument for Crystal Growth

Automatic Waste Fluid Disposition Apparatus

Polarimeter

Zone Refiners

Auto Annular Teflon Spinning Band

Spaltrohr-System

Ultra Low Temperature

Refrigerated Circulating Bath

JEOL JMS D300 equipped with EI, CI, and FD ion sources, and JMA-2000 mass data analysis system
Varian EM-390

JASCO TRI ROTAR and JASCO FAMILIC-1000

Vacuum Atmospheres Co. MO-40-2V DRI-TRAIN

LUMONICS 203

Hitachi 295

Assembled in IMS

Yanaco YWT-1

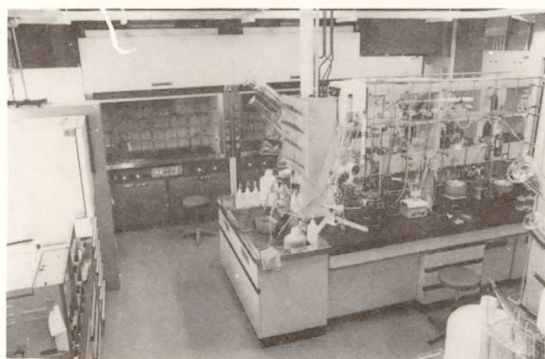
JASCO DIP-4

Shibayama SS-960 and Instruments Assembled in IMS

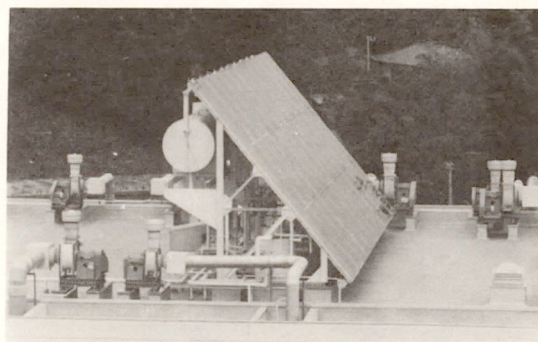
Perkin-Elmer 251

Fischer HMS 300

NESLAB ULT-80



Experimental Room



Solar-Energy Collecting System

Instrument Center

For the efficient use of instruments, the Instrument Center is equipped with instruments for general use as listed below. The Center also lends out the total of some fifty electronic and optical instruments, such as oscilloscopes, amplifiers, signal averagers, function generators, electrometers, power supplies, recorders,

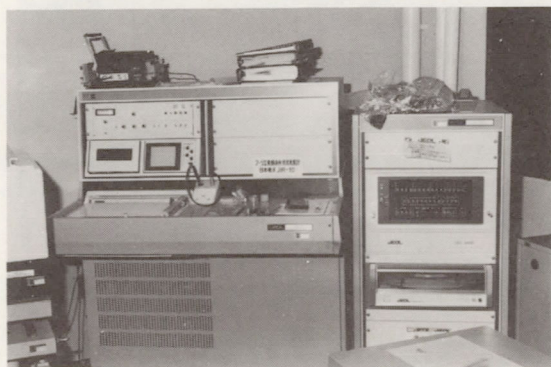
monochromators, which are used inside the campus of IMS.

The Center had many visiting research scientists and graduate students from universities and the users of this facility amounted to the total man-day of 284 in the fiscal year of 1979.

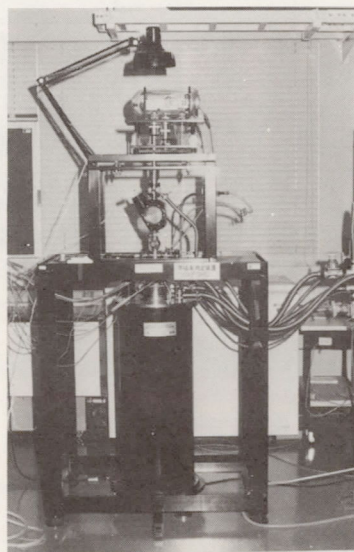
The Center staffs operate and do the maintenance work for these instruments and also conduct their own research by developing new instrumental techniques.

The major instruments are as follows:

Spectrophotometer	CARY 17
Dual-wavelength Spectrophotometer	HITACHI 556
Fourier-Transform IR Spectrophotometer	JEOL JIR-10
Fourier-Transform IR Spectrophotometer	NICOLET 7199A
Automatic Recording Spectropolarimeter	JASCO J40C
Corrected Recording Spectrofluorophotometer	SHIMADZU RF-502
1-Meter VUV Scanning Monochromator	GCA MCPHERSON 225
Photoelectron Spectrometer	PERKIN ELMER PS-18
Laser-Raman Spectrophotometer	JEOL JRS-400T
Nanosecond Spectrometer	APPLIED PHOTOPHYSICS SP-3X + ORTEC
Argon Ion Laser	SPECTRA-PHYSICS 164-05
Helium-Neon laser	SPECTRA-PHYSICS 125A
CW Dye Laser	SPECTRA-PHYSICS 375-90
Pulsed Dye Laser	MOLECTRON UV-24 + DL14
Pulsed Dye Laser	CHROMATIX CMX-4
X-ray Diffractometer	RIGAKU DENKI GEIGER FLEX 2027
Single Crystal Automatic Four Circle X-ray Diffractometer	RIGAKU DENKI AFC-5
Surface Roughness Tester	SLOAN DEKTAK
Thermal Analyzer	DUPONT 990
High Vacuum Evaporator	ULVAC EBH-6
Scanning Electron Microscope	HITACHI S-450
Magnetic Balance	OXFORD
Fourier-Transform NMR Spectrometer	JEOL JNM-FX 100
ESR Spectrometer	VARIAN E-112/E-900
High Speed Refrigerated Centrifuge	KUBOTA KR-180A



FT-IR Spectrometer



Magnetic Balance

DEVELOPMENT WORKSHOP

Development Workshop is expected to play a unique and important role in research activities at IMS. It designs and constructs instruments based on IMS's own ideas. It also improves existing research equipments. Technicians are making interplay with scientific staff members to support activities of the Workshop. Technical meetings are regularly held twice a year, which provide opportunities for technicians to exchange information and to discuss technical problems with those from other institutes and universities.

Development Workshop consists of machine shop, electronic shop, and glass-blowing shop.

1) Machine Shop

The facilities constructed or to be constructed at IMS include high-vacuum apparatus, lasers, microwave spectrometers as well as various types of equipments operated at the liquid-helium temperature. All these are of high performance and thus require very fine engineering to prepare their parts. Therefore, in addition to lathes, milling machines, drilling machines, and grinders of common use we have installed the following special machines:

- (i) NC Lathe (OKUMA TEKKOSHO LS-N). This computer-controlled lathe has been used to prepare microwave lenses with spherical and/or paraboloidal surfaces, made of Teflon, TPX, or metals. It also prepared spherical collectors for electron spectroscopy. None of these parts can be constructed with a normal lathe. The electronic shop develops microcomputer facilities to feed tapes in the NC lathe.
- (ii) Spark erosion machine (MAKINO SODICK GP-20L). This has been used to make a 50 mm diameter stainless steel cylinder of 0.025 mm thickness, which is to support an optical window in a low-temperature apparatus. It has also been used to drill a very fine slit (0.04 mm wide and 30 mm long).
- (iii) Electron-beam welder (NEC EBW). This can weld tightly two different kinds of metals (e.g. copper and stainless steel). This welding eliminates possible leakage in a vacuum apparatus operated at a very low temperature, especially in those parts that suffer from frequent changes of temperature. We can use a beam of 10 mA accelerated at a voltage of 150 kV under the pressure of 5×10^{-2} Pa or less. The maximum beam power is 1.5 kW.
- (iv) Helium/nitrogen leak detector (ULVAC DLM 33). This detects a leakage in an ultra-high vacuum apparatus as small as 3×10^{-9} l-Pa/s. It may even detect the nitrogen gas. This machine consists of a detector combined with a vacuum system designed by the Machine Shop. It is equipped with a microcomputer that automatically eliminates backgrounds and noise signals.
- (v) NC Milling Machine (MAKINO KGNCC-70). This has been used for some complicated fabrication which was not possible with a normal milling machine. The electronic shop develops microcomputer facilities to feed tapes in this machine.

2) Electronic Shop

The major instruments installed are:

Oscilloscope	TEKTRONICS 7904 (500 MHz)
Oscilloscope	TEKTRONICS 475 (200 MHz)
Storage oscilloscope	HEWLETT PACKARD 1741A (100 MHz)
Sampling oscilloscope	IWATSU SAS-610B (12.4 GHz)
Spectrum analyzer	TAKEDA RIKEN 4110M (200 Hz — 1.3 GHz)
Frequency counter	TAKEDA RIKEN 5502C (≤ 1.4 GHz)
Lock-in amp	PAR 124
Boxcar integrator	PAR 162
LCR meter	HEWLETT PACKARD 4262A
Teletype	CASIO 502
Minicomputer system	NIHON MINICON ECLIPSE S-130

The Electronic Shop has designed and constructed a high-precision wavelength meter for infrared diode laser, a data processing system for a magnetic balance, and a microcomputer-controlled picture analyzer for a picosecond streak camera. It is also setting up a laser wavelength conversion unit utilizing parametric oscillation and also an interface for spectroscopic measurements in the vacuum ultraviolet region.

3) Glass-blowing Shop

We have installed the following machines:

Glass lathe

Spot welder

Water welder

Glass grinder

Glass cutter

Ultrasonic microboring machine

Ultrasonic soldering machine

RIKEN SEIKO RGL-4DLH (max. diameter of the glass pipe is 20 mm)

NIPPON AVIOTRONICS NW-29 DS (100 W)

FUJI BUSSAN S51-4 (oxygen/hydrogen evolving rate is 170 l/h)

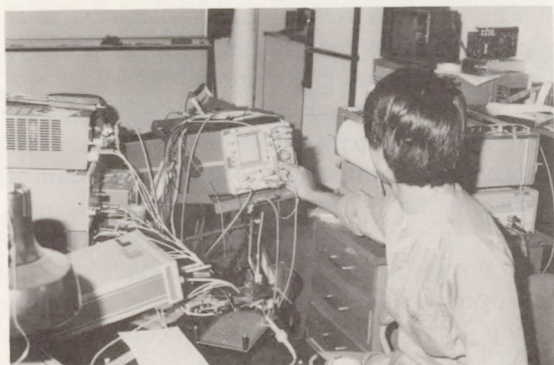
SANWA DIAMOND SDK 20-B (diamond disk 300 mm ϕ with an angle holder)

ITO DP-3 (diamond disk 200 mm ϕ with an angle holder)

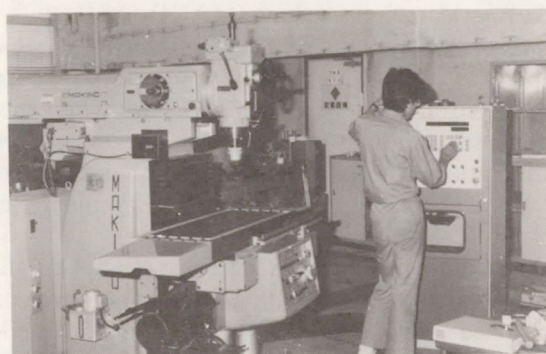
CHO-OMPA KOGYO UM-2-7B

ASAHI GLASS SUNBONDER USM-II

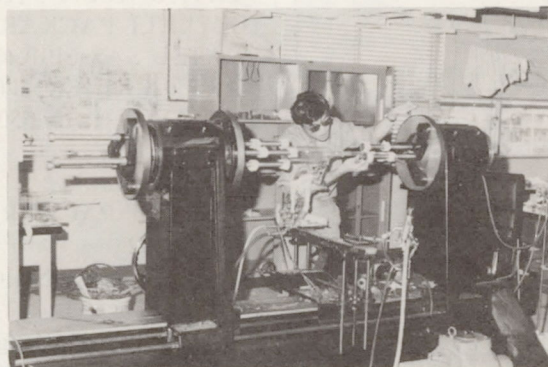
The shop has constructed, among others, high vacuum glass apparatus and laser tubes.



Electronic Shop



NC Milling Machine



Glass-blowing Shop

LARGE SCALE RESEARCH EQUIPMENTS

1) Picosecond Continuously Tunable Laser from UV to IR

We have been developing a picosecond continuously tunable laser from UV to IR for a couple of years (See IMS Annual Review, 1979). Recently we have obtained a high peak power in OPA (optical parametric amplification) enough for practical uses by expanding the former optical arrangement. A single pulse selected from a mode-locked YAG laser and amplified (20 ps and 50 — 100 mJ at 1064 nm) is split into two beams acting separately as pumping lights for OPO and OPA as shown in Fig. 1. Two kinds of crystals were used in the condition of angle tuning; one is KD*P in TYPE-II which is pumped by a 3rd harmonic (355 nm) of the YAG laser and covers the spectral ranges of 450 — 650 nm and 780 — 1670 nm, and the other is LiNbO₃ in TYPE-I pumped by a fundamental of the YAG laser and the tuning range is from 1.4 to 4.4 μ m. Angle tuning of the cascaded crystals was controlled by a microcomputer. The result is summarized in Table 1. By introducing the pumping beam for OPO and OPA separately we have obtained the high power output without exposing the crystals to the danger of damage and "walk off" and "walk through" effect were diminished.

Table 1. Experimental conditions and results on OPO and OPA.

crystal	excitation wavv-length	phase match condition	tuning range	average output energy	conversion efficiency
KD*P	355 nm	TYPE-II	450-650nm 780-1670nm	1mJ	5%
LiNbO ₃	1064nm	TYPE-I	1.4-4.4 μ m	10mJ	10%

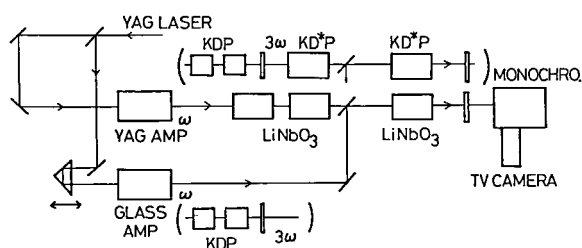


Figure 1. A block diagram of the arrangement for OPO and OPA.

Frequencies of these outputs will be extended to UV and IR out of the region between 400 nm and 4 μ m by frequency mixings.

2) High Resolution Spectroscopy

The system consists of two cw tunable lasers with high spectral purity, one in the visible region and the other in the infrared region.

2-a) Dye lasers in the visible region

Three dye lasers are available: (1) Spectra Physics 580A, (2) Coherent Radiation 599 — 21, and (3) Spectra Physics 380A. Figure 1 shows a picture of the SP 380A ring laser. These dye lasers are pumped by either a Spectra Physics 171 — 05 or 171 — 17 Ar⁺ laser. The two SP dye lasers have the spectral width of a few MHz with the stability of about ± 20 MHz, whereas the CR 599 — 21 has both stability and spectral purity of about 1 MHz, thanks to a feedback loop. The output power is 20 to 150 mW for SP 580A and CR 599 — 21, but is much larger, up to 800 mW, for the ring laser, SP 380A. Rhodamine dyes allow to oscillate the lasers in the region 540 to 650 nm.

The dye lasers have been mainly used to induce fluorescence of unstable molecules, as described in Research Activities II-A. They have also been proven useful in carrying out sub-Doppler spectroscopy: e.g. intermodulated fluorescence spectroscopy as applied to PH₂ (II-A-8), microwave optical double resonance to HNO (II-A-5), and infrared optical double resonance to NH₂ (II-A-10). Professor K. Takagi (*Toyama Univ.*) and Dr. T. Amano (*Univ. of Tokyo*) have participated, respectively, in the works on HNO and NH₂, under a Joint Studies Program of IMS. The same program has facilitated the observation by Dr. N. Ohashi (*Kanazawa Univ.*) of the laser excitation spectra of singlet methylene (II-A-16). Professor F. Shimizu (*Univ. of Tokyo*) and his student are using two dye laser beams to determine velocity distributions of molecules. C. Yamada and Y. Endo (IMS) have generated infrared light at 3 μ m by mixing the outputs of a dye laser and an Ar⁺ laser in a LiNbO₃ crystal (II-A-15).

2-b) Diode lasers in the infrared region

The source is a Laser Analytics LS-3 spectrometer, which may be equipped with four diodes at the same time. At present nearly 20 diodes are available in the region from 660 to 2600 cm^{-1} . The stability and spectral purity are of the order of 10^{-4} cm^{-1} , and the output of about 0.1 mW is normally distributed among a few modes. A high-precision wavelength meter has been constructed, which measures the wavenumber of an absorption line to the accuracy 10^{-3} to 10^{-4} cm^{-1} . Figure 2 shows a typical arrangement for detecting paramagnetic species. Zeeman modulation has been found particularly useful for that purpose. An absorption line is normally measured relative to a reference line, by counting the number of fringes from an air-spaced etalon. These measurements can be done with the aid of a mini-computer. As described in Research Activities II—A, more than ten free radicals have been detected in this way.

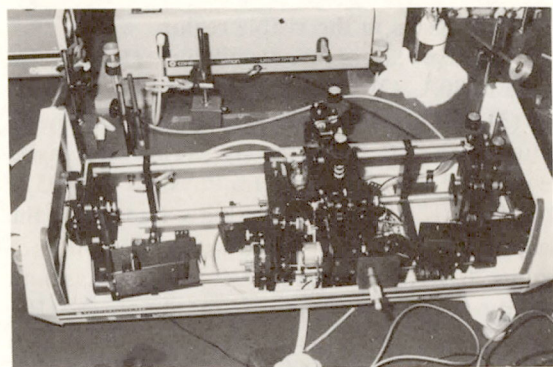


Figure 1. Spectra Physics 380A ring dye laser.

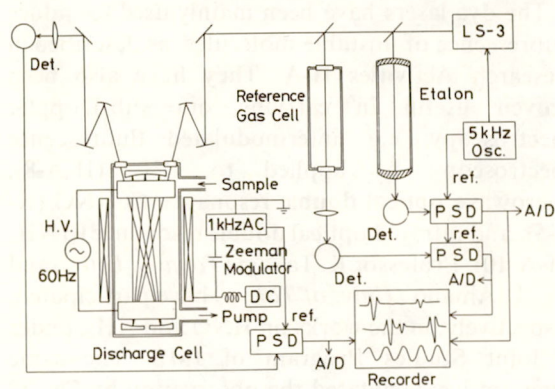


Figure 2. A schematic diagram of a Zeeman-modulated infrared diode laser spectrometer.

Dr. M. Takami (*IPCR and IMS*) had demonstrated the feasibility of microwave diode-laser double resonance using the $\text{CF}_4 \nu_3$ band as an

example. Other examples of diode laser spectroscopy (straight absorption spectroscopy) are listed below:

CH_3CN	by Dr. T. Nakagawa (<i>Univ. of Tokyo</i>)
NH_3	by Drs. K. Yamada and M. Takami (<i>IPCR</i>)
ClO_2	by Dr. K. Tanaka (<i>Kyushu Univ.</i>)
N_2H_4	by Prof. M. Tsuboi and Dr. Y. Hamada (<i>Univ. of Tokyo and IMS</i>)
CH_3NH_2	
HCOOH	by Mr. H. Kuze (<i>Univ. of Tokyo</i>)
CH_3OH	by Dr. T. Amano (<i>Univ. of Tokyo</i>)
CHF_3	by Mr. S. Sofue and Prof. T. Fujiyama (<i>IMS</i>)

3) High Resolution Spectroscopic System in the Far-Infrared Region

The system is being developed according to the plan described in detail in the *IMS Annual Review 1979*, pp. 148 — 149. The main parts, such as a high-power CO_2 laser, an electromagnet, InSb far-infrared and mm-wave detectors, a backward wave oscillator (BWO) and other mm-wave sources, have already been installed.

4) Ultraviolet Synchrotron Orbital Radiation (UVSOR) Facility — Experiment Systems

Synchrotron orbital radiation (abbreviated hereafter as SOR) has now opened new possibilities in research and technology due to its unique characteristics. In the world there are many SOR facilities in operation as well as those under construction. Since 1974, the construction of a SOR facility with a 0.6 GeV storage ring has been repeatedly proposed for research in molecular science and its related fields. The facility proposed here is called 'UVSOR'. A detailed proposal for the UVSOR project has been elaborated by its working group at IMS, and has been summarized in Pamphlet UVSOR-3 recently published from IMS. The entire UVSOR facility proposed consists of a 0.6 GeV storage ring, a 0.6 GeV synchrotron (with a 12 MeV linac), and experiment systems.

The main research fields to be covered by UVSOR are divided into the following four categories, 1) optical spectroscopy, 2) photoelectron spectroscopy, 3) photochemistry, and 4) elementary chemical reactions. Some of the typical

apparatuses to be constructed in the UVSOR project are schematically illustrated in Pamphlet UVSOR-3.

A starting budget for the UVSOR project has been approved in the fiscal year of 1980, mainly covering some part of the experiment systems.

During the present fiscal year a few vacuum monochromators of 1m Seya-Namioka type and main experimental apparatus are to be constructed. Discussions about the detailed designs of monochromators and main apparatus are now

going on in the working group. Final conclusions on the detailed designs will be obtained very soon. The purchase of vacuum equipments and electronics instruments necessary for UVSOR experiments has already been started.

The current working group for the UVSOR experiment systems comprises Profs. H. Inokuchi, K. Kimura, I. Koyano, K. Shobatake, and M. Watanabe, and Drs. Y. Achiba, K. Seki, and K. Tanaka, and Mr. A. Uchida (Technical Chief).

SPECIAL RESEARCH PROJECT

IMS has special research projects supported by national funds. The following two projects were carried out during the first five years (1974—1979): (1) Molecular designing for interesting and useful materials. (2) Investigation of energy conversion processes at the molecular level. The second five year plan started this fiscal year, and the two new projects are (1) The development and control of molecular functions; (2) Energy transfer and energy conversion through molecular processes. These projects are being carried out with close collaboration between research divisions and facilities. Collaboration from outside also makes important contributions. Research fellows join these projects. In this report, the results of the previous projects in 1979 are reviewed.

(1) Molecular Designing for Interesting and Useful Materials

Theoretical Studies on Potential Energy Surfaces of Elementary Reaction Processes

Keiji MOROKUMA*, Shigeki KATO, Iwao OHMINE, Kazuo KITAURA and Shigeru NAGASE

Theoretical studies of elementary molecular processes including chemical reactions provide basic information for the energy conversion through chemical reaction and for the molecular designing of useful materials. For this purpose we have performed some research projects with the use of ab initio electronic structure method.

Potential energy surfaces of some ground and excited state reactions have been calculated. The mechanism of energy conversion occurring in the reaction processes has been discussed on the basis of characteristic features of potential energy surface. For example, the vibrational enhancement of reaction products has been interpreted from the structures of transition state and reaction coordinate. We also treated the reaction which produces the electronically excited species. As an example, the energy surfaces of $C^+ + H_2 \rightarrow CH^+ + H$ has been studied.

In order to understand the mechanism of catalytic reactions, we examined the electronic structure of some transition metal complexes and reaction intermediates involved in the reactions. The results obtained from these calculations have been used to extract the essential feature of catalytic reactions which is important in molecular designing.

Theory of Electronic Structure on Solid Surfaces and its Catalytic Activities

Masaru TSUKADA* and Chikatoshi SATOKO

A variety of processes occur on solid surfaces, which are important from the view point of application. This project is aimed at the elucidation of the electronic structure of solid surfaces and their interaction with adsorbates, to give a firm basis of the study of complicated surface processes.

Various oxide surfaces are investigated by the DV-X α cluster method and general features of their electronic structure are clarified. The reduction of the Madelung potential and strong electric field on the surface ionic site result in the formation of an intrinsic surface state. At the same time the enhanced covalency on the surface considerably compensates the above electrostatic effects. Thus self-consistent first principle calculations are essential for the surface of partially ionic solids. The character of the localized state associated with surface defects such as vacancy, edge and corner is also analyzed from the generalized view point. Problems in polar surfaces are discussed for the ReO_3 surface, as well as its catalytic activities. The interaction mechanism of the surfaces with adparticles is investigated for many types of the system, as described in "Research Activities I".

Molecular Structure and Chemical Reaction of Highly Excited Atoms and Molecules and of Molecular Ions

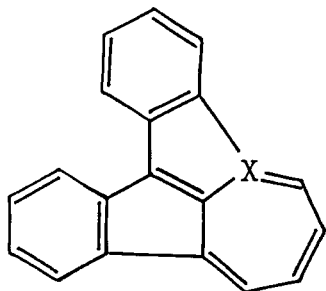
Eizi HIROTA*, Shuji SAITO, Chikashi YAMADA, Yasuki ENDO, Kentarou KAWAGUCHI, Masao KAKIMOTO, Keiichi NAGAI, and Tetsuo SUZUKI

Experiments on molecular ions have not been successful, but many unstable, neutral species, in particular, free radicals were detected and characterized by straight absorption infrared diode laser spectroscopy, dye laser excitation spectroscopy, and double resonance spectroscopy. The following species should be mentioned in the case of infrared diode laser spectroscopy: CF_3 (ν_3 band), FCO (ν_2 and ν_3 bands), HO_2 (ν_2 band), HNO (ν_2 band in the \tilde{a}^3A'' state), and FSO (ν_1 band), in addition to the species mentioned in the last year. Dye laser excitation spectroscopy has been applied to carbenes (HCF , DCF , HCCl , and CH_2) as well as to dihydrides, PH_2 and SiH_2 . Particular attention was given here to metastable states with multiplicity different from that of the ground state, because the reactivity of species is very much dependent on the multiplicity. Double-resonance spectroscopy of various kinds was developed and applied; microwave (or radio-frequency) optical double resonance to HNO and infrared optical double resonance to NH_2 . New light sources are also being developed in the infrared and near-infrared regions, that is, a difference-frequency laser and a diode laser, respectively, to obtain new information in these regions.

Molecular Designing of Novel π -Donors

Hiizu IWAMURA,* Tadashi SUGAWARA, Yuzo KAWADA, Yoshinori NISHIZAWA, and Yoshiteru SAKATA (*Osaka Univ. and IMS*)

As a continuation of our effort to elucidating the structural and electronic factors related to development of organic photoconductors and superconductors, we prepared a number of new π -donors of considerable strength. A couple of examples are 2,7-bis(dimethylamino)pyrene and benz[a]indeno[1,2,3-cd]azulene. The former formed the TCNQ complex which showed the electrical conductivity of $10^{-2} \text{ ohm}^{-1} \text{ cm}^{-1}$ at room temperature. Compound I obtained by judicious



I ($X = \text{C}$ and N^+)

molecular designing of the photorearrangement of triptycenes is isomeric to benz[a]pyrene and was found to be the strongest π -donor among the pentacyclic hydrocarbons. Red-brown needles of $\text{C}_{20}\text{H}_{12}\cdot\text{TCNQ}$: mp 150°C decomp.; CT-absorption max. at 1015 nm , were obtained. (See Research Activities V—A)

Electronic Characters of Organic Solids Having Interesting Physical and Chemical Properties

Naoki SATO, Kazuhiko SEKI and Hiroo INOKUCHI*

We are trying to find a principle for molecular design of organic solids with interesting physical and chemical properties by characterizing the electronic properties of organic solids. We constructed a new ultrahigh vacuum (10^{-8} Pa) photoelectron spectrometer for solids, with equipments of controlling the substrate temperature and characterizing the specimen. With this, we studied the electronic structure of aliphatic compounds condensed on cold substrate. (See Research Activities IV-A-2)

A Study of Vibrational Relaxation of Molecules by Photon Echo and Free Induction Decay

Masahiro MATSUOKA,* Masayuki FUJITA, and Shuji ASAKA (*Kyoto Univ. and IMS*)

Understanding of relaxation paths and rates of vibrational excitations in molecules under laser irradiation is an important problem toward the laser controlled chemical reaction. The photon echo and free induction decay (FID) methods can measure intramolecular and intermolecular relaxations separately.

We have succeeded in picosecond photon echo and FID using the backward echo and FID methods. Here in the first experiment, molecular sodium Na_2 was investigated using a synchronously-pumped-and-amplified mode-locked dye-laser system.

In the second stage some simple molecules in gas phase will be investigated in the ultra-violet and visible regions. The lifetimes of vibrational modes are expected to extend widely from the nanosecond to picosecond time scale. The laser wavelength must be varied widely before we will find out suitable modes, the lifetimes of which lie in a suitable range for the experiment.

Development of Ultrahigh Vacuum Technique

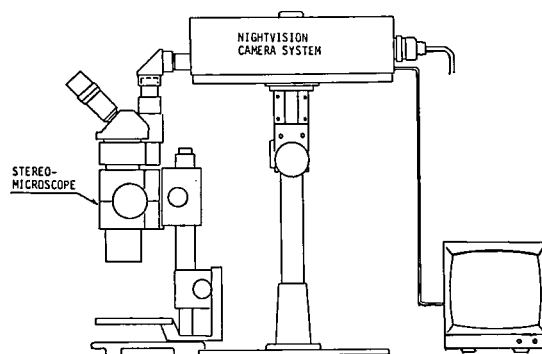
Makoto WATANABE, Kusuo SAKAI, and Shigetoshi TAKAHASHI

The chemical properties of materials such as energy conversion, catalysis and corrosion, are in many cases due to the surface characteristics of materials. Since the characterization of the surface requires the clean surfaces of the materials, the application of the ultrahigh vacuum (UHV) technique is inevitable. In IMS, there is a big demand that the UHV instruments such as chambers, cryostats,, are readily and quickly fabricated by its own Development Workshop. Therefore we initiated the development study of the UHV techniques which enable us to make homemade instruments evacuated to UHV. We have constructed a test chamber made of stainless steel, which is 200 mm ϕ in diameter and 800 mm long. The surface of the chamber was etched electrolytically. The chamber is pumped with a 110 l/s sputter ion pump and a titanium sublimation pump. The pressure reached $\sim 10^{-10}$ Torr, after 24 hours baking at 250°C. We are preparing for argon discharge cleaning in order to attain the 10^{-12} Torr vacuum. In near future, we will test usability of various kinds of metal gaskets and measure the outgassing rate of a large number of materials.

A Device for Manipulation of Air- and/or Moisture-sensitive Compounds in the Single Crystal X-ray Analyses

Tasuku ITO* and Koshiro TORIUMI

For designing new molecules having interesting chemical and physical properties, it is necessary and desirable to determine the crystal and molecular structures of their related compounds by X-ray diffraction. Chemically interesting materials such as functional transition metal complexes, metal complexes with unusual valence states, and reaction intermediates are often air- or moisture-sensitive. Usually the X-ray analyses of such compounds accompany with technical difficulties, because the crystals must be handled under an inert and dry atmosphere. To solve the problems, we have constructed a device which consists of a stereomicroscope and a high-sensitive television camera system (Figure 1). The apparatus is designed to be assembled and used in an argon box (Dri-lab glove box, Vacuum Atmospheres Corp).



Currently, we are applying this apparatus to the single crystal X-ray analyses of macrocyclic complexes which show spin-state variations or have unusual valence states (See Research Activities V—D and V-E-1).

Molecular Design and Synthesis of Highly Efficient Organotransition Metal Catalysts.

Akira MIYASHITA, Arata YASUDA, and Hidemasa TAKAYA*

We have reported the synthesis of 2,2'-bis-(diphenylphosphino)- 1,1'-binaphthyl (abbreviated to BINAP), a new type of chiral bis(triaryl)-phosphine ligand,¹⁾ and the molecular structure determination of $[\text{Rh}(+)\text{BINAP}(\text{nbd})]\text{-ClO}_4$ (nbd = norbornadiene) by the X-ray crystallographic analysis.²⁾ This time, the high efficiency of the chiral Rh(I) — BINAP complexes as a catalyst for asymmetric hydrogenation has been demonstrated by the synthesis of various amino acids from α -acylaminoacrylic acids in very high optical purity (65 — 100% ee). The ^{31}P NMR measurements revealed the mechanism of the asymmetric hydrogenations and the factors controlling the enantioselectivity. Results are summarized in VI-D-1.

References

- 1) H. Takaya, T. Souchi, A. Yasuda, and R. Noyori, *IMS Ann. Rev.*, 92(1978).
- 2) K. Toriumi, T. Ito, and H. Takaya, *IMS Ann. Rev.*, 118(1979).

(2) Investigation of Energy Conversion Processes at the Molecular Level

"The Energy Conversion in Ion-Molecule Reactions"

***Inosuke KOYANO, Kenichiro TANAKA, and Tatsuhisa KATO**

The purpose of this project has been to elucidate the evolution of specific forms of reactant energy and reaction exoergicity to specific forms of product energy in elementary reactions. To pursue this evolution in ion-molecule reactions, reactions of state-selected molecular ions have been studied at specified translational energies. The apparatus "TEPSICO" which has been constructed for this purpose and its performance have been described previously. (See IMS Ann. Rev. 1978, pp. 73 and 104)

Following the studies of vibrational state selection reported previously (IMS Ann. Rev. 1979, p.151), selection of spin-orbit coupling states has successfully been performed in the reaction $\text{Ar}^+(\text{}^2\text{P}_1) + \text{H}_2(\text{D}_2) \rightarrow \text{ArH}^+(\text{ArD}^+) + \text{H}(\text{D})$. It has been found that the excited $\text{}^2\text{P}_{1/2}$ state reacts with H_2 1.5 times faster than the $\text{}^2\text{P}_{3/2}$ ground state. The reaction $\text{H}_2^+(\text{v}) + \text{Ar}$ has also been studied and the resonant enhancement of the charge transfer channel (forming $\text{H}_2 + \text{Ar}^+$) has been observed at $\text{v} = 2$. (See Research Activities IV—E)

Picosecond Transient Behavior of the Reaction-Center Particles of Photosystem I Isolated from Spinach Chloroplast.

I. Decay Characteristics of Excited Chlorophylls.

II. Energy Transfer and Electron Transfer at Weak Light Excitation.

Akira NAMIKI, Keiji KAMOGAWA, Nobuaki NAKASHIMA, Keitaro YOSHIHARA,* and Isamu IKEGAMI (Tikyo Univ.)

See Research Activities III-C-2, and III-C-3.

Hydrogen Evolution from Water and Natural Resources by Heterogeneous Photocatalytic Reactions

Tomoji KAWAI, Kazuhito HASHIMOTO, and Tadayoshi SAKATA*

Surface modification of powdered TiO_2 by Pt, Rh, Pd or RuO_2 increased remarkably the photocatalytic activity. One of these photocatalysts, $\text{RuO}_2/\text{TiO}_2/\text{Pt}$ decomposes water, even though the quantum yield of the reaction is low ($\sim 2 \times 10^{-4}$). When alcohols or various organic compounds are added to the aqueous suspension of these photocatalysts, the hydrogen evolution rate is increased enormously under band-gap irradiation. For the decomposition of methanol, quantum yield of hydrogen evolution exceeds 50%. In these photocatalytic reactions, water were found to work as an oxidizing agent. This new method would be applied to the hydrogen production from various biomasses if one could succeed in exploiting a new photocatalyst which works efficiently with visible light. (See Research Activities III—D)

IR-IR Double Resonance Using a Tunable Diode Laser for Investigation of Collisional Energy Transfers in Polyatomic Molecules

Michio TAKAMI (Inst. Phy. Chem. Res. and IMS)

In infrared-infrared double resonance, a non-Boltzmann population distribution produced by an intense infrared pumping radiation is monitored by another probing infrared radiation. This method is permanent dipole moment prevents the application of other methods such as infrared-microwave double resonance. As the first stage of such works, double resonance and high resolution infrared spectroscopy of the CF_4 ν_3 fundamental was performed using a tunable diode laser. Many pure rotational transitions of CF_4 in the ν_3 excited state, which were allowed by a small vibrationally-induced dipole moment, were observed by infrared-radiofrequency and infrared-microwave double resonance. The double resonance measurement also made it possible to analyze the badly overlapped ν_3 Q-branch spectrum of CF_4 . Many accurate molecular constants were determined from the experimental results.

OKAZAKI CONFERENCES

"Okazaki Conferences" are principal symposia at IMS, which are held on the subjects related to the "Special Research Projects". They are held usually twice a year, with a moderate number of participants around 50, including several invited foreign speakers. The formal language for the conference is English. Eight conferences have been already held successfully. Outlines of the ninth and tenth conferences are as follow

The Ninth Okazaki Conference

Molecular Designing of Reactive Intermediates — A Case of Carbenes (January 7—9, 1980)

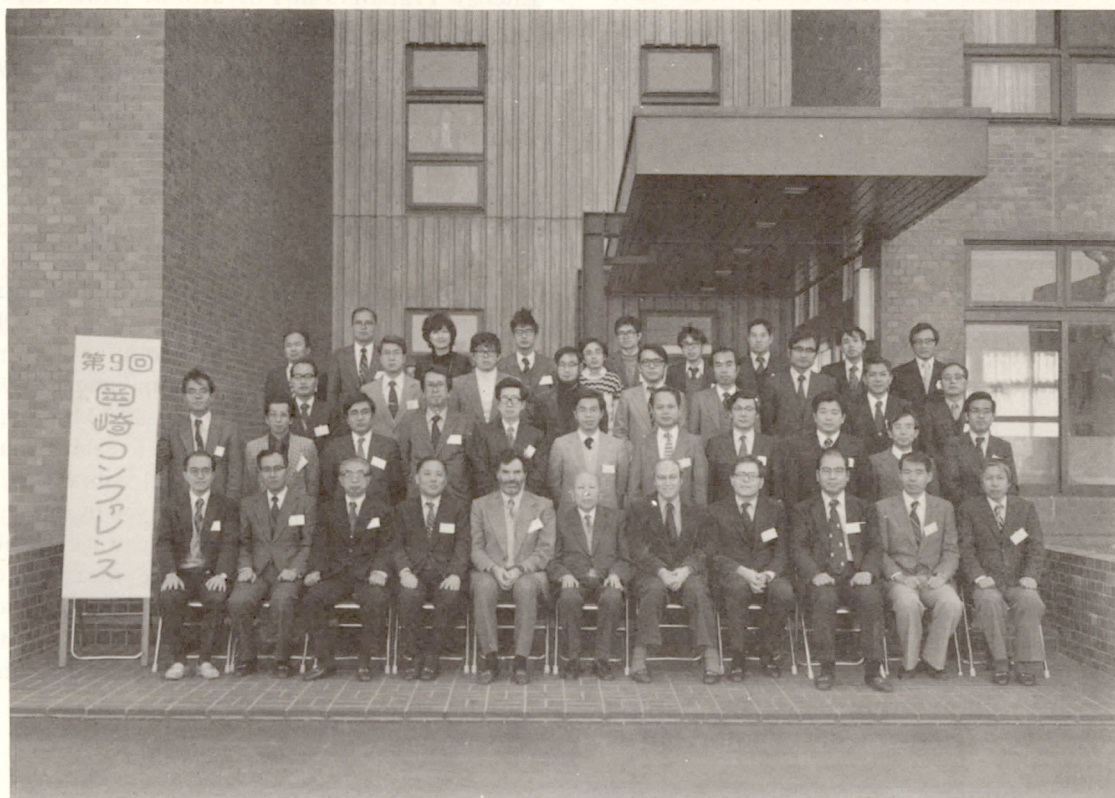
Organizer: H. Iwamura (*IMS*)

Invited Speakers: R. A. Moss (*Rutgers*), M. Jones, Jr. (*Princeton Univ.*) and P. P. Gaspar (*Washington Univ.*)

Just as molecular designing of stable molecules is made for getting interesting and useful materials, so molecular designing of reactive intermediates could lead to development and control of chemical reactions of interest. In this conference due attention was paid to carbenes (:CH_2 and its derivatives) which can show many facets of reactivity, namely carbocationic, carbanionic and

diradical characters. About fifty scientists actively engaged in the structural theory, spectroscopy, reaction mechanistic studies, studies of reactions of synthetic values, and so on participated in the conference.

Professor Moss proposed a unifying theory on structure vs. reactivity relationships. His selectivity index m_{CXY} for a wide variety of carbenes :CXY drew experimental support from ^{17}O NMR chemical shift data of tungsten carbonyl complexes such as $(\text{OC})_5\text{W:CXY}$ by the IMS group. The electronic states, structures and reactivities of the silicon and germanium analogs of carbenes were discussed by Professor Gaspar. The design of carbene species as high energy intermediates in the synthesis of novel strained molecules was beautifully elaborated by Professor M. Jones, Jr. Lively discussions were devoted to the formation of carbene complexes with metals to give new intermediates for versatile purposes.



The Ninth Okazaki Conference Jan. 7—9, 1980

The Tenth Okazaki Conference

Excitons in Molecular Crystals — from the Viewpoint of Transport Processes

(February 3—6, 1980)

Organizers: H. Inokuchi (*IMS*) and M. Sano (*Univ. of Electro-Communication & IMS*)

Invited Speakers: H. C. Wolf (*Univ. of Stuttgart*), G. J. Sloan (*de Pont de Nemours, Wilmington*) and A. Zewail (*California Inst. of Technology*)

Excitons in molecular crystals have long been studied both experimentally and theoretically. Recently a deeper understanding has been

obtained, due to the developments of new experimental techniques and the efforts to establish a unified theoretical view including also other kind of compounds such as ionic compounds and semiconductors. On the occasion of the stay of Professor D. Fox (State Univ. of New York), one of the pioneers in this field, at IMS, this Conference was arranged to review these developments and to get insight into the future trends. Stimulating discussions were devoted not only to excitons in molecular crystals, but also to excitons in inorganic crystals or amorphous molecular solids, and charge carriers in organic crystals. The Conference was closed with an impressive talk by Dr. Sloan about the purification and crystal growth of molecular crystals, based on his long experience at du Pont.



The Tenth Okazaki Conference Feb. 3—6, 1980

JOINT STUDIES PROGRAMS

As one of the important functions of an inter-university research institution, IMS undertakes joint studies programs for which funds are available to cover research expenses as well as travel and living expenses of individuals. The proposals from domestic scientists are reviewed and controlled by the inter-university committee. The programs are carried out under one of four categories:

- 1) Joint Studies on special projects (a special project of significant relevance to the advancement of molecular science can be carried out by a team of several groups of scientists).
- 2) Research Symposia (on timely topics in collaboration with both outside and IMS scientists).
- 3) Cooperative Research (carried out in collaboration with both outside and IMS scientists).
- 4) Use of Facility (the Computer Center, Instrument Center and other research facilities at IMS are open to all researchers throughout the country).

In the fiscal year 1979, numbers of joint studies programs accepted amounted to 5, 16, and 162 for categories 1) ~ 3), respectively.

1) Joint Studies

Accurate Determination of Electron-Density Distribution in Crystals and Developments of Techniques for Improving Accuracy

Coordinators: Yoshihiko SAITO (Univ. of Tokyo),
Tasuku ITO (Division of Applied Molecular Science)

A gas-stream cooling device for four-circle diffractometer was designed and made on experimental basis in order to collect accurate intensity data at low temperature. This development was performed by the Tokyo group during 1978—1979. An improved version of this device was constructed and installed at IMS. Prior to designing a new cooling device at IMS, meetings concerning improvements of a cooling device and a low-temperature measurement were held twice at IMS in 1979. In the meetings, some basic problems on a low-temperature measurement, such as temperature control and ice formation on a crystal specimen, were discussed and some useful advices on a gas-stream cooling device were pointed out. An efficient cooling device was designed and constructed at IMS. In this system, a stream of cold gas, generated by boiling a liq. N₂, is directed over the sample. In order to achieve a precise temperature control of a cold gas stream, a gas generator is continually refilled by liq. N₂, transported through an insulated transfer tube from a 100L strage vessel, keeping liq. N₂ level constant. At the steady state, the temperaure can be nicely maintained within the range of ± 1 K at 100K. The cold gas transfer line, made up of a flexible metal transfer tube, makes possible to locate its

nozzle at the most suitable position to the crystal specimen.

Developments and Applications of New Spectroscopic Methods Using Tunable, Coherent, and High-Resolution Light Sources

Coordinators: Eizi HIROTA (Division of Molecular Structure)
Shuji SAITO (Division of Molecular Structure)

According to a suggestion of Prof. F. Shimizu (Univ. of Tokyo) a high-precision wavelength meter was set up, which allows us to determine the wavelength of diode laser light to a precision of 10^{-7} . Two coherent and high-resolution light sources have been combined to develop double-resonance spectroscopic techniques. Microwave-optical double resonance was successfully applied to HNO [Prof. K. Takagi (Toyama Univ.) and S. Saito], infrared (CO₂/N₂O laser) optical double resonance to NH₂ [Dr. T. Amano (Univ. of Tokyo), K. Kawaguchi, M. Kakimoto, and S. Saito], and microwave infrared (diode laser) double resonance to CF₄ [Dr. M. Takami (IPCR and IMS)].

Activity of Hydrogenase: Physico—chemical properties of Cytochrome c₃

Coordinators: Hiroo INOKUCHI (Division of Molecular Assemblies)
Tatsuhiko YAGI (Shizuoka University)

The following works were carried out; (1) electrical conductivity measurement of an anhydrous cytochrome c_3 film as function of temperature and ambient pressure, (2) preparation of cytochrome c_3 single crystal for the crystal structural analysis, (3) observation of direction reduction of oxygen to water catalyzed by cytochrome c_3 , and (4) kinetic study of cytochrome c_3 reduction with hydrogenase by means of Mössbauer effect measurement.

In the work of (3), we found that cytochrome c_3 catalyzes the electrochemical reduction of oxygen from two-electron pathway via hydrogen peroxide to four-electron pathway directly to water at mercury electrode in neutral phosphate buffer solution.

Construction of Ab Initio Force Field and Its Application to Molecular Science

Coordinators: Eiji ŌSAWA (Hokkaido Univ.)

The project consists of two parts. The first part is a preliminary attempt to construct empirical force field model based entirely on the results of *ab initio* molecular orbital calculations instead of relying upon insufficient experimental data especially for hetero-atom systems. Simple hydrocarbons up to four carbon atoms have been subjected to calculations using GAUSSIAN 70 package with complete geometry optimization. The second part concerns the applications of empirical potential calculations with existing force fields to various practical problems of organic chemistry. Both parts gave progress which would have been impossible in other institutes. Results will be published upon completion.

Electronic Structure of Solid Surfaces and Surface Chemical Reactions

*Coordinators: Masaru ONCHI (Kyoto Univ.)
Iwao YASUMORI (Tokyo Inst. of Tech.)*

Recently, thanks to the development of new techniques, reliable experimental informations on the surface electronic structure have been accumulated. On the other hand, a powerful method called DV- $X\alpha$ cluster method has been developed for the theoretical study of surface systems.

Through discussions of all the members in the joint study, several problems with fundamental importance were chosen to be studied by the DV-

$X\alpha$ calculation. These subjects include the chemisorption systems such as Zn/O, V, Cr, Fe, Mo/O, and Pd/S. The numerical works have been carried out at the IMS Computer Center by several groups of the joint study. The results were analyzed and discussed by all the members and the future prospects of the study was explored. Some of the results are reported in "Research Activities I—E,F".

2) Research Symposia

Under this program 16 symposia were held during the fiscal year of 1979. The first two symposia are the satellite meetings of the international conferences held in Japan as shown below.

1. Dynamics of Molecular Collisions*
(September 6th — 7th, 1979)
Organizers: K. Kuchitsu (Univ. of Tokyo), I. Kusunoki (Tohoku Univ.) and K. Morokuma (IMS)
No. of Participants: 70
No. of Foreign Participants: 30.
2. Theoretical Aspects of Chemical Reactions and Molecular Interactions*
(November 5th — 6th, 1979)
Organizers: T. Fueno (Osaka Univ.), S. Iwata (Inst. Phys. Chem. Res. and IMS) and K. Morokuma (IMS)
No. of Participants: 80
No. of Foreign Participants: 40.
3. Development of Large Scale Programs and Languages for Molecular Science
(May 25th — 26th, 1979)
Organizer: H. Kashiwagi (IMS)
No. of Participants: 35.
4. Application of Lasers to Chemical Reactions
(July 2nd — 3rd, 1979)
Organizer: K. Yoshihara (IMS)
No. of Participants: 50.
5. Intermolecular Interactions in Solutions
(July 12th — 13th, 1979)
Organizer: H. Ohtaki (Tokyo Inst. of Tech.)
No. of Participants: 40.
6. Solar Energy Storage and Conversion*
(October 23rd, 1979)
Organizer: H. Inokuchi (IMS)
No. of Participants: 60
No. of Foreign Participants: 3.
7. Physics and Chemistry of Layered Compounds
(November 21st — 22nd, 1979)
Organizer: M. Sano (IMS and Univ. of Electro-commun.)
No. of Participants: 35.

8. Micelles Including Membranes and Vesicles — Structures and Properties
(November 30th — 31st, 1979)
Organizer: A. Kitahara (Science Univ. of Tokyo)
No. of Participants: 30.
9. Ultraviolet Synchrotron Orbital Radiation Source
(December 17th — 18th, 1979)
Organizer: K. Kimura (IMS)
No. of Participants: 66.
10. What should be the Future Research Projects in Molecular Science?
(December 22nd, 1979)
Organizer: H. Akamatsu (IMS)
No. of participants: 33.
11. Purification and Crystal Growth for Molecular Crystals
(February 7th, 1980)
Organizer: M. Sano (IMS and Univ. of Electro-commun.)
No. of Participants: 20
No. of Foreign Participants: 3.
12. Primary Photochemical Processes of Benzene, Substituted Benzenes and Azabenzenes
(February 14th — 15th, 1980)
Organizer: K. Yoshihara (IMS)
No. of Participants: 30.
13. Theoretical and Experimental Approaches to the Understanding of Chemical Reactivities
(February 22nd — 23rd, 1980)
Organizer: J. Hayami (Kyoto Univ.)
No. of Participants: 40.
14. Structure and Function of Synthetic Macrocyclic Complexes
(March 14th — 15th, 1980)
Organizer: T. Ito (IMS)
No. of Participants: 20.
15. Application of Molecular Beam Techniques to Photochemistry
(March 14th — 15th, 1980)
Organizer: K. Kimura (IMS)

No. of Participants: 45.

16. Development and Application of High-Performance and Large Scale Lasers
(March 15th, 1980)
Organizer: E. Hirota (IMS)
No. of Participants: 9.

* Official language for this symposium: English.

3) Cooperative Research

This is probably one of the most important joint studies programs IMS undertakes for conducting its own research as well as the research of the common interest to both outside and IMS scientists by using the facilities at IMS. During the first half of the fiscal year of 1979 ending on September 30, 1979, 92 outside scientists including 16 invited collaborated with IMS scientists, and during the second half of the fiscal year of 1979, 72 outside scientists including five invited worked in collaboration with IMS scientists. The names and the affiliations of these collaborators are found in the Research Activities.

4) Use of Facility

The number of projects accepted for the Use of Facility Program of the Computer Center during the fiscal year of 1979 amounted to 92 (185 users), and the computer time spent for these projects is 2,279 hours (38% of the total annual CPU time).

Fifty four projects were accepted for the Use of Facility Program of the Instrument Center during the fiscal year of 1979.

SATELLITE MEETINGS FOR INTERNATIONAL CONFERENCES

1) Dynamics of Molecular Collisions (September 6—7, 1979)

Organizers: Kozo KUCHITSU (*Univ. Tokyo*),
Isao KUSUNOKI (*Tohoku Univ.*)
and Keiji MOROKUMA (*IMS*)

This symposium was held as a satellite meeting for the 11th International Conference on the Physics of Electronic and Atomic Collisions, held in Kyoto for August 29-September 4. ICPEAC is a huge conference with a wide range of interest converging electronic, atomic, ionic and molecular collisions with an energy range of sub-eV to above KeV. The purpose of this symposium is to bring together experimentalists and theorists of chemical interest and stimulate discussions in an informal atmosphere. Thirty overseas participants and over forty domestic participants packed the IMS seminar room. Invited speeches were: P. J. Dagdigian (Johns Hopkins; Experimental and theoretical studies of rotational energy transfer involving lithium hydride), U. Buck (MPI Göttingen; Differential cross sections for rotational transition of hydrogen molecules), J. P. Toennies (MPI Göttingen; Vibrational excitation of CH₄, CF₄ and SF₄ molecules by H⁺ and Li⁺ ions at E_{CM} = 5–10 eV), J. Los (Amsterdam; Vibronic excitation via charge-transfer), K. Shobatake (IMS; Crossed beam study of the reaction: F + D₂ → FD + D), A. Schulz (Freiburg; Spectroscopic investigations of reactive collisions. Interpretation by trajectory calculations), Ch. Ottinger (MPI Göttingen; Luminescence from ion-molecule collisions at low energy), S. Tsuchiya (Tokyo; Energy partitioning in reactions of excited mercury atoms), T. F. George (Rochester; The Interaction of Laser radiation with molecular collision processes), W. R. Gentry (Minnesota; Merged molecular beam studies of electronically nonadiabatic chemical reactions), J. Durup (Orsay; Short-distance and long-distance coupling studies by half-collision experiments) and K. Morokuma (IMS, Potential energy characteristics and chemical reaction dynamics). In addition, there were many contributed papers and informal discussions.

2) Theoretical Aspects of Chemical Reactions and Molecular Interactions (November 5—6, 1979)

Organizers: Takayuki FUENO (*Osaka Univ.*),
Suehiro IWATA (*Inst. Phys. Chem.
Res. and IMS*) and Keiji MOROKUMA (*IMS*)

The 3rd International Congress of Quantum Chemistry was held in Kyoto for October 29-November, 3 1979 and attracted over 650 theorists and experimentalists including over 150 from abroad. This symposium was one of five associated symposia held in conjunction with ICQC. It was attended by about 40 overseas participants from 15 countries as well as 40 domestic participants. The theme of this symposium was understanding of mechanism of chemical reactions and molecular interactions from point of view of the electronic structure theory.

Speakers were H. Johansen (Lyngby; electrostatic potential in transition metal complexes), M. D. Newton (Brookhaven; MO models for aqueous electron transfer), A. Tachibana (Kyoto; intrinsic reaction coordinate), E. Lindholm (Stockholm; HAM3 semiempirical MO method), Hopper (Dayton; HeH⁺ potential surface), Pople (Pittsburgh; energy gradient with electron correlation), M. Dupuis (Berkeley; alkyl free radical), L. Tomasi (Pisa; electrostatic potential), A. Komornicki (Sunnyvale; reactions of OH radicals), S. Kato (Okazaki; MCSCF energy gradient), S. Yamabe (Nara; reactivity of azo compounds), W. T. Borden (Seattle; trimethylene and Jahn-Teller effect), K. Tanaka (Sapporo; HCO potential surfaces), M. S. Gordon (North Dakota; excited states of hydrocarbons), V. Bonacic-Koutecky (Berlin; sudden polarization in polyene excited states), J. J. C. Mulder (Leiden; polyene excited states), M. Yoshimine (San Jose; Wolff rearrangement of C₂H₂O), T. Fueno (Osaka; C₂H₄ + H rate and isotope effects), I. G. Csizmadia (Toronto; triplet methyl ethane), T. Tezuka (Tsukuba; photocyclization of cycloheptatrienes) and K. N. Houk (Baton Rouge; stereoisomeric imine anions). Other overseas participants included Goscinski (Uppsala), Kutzelnigg (Bochum), Lee (Berkeley), Parr (Chapel Hill), Pyykko (Abo) and Ruedenberg (Iowa).

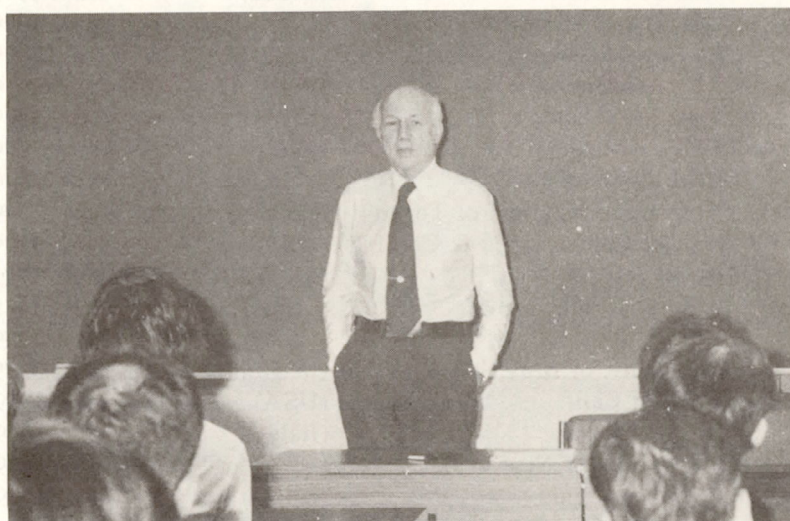
FOREIGN SCHOLARS

Visitors from abroad play an essential role in research activities and always welcome at IMS. The following is the list of foreign scientists who visited IMS in the past year (Aug. 1979 - July 1980). The sign *1 indicates a visitor invited to attend an Okazaki Conference, and *2 indicates a visitor on the Invited Foreign Scholars Program, and *3 a counsellor of IMS.

Prof. W. H. Miller	Univ. of Calif. Berkeley	(USA)	Aug. & Sept. 1979
Prof. J. Durup ^{*2}	Univ. of Paris-Sud	(France)	Aug. — Dec. 1979
Prof. R. C. Woods	Univ. of Wisconsin	(USA)	Aug. — Sept. 1979
Prof. A. J. Merer	Univ. of British Columbia	(Canada)	Aug. 1979
Prof. R. N. Dixon	Univ. of Bristol	(United Kingdom)	Aug. — Sept. 1979
Prof. A. Carrington	Univ. of Southampton	(United Kingdom)	Aug. — Sept. 1979
Dr. M. E. Jacox	NBS	(USA)	Aug. 1979
Dr. M. Nakashima	Natick Lab.	(USA)	Aug. 1979
Prof. K. V. L. N. Sastry	Univ. of New Brunswick	(Canada)	Aug. — Sept. 1979
Prof. R. W. Field	Mass. Inst. of Tech.	(USA)	Aug. — Sept. 1979
Prof. P. -M. Guyon	Univ. of Paris-Sud	(France)	Sept. 1979
Prof. B. A. Thrush	Univ. of Cambridge	(United Kingdom)	Sept. 1979
Prof. R. F. Curl	Rice Univ.	(USA)	Sept. 1979
Prof. K. H. Welge	Univ. of Bielefeld	(W. Germany)	Sept. 1979
Dr. A. R. W. Mckellar	National Research Council	(Canada)	Sept. 1979
Dr. F. Mies	NBS	(USA)	Sept. 1979
Prof. D. Wöhrle	Univ. of Bremen	(W. Germany)	Sept. 1979
Prof. H. Ehrhardt	Univ. of Kaiserslautern	(W. Germany)	Sept. 1979
Prof. J. M. Morris	Perth Inst. of Tech.	(Australia)	Sept. — Oct. 1979
Dr. D. A. Ramsay	National Research Council	(Canada)	Sept. 1979
Prof. A. R. H. Cole	Univ. of Western Australia	(Australia)	Sept. 1979
Prof. E. N. Maslen	Univ. of Western Australia	(Australia)	Sept. 1979
Dr. K. M. Evenson	NBS	(USA)	Sept. 1979
Prof. H. E. Radford	Harvard Observatory	(USA)	Sept. 1979
Prof. K. Bergmann	Univ. of Kaiserslautern	(W. Germany)	Sept. 1979
Dr. U. Buck	Max-Planck-Institut	(W. Germany)	Sept. 1979
Dr. Chung-Hsuan Chen	Oak Ridge Natl. Lab.	(USA)	Sept. 1979
Dr. M. J. Coggiola	SRI International	(USA)	Sept. 1979
Prof. Hao-Lin Chen	Lawrence Livermore Lab.	(USA)	Sept. 1979
Prof. P. J. Dagdigan	Johns Hopkins Univ.	(USA)	Sept. 1979
Prof. D. G. Fleming	Univ. of British Columbia	(Canada)	Sept. 1979
Prof. T. F. George	Univ. of Rochester	(USA)	Sept. 1979
Prof. W. R. Gentry	Univ. of Minnesota	(USA)	Sept. 1979
Dr. K. T. Gillen	SRI International	(USA)	Sept. 1979
Prof. I. V. Hertel	Free Univ. of Berlin	(W. Germany)	Sept. 1979
Dr. J. M. Launay	Observatoire de Paris	(France)	Sept. 1979
Prof. Hsi-Hu Lo	Pittsburg State Univ.	(USA)	Sept. 1979
Prof. J. Los	FOM Inst. of Atom. & Mol. Phys.	(Netherlands)	Sept. 1979
Prof. A. Rieker ^{*2}	Univ. of Tübingen	(W. Germany)	Sept. — Nov. 1979
Dr. A. G. Giardini	CNEN, Rome	(Italy)	Sept. 1979
Dr. W. Schepper	Univ. of Bielefeld	(W. Germany)	Sept. 1979
Prof. K. T. Tang	Pacific Lutheran Univ.	(USA)	Sept. 1979
Prof. J. Weiner	Univ. of Maryland	(USA)	Sept. 1979
Prof. R. M. Martin	Univ. of California	(USA)	Sept. 1979
Prof. J. Momigny	Univ. of Liege	(Belgium)	Sept. 1979
Dr. Ch. Ottinger	Max-Planck-Institut	(W. Germany)	Sept. 1979
Dr. J. Shaefer	Max-Planck-Institut	(W. Germany)	Sept. 1979

Dr. A. Schultz	Univ. of Freiburg	(W. Germany)	Sept. 1979
Dr. J. P. Toennies	Max-Planck-Institut	(W. Germany)	Sept. 1979
Prof. A. J. Yencha	State Univ. of New York	(USA)	Sept. 1979
Dr. T. Oka	National Research Council	(Canada)	Oct. 1979
Prof. M. Calvin ^{*3}	Univ. of California, Berkeley	(USA)	Oct. 1979
Prof. N. K. Ray	Univ. of Delhi	(India)	Oct. — Nov. 1979
Prof. R. G. Parr ^{*2}	Univ. of North Carolina	(USA)	Oct. — Nov. 1979
Prof. M. Kasha ^{*2}	Florida State Univ.	(USA)	Oct. 1979
Prof. H. S. Taylor	Univ. of Southern California	(USA)	Oct. 1979
Prof. Y. T. Lee	Univ. of California, Berkeley	(USA)	Nov. 1979
Prof. F. Woldbye	Tech. Univ. of Denmark	(Denmark)	Nov. 1979
Prof. F. L. Vogel	Univ. of Pennsylvania	(USA)	Nov. 1979
Dr. E. A. Silinsh	Latvian S.S.R. Acad. of Sci.	(USSR)	Nov. 1979
Prof. K. K. Shvarts	Latvian S.S.R. Acad. of Sci.	(USSR)	Nov. 1979
Dr. M. Dupuis	Lawrence Berkeley Lab.	(USA)	Nov. 1979
Dr. A. Komornicki	Ames Research Center	(USA)	Nov. 1979
Prof. I. G. Csizmadia	Univ. of Toronto	(Canada)	Nov. 1979 & Apr. 1980
Prof. W. T. Borden	Univ. of Washington	(USA)	Nov. 1979
Prof. T. C. Chang	National Cheng Kung Univ.	(Taiwan)	Nov. 1979
Prof. C. Chen	Chung-Cheng Inst. Tech.	(Taiwan)	Nov. 1979
Prof. S. Y. Chu	National Tsing Hua Univ.	(Taiwan)	Nov. 1979
Prof. M. S. Gordon	North Dakota State Univ.	(USA)	Nov. 1979
Prof. O. Goscinski	Univ. of Uppsala	(Sweden)	Nov. 1979
Dr. D. G. Hopper	Science Applications	(USA)	Nov. 1979
Prof. K. N. Houk	Louisiana State Univ.	(USA)	Nov. 1979
Prof. H. Johansen	Tech. Univ. of Denmark	(Denmark)	Nov. 1979
Prof. G. Karlström	Univ. of Lund	(Sweden)	Nov. 1979
Prof. H. F. King	State Univ. of New York	(USA)	Nov. 1979
Prof. Y. S. Kiang	Kiring Univ.	(China)	Nov. 1979
Prof. J. Koutecky	Free Univ. of Berlin	(W. Germany)	Nov. 1979
Dr. V. Koutecky	Free Univ. of Berlin	(W. Germany)	Nov. 1979
Prof. W. Kutzelnigg	Ruhr Univ. at Bochum	(W. Germany)	Nov. 1979
Prof. A. Laforgue	Univ. of Reims	(France)	Nov. 1979
Prof. J. W. McIver	State Univ. of New York	(USA)	Nov. 1979
Prof. T. C. Lee	National Tsing-Hua Univ.	(Taiwan)	Nov. 1979
Prof. J. J. C. Mulder	State Univ. of Leiden	(Netherlands)	Nov. 1979
Prof. D. Li	Lanchow Univ.	(China)	Nov. 1979
Dr. M. D. Newton	Brookhaven National Lab.	(USA)	Nov. 1979
Prof. J. A. Pople	Carnegie Mellon Univ.	(USA)	Nov. 1979
Dr. P. Pyykko	Abo Academy	(Finland)	Nov. 1979
Prof. K. Ruedenberg	Iowa State Univ.	(USA)	Nov. 1979
Prof. U. Tomasi	Univ. of Pisa	(Italy)	Nov. 1979
Dr. M. Yoshimine	IBM San Jose Lab.	(USA)	Nov. 1979
Prof. J. S. Kwiatkowski	N. Copernicus Univ. of Torun	(Poland)	Nov. 1979
Prof. Yu. N. Molin	Inst. of Chem. Kinet. & Combust.	(USSR)	Nov. 1979
Prof. E. Lindholm	Royal Inst. of Tech.	(Sweden)	Nov. 1979
Prof. R. Z. Liu	Beijing Normal Univ.	(China)	Nov. 1979
Prof. C. C. Sun	Kirin Univ.	(China)	Nov. 1979
Prof. G. Verhaegen	Free Univ. of Brussels	(Belgium)	Nov. 1979
Prof. K. C. Kim	Univ. of Calif.	(USA)	Dec. 1979
Prof. M. Spoliti	Univ. of Rome	(Italy)	Dec. 1979
Prof. D. Fox ^{*2}	State Univ. of New York	(USA)	Dec. 1979 — Mar. 1980
Dr. D. Myung-Ki	Yeungnam Univ.	(Korea)	Dec. 1979
Prof. N. F. Stepanov	Moscow M. V. L. State Univ.	(USSR)	Dec. 1979
Prof. K. J. Kaufmann	Univ. of Illinois, Urbana	(USA)	Jan. 1980
Dr. W. R. Workman	Central Research Laboratories	(USA)	Jan. 1980
Prof. N. M. Emanuel	Inst. of Chem. Acad. Sinica	(USSR)	Jan. 1980
Prof. G. E. Zaikov	Inst. of Chem. Acad. Sinica	(USSR)	Jan. 1980

Dr. E. Y. Topygin	Inst. of Chem. Acade. Sinica	(USSR)	Jan. 1980
Prof. G. Pimentel	National Science Foundation	(USA)	Jan. 1980
Prof. R. A. Moss ^{*1}	Rutgers Univ.	(USA)	Jan. 1980
Prof. P. P. Gaspar ^{*1}	Univ. of Washington	(USA)	Jan. 1980
Prof. M. Jones, Jr. ^{*1}	Princeton Univ.	(USA)	Jan. 1980
Prof. H. C. Wolf ^{*1}	Univ. of Stuttgart	(W. Germany)	Feb. 1980
Dr. G. J. Sloan ^{*1}	E. I. du Pont de Nemours & Co.	(USA)	Feb. 1980
Prof. A. Zewail ^{*1}	California Inst. of Tech.	(USA)	Feb. 1980
Dr. Cao Yong	Inst. of Chem. Acade. Sinica	(China)	Feb. 1980
Dr. J. T. Hougen	NBS	(USA)	Feb. — Apr. 1980
Dr. R. L. Jaffe	NASA Ames Research Center	(USA)	Feb. — Apr. 1980
Dr. S. R. Mosier	National Science Foundation	(USA)	Feb. 1980
Dr. E. A. Ashby	National Science Foundation	(USA)	Feb. 1980
Prof. R. L. Byer	Stanford Univ.	(USA)	Feb. 1980
Prof. Chen Yixuan	Dalian Inst. of Chem. Phys.	(China)	Apr. 1980
Prof. T. W. Hänsch	Stanford Univ.	(USA)	Apr. 1980
Prof. P. S. Song	Texas Tech. Univ.	(USA)	Apr. 1980
Prof. D. Banerjee	Univ. of Calcutta	(India)	Apr. 1980
Prof. B. Douglas	Univ. of Pittsburg	(USA)	May 1980
Prof. S. R. Hartmann	Columbia Univ.	(USA)	May 1980
Prof. K. Schulten	Max-Planck-Institut	(W. Germany)	May 1980
Prof. R. H. Grubbs	California Inst. of Tech.	(USA)	June 1980
Prof. R. Maurel	CNRS, Univ. of Poitiers	(France)	June 1980
Prof. W. A. Little	Stanford Univ.	(USA)	June 1980
Prof. Chen Nian-Yi	Shanghai Inst. of Metallurgy	(China)	June 1980
Dr. Jin Da Kang	Shanghai Inst. of Metallurgy	(China)	June 1980
Dr. Zheng Long-Zhi	Shanghai Inst. of Metallurgy	(China)	June 1980
Prof. J. Manassen	Weizmann Institute of Science	(Israel)	July 1980
Prof. G. N. Schrauzer	Univ. of California, San Diego	(USA)	July 1980
Dr. O. Inganäs	Linköping Inst. of Tech.	(Sweden)	July 1980
Mr. T. W. Ebbesen	Chaire de Biophysique	(France)	July 1980
Prof. Pichat	Inst. de Recherche sur la Catalyse	(France)	July 1980
Prof. Fraissard	Univ. P. M. Curie	(France)	July 1980
Prof. M. M. Labes	Temple Univ.	(USA)	July 1980



Prof. M. Calvin at IMS (Oct. 1979)

LIST OF PUBLICATIONS

- S. NAGASE, T. FUENO and K. MOROKUMA, "An Ab Initio Approach to Organic Reaction Rates. Kinetic Isotope Effects in the Reaction $\text{H} + \text{C}_2\text{H}_4 \rightarrow \text{C}_2\text{H}_5$ ", *J. Am. Chem. Soc.*, **101**, 5849 (1979).
- J. O. NOELL and K. MOROKUMA, "The Relative Stability of Bent and Linear Coordination of the Nitrosyl Ligand in Nitrosylpentaamminecobalt (III), $\text{Co}(\text{NH}_3)_5\text{NO}^{+2}$. An ab initio Investigation", *Inorg. Chem.*, **18**, 2774 (1979).
- H. F. KING and K. MOROKUMA, "Theory of the Rydberg Spectrum of Triatomic Hydrogen", *J. Chem. Phys.*, **71**, 3213 (1979).
- S. KATO and K. MOROKUMA, "Potential Energy Characteristics and Energy Partitioning in Chemical Reactions: Ab Initio MO Study of $\text{H}_2\text{CCH}_2\text{F} \rightarrow \text{H}_2\text{CCHF} + \text{H}$ Reaction", *J. Chem. Phys.*, **72**, 206 (1980).
- K. YAMAGUCHI, S. YABUSHITA, T. FUENO, S. KATO and K. MOROKUMA, "Geometry Optimization of the Ring-Opened Oxirane Diradical: Mechanism of the Addition Reaction of the Triplet Oxygen Atom to Olefins", *Chem. Phys. Lett.*, **70**, 27 (1980).
- K. YAMAGUCHI, S. YABUSHITA, T. FUENO, S. KATO, K. MOROKUMA and S. IWATA, "Ab Initio UHF and UHF NO CI Approaches for Quasi-Degenerate Systems: Methylene Peroxide (CH_2OO), *Chem. Phys. Lett.*, **71**, 563 (1980).
- S. NAGASE, N. K. RAY and K. MOROKUMA, "The Reaction Mechanism of Hydroboration. An Ab Initio MO Study on the $\text{C}_2\text{H}_4 + \text{BH}_3$ Reaction", *J. Am. Chem. Soc.*, **102**, 4536 (1980).
- K. MOROKUMA, S. KATO and K. HIRAO, "Substitution Effect on Formaldehyde Photochemistry. Potential Surface Characteristics of HFCO", *J. Chem. Phys.*, **72**, 6800 (1980).
- I. KUSUNOKI, S. SAKAI, S. KATO and K. MOROKUMA, "Ab Initio Calculations of the $a^3\Pi-b^3\Sigma^-$ Transition of CH^+ ", *J. Chem. Phys.*, **72**, 6813 (1980).
- T. F. GEORGE, J. -M. YUAN, R. L. JAFFE, A. KOMORNICKI, K. MOROKUMA and M. SKUSE, "Semiclassical Study of the Quenching of Excited-State Fluorine Atom by Hydrogen Molecule: Comparison between Reactive and Nonreactive Processes", *Isr. J. Chem.*, **19**, 337 (1980).
- Y. SUGAWARA, Y. HAMADA, A. Y. HIRAKAWA, M. TSUBOI, S. KATO and K. MOROKUMA, "Ab Initio MO Calculation of Force Constants and Dipole Derivatives for Formamide", *Chem. Phys.*, **50**, 105 (1980).
- K. SHIGA, Y. NISHINA, I. OHMINE, K. HORIIKE, S. KASAI, K. MATSUI, H. WATARI and T. YAMANO, "A Study of the Absorption, Circular Dichroism and Magnetic Circular Dichroism Spectra of a Flavin Derivative", *J. Biochem.*, **87**, 281 (1980).
- I. OHMINE, "Cluster Configuration Method: Application to the Spectra of π -Electron Systems", *Chem. Phys. Lett.*, **72**, 53 (1980).
- H. ADACHI, S. SHIOKAWA, M. TSUKADA, C. SATOKO and S. SUGANO, "Discrete Variational $X\alpha$ Cluster Calculations III. Application to Transition-Metal Complexes", *J. Phys. Soc. Jpn.*, **47**, 1528 (1979).
- M. TSUKADA, C. SATOKO and H. ADACHI, "Theory of the Surface Electronic Structure and Defect States of Rutile by the DV- $X\alpha$ Cluster Calculation", *J. Phys. Soc. Jpn.*, **47**, 1610 (1979).
- M. TSUKADA, C. SATOKO and H. ADACHI, "Surface Electronic Structure of SrTiO_3 by the DV- $X\alpha$ Cluster Method", *J. Phys. Soc. Jpn.*, **48**, 200 (1980).
- M. TSUKADA, N. TSUDA and F. MINAMI, "Theory of the Electronic Structure of ReO_3 (001) Surface and the Surface Oxygen Vacancy", *J. Phys. Soc. Jpn.*, **49**, 1115 (1980).
- M. TSUKADA, "Self-Consistent Madelung Potential for the Cluster Calculation of Partially Ionic Solids — Application of ReO_3 —", *J. Phys. Soc. Jpn.*, **49**, 1183 (1980).
- E. HIROTA, S. SAITO, and Y. ENDO, "Barrier to Internal Rotation in Ethane from the Microwave Spectrum of CH_3CHD_2 ", *J. Chem. Phys.*, **71**, 1183 (1979).
- E. HIROTA, "Anharmonic Potential Function and Equilibrium Structure of Methane", *J. Mol. Spectrosc.*, **77**, 213 (1979).
- Y. ENDO, S. SAITO, E. HIROTA, and T. CHIKARAISHI, "Microwave Spectrum of Sulfur Difluoride in the First Excited Vibrational States/Vibrational Potential Function and Equilibrium Structure", *J. Mol. Spectrosc.*, **77**, 222 (1979).

- K. KAWAGUCHI, C. YAMADA, and E. HIROTA, "Laser Magnetic Resonance Spectroscopy of SO in the $X^3\Sigma^-$ State with a CO₂ Laser as a Source", *J. Chem. Phys.*, **71**, 3338 (1979).
- S. SAITO and C. MATSUMURA, "Dipole Moment of the HO₂ Radical from its Microwave Spectrum", *J. Mol. Spectrosc.*, **80**, 34 (1980).
- M. KAKIMOTO, S. SAITO, and E. HITORA, "Doppler-Limited Dye Laser Excitation Spectroscopy of the HSO Radical", *J. Mol. Spectrosc.*, **80**, 334 (1980).
- K. KAWAGUCHI, C. YAMADA, E. HIROTA, J. M. BROWN, J. BUTTENSHAW, C. R. PARENT, and T. J. SEARS, "The Laser Magnetic Resonance Spectrum of the ν_2 Band of NH₂", *J. Mol. Spectrosc.*, **81**, 60 (1980).
- J. T. HOUGEN, "Double Group Considerations, Jahn-Teller Induced Rovibronic Effects, and the Nuclear Spin-Electron Spin Hyperfine Hamiltonian for a Molecule of Symmetry C_{3v} in an Electronic ²E State", *J. Mol. Spectrosc.*, **81**, 73 (1980).
- N. ITO, T. KATO, and T. FUJIYAMA, "Measurement of Rayleigh Scattering Spectra for Liquid Sample by Light Beating Method", *Bunko Kenkyu*, **29**, 106 (1980).
- T. SUZUKI, Y. K. TSUTSUI, and T. FUJIYAMA, "Shapes of the ν_1 Band of Liquid Chloroform and Intermolecular Interaction", *Bull. Chem. Soc. Jpn.*, **53**, 1931 (1980).
- T. KATO, N. ITO, and T. FUJIYAMA, "Light Scattering Study of Local Structures in Solutions. Cooperative Translational Motion of Alcohol Molecules in Carbon Tetrachloride Solutions", *Bull. Chem. Soc. Jpn.*, **53**, 2167 (1980).
- T. KATO, T. NAKANISHI, and T. FUJIYAMA, "Light Scattering Study of Local Structures in Solutions. Mean Association Numbers and Concentration Fluctuations for Alcohol-Carbon Tetrachloride Systems", *Bull. Chem. Soc. Jpn.*, **53**, 2173 (1980).
- S. HYODO and T. FUJIYAMA, "Fluctuation of Local Field and Depolarization Degree of the ν_1 Line of Carbon Tetrachloride", *Bull. Chem. Soc. Jpn.*, **53**, 2456 (1980).
- M. TAKAMI, "Dipole Moment and Infrared-Radiofrequency Double Resonance Spectroscopy of CF₄ in the $\nu_3 = 1$ State", *J. Chem. Phys.*, **71**, 4164 (1979).
- M. TAKAMI, "Double Resonance and High Resolution Infrared Spectroscopy of the CF₄ ν_3 Fundamental. I. Infrared-Radiofrequency Double Resonance", *J. Chem. Phys.*, **73**, 2665 (1980).
- K. YOSHIHARA, A. NAMIKI, S. SUMITANI, and N. NAKASHIMA "Picosecond Flash Photolysis, of cis- and trans-Stilbene. Observation of an Intense Intra-Molecular Charge-Resonance Transition", *J. Chem. Phys.*, **71**, 2892 (1979).
- M. HANABUSA, A. NAMIKI, and K. YOSHIHARA, "Laser-Induced Vapor Deposition of Silicon", *Appl. Phys. Lett.*, **35**, 626 (1979).
- M. SUMITANI, N. NAKASHIMA, and K. YOSHIHARA, "Direct Measurement of the Reaction Rate for cis \rightarrow trans Photoisomerization of Stilbene", *Chem. Phys. Lett.*, **68**, 255 (1979).
- T. KAWAI, and T. SAKATA, "Hydrogen Evolution from Water using Solid Carbon and Light Energy", *Nature*, **282**, 283 (1979).
- T. KAWAI and T. SAKATA, "Production of H₂ and CO from Liquid Water and Carbon using Solar Energy", *JCS Chem. Comm.*, 1047 (1979).
- K. TANIMURA, T. KAWAI, and T. SAKATA, "Fluorescence Quenching via Charge Injection at the Interface between Tetraphenylporphine and SnO₂", *J. Chem. Phys.*, **83**, 2639 (1979).
- M. FUJITA, H. NAKATSUKA, H. NAKANISHI, and M. MATSUOKA, "Backward Echo in Two-Level Systems", *Phys. Rev. Lett.*, **42**, 974 (1979).
- H. SAIGUSA, T. AZUMI, M. SUMITANI, K. YOSHIHARA, "Internal Heavy Atom Effect on the Triplet Spin Sublevels of the Lowest Triplet State of Naphthalene. II. Intersystem Crossing Processes from the Singlet Excited State to the Individual Spin Sublevels of the Lowest Triplet State", *J. Chem. Phys.*, **72**, 1713 (1980).
- N. NAKASHIMA, M. SUMITANI, I. OHMINE, K. YOSHIHARA, "Nanosecond Laser Photolysis of Benzene Monomer and Excimer", *J. Chem. Phys.*, **72**, 2226 (1980).
- H. SATO, Y. KUSUMOTO, N. NAKASHIMA, K. YOSHIHARA, "Picosecond Study of Energy Transfer between Rhodamine 6G and 3,3'-Diethylthiacarbocyanine Iodide in the Premicellar Region: Förster Mechanism with Increased Local Concentration", *Chem. Phys. Lett.*, **71**, 326 (1980).
- N. NAKASHIMA, K. YOSHIHARA, F. TANAKA, K. YAGI, "Picosecond Fluorescence Lifetime of the Coenzyme of D-Amino Acid Oxidase", *J. Biol. Chem.*, **255**, 5261 (1980).
- M. MIGITA, T. OKADA, N. MATAGA, N. NAKASHIMA, K. YOSHIHARA, Y. SAKATA, S. MISUMI, "Picosecond Time-Resolved Fluorescence Studies of Intramolecular Heteroexcimers", *Chem. Phys. Lett.*, **72**, 229 (1980).

- T. KAWAI, H. TRIBUTSCH, and T. SAKATA, "Time-Resolved Photocurrent at the $\text{MoSe}_2\text{-I}^-$ Photoelectrode Studied with a Nanosecond Pulsed Laser", *Chem. Phys. Lett.*, **69**, 336 (1980).
- K. TANIMURA, T. KAWAI, and T. SAKATA, "Electronic Structure of a Porphyrin Solid Film and Energy Transfer at the Interface with a Metal Substrate", *J. Phys. Chem.*, **84**, 751 (1980).
- T. KAWAI, and T. SAKATA, "Dynamics of Photoinduced Surface Reactions on Semi-Conductors Studied by a Pulsed Laser-Dynamic-Mass-Spectrometer Technique", *Chem. Phys. Lett.*, **69**, 33 (1980).
- T. KAWAI, and T. SAKATA, "Photocatalytic Decomposition of Gaseous Water over $\text{TiO}_2\text{-RuO}_2$ Surfaces", *Chem. Phys. Lett.*, **72**, 87 (1980).
- T. KAWAI, and T. SAKATA, "Conversion of carbohydrate into Hydrogen Fuel by a Photocatalytic Process", *Nature*, **286**, 474 (1980).
- T. KAWAI, and T. SAKATA, "Photocatalytic Hydrogen Production from Liquid Methanol and Water", *JCS Chem. Comm.*, 384 (1980).
- T. KAWAI, and T. SAKATA, "Photocatalytic Decomposition of Water by Solar Energy — Hydrogen Evolution, CO_2 Fixation on Powdered Semiconductors and Their Mechanisms with Pulsed Laser — Dynamic Mass Technique", *The Seventh International Congress on Catalysis*, **B38**.
- N. NISHI, H. SHINOHARA, and I. HANAZAKI, "Photochemical Conversion from Methylamine to Hydrogencyanide with an ArF Laser at 193 nm", *Chem. Phys. Lett.*, **73**, 473 (1980).
- M. MATSUOKA, H. NAKATSUKA, and M. FUJITA, "Backward Echo and FID in Two-Level systems", *Appl. Phys.*, **22**, 433 (1980).
- M. MATSUOKA, H. NAKATSUKA, and M. FUJITA, "Picosecond Backward Echo in Sodium Vapor — Relaxation and Quantum Beat Modulation", *Topical Meeting on Picosecond Phenomena, North Falmouth*, June, 1980.
- M. KAJITANI, A. SUGIMORI, N. SATO, K. SEKI, H. INOKUCHI and Y. HARADA, "Ultraviolet Photoelectron Spectra of Crown Ethers", *Bull. Chem. Soc. Jpn.*, **52**, 2199 (1979).
- Y. NAKAHARA, Keisaku KIMURA, H. INOKUCHI and T. YAGI, "Electrical Conductivity of Solid State Proteins: Simple Proteins and Cytochrome c_3 as Anhydrous Film", *Chem. Lett.*, 877 (1979).
- S. HASHIMOTO, K. SEKI and H. INOKUCHI, "Anisotropic Absorption of Oriented Syndiotactic-1,2-polybutadiene Thin Films in the Vacuum Ultraviolet Region", *Rep. Prog. Polym. Phys. Jpn.*, **22**, 439 (1979).
- K. SEKI, S. HASHIMOTO, K. INOUE, K. NAKAGAWA, N. SATO, K. TAKAGI, S. SUGA, H. KANZAKI and H. INOKUCHI, "Anisotropic Carbon $1s\text{-}\pi^*$ Extreme Ultraviolet Absorption Spectra of Oriented *St*-1,2-polybutadiene", *Rep. Prog. Polym. Phys. Jpn.*, **22**, 443 (1979).
- K. SEKI, K. NAKAGAWA, N. SATO, H. INOKUCHI, S. HASHIMOTO, K. IOUE S. SUGA, H. KANZAKI and K. TAKAGI, "Anisotropic Carbon $1s$ XUV Absorption Spectra of Oriented *St*-1,2-polybutadiene Film", *Chem. Phys. Lett.*, **70**, 220 (1980).
- N. UENO, T. FUKUSHIMA, K. SUGITA, S. KIYONO, K. SEKI, and H. INOKUCHI, "Experimental Study of Conduction Band Structure of Some *n*-Alkanes and Polyethylene by Means of Low Energy Electron Scattering and Photoelectron Spectroscopy", *J. Phys. Soc. Jpn.*, **48**, 1254 (1980).
- M. UTUNO, Keisaku KIMURA, K. ONO, H. INOKUCHI and T. YAGI, "Application of Mössbauer Spectroscopy to the Wet Bacterial Cells", *J. Biochem.*, **87**, 1257 (1980).
- M. UTUNO, Keisaku KIMURA, K. ONO, T. YAGI, and H. INOKUCHI, "Kinetics of Cytochrome c_3 Reduction with Hydrogenase Studied by Mössbauer Effect", *J. Chem. Phys.*, **72**, 2264 (1980).
- S. IWASHIMA, H. HONDA, J. AOKI and H. INOKUCHI, "Time Dependence of Crystallization of Tetrabenzos [*a, cd, j, lm*] perylene Evaporated Film as a Function of Purity", *Mol. Cryst. Liq. Cryst.*, **59**, 207 (1980).
- M. SANO, H. INOKUCHI, M. KOBAYASHI, S. KANEIWA and I. TSUJIKAWA, "Superconductivity in Graphite-Potassium Intercalation Compounds", *J. Chem. Phys.*, **72**, 3840 (1980).
- Y. NAKAHARA, Keisaku KIMURA, T. YAGI and H. INOKUCHI, "Electrocal Conductivity of an Anhydrous Cytochrome c_3 Film as Function of Temperature and Ambient Pressure", *Chem. Phys. Lett.*, **73**, 31 (1980).
- N. SATO, Keisaku KIMURA, H. INOKUCHI and YAGI, "Ionization Potential of Anhydrous Ferrocyclochrome c_3 ", *Chem. Phys. Lett.*, **73**, 35 (1980).
- K. NOMOTO, Y. ACHIBA and K. KUMURA, "HeI and HeII photoelectron Study of N_2O_4 ", *Bull. Chem. Soc. Jpn.*, **52**, 1614 (1979).
- T. KONDO, M. TANIMOTO, M. MATSUMOTO, K. NOMOTO, Y. ACHIBA and K. KIMURA, "Cyclic Peroxides: Dihedral Angle around the Peroxide Bond by Microwave and Photoelectron Spectroscopic Studies", *Tetrahedron Lett.*, **21**, 1649 (1980).

- I. KOYANO and K. TANAKA, "State-Selected Reactive Collisions of Diatomic Molecular Ions by a Coincidence Technique", *Electronic and Atomic Collisions*, Ed. by N. Oda and K. Takayanagi, North-Holland, 1980, p.547.
- I. KOYANO, and K. TANAKA, "State-Selected Ion — Molecule Reactions by a Threshold Electron — Secondary Ion Coincidence (TESICO) Technique. I. Apparatus and the Reaction $H_2^+ + H_2 \rightarrow H_3^+ + H$ ", *J. Chem. Phys.*, **72**, 4858 (1980).
- K. TANAKA, J. DURUP, T. KATO, and I. KOYANO, "Direct Determination of Individual Reaction Cross Section for the Two Spin-orbit States $Ar^+ (^2P_{3/2}, ^2P_{1/2})$ ", *J. Chem. Phys.*, **73**, 586 (1980).
- A. NATO, M. NIWA, K. HONMA, I. TANAKA, and I. KOYANO, "Effect of Structure of Reactants on the Ion — Molecule Reactions $C_3H_4^+ + C_3H_4$ ", *Int. J. Mass Spectrom. Ion Phys.*, **34**, 287 (1980).
- Y. KODAMA, K. NISHIHATA, S. ZUSHI, M. NISHIO, J. UZAWA, K. SAKAMOTO, and H. IWAMURA, "The Conformation of a Diastereoisomeric Pair of 2,2-Dimethyl-4-phenyl-3-pentanol", *Bull. Chem. Soc. Jpn.*, **52**, 2661 (1979).
- S. NAKADA, M. YAMADA, T. ITO, and M. FUJIMOTO, "Thermochromism of Metal Chelates with Triphenylmethane Complexons in Aqueous Solutions. II. Inhibitive Effects of the Protolysis of Aqua Cu^{2+} Ion on the Thermochromism of $Cu(II)$ -Xylenol Orange Chelate", *Bull. Chem. Soc. Jpn.*, **52**, 2723 (1979).
- T. SUGAWARA, Y. KAWADA, M. KATOH, and H. IWAMURA, "Oxygen-17 Nuclear Magnetic Resonance. III. Oxygen Atoms with a Coordination Number of Two", *Bull. Chem. Soc. Jpn.*, **52**, 3391 (1979).
- M. KATOH, T. SUGAWARA, Y. KAWADA, and H. IWAMURA, " ^{17}O Nuclear Magnetic Resonance Studies. V. ^{17}O Shieldings of Some Substituted Anisoles", *Bull. Chem. Soc. Jpn.*, **52**, 3475 (1979).
- Y. KAWADA, H. TSUKADA, and H. IWAMURA, "A Novel Route from Triptycenes to a Dibenzo (Hafner's Hydrocarbon), Benz [a] indeno [1,2,3-cd] azulene", *Tetrahedron Lett.*, **21**, 181 (1980).
- K. MOCHIZUKI, T. ITO, and M. FUJIMOTO, "Formation of Five-Coordinate $Ni(II)$ Complexes of 2,12-Dimethyl-3,7,11,17-tetraazabicyclo-[11.3.1]-heptadeca-1(17),2,11,13,15-pentane Analogs and Halide Ions in Nitromethane." *Bull. Chem. Soc. Jpn.*, **53**, 543 (1980).
- H. IWAMURA, M. KATOH, and H. KIHARA, "How Strained is the "Flat" Benzene Ring in Superphane?", *Tetrahedron Lett.*, **21**, 1757 (1980).
- S. NAKADA, M. YAMADA, T. ITO, and M. FUJIMOTO, "Thermochromism of Metal Chelates with Triphenylmethane Complexons in Aqueous Solutions. III. Copper(II)-Methylthymol Blue and -Methylxylenol Blue Systems." *Bull. Chem. Soc. Jpn.*, **53**, 2252 (1980).
- K. MOCHIZUKI, M. FUJIMOTO, H. ITO and T. ITO, "Spin-state Equilibria of the $Ni(II)$ Complexes of 2,12-Dimethyl-3,7,11,17-tetraazabicyclo-[11.3.1]-heptadeca-1(17),2,11,13,15-pentane Analogs in Water." *Bull. Chem. Soc. Jpn.*, **53**, 2535 (1980).
- Y. KAWADA and H. IWAMURA, "Unconventional Synthesis and Conformational Flexibility of Bis (1-triptycyl) Ether", *J. Org. Chem.*, **45**, 2547 (1980).
- M. IWAMURA, M. KATOH, and H. IWAMURA, "Rotational Barriers in Bisadducts of 1-Cyano-1-methylethyl Radicals with Nitrones and Nitroso Compounds", *Org. Magn. Reson.*, **13**, 1905 (1980).
- Keisaku KIMURA, "Ionic Radii and Metallic Radii Based on a Pseudopotential", *Phys. Lett.*, **72A**, 456 (1979).
- Y. OSANAI and H. KASHIWAGI, "Improvement of an Integral Approximation Scheme Based on Semiorthogonalized Orbitals", *Int. J. Quant. Chem.*, **17**, 1031 (1980).

Review Articles and Textbooks

- E. HITORA, "Ultra-high Resolution Infrared Spectroscopy", *Bunko Kenkyu* (in Japanese), **28**, 187 (1979).
- E. HIROTA, "Visit to Short-Lived Molecules/Recent Progress by Laser Spectroscopy", *Bunseki* (in Japanese), 886 (1979).
- E. HIROTA, "Microwave Spectroscopy", *Gendai Kagaku* (in Japanese), 40 (1980).
- E. HIROTA, "Rotational Spectrum", in "Determination of Molecular Structure, Modern Chemistry 13" (in Japanese), M. Ōki, Y. Saito and S. Nagakura Ed., *Iwanami* (1980), Chapter 3, pp. 65-103.
- S. SAITO, "High Resolution Spectroscopy of Molecular Ions", *Kagaku* (in Japanese), **35**, 257 (1980).
- N. NAKASHIMA, K. YOSHIHARA, "Electronic Excited States and Photochemical Reactions", *Chem. Rev.*, (in Japanese), **24**, 83 (1979).
- T. SAKATA, and T. KAWAI, "The Conversion of Solar Energy into Chemical Energy by using Solid Interfaces — Decomposition of Water by Photocatalytic Process", *Hyomen* (in Japanese) **10**, 618-632 (1979).
- K. YOSHIHARA, "Progress in Mechanistic Studies of Photochemistry by Picosecond Spectroscopy; cis-trans Photoisomerization of Stilbene", *Rev. Laser Engineering*, (in Japanese), **4**, 367 (1980).
- T. SAKATA, "Photocatalytic Decomposition of Water: An Approach to Artificial Photosynthesis", in "Water and Metal Cations in Biological Systems", B. Pullman and K. Yagi Ed., *Japan Scientific Society Press*, Tokyo, pp. 75-82 (1980).
- T. SAKATA, T. KAWAI, T. KOISO, and M. OKUYAMA, "Hydrogen Evolution by Photocatalytic Reactions of Some Organic Dyes and Semiconductors", in "Hydrogen Energy Progress", Proceedings of the 3rd World Hydrogen Energy Conference held in Tokyo, T. N. Veziroglu, K. Fueki and T. Ohta Ed., *Pergamon Press*, pp. 773-780 (1980).
- N. NISHI, "Electron Spin Echo", in "Fast Reactions in Biological System", T. Ishimura, H. Hatano, K. Hayashi, and K. Hiromi Ed., *Kagaku Dojin*, (in Japanese), **91**, (1979).
- H. INOKUCHI, "Solid State Chemistry", in "Chemistry of Molecular Assemblies" (in Japanese), H. Inokuchi, R. Tamamushi and M. Tanaka Ed., *Iwanami* (1980), pp. 211-332.
- I. KOYANO and H. HORIGUCHI, "Chemical Reactions of Vibrationally and Rotationally Excited Molecules", *Kagaku Sosetsu* (in Japanese), **26**, 113 (1980).
- K. KIMURA, "Ionic Photodissociation of Weak Ground State Electron-Donor-Acceptor Complexes", *Rev. Chem. Intermediates*, **2**, 321 (1979).
- K. KIMURA, "Electronic Spectra and Photoelectron Spectra" (in Japanese), Ed. by M. Ooki, Y. Saito and S. Nagakura, *Iwanami* (1980), pp. 125-152.
- H. IWAMURA and K. MARUYAMA, "Design of Organic Syntheses with the Aid of a Computer", *Kagaku Sosetsu* (in Japanese), **18** (Information Chemistry), *Chem. Soc. Jpn.*, Ed., (1978), pp. 179-201.
- T. ITO, "Complexation Reactions" in "Fundamental Chemical Reactions in Analytical Chemistry", Ed. by The Japan Society for Analytical Chemistry, Hokkaido Branch, (in Japanese), *Baifukan*, (1980), pp. 58-83.
- H. TUKADA and H. IWAMURA, "The Chemistry of Three-dimensional Molecules Constructed with Aromatic Ring", *Kagaku no Ryoiki* (in Japanese), **34**, 27 (1980).
- T. SUGAWARA, Y. KAWADA, and H. IWAMURA, "Information from ^{17}O NMR", *Kagaku no Ryoiki* (in Japanese), **34**, 35 (1980).
- N. INAMOTO, H. IWAMURA, and I. NAKAGAWA, "Practice in Conformational Analyses" (in Japanese), *Nankodo* (1980).
- H. IWAMURA, "Theoretical Prediction of Molecular Structure", *Gendai Kagaku* (in Japanese), **13**, (1980), pp. 289-310.

Institute for Molecular Science, Myodaiji, Okazaki 444, Japan